Towards the development of synthetic vaccines against tuberculosis

Marino, L.

Towards the development of synthetic vaccines against tuberculosis

Proefschrift

ter verkrijging van
de graad van doctor aan de Universiteit Leiden,
op gezag van rector magnificus prof.dr.ir. H. Bijl,
volgens besluit van het college voor promoties
te verdedigen op dinsdag 7 juni 2022
klokke 10:00 uur

Laura Marino

Geboren te Villaricca, Italië
in 1990

Promotores:
Prof.dr. J.D.C. Codée
Prof.dr. T.H.M. Ottenhoff

Promotiecommissie:
Prof.dr. G.A. van der Marel
Dr. I. van Rhijn (Brigham and Women's Hospital)
Prof.Dr. A. Geluk (LUMC)
Dr. D.V. Filippov
Prof.dr. A.J. Minnaard (University of Groningen)

ISBN: 978-94-93289-01-7
Printed by: Printsupport4u

In memory of Aurelia Tripodo,
for her kindness and perseverance.

Table of contents

List of abbreviations ii

Chapter 1 1
General Introduction

Chapter 2 21
Design and synthesis of stabilized mannosyl phosphomycoketide analogues

Chapter 3 61
Design and immunological evaluation of conjugates containing Mincle ligands

Chapter 4 117
Synthesis and immunological evaluation of conjugates containing a TLR2 agonist

Chapter 5 151
Mincle/TLR2 co-stimulation using synthetic ligands

Chapter 6 175
Summary and prospects

Nederlandse Samenvatting 189

About the author 191

Acknowledgments 193

List of abbreviations

a.a.	amino acids
AIBN	2,2′-azobis(2-methylpropionitrile)
ANOVA	analysis of variance
APC	antigen-presenting cell
APT	attached proton test
aq	aqueous
arom	aromatic
BCG	bacillus Calmette–Guérin
BMM	bone-marrow derived macrophage
BnBr	benzyl bromide
BSA	bovine serum albumin
CCL*	chemokine ligand
CCR*	chemokine receptor
CD*	cluster of differentiation
CE	cyanoethyl
CFU	colony forming unit
CLEC4E	C-type lectin domain family 4 member E
CLR	C-type lectin receptor
COSY	correlation spectroscopy
CPG	controlled pore glass
CpG	cytosine-phosphorothioate-guanine oligodeoxynucleotides
CSO	*(1S)*(+)-(10-camphorsulfonyl)oxaziridine
CTL	cytotoxic T lymphocytes
δ	chemical shift
d	doublet
DAMP	damage-associated molecular pattern
DC	dendritic cell

DC-SIGN	DC-specific ICAM-3 grabbing non-integrin
DCI	4,5-dicyanoimidazole
DCM	dichloromethane
DDA	dimethyldioctadecylammonium
DDQ	2,3-dichloro-5,6-dicyano-1,4-benzoquinone
DEAD	diethyl azodicarboxylate
DIC	diisopropylcarbodiimide
DIPA	diisopropylamine
DIPEA	*N,N*-diisopropylethylamine
DMAP	4-dimethylaminopyridine
DMEM	Dulbecco's modified Eagle medium
DMF	dimethylformamide
DMSO	dimethyl sulfoxide
DMT	(4,4'-dimethoxytrityl)
DNA	deoxyribonucleic acid
DOPC	1,2-dioleoyl-*sn*-glycero-3-phosphocholine
DOTAP	dioleoyl-trimethylammonium propane
DPAP	2,2-dimethoxy-2-phenylacetophenone
DTT	dithiothreitol
EDCI	1-ethyl-3-(3-dimethylaminopropyl)carbodiimide
EDTA	ethylenediamine tetraacetic acid
ELISA	enzyme-linked immunosorbent assay
eq	equivalents
ESI	electrospray ionization
et al.	*et alia*, 'and others'
EtOAc	ethyl acetate
FACS	fluorescence-activated cell sorting
FBS	fetal bovine serum
FCS	fetal calf serum
GM-CSF	granulocyte-macrophage colony-stimulating factor
GMM	glucose monomycolate
HEK	human embryonic kidney
HIV	human immunodeficiency virus
HLA	human leukocyte antigen

HMDS	hexamethyldisilazane
HPLC	high-performance liquid chromatography
HRMS	high resolution mass spectrometry
HRP	horseradish peroxidase
HSQC	heteronuclear single quantum coherence
IBX	2-iodoxybenzoic acid
IFN-γ	interferon γ
IL*	interleukin
IMDM	Iscove's modified Dulbecco's medium
IR	infrared
ITAM	immunoreceptor tyrosine-based activation motif
J	J-coupling
KHMDS	potassium bis(trimethylsilyl)amide
KLRG1	killer cell lectin-like receptor subfamily G member 1
LAL	limulus amebocyte lysate
LC-MS	liquid chromatography mass spectrometry
LDA	lithium diisopropylamide
LN	lithium naphthalenide
LPS	lipopolysaccharides
m	multiplet
M-CSF	macrophage-colony stimulating factor
M1	macrophage type 1
M2	macrophage type 2
MACS	magnetic-activated cell sorting
MALDI-TOF	matrix-assisted laser desorption-ionisation-time of flight mass spectrometry
MAP*	mitogen-activated protein kinases
MCL	macrophage C-type lectin
*m*CPBA	*meta*-chloroperoxybenzoic acid
MFI	median fluorescence intensity
MHC	major hystocompatibility complex
Mincle	macrophage-inducible C-type lectin
MIP*	macrophage inflammatory protein
moDC	monocyte-derived dendritic cell
MPL	monophosphoryl lipid A

MPM	mannosyl phosphomycoketide
MR	mannose receptor
Mtb	*Mycobacterium tuberculosis*
MW	molecular weight
MyD88	myeloid differentiation primary response protein 88
NapBr	1-bromonaphthalene
NBS	*N*-bromosuccinimide
NLRP*	nucleotide-binding oligomerization domain
NMR	nuclear magnetic resonance
NOD*	nucleotide-binding and oligomerization domain
NOE	nuclear Overhauser effect
NOESY	nuclear Overhauser effect spectroscopy
NOS	nitrogen oxide species
OD	optical density
PAMP	pathogen-associated molecular pattern
PBMC	peripheral blood mononuclear cell
PBS	phosphate-buffered saline
PCR	polymerase chain reaction
PD-L*	programmed death ligand
PD*	programmed cell death protein
PDI	polydispersity index
Ph	phenyl
PM	phosphomycoketide
ppm	parts per million
PRR	pattern recognition receptor
*p*TsOH	*para*-toluenesulfonic acid
q	quartet
quant.	quantitative
RIG*	retinoic acid-inducible gene
RNA	ribonucleic acid
RPMI	Roswell Park Memorial Institute
RT	room temperature
s	singlet
s.c.	subcutaneous

SD	standard deviation
SEAP	secreted embryonic alkaline phosphatase
SEM	standard error of the mean
SLP	synthetic long peptide
SYK	spleen tyrosine kinase
t	triplet
TB	tuberculosis
TBAF	tetra-*n*-butylammonium fluoride
TBAI	tetra-*n*-butylammonium iodide
TCEP	(tris(2-carboxyethyl)phosphine)
TCR	T cell receptor
TDB	trehalose-6,6'-dibehenate
TDM	trehalose-6,6'-dimycolate
TDS	trehalose-6,6'-distearate
TDSCl	chloro(dimethyl)thexylsilane
TFA	trifluoroacetic acid
Th*	T helper cell
THF	tetrahydrofuran
TIRAP	TIR-containing adaptor protein
TIS	triisopropyl silane
TLC	thin-layer chromatography
TLR*	toll-like receptor
TMB	3,3′,5,5′-Tetramethylbenzidine
TMS	trimethylsilyl
TNF-α	tumor necrosis factor α
TRIF	TIR-domain-containing adapter-inducing interferon-β
UV	ultraviolet
WHO	World Health Organization

NB: The asterisk symbol (*) used in the list of abbreviations is the wildcard character for any number which indicates a different member of the indicated family.

1

1

General introduction

Mycobacterium tuberculosis (*Mtb*), the causative agent of tuberculosis (TB), is responsible for the death of around 1.4 million people every year.[1] Although there is a commercially available vaccine, the *bacillus of Calmette Guérin* (BCG), an attenuated version of *Mycobacterium bovis*, studies have shown that this is not always effective and it can cause disseminated disease in immunocompromised individuals.[2,3] A safe and effective vaccine is required to contain and, possibly, eradicate *Mtb*. Technological advances accomplished in the fields of chemistry and immunology offer the opportunity to discover efficient, safe and economical vaccines. The overarching goal of this Thesis is to devise synthetic strategies for the generation of novel, rationally designed synthetic vaccines against TB.

Immune response upon pathogen encounter and vaccination

The immune system is a defense mechanism against pathogens which can be exploited in vaccination to reduce the chance of developing a life-threatening disease. The immune system is described as consisting of an innate and an adaptive part.[4]

The innate immune system is a fast-acting defense mechanism that all animals have. It comprises the complement system of proteins, natural killer cells and several professional phagocytes (such as monocytes, macrophages and dendritic cells). In the course of this introduction, the focus will be placed on the role and function of macrophages and dendritic cells as key cellular targets for the design of a vaccine. Macrophages and dendritic cells express pattern recognition receptors (PRRs) on their cellular surface. PRRs are able to recognize components of pathogens that are common among different microorganisms and that are known as pathogen-associated molecular patterns (PAMPs). Upon PAMP recognition, a macrophage or dendritic cell can engulf the pathogen by phagocytosis. Phagocytosis can lead to direct killing of the pathogen and/or release of messenger cytokines and chemokines. Besides their role as professional phagocytes in immune responses, macrophages and dendritic cells are key players in bridging innate and adaptive immune responses *via* a process known as antigen presentation (see Figure 1 for a graphical depiction of the two systems and the key role of macrophages and dendritic cells in bridging the innate and adaptive immune response). Molecular components of a pathogen, called antigens, get processed and presented to other immune cells, such as T cells which are part of the adaptive immune system. For this function, macrophages and dendritic cells are grouped in the family of antigen presenting cells (APCs) together with other immune cells (monocytes, B cells).

Antigen presentation is a fundamental aspect of the adaptive immune system, which is typical of vertebrates. The adaptive immune response is very specific to a certain antigen, and its activation is functional to the development of immunological memory, which is the goal of prophylactic vaccination. The adaptive immune system comprises plasma cells, T cells, B-cells and antibodies.

Antibodies circulate in the blood of immunized individuals and are produced by B-cells upon B-cell activation. They bind to extracellular bacteria and viruses tagging them for destruction. Several subclasses of antibodies have been identified in humans and mice, which are the two organisms used in the research in this Thesis for the evaluation of novel vaccine modalities. Immunoglobulin G (IgG) is the major antibody type found in the blood of humans, representing about 75% of total immunoglobulins. Table 1 provides an overview of the existing antibody IgG subclasses and their properties to initiate complement activation and triggering of FcγR-expressing cells, mechanisms that can eventually result in destruction of the invading pathogen.[5,6]

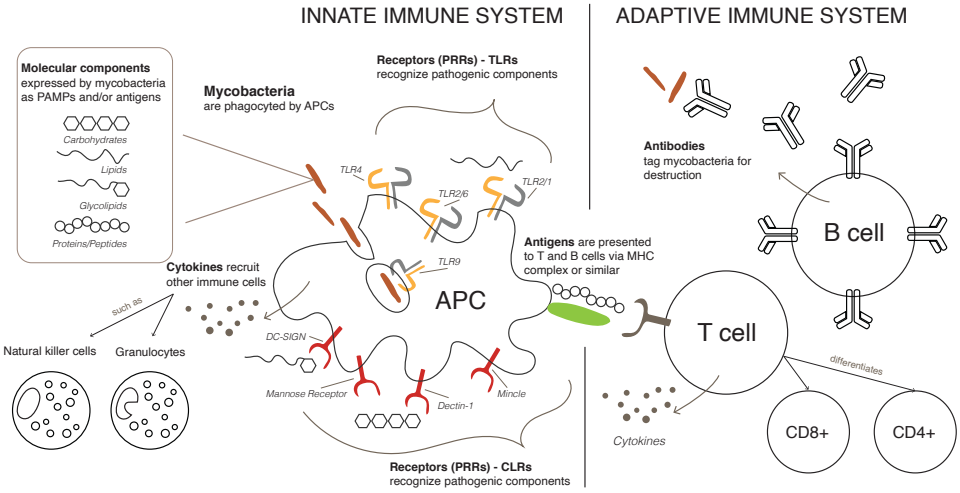

Figure 1 – Graphical depiction of key players of innate and adaptive immune response with focus on central role of antigen presenting cells (APCs) to bridge innate and adaptive system. The left side shows three cellular components of the innate immune system: APCs, natural killer cells (NKs) and granulocytes. These are activated during the innate immune response to mycobacteria. The recognition of mycobacteria by APCs is mediated by pattern recognition receptors (PRRs), capable of binding pathogen associated molecular patterns (PAMPs), such as carbohydrates, lipids, glycolipids and proteins or peptides. PRRs proven to interact with mycobacterial components are here depicted and classified in two categories: Toll-like receptors (TLRs), such as TLR2/1, TLR2/6, TLR4, TLR9, and C-type lectin receptors (CLRs), such as Mincle, Dectin-1, Mannose Receptor and DC-SIGN. Recognition and binding of mycobacterial molecular components to TLRs and CLRs results in activation of specific signaling pathways which result in production of cytokines to recruit other immune cells, such as NK and granulocytes. Additionally, APCs are able to detect and present other mycobacterial components that are phagocyted and loaded onto MHC proteins – or MHC-like molecules such as CD1. This process is key to activation of the adaptive immune system. The right side of the figure depicts three fundamental players of the adaptive immune response: T cells, B cells and antibodies.

Table 1 - Properties of the murine and human IgG subclasses. Ability to fixate the complement and affinity to the Fcγ receptor are selected functions which provide an indication of the ability of an antibody to tag a pathogen for destruction through activation of either the complement system or phagocytosis. Properties of murine IgG2c are not shown as this subclass is not well characterized.[5,6]

Murine IgG antibodies			Human IgG antibodies		
IgG subtype	**Complement fixation**	**Affinity to Fcγ receptor**	**IgG subtype**	**Complement fixation**	**Affinity to Fcγ receptor**
IgG1	-	+	*IgG1*	++	+++
IgG2a	++	+++	*IgG2*	+	+
IgG2b	++	+++	*IgG3*	+++	++++
IgG3	++	-	*IgG4*	-	++

Although antibodies can tag extracellular pathogens for phagocytic uptake, they cannot easily access pathogens once these are inside a cell. T cells, on the contrary, have the ability to recognize infected cells and destroy them. Different classes of T cells exist and their roles span from T-helper lymphocytes ($CD4^+$) to cytotoxic T lymphocytes ($CD8^+$). When APCs present antigens to T cells, the latter can identify the antigen-protein complex via T cell receptors (TCRs) if the right co-stimulatory signals and cytokines are present.[7] Although both $CD4^+$ and $CD8^+$ T cells are activated via antigen presentation, the mechanism of antigen presentation differs for the two. $CD8^+$ T cell activation requires processing of intracellular antigenic proteins or peptides and loading on the major histocompatibility complex class I (MHC-I).[8] $CD4^+$ T cell activation requires engulfment of extracellular proteins or peptides, processing, and loading of the antigen on the major histocompatibility complex class II (MHC-II).[9] Other T cell classes have been discovered, some of which contain TCRs able to interact with lipid antigens presented on MHC class I like cluster of differentiation-1 (CD1) molecules.[10] T cell differentiation into further subtypes producing specific cytokines is functional to the diversification of the immune-response and the recruitment of different immune cells. Depending on the type of cytokines released by T-helper cells, the cellular adaptive immune response can be classified further.

In TB vaccination, relevant T cell responses include Th1- and Th17-cellular responses.[11] These cells produce cytokines, including IL-2, IFN-γ, TNF-α and IL-17 that stimulate macrophages and dendritic cells to upregulate phagocytosis and antigen presentation. Notably, Th1 and Th17 cellular responses have been regarded as markers of protection. The suppression of IFN-γ and IL-17 production has been shown to increase TB susceptibility.[12–15] On the other end of the spectrum are Th2 immune responses, which are characterized by production of IL-4 and IL-10, and are associated with latent TB infection, reactivation and advanced TB.[16]

The selection of an antigen is of fundamental importance when designing a vaccine against a certain pathogen because it determines the specificity of the immunological memory. Molecules derived from *Mtb*, or synthetically made on the basis of the natural components, can be employed to render a vaccine specific against TB. However, an antigen alone is usually not sufficient to efficiently activate the immune system.[17] Therefore, the antigen needs to be delivered together with one or more immune stimulatory agents, called adjuvants when they are included in a vaccine formulation. The main role of an adjuvant is to amplify and direct the responses to the antigen towards specific cell subsets, such as dendritic cells and macrophages, or certain compartments within the cell.

Immunological memory is generated when memory B or T cells are generated after prior exposure to the specific antigen and antigen-specific T cells and antibodies rapidly increase in the circulation after exposure to the specific antigen (humoral component of the immunological memory).

Table 2 - Properties of selected cytokines that are produced upon mycobacterial infection and that can be monitored to evaluate vaccine immunogenicity. The first two columns summarize the origin and functions of each cytokine. The last two columns provide an indication of the susceptibility to mycobacterial infection in the absence or alteration of the expression of each cytokine in either mice (knock-out) or humans (genetic deficiencies).[18,19]

	Cytokine in relation to the immune system		**Susceptibility to *Mtb* infection**	
	produced by:	**recognized functions:**	**Cytokine-knockout mice**	**Humans with disregulated cytokine expression**
IL-6	monocytes, DCs, B cells, fibroblasts and endothelial cells	↓ inhibitory activity towards Th1 and Treg function; ↑ promotes Th2 and Th17 differentiation	enhanced susceptibility during early *Mtb* infection	genetic variation in IL-6 gene associated with TB disease
IL-10	DCs, macrophages, Th0, Th1, Th2 and T regs phenotypes	↓ deactivation of macrophages; ↓ downregulation of Th1 and NK immune-responses	similar susceptibility to *Mtb* infection	N/A
IL-12	DCs, macrophages, B cells	↑ induction of IFN-γ production and polarization to Th1 responses; promotion of macrophage and NK cell activity	enhanced susceptibility to *Mtb* infection	patients with genetic defects in IL-12/IFN-γ pathway are more susceptible
IFN-γ	macrophages, Th1, CTL, NK cells	↑ promotion of antigen presentation and recruitment of $CD4^+$ and $CD8^+$ T cells; promotion of B cell, macrophage, NK activity	enhanced susceptibility to *Mtb* infection	patients with genetic defects in IL-12/IFN-γ pathway are more susceptible
TNF-α	DCs, macrophages, Th1, some Th2 and some CTL phenotypes	↑ induction of NO production; ↑ contribution to granuloma formation; promotion DC activity	enhanced susceptibility to *Mtb* infection	TNF-α neutralization correlates with an increased risk of reactivation of latent tuberculosis
IL-17	Th17 cells; dependent on IL-23, IL-1beta, tgf-beta and IL-6.	↑ recruitment of neutrophils; ↑contribution to granuloma formation	N/A	N/A

Through targeting of certain cells or compartments within APCs it's possible to promote the induction of specific cytokines and chemokines to attract other immune cells or promote the diversification of T cell response, eventually leading to immunological memory. Table 2 provides an overview of the functions of selected cytokines that are involved in immune-responses against TB. These cytokines were chosen on the basis of their origin (which immune cells produces them), their relevance in the recruitment of phagocytes or polarization of T cell responses. Additionally, their significance for the susceptibility to *Mtb* infection in cytokine knock-out mice and cytokine-deficient individuals is defined.

Current vaccines against *Mtb*

The first vaccine employed against *Mtb* was developed in Lille at the Pasteur Institute through attenuation of the virulent *Mycobacterium bovis* and used for the first time in humans back in 1921.[20] This was the first step towards the widespread use of the BCG vaccine, the sole *Mtb* vaccine licensed and in use today. The administration of the BCG vaccine, however is connected to the risk of disseminated BCG-osis, a disease occurring particularly in immunocompromised vaccinated infants (due to HIV infection), and occasionally in immune-compromised adults. BCG's main drawback is its limited and varying (0-80%) efficacy in providing protection against TB in adults. These challenges could be overcome by developing new vaccination strategies that are more efficacious, safer and preferably both.[21,22] In the past 100 years, six different strains of BCG have been employed and there is evidence suggesting that the outcome of immunization may be related to which strain is used and/or batch to batch variation.[23] Controversy regarding the efficacy of the BCG vaccine in adults and immune-compromised individuals has prompted the investigation of other vaccination approaches.[2,3,23] Moreover, the immunological mechanisms of protection after BCG vaccination have not been completely elucidated.

For a long time, TB vaccines were designed and evaluated with a focus on the induction of cellular Th1 responses on the assumption that this mechanism is primarily responsible for BCG-induced protection.[24] The key role of IFN-γ and Th1 cellular responses was deducted from the observation that a Th1 immune response was detected in BCG-immunized infants, and the additional observation that IFN-γ-secreting BCG-specific T cells were associated with protection against active TB in the following three years of life.[25–27] However, there is little evidence that IFN-γ and Th1 cellular responses are the only correlates of BCG-induced protection. The $CD4^+$ Th1 paradigm of protection has been subsequently challenged, especially after recognizing the low performance of Th1-inducing vaccine candidates once they reached human clinical trials.[20,28–30] For example, the MVA85A vaccine, which induced robust Th1 antigen-specific T cell responses in infants and adults, failed to provide protection against incident *Mtb* infection or active disease.[31,32]

Currently, there are 15 vaccine candidates in various stages of clinical trials,[2] which can be grouped in three main categories: attenuated/inactivated/recombinant pathogens, virally vectored- and recombinant protein subunit vaccines. The first category includes among others a recombinant BCG vaccine (VPM1002), a non-tuberculous mycobacterium (DAR-901), and a live genetically double attenuated vaccine based on a human isolate of *Mtb* (MTBVAC), as shown in Table 3. Advantages of using this vaccine modality include the simultaneous delivery of multiple epitopes and PAMPs, which can induce a strong pro-inflammatory response in the host and act via several different immune stimulating and modulating mechanisms, leading to

both innate and adaptive immune responses.[33] On the other hand, attenuated and inactivated micro-organisms might present safety concerns due to the intrinsic risk of mutation, reversion and contamination.[34] Even when using genetic modification approaches to inactivate genes, the problem of balancing immunogenicity and reactogenicity persists.[33]

The second category includes virally vectored vaccines, with the most studied vectors being adenoviral vectors.[35] Currently there are two such vaccines in clinical trials against TB (see Table 3) and they include an adenovirus serotype 5 (Ad5Ag85A) and a recombinant chimpanzee adenoviral vector, both expressing an *Mtb* protein antigen. This vaccine modality presents similar advantages to whole-cell vaccines, delivering multiple PAMPs simultaneously. However, preexisting immunity in humans due to natural adenoviral infections can significantly reduce uptake of the vaccine by APCs as a consequence of neutralization of the viral vector by virus-neutralizing antibodies.[36]

The third category, comprising subunit vaccines, is characterized by the use of (macro)molecules (proteins and peptides) derived from *Mtb* as molecular antigens in combination with other components, such as PAMPs (TLR4, TLR9), aluminum hydroxide or additional lipids assembling into liposomal bilayer/particles/emulsions. An advantage of both the second and third strategies is the reduction of safety concerns, together with the potential to change the antigen(s) included.[37,38] An important characteristic of subunit vaccines, and in particular synthetic subunit vaccines, is the chance for step-wise improvements to optimize vaccine formulation in terms of, for example, solubility and delivery kinetics, together with the opportunity to target specific immune cells or cell compartments. An example of the potential of subunit vaccines can be seen in the recent study using M72/AS01E, showing a vaccine efficacy of 54% for the prevention of TB development in latently-infected individuals.[3940]

Table 3 - Vaccines against *Mtb* in different phases of clinical trials. The vaccines are grouped in three categories: viral, subunit and whole-cell. For each vaccine an indication of the stage of clinical evaluation is provided. Viral vector and type of whole-pathogen are specified for the viral and whole-pathogen vaccines. For subunit vaccines, details of the antigen(s) including the targeted PRR and delivery system are provided.

		Vaccine	Viral vector	Protein/peptide antigen	PAMP adjuvant	Delivery system	Whole-pathogen	Ref.
Phase II	Whole-cell	MTBVAC					attenuated *M. tuberculosis*	41
		RUTI					inactivated *M. tuberculosis*	42
		DAR-901					inactivated *M. obuense*	43
Phase III		VPM1002					recombinant BCG	44
		MIP					inactivated *M. incidus pranii*	45
		Vaccae					inactivated *M. vaccae*	46
Phase I	Viral	Ad5Ag85A	adenovirus serotype 5					47
		ChadOx1 + Ag85A	chimpanzee adenovirus					48
Phase II	Subunit	AEC + BC02		Ag85B and ESAT6-CFP10	TLR9			49
		GamTBVac		modified-Ag85B and ESAT6-CFP10	TLR9	dextran nanoparticles		50
		ID93 + GLA-SE		Rv1813, Rv2608, Rv3619 and Rv3620	TLR4	oil-in-water emulsion		51
		H1:IC31		Ag85B and ESAT-6	TLR9	cationic particles		52
		H4:IC31		Ag85B and TB10.4	TLR9	cationic particles		53
		H56:IC31		Ag85B, ESAT-6 and Rv2660c	TLR9	cationic particles		54
		M72 + AS01E		Mtb39A and Mtb32A	TLR4	liposome		40

Synthetic organic chemistry to generate effective & economical subunit vaccines

Synthetic organic chemistry offers the tools for the generation of highly pure, well defined and modifiable vaccine components that can be used to create new generations of vaccines: synthetic subunit vaccines. Currently, one challenge associated with the design of synthetic subunit vaccines against TB is the requirement for a good understanding of the processes and players involved in mycobacterial infection-induced immune responses. A thorough understanding of these processes is key to the definition of relevant antigenic targets, adjuvants and delivery systems for targeting relevant cell populations and their responses.[55,56] The rapid advances in the field of molecular biology will possibly pave the way to the definition of many new molecular targets that can be employed in the rational design of vaccines.

Molecules from the cell wall of mycobacteria can be used for the development of new vaccine components, such as antigens and adjuvants (see Figure 2). To date, the most studied antigens from *Mtb* are proteins or peptides, as evident from their widespread use in TB vaccines that are currently in clinical trials (see Table 3). However, a plethora of antigenic lipids or glycolipids are present on the cell surface of *Mycobacterium tuberculosis* and some of them have antigenic properties, being recognized by the human immune system as foreign.[57,58] An example is provided by β-mannosylphosphomycoketide (MPM), a glycolipid shown to act as epitope for the CD1c receptor (Chapter 2), a protein expressed on B cells and subsets of dendritic cells and required for subsequent presentation to T cells.[59–62]

Unfortunately, technical advances in glycobiology have been slower as compared to those that allowed the study of RNA and proteins. RNA and proteins sequences can be elucidated from the complementary DNA and their functions can be more easily understood due to the ready access to synthetic structures.[63,646566] The processing and presentation of protein-derived peptides by the MHC I and II systems has been extensively researched.[7,67] In addition to their proven antigenicity, proteins and peptides are commonly incorporated in vaccines due to the availability of scalable and efficient synthetic methods for their production, such as the use of automated solid phase synthesis for peptides[64] and recombinant methodologies or chemical ligation for proteins[68,69]. The development of automated synthetic strategies for the generation of key glycans is currently hampered by the requirements for numerous different building blocks.[70] Nevertheless, glycolipids remain interesting targets and synthetic routes may be devised and optimized that render their production feasible and scalable, especially when the natural structures are simplified and the fundamental epitopes discovered.

Independently of the chosen antigen, to induce a long-lasting strong immune response it is necessary to deliver the antigen together with relevant immunostimulatory molecules. The co-delivery of proteins or peptides with immune adjuvants, such as PAMPs, has proven to be a successful method to overcome their inherent poor immunogenicity as single entities, as well as to increase and direct the type of immune response.[17,37,71]

The subunit vaccines against *Mtb* that are currently in clinical trials all make use of TLR4 or TLR9 ligands, which have been shown to induce strong cellular immunity with Th1-polarized immune responses. One such TLR4 ligand is employed in the TB M72/AS01E vaccine formulation by Glaxo Smith Klein, notably the monophosphoryl lipid A (MPL), a synthetic glycolipid whose structure is derived from the *Salmonella minnesota* lipopolysaccharide.[39] The use of TLR9 ligands in the IC31 cationic particles developed by Intercell AG in the context of TB relies on the use of ODN1a, a synthetic oligodeoxynucleotide.[52–54] Expanding the research on novel vaccine adjuvants outside the current focus on TLR4 and TLR9 activators is a strategy that can improve the development of rationally designed vaccines.

By understanding the molecular mechanism of action for different PAMPs and by defining the required immune responses, combinations of multiple PAMPs can be employed in search for a synergistic stimulating effect. Another important parameter in the design of subunit vaccines is the type of formulation and delivery system. Examples of vaccine formulations that are approved for use in humans include oil in water emulsions and liposomal formulations.[72] These formulations ensure that antigen and adjuvants are co-delivered to the target immune cells, resulting in efficacious activation of APCs. However, they are relatively unstable and suffer from the requirement of cold chain storage, increasing costs and waste and decreasing accessibility of the vaccine to low-income countries.

These problems can be solved by the development of systems that rely on chemical bonds and not physical interactions, with chemical bonds being intrinsically more stable. Fully synthetic single molecule vaccines can be rationally designed to include antigen(s) and adjuvant(s) that are chemically linked to each other. To reach the point where this vaccine strategy can be employed, more fundamental and applied research is required. In this Thesis, efforts towards the development of fully synthetic vaccines are provided with the aim of generating knowledge and insights into this class of simple and stable vaccines against TB.

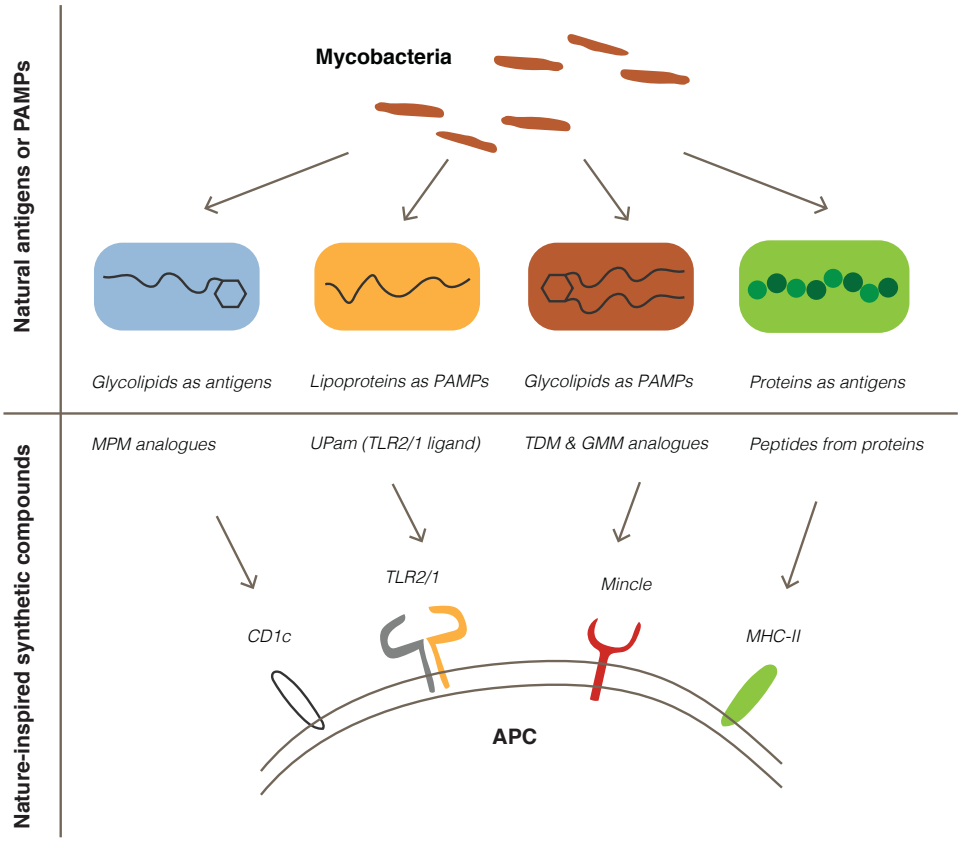

Figure 2 – Graphical depiction of rational design strategy to vaccine design in this Thesis. The rational design of vaccines begins with antigen discovery and the selection of relevant PAMPs, immunostimulatory molecules expressed by the pathogen that are recognized by PRRs, such as TLR2/1 and Mincle. TLR2/1 and Mincle get activated upon engagement with mycobacterial lipoproteins and glycolipids, respectively. Natural antigens expressed by mycobacteria and recognized by the human immune system include glycolipids and proteins/peptides. Synthetic chemistry can be employed to generate simplified/stabilized and biologically active analogues of the natural immunogenic structures. These nature-inspired synthetic compounds can be assayed for their ability to induce desired immune responses.

Thesis outline

The aim of this Thesis is to exploit synthetic chemistry to better understand processing of natural glycolipid antigens (Chapter 2), and to generate single molecule vaccines (Chapters 3 & 4), in which well-defined antigens and molecular adjuvants are combined. Co-stimulation by two synthetic PAMPs is investigated with the aim to probe synergistic immune activation (Chapter 5).

Chapter 2 applies rational antigen design to create a stabilized mannose phosphomyoketide (MPM) that stimulates human T cell responses against the natural *Mtb*-derived glycolipid. Through the development of versatile synthetic strategies three stabilized MPM analogues were generated and tested for their antigenicity and cross-reactivity with nature-identical MPM. Overall, this work has provided detailed insights into presentation of MPM by CD1c.

Chapter 3 presents the first biologically active conjugate vaccine containing a peptide covalently linked to a synthetic analogue of the *Mtb*-derived glycolipid trehalose dimycolate (TDM) showing the *in vivo* efficacy of these constructs. The design and synthetic strategy for the generation of four TDM-inspired glycolipids is described, followed by the *in vitro* characterization of the glycolipid-derived conjugates. Finally murine experiments demonstrate the ability of one of the constructs to reduce the bacterial load in the spleen, correlating to strong humoral immune responses.

In **Chapter 4** the activation of TLR2 is explored in UPam-peptide conjugates for the induction of antimycobacterial responses in the context of different peptide epitopes. Three conjugates were generated, that have been shown to induce strong activation of human dendritic cells and macrophages *in vitro*. Further *in vitro* testing suggests that antigen presentation to T cells was not affected by the conjugation to the TLR-ligand. Finally, one conjugate was used to immunize mice with preliminary data indicating generation of humoral and cellular responses.

In **Chapter 5** two synthetic ligands, that are able to interact with Mincle and TLR2 were generated and assayed *in vitro* in search of functional synergies. It was shown that at certain concentrations a synergistic effect of the two ligands could be achieved, leading to increased cytokine production by human monocyte-derived dendritic cells. T cell antigen presentation experiments were also performed, suggesting that co-stimulation could not further increase presentation.

Finally, **Chapter 6** contains a summary of the results reported in this Thesis together with a discussion on the next steps required for the further development, refinement and future implementation of synthetic methods in *Mtb* vaccine development.

References

1. Geneva: World Health Organization. Global tuberculosis report 2020. 2020.

2. Cho T, Khatchadourian C, Nguyen H, Dara Y, Jung S, Venketaraman V. A review of the BCG vaccine and other approaches toward tuberculosis eradication. Hum Vaccines Immunother. 2021 Mar 26;1–17.

3. Foster M, Hill PC, Setiabudiawan TP, Koeken VACM, Alisjahbana B, Crevel R. BCG-induced protection against *Mycobacterium tuberculosis* infection: Evidence, mechanisms, and implications for next-generation vaccines. Immunol Rev. 2021 May;301(1):122–44.

4. Kenneth M. Murphy. Janeway's Immunobiology, 8th Edition. 2012.

5. Collins AM. IgG subclass co-expression brings harmony to the quartet model of murine IgG function. Immunol Cell Biol. 2016 Nov;94(10):949–54.

6. Vidarsson G, Dekkers G, Rispens T. IgG Subclasses and Allotypes: From Structure to Effector Functions. Front Immunol. 2014 Oct 20;5.

7. Neefjes J, Jongsma MLM, Paul P, Bakke O. Towards a systems understanding of MHC class I and MHC class II antigen presentation. Nat Rev Immunol. 2011 Dec;11(12):823–36.

8. Williams A, Peh CA, Elliott T. The cell biology of MHC class I antigen presentation: Williams et al : MHC class I antigen presentation. Tissue Antigens. 2002 Jan;59(1):3–17.

9. Roche PA, Furuta K. The ins and outs of MHC class II-mediated antigen processing and presentation. Nat Rev Immunol. 2015 Apr;15(4):203–16.

10. Brigl M, Brenner MB. CD1: Antigen Presentation and T Cell Function. Annu Rev Immunol. 2004 Apr;22(1):817–90.

11. Lyadova IV, Panteleev AV. Th1 and Th17 Cells in Tuberculosis: Protection, Pathology, and Biomarkers. Mediators Inflamm. 2015;2015:1–13.

12. Dalton D, Pitts-Meek S, Keshav S, Figari I, Bradley A, Stewart T. Multiple defects of immune cell function in mice with disrupted interferon-gamma genes. Science. 1993 Mar 19;259(5102):1739–42.

13. Kaufmann SHE. Protection against tuberculosis: cytokines, T cells, and macrophages. Ann Rheum Dis. 2002 Nov;61 Suppl 2:ii54-58.

14. Qiu L, Huang D, Chen CY, Wang R, Shen L, Shen Y, et al. Severe Tuberculosis Induces Unbalanced Up-Regulation of Gene Networks and Overexpression of *IL-22, MIP-1α, CCL27, IP-10, CCR4, CCR5, CXCR3, PD1, PDL2, IL-3, IFN-β, TIM1,* and *TLR2* but Low Antigen-Specific Cellular Responses. J Infect Dis. 2008 Nov 15;198(10):1514–9.

15. Segueni N, Tritto E, Bourigault M-L, Rose S, Erard F, Le Bert M, et al. Controlled *Mycobacterium tuberculosis* infection in mice under treatment with anti-IL-17A or IL-17F antibodies, in contrast to TNFα neutralization. Sci Rep. 2016 Dec;6(1):36923.

16. Ashenafi S, Aderaye G, Bekele A, Zewdie M, Aseffa G, Hoang ATN, et al. Progression of clinical tuberculosis is associated with a Th2 immune response signature in combination with elevated levels of SOCS3. Clin Immunol. 2014 Apr;151(2):84–99.

17. Guy B. The perfect mix: recent progress in adjuvant research. Nat Rev Microbiol. 2007 Jul;5(7):396–7.

18. Romero-Adrian TB. Role of cytokines and other factors involved in the *Mycobacterium tuberculosis* infection. World J Immunol. 2015;5(1):16.

19. Hossain MdM, Norazmi M-N. Pattern Recognition Receptors and Cytokines in *Mycobacterium tuberculosis* Infection—The Double-Edged Sword? BioMed Res Int. 2013;2013:1–18.

20. Tran V, Liu J, Behr MA. BCG Vaccines. In: Molecular Genetics of Mycobacteria. Washington, DC, USA: ASM Press; 2015. p. 49–59.

21. Fine PEM. Variation in protection by BCG: implications of and for heterologous immunity. The Lancet. 1995 Nov;346(8986):1339–45.

22. Whitlow E, Mustafa AS, Hanif SNM. An Overview of the Development of New Vaccines for Tuberculosis. Vaccines. 2020 Oct 5;8(4):586.

23. Dockrell HM, Smith SG. What Have We Learnt about BCG Vaccination in the Last 20 Years? Front Immunol. 2017 Sep 13;8:1134.

24. Ahmed A, Rakshit S, Adiga V, Dias M, Dwarkanath P, D'Souza G, et al. A century of BCG: Impact on tuberculosis control and beyond. Immunol Rev. 2021 May;301(1):98–121.

25. Vekemans J, Amedei A, Ota MO, D'Elios MM, Goetghebuer T, Ismaili J, et al. Neonatal bacillus Calmette-Guérin vaccination induces adult-like IFN-gamma production by CD4+ T lymphocytes. Eur J Immunol. 2001 May;31(5):1531–5.

26. Marchant A, Goetghebuer T, Ota MO, Wolfe I, Ceesay SJ, De Groote D, et al. Newborns develop a Th1-type immune response to *Mycobacterium bovis* bacillus Calmette-Guérin vaccination. J Immunol Baltim Md 1950. 1999 Aug 15;163(4):2249–55.

27. Fletcher HA, Snowden MA, Landry B, Rida W, Satti I, Harris SA, et al. T-cell activation is an immune correlate of risk in BCG vaccinated infants. Nat Commun. 2016 Apr 12;7:11290.

28. Andersen P, Woodworth JS. Tuberculosis vaccines – rethinking the current paradigm. Trends Immunol. 2014 Aug;35(8):387–95.

29. Achkar JM, Casadevall A. Antibody-Mediated Immunity against Tuberculosis: Implications for Vaccine Development. Cell Host Microbe. 2013 Mar;13(3):250–62.

30. Levitz SM, Golenbock DT. Beyond Empiricism: Informing Vaccine Development through Innate Immunity Research. Cell. 2012 Mar;148(6):1284–92.

31. Tameris MD, Hatherill M, Landry BS, Scriba TJ, Snowden MA, Lockhart S, et al. Safety and efficacy of MVA85A, a new tuberculosis vaccine, in infants previously vaccinated with BCG: a randomised, placebo-controlled phase 2b trial. The Lancet. 2013 Mar;381(9871):1021–8.

32. Ndiaye BP, Thienemann F, Ota M, Landry BS, Camara M, Dièye S, et al. Safety, immunogenicity, and efficacy of the candidate tuberculosis vaccine MVA85A in healthy adults infected with HIV-1: a randomised, placebo-controlled, phase 2 trial. Lancet Respir Med. 2015 Mar;3(3):190–200.

33. Dougan G, Hormaeche C. How bacteria and their products provide clues to vaccine and adjuvant development. Vaccine. 2006 Apr;24:S13–9.

34. Vetter V, Denizer G, Friedland LR, Krishnan J, Shapiro M. Understanding modern-day vaccines: what you need to know. Ann Med. 2018 Feb 17;50(2):110–20.

35. Liniger M, Zuniga A, Naim HY. Use of viral vectors for the development of vaccines. Expert Rev Vaccines. 2007 Apr;6(2):255–66.

36. Tatsis N, Ertl HCJ. Adenoviruses as vaccine vectors. Mol Ther. 2004 Oct;10(4):616–29.

37. Moyle PM, Toth I. Modern Subunit Vaccines: Development, Components, and Research Opportunities. ChemMedChem. 2013 Mar;8(3):360–76.

38. Bobbala S, Hook S. Is There an Optimal Formulation and Delivery Strategy for Subunit Vaccines? Pharm Res. 2016 Sep;33(9):2078–97.

39. Van Der Meeren O, Hatherill M, Nduba V, Wilkinson RJ, Muyoyeta M, Van Brakel E, et al. Phase 2b Controlled Trial of M72/AS01E Vaccine to Prevent Tuberculosis. N Engl J Med. 2018 Oct 25;379(17):1621–34.

40. Tait DR, Hatherill M, Van Der Meeren O, Ginsberg AM, Van Brakel E, Salaun B, et al. Final Analysis of a Trial of M72/AS01E Vaccine to Prevent Tuberculosis. N Engl J Med. 2019 Dec 19;381(25):2429–39.

41. Clark S, Lanni F, Marinova D, Rayner E, Martin C, Williams A. Revaccination of Guinea Pigs With the Live Attenuated *Mycobacterium tuberculosis* Vaccine MTBVAC Improves BCG's Protection Against Tuberculosis. J Infect Dis. 2017 Sep 1;216(5):525–33.

42. Vilaplana C, Montané E, Pinto S, Barriocanal AM, Domenech G, Torres F, et al. Double-blind, randomized, placebo-controlled Phase I Clinical Trial of the therapeutical antituberculous vaccine RUTI®. Vaccine. 2010 Jan;28(4):1106–16.

43. von Reyn CF, Lahey T, Arbeit RD, Landry B, Kailani L, Adams LV, et al. Safety and immunogenicity of an inactivated whole cell tuberculosis vaccine booster in adults primed with BCG: A randomized, controlled trial of DAR-901. PLOS ONE. 2017 May 12;12(5):e0175215.

44. Nieuwenhuizen NE, Kulkarni PS, Shaligram U, Cotton MF, Rentsch CA, Eisele B, et al. The Recombinant Bacille Calmette–Guérin Vaccine VPM1002: Ready for Clinical Efficacy Testing. Front Immunol. 2017 Sep 19;8:1147.

45. Sharma SK, Katoch K, Sarin R, Balambal R, Kumar Jain N, Patel N, et al. Efficacy and Safety of *Mycobacterium indicus pranii* as an adjunct therapy in Category II pulmonary tuberculosis in a randomized trial. Sci Rep. 2017 Dec;7(1):3354.

46. Yang X-Y, Chen Q-F, Li Y-P, Wu S-M. *Mycobacterium vaccae* as Adjuvant Therapy to Anti-Tuberculosis Chemotherapy in Never-Treated Tuberculosis Patients: A Meta-Analysis. PLoS ONE. 2011 Sep 6;6(9):e23826.

47. Zhu F-C, Hou L-H, Li J-X, Wu S-P, Liu P, Zhang G-R, et al. Safety and immunogenicity of a novel recombinant adenovirus type-5 vector-based Ebola vaccine in healthy adults in China: preliminary report of a randomised, double-blind, placebo-controlled, phase 1 trial. The Lancet. 2015 Jun;385(9984):2272–9.

48. Wilkie M, Satti I, Minhinnick A, Harris S, Riste M, Ramon RL, et al. A phase I trial evaluating the safety and immunogenicity of a candidate tuberculosis vaccination regimen, ChAdOx1 85A prime – MVA85A boost in healthy UK adults. Vaccine. 2020 Jan;38(4):779–89.

49. Lu J, Chen B, Wang G, Fu L, Shen X, Su C, et al. Recombinant tuberculosis vaccine AEC/BC02 induces antigen-specific cellular responses in mice and protects guinea pigs in a model of latent infection. J Microbiol Immunol Infect. 2015 Dec;48(6):597–603.

50. Vasina DV, Kleymenov DA, Manuylov VA, Mazunina EP, Koptev EY, Tukhovskaya EA, et al. First-In-Human Trials of GamTBvac, a Recombinant Subunit Tuberculosis Vaccine Candidate: Safety and Immunogenicity Assessment. Vaccines. 2019 Nov 1;7(4):166.

51. Penn-Nicholson A, Tameris M, Smit E, Day TA, Musvosvi M, Jayashankar L, et al. Safety and immunogenicity of the novel tuberculosis vaccine ID93 + GLA-SE in BCG-vaccinated healthy adults in South Africa: a randomised, double-blind, placebo-controlled phase 1 trial. Lancet Respir Med. 2018 Apr;6(4):287–98.

52. Mearns H, Geldenhuys HD, Kagina BM, Musvosvi M, Little F, Ratangee F, et al. H1:IC31 vaccination is safe and induces long-lived TNF-α+IL-2+CD4 T cell responses in M. tuberculosis infected and uninfected adolescents: A randomized trial. Vaccine. 2017 Jan;35(1):132–41.

53. Nemes E, Geldenhuys H, Rozot V, Rutkowski KT, Ratangee F, Bilek N, et al. Prevention of *M. tuberculosis* Infection with H4:IC31 Vaccine or BCG Revaccination. N Engl J Med. 2018 Jul 12;379(2):138–49.

54. Luabeya AKK, Kagina BMN, Tameris MD, Geldenhuys H, Hoff ST, Shi Z, et al. First-in-human trial of the post-exposure tuberculosis vaccine H56:IC31 in *Mycobacterium tuberculosis* infected and non-infected healthy adults. Vaccine. 2015 Aug;33(33):4130–40.

55. Stewart E, Triccas JA, Petrovsky N. Adjuvant Strategies for More Effective Tuberculosis Vaccine Immunity. Microorganisms. 2019 Aug 12;7(8):255.

56. Duthie MS, Windish HP, Fox CB, Reed SG. Use of defined TLR ligands as adjuvants within human vaccines. Immunol Rev. 2011 Jan;239(1):178–96.

57. Jackson M. The Mycobacterial Cell Envelope--Lipids. Cold Spring Harb Perspect Med. 2014 Oct 1;4(10):a021105–a021105.

58. Mendelson M, Walters S, Smith I, Kaplan G. Strain-specific mycobacterial lipids and the stimulation of protective immunity to tuberculosis. Tuberculosis. 2005 Sep;85(5–6):407–13.

59. Moody DB, Ulrichs T, Mühlecker W, Young DC, Gurcha SS, Grant E, et al. CD1c-mediated T-cell recognition of isoprenoid glycolipids in *Mycobacterium tuberculosis* infection. Nature. 2000 Apr;404(6780):884–8.

60. de Jong A, Arce EC, Cheng T-Y, van Summeren RP, Feringa BL, Dudkin V, et al. CD1c Presentation of Synthetic Glycolipid Antigens with Foreign Alkyl Branching Motifs. Chem Biol. 2007 Nov;14(11):1232–42.

61. Ly D, Kasmar AG, Cheng T-Y, de Jong A, Huang S, Roy S, et al. CD1c tetramers detect ex vivo T cell responses to processed phosphomycoketide antigens. J Exp Med. 2013 Apr 8;210(4):729–41.

62. Roy S, Ly D, Li N-S, Altman JD, Piccirilli JA, Moody DB, et al. Molecular basis of mycobacterial lipid antigen presentation by CD1c and its recognition by T cells. Proc Natl Acad Sci. 2014 Oct 28;111(43):E4648–57.

63. Damha MJ, Zabarylo S. Automated solid-phase synthesis of branched oligonucleotides. Tetrahedron Lett. 1989 Jan;30(46):6295–8.

64. Albericio F. Developments in peptide and amide synthesis. Curr Opin Chem Biol. 2004 Jun;8(3):211–21.

65. Varki A. Biological roles of glycans. Glycobiology. 2017 Jan;27(1):3–49.

66. Ferreira SS, Passos CP, Madureira P, Vilanova M, Coimbra MA. Structure–function relationships of immunostimulatory polysaccharides: A review. Carbohydr Polym. 2015 Nov;132:378–96.

67. Mantegazza AR, Magalhaes JG, Amigorena S, Marks MS. Presentation of Phagocytosed Antigens by MHC Class I and II: Presentation of Phagocytosed Antigens. Traffic. 2013 Feb;14(2):135–52.

68. Cox MMJ. Recombinant protein vaccines produced in insect cells. Vaccine. 2012 Feb;30(10):1759–66.

69. Kent SBH. Total chemical synthesis of proteins. Chem Soc Rev. 2009;38(2):338–51.

70. Bojar D, Powers RK, Camacho DM, Collins JJ. SweetOrigins: Extracting Evolutionary Information from Glycans. Bioinformatics; 2020 Apr.

71. Black M, Trent A, Tirrell M, Olive C. Advances in the design and delivery of peptide subunit vaccines with a focus on Toll-like receptor agonists. Expert Rev Vaccines. 2010 Feb;9(2):157–73.

72. Baldwin SL, Bertholet S, Reese VA, Ching LK, Reed SG, Coler RN. The Importance of Adjuvant Formulation in the Development of a Tuberculosis Vaccine. J Immunol. 2012 Mar 1;188(5):2189–97.

2

Design and synthesis of stabilized mannosyl phosphomycoketide analogues

Laura Marino[4,*], Josephine F. Reijneveld[1,2,3,*], Thinh-Phat Cao[5,*], Tan-Yun Cheng[1], Dennis Dam[4], Adam Shahine[5,6], Martin D. Witte[3], Dmitri Filippov[4], Sara Suliman[1], Gijsbert A. van der Marel[4], D. Branch Moody[1], Adriaan J. Minnaard[3], Jamie Rossjohn[5,6,7], Jeroen D.C. Codée[4], Ildiko Van Rhijn[1,2*]

[1] Division of Rheumatology, Inflammation, and Immunity, Brigham and Women's Hospital and Harvard Medical School, Boston, MA, United States

[2] Department of Infectious Diseases and Immunology, Faculty of Veterinary Medicine, Utrecht University, Utrecht, Netherlands

[3] Stratingh Institute for Chemistry, University of Groningen, Groningen, The Netherlands

[4] Department of Bio-organic Synthesis, Faculty of Science, Leiden Institute of Chemistry, Leiden University, Leiden, The Netherlands.

[5] Infection and Immunity Program and Department of Biochemistry and Molecular Biology, Biomedicine Discovery Institute, Monash University, Clayton, Victoria, Australia.

[6] Australian Research Council Centre of Excellence in Advanced Molecular Imaging, Monash University, Clayton, Victoria, Australia

[7] Institute of Infection and Immunity, Cardiff University, School of Medicine, Heath Park, Cardiff, United Kingdom

* These authors contributed equally: Josephine F. Reijneveld, Laura Marino, Thinh-Phat Cao.

2

Abstract

Mannose phosphomycoketide (MPM) is a glycolipid expressed on the cell wall of *Mycobacterium tuberculosis*, which has been shown to be presented by the CD1c protein to human interferon-γ (IFN-γ) producing T-cells. Although the ability of T-cells to respond to peptides presented by the major histocompatibility complex (MHC) protein is more widely known than their ability to respond to lipids presented by MHC class I-like CD1 proteins, the CD1c non-polymorphic nature makes it a very interesting target for the development of vaccines against tuberculosis (TB). Currently, two structurally related mycoketides have been shown to be antigenic to T-cells via CD1c: the MPM glycolipid and the phosphomycoketide (PM) lipid. Processing of MPM to PM by antigen-presenting cells like dendritic cells can reduce the availability of MPM during *in vitro* and *in vivo* experiments. In order to improve the stability of the glycosidic linkage between mannose and the phosphomycoketide moiety, which is the most likely point of degradation of MPM to PM, three synthetic analogues of MPM were designed and synthesized. These analogues, comprising a carba-mannose, a methyl *C*-glycoside and a difluoro-*C*-glycoside, were used to stimulate human monocyte-derived dendritic cells in the presence of either T-cells, that specifically recognize MPM (the CD8-1 T-cell) or PM (the DN6 cell). The difluoro-*C*-glycoside was shown to induce activation of the CD8-1 but not the DN6 T-cell line, indicating that this analogue did not give rise to PM in an antigen presentation assay nor did it cross-react with the DN6 T-cell receptor. Because of its desirable characteristics, the difluoro-*C*-mannoside was used to expand antigen-specific T-cells, which were then shown to cross-react to the natural MPM. IFN-γ dose-response curves obtained from the novel T-cell clone indicated that the stabilized difluoro-*C*-mannoside was more antigenic than MPM.

Introduction

Mannose phosphomycoketide (MPM, See Figure 1a), a naturally occurring glycolipid expressed on the cell wall of *Mycobacterium tuberculosis* (*Mtb*), is a known antigen presented by dendritic cells (DCs) to T-cells via cluster of differentiation 1c (CD1c).[1–4] Given its non-polymorphic nature and its ability to present *Mtb*-derived glycolipids to T-cells, CD1c represents an interesting target to exploit for development of vaccines against tuberculosis (TB).[5] CD1c is a protein expressed with high density on subsets of human dendritic cells and B cells. It resembles the major histocompatibility complex I (MHC-I) in its ability to present foreign and self-molecules to T-cells.[6–9] Unlike the MHC-I, which forms complexes with peptides, CD1c presents foreign and self-lipids to T-cells.[10] As shown in Figure 1, different classes of lipids have been identified as ligands for this receptor, including cholesteryl esters (Figure 1c) and phosphatidylcholines (Figure 1d),[1,11–13] in addition to phosphomycoketides (Figure 1a-b).[1,2] Although many lipids and glycolipids are presented by multiple CD1 receptors, phosphomycoketides are not recognized by the other members of the CD1 family. T-cells reactive to CD1c in complex with phosphomycoketides from *Mtb* are thought to have important effector functions, given their ability to produce IFN-γ, a cytokine involved in killing of intracellular mycobacteria through stimulation of endosomal maturation.[14–16]

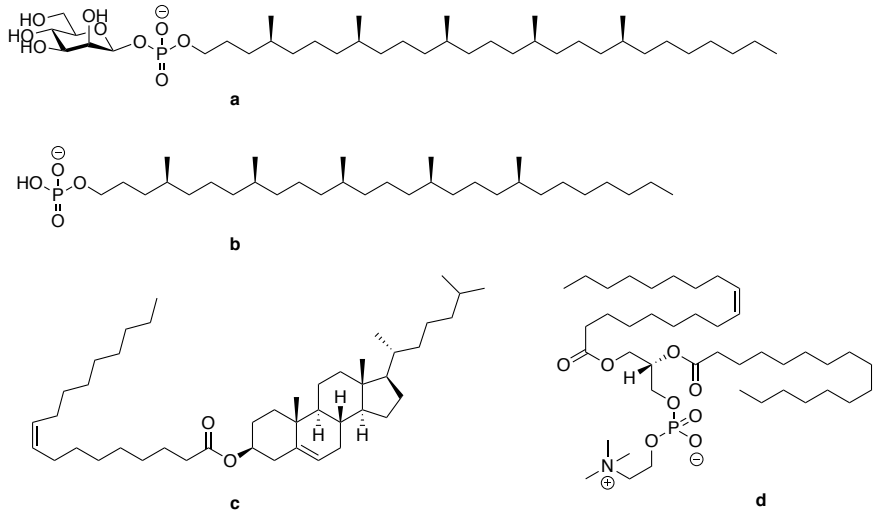

Figure 1 – Chemical structures of lipids that have been shown to interact with the CD1c receptor. a) β-D-mannosyl phosphomycoketide; b); Phosphomycoketide; c) cholesteryl esters; d) phosphatidylcholines (here PC(16:0/18:1) is shown).

The first example of CD1c presentation of MPM to T-cells dates back to 2000, when Moody and co-workers used a DC-mediated antigen presentation assay to prove that this glycolipid was presented to the CD1c restricted T-cell clone, CD8-1.[1] Thirteen years later, Ly *et al.* were able to show that another CD1c restricted T-cell line, DN6, was responding to dendritic cells stimulated by two lipids: MPM and phosphomycoketide (Figure 1a-b) (PM), a phospholipid differing from MPM only in the absence of the carbohydrate moiety.[2] Interestingly, DN6 T-cells did not respond to plate bound CD1c in the presence of MPM, but only in the presence of PM. This result led to the hypothesis that the mannose group is hydrolyzed by antigen-presenting cells via mannosidase enzymes or in the acidic endosomal compartment, yielding PM as a neo-epitope. The crystal structure later revealed PM to be the real epitope for DN6 T-cells.[4]

MPM has been suggested as a promising antigen for the development of anti-TB vaccines. However, natural processing of MPM to PM reduces the levels of the antigen, which is present in the mycobacterial cell wall in low quantities. To further probe MPM as an antigen, stabilized analogues of the glycolipid, which are not (as readily) transformed into PM, could be attractive tools. To this end, this Chapter reports the design and synthesis of three novel MPM analogues. These synthetic analogues, whose structures are shown in Figure 2, comprise a carba-mannose, where the ring oxygen is replaced by a methylene group (compound **1**), and two *C*-mannosides, where the anomeric oxygen is replaced by a methylene group or a difluoro methylene moiety (compounds **2** and **3**, respectively). These modifications render the molecules (more) stable towards chemical and enzymatic hydrolysis making these MPM-analogues ideal candidates to explore their antigenic potential in the context of TB vaccination and further understand the immune function of CD1c receptor.

The stability of the three analogues towards mannosidase enzymes can be explained on the basis of the mechanism of action of the glycosidases. During glycosidase-induced hydrolysis an oxocarbenium ion forms,[17] whose formation is not possible once the carbohydrate hemiacetal is replaced by the ether linkage in the carba- and *C*-glycosides here described. It is not possible to exclude occurrence of enzymatic hydrolysis induced by phosphatases during processing by antigen-presentation dendritic cells. However, in analogues **2** and **3** this would lead to formation of lipid **4** (Figure 2), which cannot be bound to the CD1c receptor. One challenge associated to the use of glycomimetics is related to the changes in conformation of the carbohydrate ring. Altering the structure of the mannose moiety of MPM to generate the more stable glycomimetic can result in conformational changes of the key exo-cyclic phosphate substituent. The exo-anomeric effect that determines the orientation of the exo-cyclic substituent is missing in all three stabilized analogues. The overall dipole of the molecules will be different as well as hydrogen bonding and accepting properties. Finally, the pKa of the phosphate in the analogies will differ

from the parent compound. These effects should be minimized in *C*-mannoside **3**, since the difluoro methylene has most similar electronic properties compared to those of the anomeric oxygen, present in the naturally occurring MPM.[18,19]

Results and discussion

Previously, van Summeren *et al.* have shown the importance of the stereochemistry of the lipid moiety in phosphomycoketides for T-cell response with the first stereoselective total synthesis of a β-D-mannosyl phosphomycoketide.[20] The same lipid moiety, compound **4** (Figure 2), was used to generate the three stabilized MPM-analogues described in the present work.

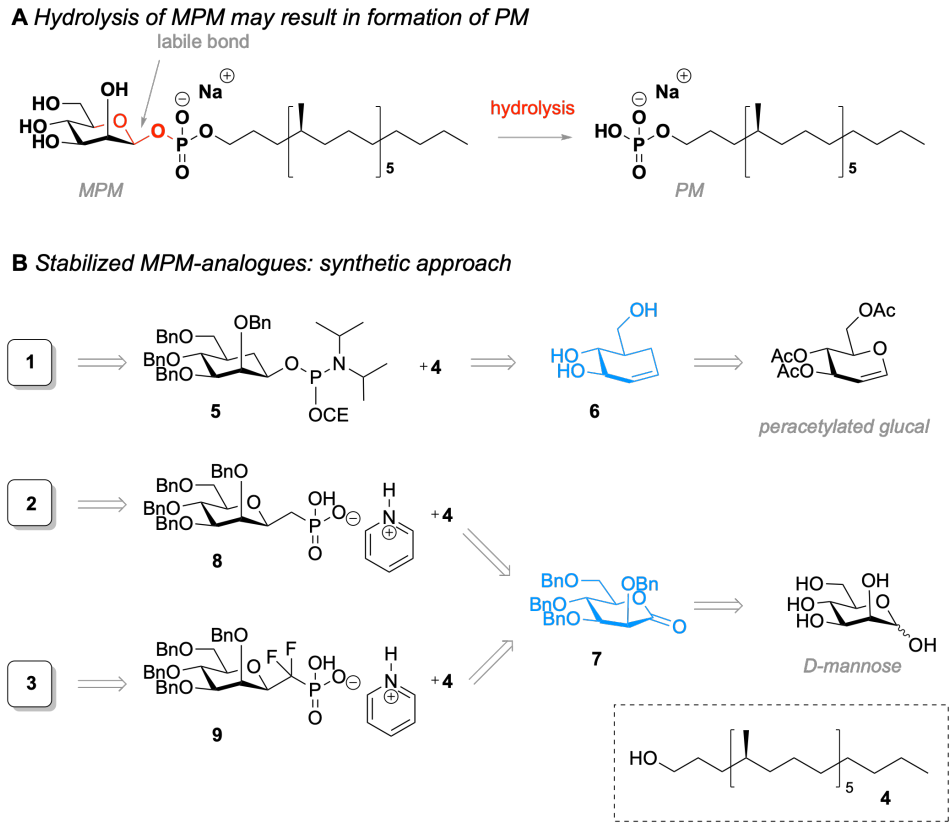

Figure 2 – (A) Chemical structures of β-D-mannosyl phosphomycoketide (MPM) and its synthetic analogues: carba-mannose **1** (MPM-1), and *C*-mannosides **2** (MPM-2) and **3** (MPM-3). Structural modifications, responsible for improved stability towards chemical and enzymatic hydrolysis, are highlighted in green. **(B)** Retrosynthetic approach to generation of carba-mannose (compound **1**) and two *C*-mannosides (compounds **2** and **3**), glycomimetics of MPM. Key intermediates, pseudo-glucal **6** and manno-lactone **6**, are highlighted in blue.

As represented in the retrosynthetic scheme of Figure 2, to generate the carba-analogue **1**, a phosphoramidite chemistry approach was chosen in coupling lipid **4** to β-carba-mannopyranoside **5**. Multiple synthetic strategies have been devised to generate carba-sugars, including those based on carbohydrate precursors as the prime source of chirality.[21–23] A route towards carba mannose **5** originating from pseudo-glucal **6** is shown in this chapter. This pseudo-glucal can be readily obtained from D-glucal. The two *C*-glycosides **2** and **3** can be obtained from D-mannose via lactone intermediate **7**, which can be converted to phosphonates **8** and **9**. Coupling between phosphonate **8** or **9** and lipid **4** then yields the desired analogues **2** and **3**. Importantly, chemical hydrolysis of the two *C*-mannopyranoside analogues **2** and **3** can never lead to formation of PM, as lipid **4** would be the hydrolysis product.

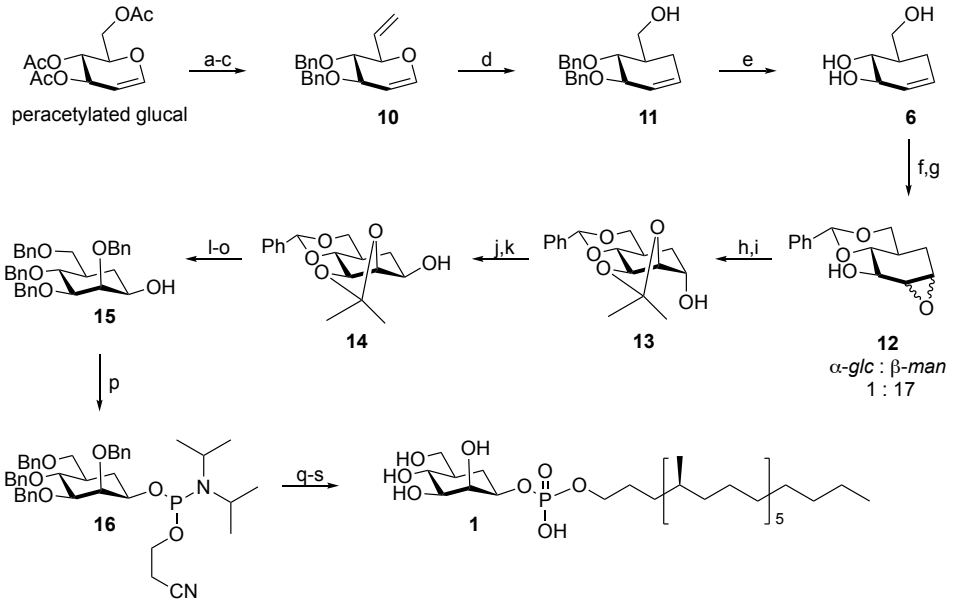

Figure 3 - Synthetic scheme for the generation of carba-mannose (compound 1). a) i. K_2CO_3, MeOH, ii. TDSCl, imidazole, DMF, -20°C, 82%, b) i. BnBr, NaH, TBAI, THF, ii. TBAF, THF, 69%, c) i. IBX, EtOAc, reflux, ii. PPh_3CH_3I, KHMDS, THF, -78°C to RT, 88%, d) i. *o*-dichlorobenzene, 230°C, ii. $NaBH_4$, EtOH/THF, 94%, e) Li-naphthalenide, THF, -20°C, 81%, f) $PhCH(OMe)_2$, *p*TsOH, DMF, 60°C, 67%, g) *m*-CPBA, PBS buffer, DCM, α 5%, β 86%, h) KOH, dioxane, H_2O, 90°C, quant., i) 2,2-dimethoxypropane, pTsOH, DMF, 90%, j) IBX, EtOAc, reflux, 82%, k) $NaBH_4$, DCM/MeOH, 0°C, 77%, l) NapBr, NaH, TBAI, THF/DMF, 88%, m) pTsOH, MeOH, 92%, n) BnBr, NaH, TBAI, DMF, 86%, o) DDQ, DCM/H_2O, 73%, p) (CEO)PCl(N-*i*Pr_2), DIPEA, DCM, 68%, q) i. compound **4,** DCI, CH_3CN, ii. CSO, CH_3CN, 70%, r) Et_3N, CH_3CN, 74%, s) Pd/C, H_2, $CHCl_3$:MeOH (1:1 v/v), 47%.

The synthesis of MPM-1 is depicted in Figure 3. First, pseudo-glucal **11** was synthesized from the commercially available peracetylated glucal, following the steps of Gao *et al.* with a key Claisen rearrangement reaction on substrate **10** to replace the ring oxygen atom with a methylene group.[24] The removal of the benzyl groups from compound **11** proved challenging, as most oxidative and reductive methods are not compatible with the presence of alkenes. Attempts of using the strong Lewis acids $FeCl_3$, BBr_3 and BCl_3 were unsuccessful (Table 1). Deprotection using $TiCl_4$, however, was successful as confirmed by NMR analysis. The downside of this Lewis acid was the formation of an unknown side-product, which proved difficult to remove by silica gel chromatography. Finally, a modified Birch-type reduction using lithium naphthalenide (LN) yielded compound **6** with reproducible results, independent on the reaction scale.

Table 1 – Optimization reaction conditions for debenzylation of substrate 11.

entry #	mmol 11	reagent (eq)	solvent	temperature (°C)	time (h)	yield (%)
1	0.39	$TiCl_4$ (2.5)	DCM	-78	1	N/A*
2	0.40	$TiCl_4$ (4.5)	DCM	-78	1.5	53
3	0.33	BCl_3 (20)	DCM	-78	16	N/A
4	0.33	BBr_3 (8.5)	DCM	-78	5	N/A
5	0.46	$FeCl_3$ (7)	DCM	0	2	N/A
6	0.42	LN (1.1)	THF	-78 to 0	16	18
7	0.32	LN (5)	THF	-78 to -20	1	30
8	0.30	LN (7.5)	THF	-78 to -20	16	79
9	27.8	LN (7.5)	THF	78 to -20	46	81
***50% monobenzylated product found**						

Pseudo-glucal **6** was then converted to α-carba-mannopyranoside **13** via epoxidation of the cyclic olefin, followed by opening of the epoxide in basic conditions and subsequent protection. Noteworthy is the stereo-convergence of epoxide formation and opening events, where both the "α-gluco" and "β-manno" configured epoxides (formed in a 1:17 ratio, isolated and reacted separately) lead to formation of the same α-carba-mannopyranoside. The opening of the epoxides follows a reaction trajectory that is in accordance with the Fürst-Plattner rule. Inversion of the pseudo-anomeric alcohol using an oxidation/reduction sequence, yielded the desired β-carba-mannopyranoside configuration of compound **14**. As expected, the intermediate ketone was reduced in an axial fashion by $NaBH_4$ and the small amount of the axial alcohol was readily removed by column chromatography. The free hydroxyl group of compound **14** was protected with a naphthyl ether (Nap)

before acidic removal of the two acetal protecting groups. Benzyl groups were introduced on the freed hydroxyls after which the Nap group was cleaved oxidatively with 1 equivalent of DDQ yielding intermediate **15**. Formation of a side product due to oxidative removal of benzyl protecting group from the C-3 position (mannose numbering) was observed when using DDQ in excess, as confirmed by NMR analysis. Compound **15** was then converted to the phosphoramidite **16** by treatment with 2-cyanoethyl *N,N*-diisopropylchlorophosphoramidite under influence of *N,N*-diisopropylethylamine (DIPEA). Intermediate **16** was coupled to lipid **4** using DCI as activator, followed by oxidation of the intermediate phosphite with *(1S)*(+)-(10-camphorsulfonyl)oxaziridine (CSO) to give the corresponding phosphotriester. After removal of cyanoethyl protecting group and dehydrogenation MPM-analogue **1** was isolated in an overall yield of 1.4% over 19 steps starting from D-glucal.

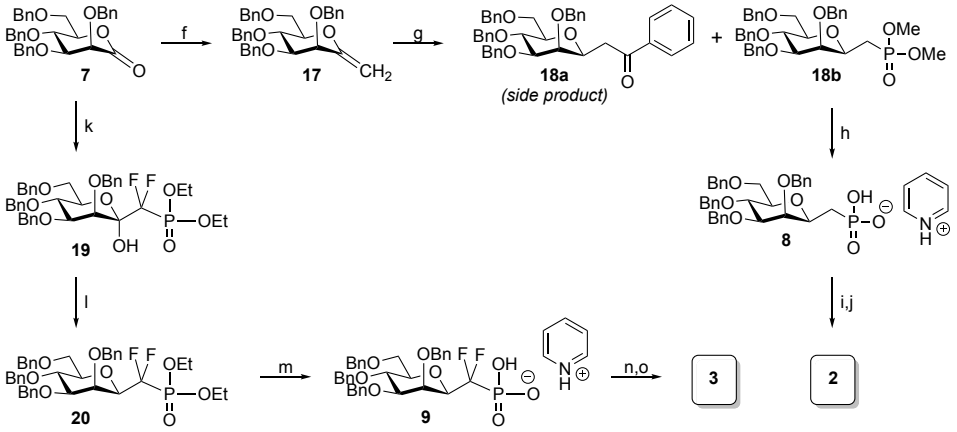

Figure 4 - Synthetic scheme for the generation of the two C-mannosides (compounds 2 and 3). a) Cp_2TiMe_2, toluene, 60°C, 79%, b) $(MeO)_2P(=O)H$, DPAP, neat, hν = 375 nm, y **18a**: 14%, y **18b**: 59%, c) TMSBr, pyridine, CH_3CN, 85%, d) compound **4**, *i*Pr_3PhSO_2Cl, pyridine, 50°C, 50%, e) Pd/C, H_2, THF/H_2O (1:1, v/v), 80%, f) LDA, $(EtO)_2P(=O)CHF_2$, THF, 98%, g) i. $MeO_2CC(=O)Cl$, DCM, ii. AIBN, Bu_3SnH, toluene, 30%, h) TMSBr, pyridine, CH_3CN, quant., i) compound **4**, *i*Pr_3PhSO_2Cl, toluene:DMF:pyridine (1.25:1:0.5, v/v/v), 50°C, 64%, j) Pd/C, H_2, THF:H_2O (2:1, v/v), 82%.

Next, the synthesis of *C*-mannosides **2** and **3** was undertaken. *C*-Glycosides are commonly synthesized by generating the anomeric C-C bond starting from carbohydrate substrates, such as glycosyl halides, sugar lactols or lactones, 1,2-anhydrosugars, thioglycosides/sulfoxides/sulfones or glycosyl imidates/phosphonates.[25] For the synthesis of the *C*-mannoside analogues **2** and **3**,

two separate reaction routes were developed, both starting from manno-lactone **7**, as shown in Figure 4. The approach chosen for the generation of compound **2** consisted of the conversion of the lactone into exo-glycal **17** using the Petasis reagent, followed by radical hydrophosphonylation to obtain the desired β-stereoisomer. This less common approach was inspired by the work of Dondoni *et al.*, where a similar hydrophosphonylation reaction was performed on peracetylated exo-glucal.[26] A plausible reaction mechanism, explaining the observed stereochemistry is shown in Figure 5. According to this mechanism, a phosphonate radical forms after hydrogen abstraction by radical fragments of the DPAP initiator. The phosphonate radical, in turn, adds to the exo-cyclic olefin, resulting in the generation of an anomeric radical. Abstraction of a hydrogen from dimethyl-H-phosphonate by this radical preferentially occurs from the more accessible bottom face, leading to the formation of the sterically more favorable equatorial *C*-phosphonate.

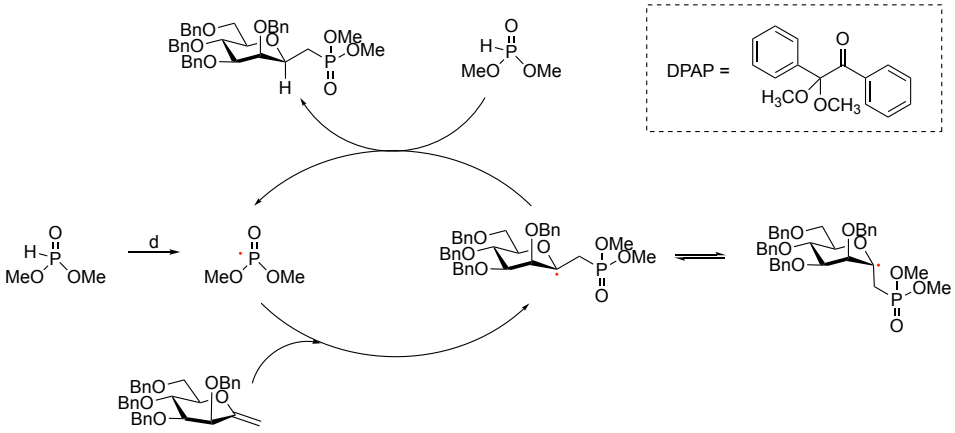

Figure 5 – Proposed reaction mechanism to explain stereochemical outcome of hydrophosphonylation reaction.

The reaction yield for the hydrophosphonylation was 43% when this reaction was performed under unfocused sunlight and it increased to 59% when using focused UV light (375 nm). Side-product **18a** formed by the undesired reaction of compound **17** with the radical initiator, was isolated in 14% yield and identified via H-NMR.[1] The

[1] Nucleophilic addition of methyl diethyl phosphonate carbanion to manno-lactone was considered as an alternative method to hydrophosphonylation, but not pursued due to the additional reaction steps and formation of an exo-cyclic olefin upon dehydroxylation of the newly formed lactol.

β-mannosyl phosphonate **18b** was demethylated to obtain free phosphonic acid **8** using TMSBr in the presence of pyridine to quench the forming acidic species.[2] The stereochemistry of the *C*-phosphonate was confirmed at this stage using Nuclear Overhauser Enhancement Spectroscopy (NOESY) experiments. The correlation between the H-1 and H-5 protons, and between H-1 and H-3, as shown in Figure 6, confirms the formation of the desired β-stereoisomer. Phosphonate **8** was finally coupled to lipid **4** by activation of the acid using 2,4,6-tri-*iso*-propylbenzenesulfonyl chloride, after which the protected glycolipid was deprotected via hydrogenation, yielding the desired MPM analogue **2** in an overall yield of 6.7% over 10 steps starting from D-mannose.

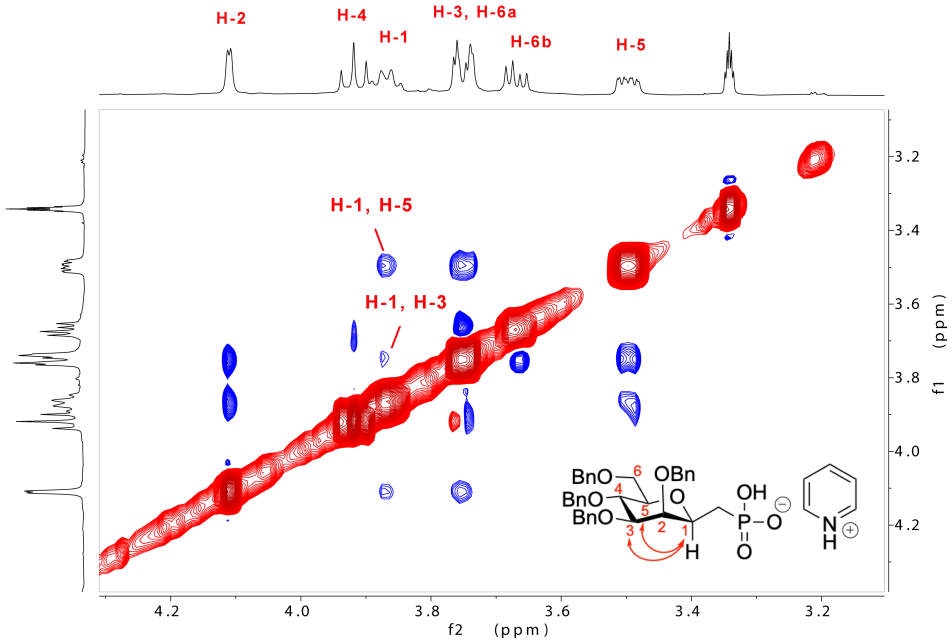

Figure 6 – NOESY spectrum of compound 8. The key NOE interaction can be found between H-1 and H-5, H-1 and H-3.

Although several synthetic strategies have been devised for the synthesis of anomeric phosphates/phosphonates,[27,28] as well as for the synthesis of fluorinated phosphonates,[29] the literature describing synthetic approaches to the generation of anomeric difluoro-*C*-phosphonates is relatively scarce. Examples of synthetic

[2] Key for obtaining good resolution NMR measurements has been the use of ultrapure silica for purification purposes, followed by treatment of the product with a Chelex® 100 resin. The use of glass-covered stirring rods in place of the classical Teflon-covered rods is recommended.

approaches to this class of compounds include the use of sugar-lactones or 1,2-anhydrosugars for a nucleophilic addition reaction of lithiated (difluoromethyl)phosphonates,[30,31] or the use of gem-difluoro exo-glycal intermediates in a phosphonyl radical addition.[32] In this work, a route involving a nucleophilic addition to the lactone was employed.

To assemble the MPM difluoro-*C*-mannoside analogue **3**, lactone **7** was treated with the carbanion formed from reaction of diethyl (difluoromethyl)phosphonate with LDA to provide lactol **19** in near quantitative yield (Figure 4). Removal of the newly formed anomeric alcohol, however, proved challenging. A Barton McCombie approach led to formation of a difluoro exo-glycal, as determined by NMR analysis. Treatment of the alcohol with catalytic quantities of Et_3SiH did not result in any product formation, while using an excess of silane exclusively led to the formation of the TES-protected hydroxyl. Reduction of the lactol eventually succeeded via the formation of the intermediate methyloxalate using monomethyl oxalyl chloride, followed by treatment with Bu_3SnH. In line with the synthesis of *C*-mannoside **2**, the phosphonate was converted into phosphonic acid **9**. NOESY-NMR confirmed the β-stereochemistry (see Figure 7).

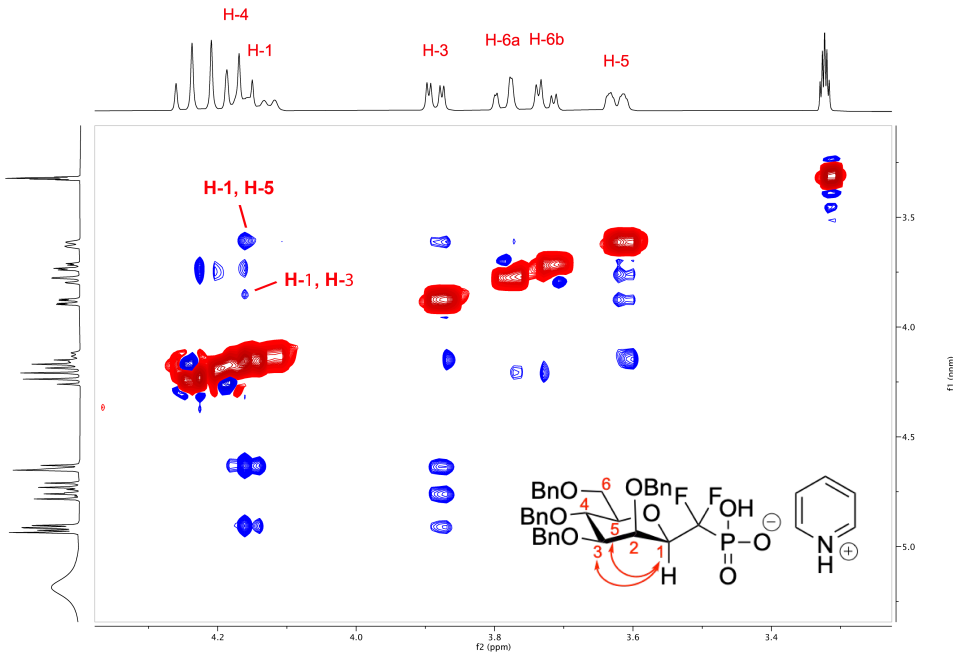

Figure 7 – NOESY spectrum of compound 9. The key NOE interaction can be found between H-1 and H-5, and H-1 and H-3.

Coupling of lipid **4** to difluoro-*C*-mannosyl phosphonic acid **9** was accomplished using *i*Pr$_3$PhSO$_2$Cl as condensing agent in a mixture of DMF/toluene/pyridine, which was required to solubilize all reagents. It was observed that an excess of lipid **4** was required for the coupling reaction to prevent formation of the pyrophosphonate side product (the identity of which was proven via NMR and LC-MS analysis). Finally, a hydrogenation reaction was performed to obtain the desired MPM difluoro-*C*-mannoside **3** which was obtained in 15 % overall yield starting from manno-lactone **7**.

With the stabilized MPM-analogues in hand, the consequences of the structural modifications on antigen presentation were assessed (see Figure 8A for a visual depiction of the chosen approach). The stabilized analogues were used to stimulate human monocyte-derived dendritic cells in the presence of either DN6 or CD8-1 T-cells.

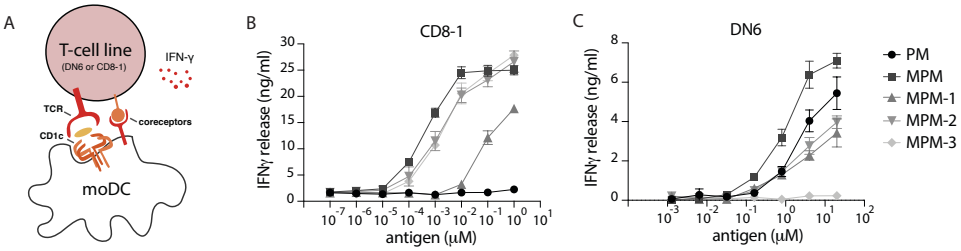

Figure 8 - MPM-3 withstands hydrolysis and cross-reacts with natural MPM. (A) Visual depiction of antigen presentation assay performed to compare IFN-γ production by CD8-1 or DN6 T-cells in the presence of lipid antigen. **(B)** IFN-γ production by MPM-specific CD8-1 T-cells co-cultured with moDCs in the presence of natural MPM or MPM analogues. **(C)** IFN-γ production by PM-specific DN6 T-cells co-cultured with moDCs in the presence of natural MPM and MPM analogues. Data are mean ± SD of triplicate measurements representative of three experiments.

Figure 8B shows that the three analogues were recognized by the CD8-1 T-cell receptor (TCR), which is known to interact with MPM but not with PM. Previously, the DN6 TCR has been shown to be specific for PM, formed from MPM after cellular processing. Unexpectedly, as determined by quantification of the IFN-γ response, carba-mannose **1** and *C*-mannoside **2** were able to activate the DN6 T-cell line, although to a lower extent than natural MPM (Figure 8C).[3] This could indicate that MPM-1 is hydrolyzed under the assay conditions to provide PM. Hydrolysis of *C*-mannoside **2** however would lead to the formation of lipid **4**, which cannot be

[3] As cross-contamination or hydrolysis during storage was unlikely and the samples were tested for the presence of traces amounts of PM using HPLC-MS (see supporting figure), an alternative possible explanation for the unexpected result is that the DN6 TCR recognizes the intact analogues in a cross-reactive manner.

presented by CD1c. Alternatively, it may be speculated that **1** and **2** bind to CD1c in such a manner that it exposes the PM moiety while folding away the mannoside. In contrast, the difluoro-*C*-mannoside **3** did not induce activation of the DN6 T-cell line, indicating that this analogue does not give rise to PM in an antigen presentation assay and that it does not cross-react with the DN6 TCR.

Because of its desirable characteristics, difluoro-*C*-mannoside **3** was used to generate a T-cell line named HD56-MPM-3, which was shown to be cross-reactive to natural MPM (see Figure 9A for a visual depiction of the chosen approach).

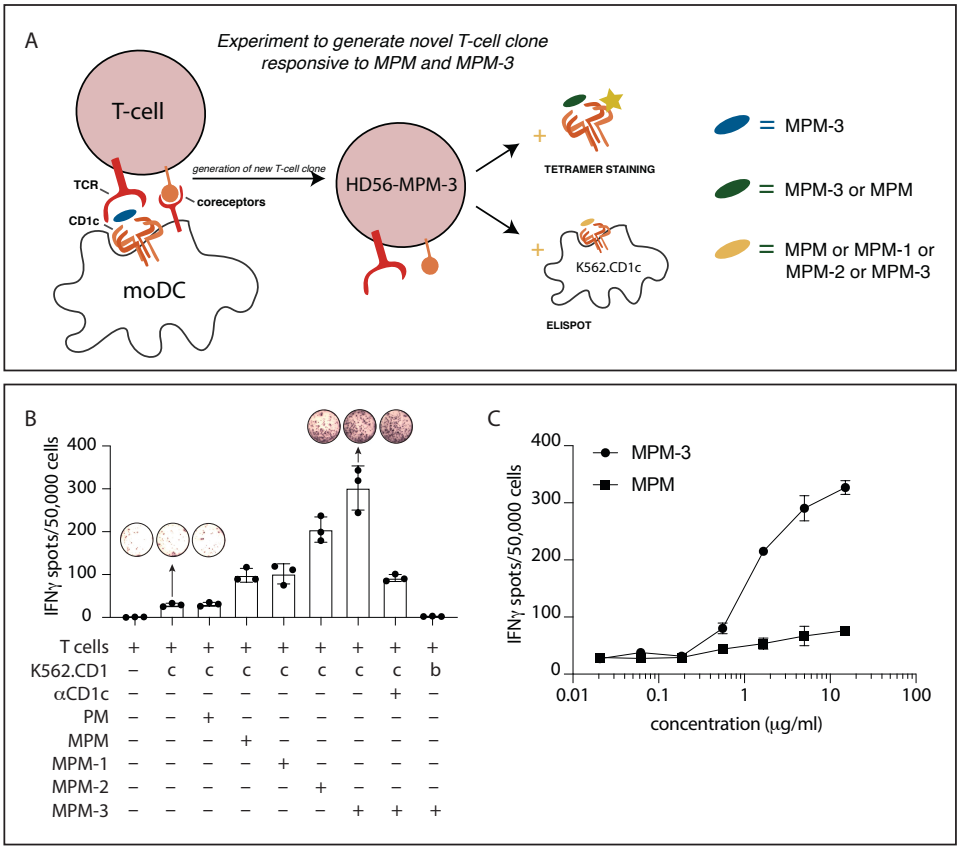

Figure 9 - HD56-MPM-3 T-cells produce IFN-γ after stimulation with MPM-3 and natural MPM. (A) Visual depiction of experimental approach to the generation and characterization of novel T-cell clone: the difluoro-C-mannoside **3** was used to generate T-cell clone HD56-MPM-3, which was shown to recognize both MPM and MPM-3 by flow cytometry using CD1c-tetramers and by ELISPOT using the myelogenous leukemia cell line K562 transduced with CD1c (K562.CD1c). **(B)** IFN-γ ELISPOT the HD56 cell line stimulated with K562.CD1c or K562.CD1b cells in the presence of the indicated lipid antigens. Error bars represent the SEM of triplicate wells. One representative experiment of three is shown. **(C)** Dose response curve of HD56-MPM-3 stimulated with K562.CD1c and lipid antigens.

The cross-reactivity was demonstrated by tetramer staining using CD1c tetramers loaded with either MPM or the difluoro-*C*-mannoside (data not shown). To further characterize the response of the HD56-MPM-3 cell line to MPM and its synthetic analogues, an antigen presentation assay using the myelogenous leukemia cell line K562 transduced with CD1c (K562.CD1c) was performed. The detected ELISPOT responses indicate that difluoro-*C*-mannoside **3** and MPM are both recognized by the HD56-MPM-3 cell line, with the synthetic analogue eliciting a stronger IFN-γ response (Figure 9B). Additionally, also the other synthetic analogues carba-mannoside **1** and *C*-mannoside **2** induced a low to intermediate response, while the amount of IFN-γ detected upon stimulation with PM is comparable to the background level of IFN-γ from T-cells stimulated without antigen.

Furthermore, no IFN-γ is detected in the presence of difluoro-*C*-mannoside **3** when K562.CD1c cells are absent, indicating that processing by the K562.CD1c cells is required. The requirement for processing by the K562.CD1c cell line with presentation via CD1c is shown by the decreased responses in the presence of anti-CD1c antibodies (α-CD1c) as compared to the difluoro-*C*-mannoside **3** stimulation condition. To further evaluate the responsiveness of the HD56-MPM-3 cell line to MPM and difluoro-*C*-mannoside analogue **3**, IFN-γ dose response curves were compared (Figure 9C), demonstrating that MPM is less antigenic than the stabilized difluoro-analogue **3**. This finding suggests that the hydrolysis of MPM to PM reduces the amount of available antigen, while the difluoro-*C*-mannoside **3** is not sensitive to hydrolysis.

Conclusions

The CD1c receptor expressed on antigen-presenting cells represents an attractive target for the development of vaccines against tuberculosis, given its non-polymorphic nature and its ability to present *Mtb*-specific glycolipids to T-cell. MPM is one of such glycolipids and its ability to induce strong T cell responses makes it a good candidate for subunit vaccine applications. However, the processing of MPM to PM by antigen presenting cells like dendritic cells reduces the availability of MPM *in vivo*.

In this chapter, the synthesis of three MPM-analogues, a carba-analogue and two *C*-mannosides, is presented. Characteristic of these analogues is their improved stability towards chemical and enzymatic hydrolysis. For the generation of the carba-analogue, a phosphoramidite chemistry approach was chosen to couple lipid alcohol to β-carba-mannopyranoside, which was obtained from a pseudo-glucal intermediate. The two *C*-glycosides were synthesized starting from D-mannose via a lactone intermediate, which was subsequently converted to the phosphonates using two different synthetic strategies. The coupling reaction between these phosphonates and lipid alcohol yielded the desired analogues in satisfactory yields.

The synthetic analogues were used to stimulate human monocyte-derived dendritic cells in the presence of two well-established T-cell clones, that can recognize CD1c presented MPM and PM analogues, respectively. The difluoro-*C*-mannoside **3** was shown to induce activation of the CD8-1 but not the DN6 T-cell line, indicating that this analogue did not give rise to PM in an antigen presentation assay and did not cross-react with the DN6 TCR.

Because of its desirable characteristics, difluoro-*C*-mannoside **3** was used to expand antigen-specific T-cells, which were further shown to cross-react to the natural MPM. IFN-γ dose-response curves obtained from the novel T-cell clone indicated that the stabilized difluoro-analogue **3** was more antigenic than MPM. Further studies, including experiments to assess recognition of the novel analogue by T-cells of individuals infected with *Mtb* and *in vivo* experiments, will be performed to provide more information regarding the potential of the difluoro-*C*-mannoside analogue for the development of TB vaccines.

Materials and methods

General methods

All reagents were of commercial grade and used as received unless stated otherwise. Ethyl acetate and toluene were distilled before use. Glassware was oven dried at 80°C. Anhydrous solvents used for water-sensitive reactions were stored on activated molecular sieves 3 Å for at least 24 hours before use. Molecular sieves 3 Å were flame dried under reduced pressure.

Reactions that required anhydrous conditions were co-evaporated as described in the experimental procedure to remove traces of water, and the reactions were performed under argon or nitrogen atmosphere. Reactions that required a microwave irradiation were performed using a Biotage initiator 2.5. Reactions that required UV irradiation (375 nm; 200 mW; 350 mA; 3.7 V) were performed in the dark using a high-power single chip led (H2A1 series, Roithner LaserTechnik), and the led was fastened to a plastic adapter (for flasks NS 14/23) with distance from the reaction mixture of 5 to 7 cm.

Flash chromatography was performed on Screening Devices silica gel 60 (0.040 - 0.063 mm). Size exclusion chromatography was performed on Sephadex LH-20 gel. The progress of each reaction was followed via TLC-analysis, conducted on DC-alufolien (Merck, Kieselgel 60, F245) with detection by UV-absorption (254 nm) for UV-active compounds and by spraying with one of the following TLC stain solutions: 20% H_2SO_4 in ethanol; 5% anisaldehyde and 5% H_2SO_4 in ethanol; $(NH_4)_6Mo_7O_{24}.4H_2O$ (25 g/L), $(NH_4)_4Ce(SO_4)_4.2H_2O$ (10 g/L), 10% H_2SO_4 in H_2O; $KMnO_4$ (10 g/L) and K_2CO_3 (67 g/L) in H_2O; the staining was followed by charring at 150°C.

^{1}H, ^{13}C and ^{31}P NMR spectra were recorded on a Bruker AV 300 (300/75/121 MHz), Bruker DMX-400 (400/101 MHz), a Bruker AV 400 (400/101/126 MHz), a Bruker AV 500 (500/126/202 MHz) or a Bruker AV 600 (600/151 MHz) spectrometer. ^{19}F NMR spectra were recorded on a Bruker AV 500 (471 MHz) spectrometer. Chemical shifts (δ) are given in ppm relative to the residual solvent peak or tetramethylsilane as internal standard. Coupling constants (J) are given in Hz. All given ^{13}C, ^{31}P and ^{19}F spectra are proton decoupled unless stated otherwise.

High-resolution mass spectrometry (HRMS) was performed on a Thermo Finnigan LTQ Orbitrap mass spectrometer equipped with an electrospray ion source in positive-ion mode (source voltage 3.5 kV, sheath gas flow 10, capillary temperature 275 °C) with resolution R = 60.000 at m/z 400 (mass range of 150-4000) and dioctylphtalate (m/z=391.28428) as lock mass, or on a Waters Synapt G2-Si (TOF) equipped with an electrospray ion source in positive mode (source voltage 3.5 kV) and LeuEnk (m/z = 556.2771) as internal lock mass.

C-mannosyl-1-phosphomycoketide

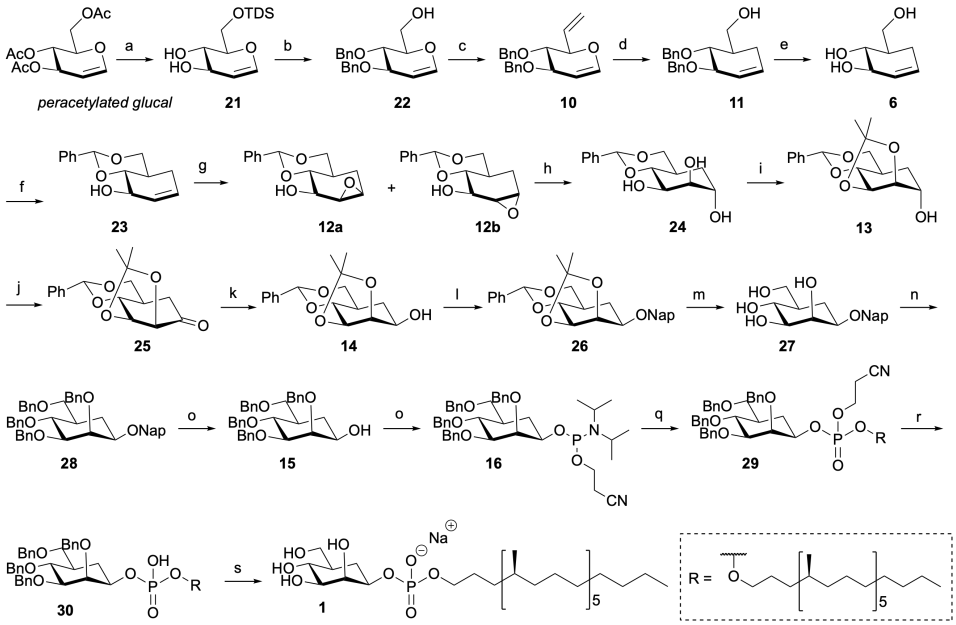

S1 Figure - Synthetic scheme for the generation of carba-mannose (compound 1). a) i. K_2CO_3, MeOH, ii. TDSCl, imidazole, DMF, -20°C, 82%, b) i. BnBr, NaH, TBAI, THF, ii. TBAF, THF, 69%, c) i. IBX, EtOAc, reflux, ii. PPh_3CH_3I, KHMDS, THF, -78°C to RT, 88%, d) i. *o*-dichlorobenzene, 230°C, ii. $NaBH_4$, EtOH/THF, 94%, e) Li-naphthalenide, THF, -20°C, 81%, f) $PhCH(OMe)_2$, pTsOH, DMF, 60°C, 67%, g) *m*-CPBA, PBS buffer, DCM, α 5%, β 86%, h) KOH, dioxane, H_2O, 90°C, quant., i) 2,2-dimethoxypropane, pTsOH, DMF, 90%, j) IBX, EtOAc, reflux, 82%, k) $NaBH_4$, DCM/MeOH, 0°C, 77%, l) NapBr, NaH, TBAI, THF/DMF, 88%, m) pTsOH, MeOH, 92%, n) BnBr, NaH, TBAI, DMF, 86%, o) DDQ, DCM/H_2O, 73%, p) (CEO)PCl(N-*i*Pr_2), DIPEA, DCM, 68%, q) i. compound **4,** DCI, CH_3CN, ii. CSO, CH_3CN, 70%, r) Et_3N, CH_3CN, 74%, s) Pd/C, H_2, $CHCl_3$:MeOH (1:1 v/v), 47%.

6-O-dimethylthexylsilyl-D-glucal (21).

3,4,6-O-acetyl-D-glucal (81.6 g, 300 mmol, 1.0 eq) was dissolved in MeOH (500 ml, 0.6M). To the solution K_2CO_3 (4.15 g, 30 mmol, 0.10 eq) was added and the reaction mixture was stirred for 1 hour at room temperature. Volatiles were then removed *in vacuo* and the crude was co-evaporated (1x) with toluene before being dissolved in dry DMF (500 ml, 0.6M). To this solution imidazole (68.1 g, 900 mmol, 3.0 eq) was added and the mixture was cooled to -20°C. TDSCl (65 ml, 330 mmol, 1.1 eq) was added dropwise via cannula and the reaction mixture was stirred overnight at -20°C. After warming to room temperature the reaction mixture was concentrated *in vacuo*, dissolved in EtOAc and transferred to a separatory funnel. The organic layer was washed with water (4x) and with brine (2x). The combined water layers were extracted (1x) with DCM and the combined organic layers were dried over $MgSO_4$, filtered and concentrated *in vacuo*. Compound **21** was obtained after silicagel chromatography

(Pentane/EtOAc 4:1→1:1; DCM loading of crude) as a yellow oil (71 g, 246 mmol, 82%). ^{1}H NMR (300 MHz, $CDCl_3$) δ: 6.31 (dd, J = 6.1, 1.8 Hz, 1H, H-1), 4.72 (dd, J= 6.1, 2.2 Hz, 1H, H-2), 4.34 – 4.20 (m, 1H, H-3), 4.02 – 3.93 (m, 1H, H-6a), 3.93 – 3.84 (m, 1H, H-6b), 3.82 – 3.74 (m, 2H, H-4, H-5), 3.27 (bs, 1H, OH-3), 2.59 (bs, 1H, OH-2), 1.70 – 1.54 (m, 1H, CH-TDS), 0.90 – 0.84 (m, 12H, CH_3-TDS), 0.16 – 0.10 (m, 6H, CH_3-Si). ^{13}C-APT NMR (75 MHz, $CDCl_3$) δ: 144.3 (C-1), 102.6 (C-2), 76.7 (C-5), 72.7 (C-4), 69.5 (C-3), 63.8 (C-6), 34.2 (CH-TDS), 20.4 (CH_3-TDS), 18.6 (CH_3-Si).

3,4-di-O-benzyl-D-glucal (22).

Compound **21** (1.45 g, 5.0 mmol, 1 eq) was co-evaporated (3x) with toluene and dissolved in dry THF (10 mL). The solution was cooled to 0°C and TBAI (190 mg, 0.5 mmol, 0.1 eq), BnBr (2.4 mL, 20 mmol, 4 eq) and a 60% suspension in mineral oil of NaH (505 mg, 13 mmol, 2.6 eq) were added sequentially. The reaction mixture was stirred at RT overnight. Upon completion, the reaction mixture was quenched with the addition of MeOH, diluted in EtOAc and transfer- red to a separatory funnel. The organic layer was washed (3x) with water and (1x) with brine. The organic layer was dried over $MgSO_4$, filtered and concentrated *in vacuo*. The resulting crude fully protected glucal was dissolved in dry THF (10 mL) and cooled to 0°C. Then a 0.1 M solution of TBAF (70.5 mL, 7.5 mmol, 1.5 eq) in THF was added dropwise to the reaction mixture via cannula. Upon complete addition, the reaction mixture was stirred at RT overnight and subsequently quenched with the addition of a saturated solution of NH_4Cl(aq). The reaction mixture was then diluted in DCM and transferred to a separatory funnel. The organic layer was washed (1x) with brine, dried over $MgSO_4$, filtered and concentrated *in vacuo*. Compound **22** was obtained after silicagel chromatography (Pentane/Et_2O 9:1→1:1; DCM loading of crude) as a yellow syrup (1.13 g, 3.5 mmol, 69%). NMR analysis confirmed purity of the product, whose ^{1}H NMR and ^{13}C NMR spectra were in agreement with published literature.[33]

3,4-di-O-benzyl-6,7-ene-D-glucal (10).

Compound **22** (19.6 g, 60.3 mmol, 1 eq) was dissolved in dry EtOAc (1.2 L) after which IBX (84.6 g, 302 mmol, 5 eq) was added. The reaction mixture was stirred under reflux for 6 hours and then cooled to RT, filtered over celite and concentrated *in vacuo* to give the crude aldehyde. The crude aldehyde was co-evaporated (2x) with toluene and dissolved in dry THF (60 mL). A phosphonium ylide solution was then prepared by suspending PPh_3CH_3Br (43.0 g, 120.5 mmol, 2 eq) in dry THF (300 mL), cooling the suspension to -78°C and adding a 0.5 M solution of KHMDS in toluene (241 mL, 120.5 mmol, 2 eq) dropwise to the suspension via cannula. The solution was stirred for 30 minutes at -78°C and left to warm up to -50°C to obtain an intensely yellow colored solution. The phosphonium ylide solution was then cooled to -78°C and the crude aldehyde solution was added dropwise. The reaction mixture was then stirred at RT overnight. Upon completion, the reaction was quenched with the addition of a saturated solution of NH_4Cl(aq) (150 mL), then diluted in DCM and transferred to a separatory funnel. The organic layer was washed (1x) with brine and the water layer was extracted (1x) with DCM. The combined organic layers were dried over $MgSO_4$, filtered and concentrated *in vacuo*. Compound **10** was obtained after silicagel chromatography (Pentane/ Et_2O 39:1→3:2; DCM loading of crude) as a light brown syrup (17.1 g, 53.1 mmol, 88%). NMR analysis confirmed purity of the product, whose ^{1}H NMR and ^{13}C NMR spectra were in agreement with published literature.[34]

3,4-di-O-benzyl-pseudo-D-glucal (11).

Compound **10** (645 mg, 2 mmol, 1 eq) was co-evaporated (3x) with toluene, transferred to a 5 mL microwave vial purged with N_2 and dissolved in dry *o*-dichlorobenzene (5 mL). The microwave vial was purged once more with N_2 and stirred under microwave irradiation for 20 minutes at 230°C. The intermediate aldehyde was then reduced by pouring the reaction mixture in a solution on of $NaBH_4$ (113 mg, 3 mmol, 1.5 eq) in THF/EtOH 2:1 (5 mL). This mixture was stirred for 15 minutes and quenched with the addition of water before being transferred to a separatory funnel. The water layer was extracted (3x) with DCM. The combined organic layers were washed (1x) with brine, dried over $MgSO_4$, filtered and concentrated *in vacuo*. Compound **11** was obtained after silicagel chromatography (Pentane/Et_2O 9:1→1:9; DCM loading of crude) as a yellow syrup (610 mg, 1.88 mmol, 94%). NMR analysis confirmed purity of the product, whose ^1H NMR and ^{13}C NMR spectra were in agreement with published literature.[34]

pseudo-D-glucal (6).

Naphthalene (26.8 g, 209 mmol, 7.5 eq) and freshly cut lithium pieces (10 eq) were suspended in freshly distilled dry THF (320 mL) under an argon atmosphere. The solution was then sonicated for 30 seconds, resulting in a dark green solution of naphthalenide radicals. Dibenzylated **11** (9.02 g, 27.8 mmol, 1 eq) was co-evaporated with toluene under argon and dissolved in freshly distilled dry THF (140 mL). The resulting solution was then added dropwise via a cannula to the lithium naphthalenide solution at -78°C and stirred for 2 days at -20°C. Upon completion, non-distilled THF was added and the reaction mixture was diluted with MeOH until the dark green color disappeared. The strongly basic solution was then neutralized using Amberlite H^+, resulting in a clear solution that was filtered and concentrated *in vacuo*. Compound **6** was obtained after silicagel chromatography (EtOAc/MeOH 1:0→4:1; EtOAc loading of crude) as white crystals (3.25 g, 22.5 mmol, 81%). $[a]_D^{20}$= - 13.7 °(c = 0.010, MeOH). ^1H NMR (400 MHz, MeOD) δ: 5.79 – 5.67 (m, 1H, H-1), 5.61 – 5.49 (m, 1H, H-2), 4.11 – 4.01 (m, 1H, H-3), 3.81 (dd, J = 10.9, 4.4 Hz, 1H, H-6a), 3.68 (dd, J = 10.8, 6.1 Hz, 1H, H-6b), 3.44 (dd, J = 11.1, 7.7 Hz, 1H, H-4), 2.33 – 2.21 (m, 1H, H-7a), 2.08 – 1.96 (m, 1H, H-7b), 1.93 – 1.79 (m, 1H, H-5). ^{13}C-APT NMR (101 MHz, $CDCl_3$) δ: 130.2 (C-2), 128.3 (C-1), 76.0 (C-4), 74.7 (C-3), 64.5 (C-6), 42.5 (C-5), 29.5 (C-7). HRMS $[M+Na]^+$: 167.06818 found, 167.06787 calculated.

4,6-O-benzylidene-pseudo-D-glucal (23).

Fully deprotected pseudo-glucal **6** (3.0 g, 20.8 mmol, 1 eq) was dissolved in dry DMF (42 mL). Benzaldehyde dimethyl acetal (4.65 mL, 31.2 mmol, 1.5 eq) and pTsOH (363 mg, 0.2 mmol, 0.1 eq) were added and the flask containing the reaction mixture was spun on a rotary evaporator under reduced pressure at 60°C. After 1 hour a saturated solution of $NaHCO_3$(aq) was added and the reaction mixture was diluted in water and Et_2O and transferred to a separatory funnel. The water layer was extracted (3x) with Et_2O. The combined organic layers were washed (1x) with brine, dried over $MgSO_4$, filtered and concentrated *in vacuo*. Compound **23** was obtained after crystallization from EtOH as white crystals (3.24 g, 14 mmol, 67%). $[a]_D^{20}$= - 11.6 °(c = 0.010, DCM). ^1H NMR (400 MHz, $CDCl_3$) δ: 7.58 – 7.48 (m, 2H, H-arom), 7.44 – 7.33 (m, 3H, H-arom), 5.74 (ddd, J = 8.9, 4.5, 2.2 Hz, 1H, H-1), 5.69 – 5.59 (m, 2H, H-2, CH-Ph), 4.48 – 4.38 (m, 1H, H-3), 4.22 (dd, J = 11.2, 4.8 Hz, 1H, H-6a), 3.75 – 3.62 (m, 2H, H-4, H-6b), 2.24 – 2.04 (m,

2H, H-5, H-7a), 1.84 – 1.77 (m, 1H, H-7b). ^{13}C-APT NMR (101 MHz, $CDCl_3$) δ: 138.2 (C-arom), 129.2 (C-arom), 128.6 (C-arom), 128.5 (C-2), 126.8 (C-1), 126.3 (C-arom), 101.8 (CH-Ph), 83.5 (C-4), 71.3 (C-6), 70.5 (C-3), 34.0 (C-5), 26.6 (C-7). HRMS $[M+Na]^+$: 255.09920 found, 255.09917 calculated.

1,2-oxirane-4,6-O-benzylidene-pseudo-D-pyranoside (12a & 12b).

Benzylidene protected pseudo-glucal **23** (2.5 g, 8.7 mmol, 1 eq) was dissolved in an emulsion of DCM (29 mL) and PBS (10.5 mL). Then *m*CPBA (4.0 g, 17.4 mmol, 2 eq) was added in various portions to the emulsion. After stirring for 2 hours, the reaction mixture was diluted in DCM and transferred to a separatory funnel. The organic layer was washed (1x) with water, (1x) with a saturated solution of $Na_2S_2O_3$(aq), (1x) with water and (1x) with brine. The organic layer was then dried over $MgSO_4$, filtered and concentrated *in vacuo*. Compound **12a** was obtained after silicagel chromatography (Pentane/ Et_2O 7:3→0:1; DCM loading of crude) as a white solid (1.9 g, 7.5 mmol, 86%).

2

β-manno: $[a]_D^{20}$= - 0.4 °(c = 0.010, DCM). ^{1}H NMR (400 MHz, $CDCl_3$) δ: 7.51 – 7.44 (m, 2H, H-arom), 7.42 – 7.32 (m, 3H, H-arom), 5.49 (s, 1H, CH-Ph), 4.19 – 4.07 (m, 2H, H-6a, H-3), 3.72 (dd, J = 10.6, 8.4 Hz, 1H, H-4), 3.52 (pt, J = 10.9 Hz, 1H, H-6b), 3.41 (dd, J = 4.0, 2.0 Hz, 1H, H-2), 3.34 (dd, J = 4.8, 3.9 Hz, 1H, H-1), 2.55 (s, 1H, OH), 2.05 – 1.85 (m, 2H, H-7a, H-5), 1.63 – 1.52 (m, 2H, H-7b). ^{13}C-APT NMR (101 MHz, $CDCl_3$) δ: 138.0 (C-arom), 129.3 (C- arom), 128.5 (C-arom), 126.3 (C-arom), 101.7 (CH-Ph), 79.9 (C-4), 71.6 (C-3), 70.8 (C-6), 56.1 (C-2), 52.9 (C-1), 34.2 (C-5), 24.8 (C-7). HRMS $[M+Na]^+$: 271.09394 found, 271.09408 calculated.

The α-epoxide **12b** was also isolated as a white solid (108 mg, 0.44 mmol, 5%).

α-gluco: $[a]_D^{20}$= + 1.6 °(c = 0.010, DCM). ^{1}H NMR (400 MHz, $CDCl_3$) δ: 7.50 – 7.43 (m, 2H, H-arom), 7.40 – 7.31 (m, 3H, H-arom), 5.45 (s, 1H, CH-Ph), 4.12 (dd, J = 11.2, 4.8 Hz, 1H, H-6a), 3.88 (dd, J = 8.2, 0.7 Hz, 1H, H-3), 3.47 (pt, J = 11.2 Hz, 1H, H-6b), 3.35 (dd, J = 10.9, 8.2 Hz, 1H, H-4), 3.18 (dt, J = 3.7, 1.9 Hz, 1H, H-1), 3.04 (pd, J = 3.5 Hz, 1H, H-2), 2.01 (ddd, J = 14.7, 4.6, 2.0 Hz, 1H, H-7a), 1.91 – 1.76 (m, 1H, H-5), 1.38 (ddd, J = 14.8, 11.9, 1.7 Hz, 1H, H-7b). ^{13}C-APT NMR (101 MHz, $CDCl_3$) δ: 137.8 (C-arom), 129.2 (C-arom), 128.4 (C-arom), 126.3 (C-arom), 101.6 (CH-Ph), 82.7 (C-4), 71.2 (C-6), 69.3 (C-3), 55.7 (C-2), 52.0 (C-1), 27.4 (C-5), 25.5 (C-7). HRMS $[M+Na]^+$: 271.09443 found, 271.09408 calculated.

4,6-O-benzylidene-7-carba-α-D-mannopyranoside (24).

A mixture of the epoxides **12a** and **12b** (745 mg, 3.0 mmol, 1 eq) was dissolved in dioxane (6 mL) and a 5M solution of KOH (54 mL) was added. The reaction mixture was stirred at 90°C for 2 hours and 30 minutes and upon completion cooled to 0°C, diluted in water and transferred to a separatory funnel. The water layer was extracted (3x) with EtOAc and the combined organic layers were washed (1x) with brine, dried over $MgSO_4$, filtered and concentrated *in vacuo*. Compound **24** was obtained as a white solid (796 mg, 3 mmol, quant.) without any further purification. $[a]_D^{20}$= - 44.7 °(c = 0.010, MeOH). ^{1}H NMR (400 MHz, MeOD) δ: 7.62 – 7.48 (m, 2H, H-arom), 7.48 – 7.30 (m, 3H, H-arom), 5.64 (s, 1H, CH-Ph), 4.10 (dd, J = 10.9, 4.4 Hz, 1H, H-6a), 4.02 – 3.96 (m, 2H, H-1, H-2), 3.94 (dd, J = 9.6, 2.8 Hz, 1H, H-3), 3.86 (pt, J = 9.8 Hz, 1H, H-4), 3.70 (t, J = 11.0 Hz, 1H, H-6b), 2.32 – 2.11 (m, 1H, H-5), 1.62 (td, J = 13.4, 2.4 Hz, 1H, H-7a), 1.55 – 1.41 (m, 1H, H-7b). ^{13}C-APT NMR (101 MHz, $CDCl_3$) δ: 140.1 (C-arom), 129.7 (C-arom), 129.0 (C-arom), 127.5 (C-arom), 103.3 (CH-Ph), 82.2 (C-4), 74.8 (C-3),

72.4 (C-6), 71.1 (C-2), 70.7 (C-1), 34.1 (C-5), 28.4 (C-7). HRMS $[M+Na]^+$: 289.10451 found, 289.10464 calculated.

2,3-O-isopropylidene-4,6-O-benzylidene-7-carba-α-D- mannopyranoside (13).

Benzylidene protected pseudo-mannoside **24** (591 mg, 2.2 mmol, 1 eq) was dissolved in dry DMF (22 mL). The solution was then cooled to 0°C and 2,2-dimethoxypropane (1.1 mL, 8.8 mmol, 4 eq) and pTsOH (42 mg, 0.22 mmol, 0.1 eq) were added. The reaction mixture was left to stir at RT overnight. Then the reaction was quenched with Et_3N, diluted in water and transferred to a separatory funnel. The water layer was extracted (3x) with Et_2O. The combined organic layers were washed (1x) with brine, dried over $MgSO_4$, filtered and concentrated *in vacuo*. Compound **13** was obtained after silicagel chromatography (Pentane/Et_2O 9:1→0:1; DCM loading of crude; silica was neutralized with Et_3N) as a white solid (606 mg, 1.98 mmol, 90%). Note: this compound readily degrades in non-neutralized $CDCl_3$. $[\alpha]_D^{20}$= -51.6 °(c = 0.010, DCM). ^{1}H NMR (400 MHz, $CDCl_3$) δ: 7.56 – 7.45 (m, 2H, H-arom), 7.42 – 7.28 (m, 3H, H-arom), 5.55 (s, 1H, CH-Ph), 4.32 (dd, J = 7.8, 5.3 Hz, 1H, H-3), 4.24 – 4.15 (m, 3H, H-1, H-2, H-6a), 3.69 (dd, J = 11.2, 7.7 Hz, 1H, H-4), 3.61 (pt, J = 11.0 Hz, 1H, H-6b), 2.26 – 2.11 (m, 1H, H-5), 1.87 (s, 1H, OH), 1.64 – 1.41 (m, 5H, H-7, CH_3-isopr), 1.38 (s, 3H, CH_3-isopr). ^{13}C-APT NMR (101 MHz, $CDCl_3$) δ: 138.1 (C-arom), 129.0 (C-arom), 128.3 (C-arom), 126.5 (C-arom), 109.6 (C-isopr), 101.9 (CH-Ph), 82.3 (C-4), 78.8 (C-2), 76.9 (C-3), 71.5 (C-6), 67.2 (C-1), 30.3 (C-5), 28.6 (C-7), 28.3 (CH_3-isopr), 26.0 (CH_3-isopr). HRMS $[M+Na]^+$: 329.13530 found, 329.13594 calculated.

1-one-2,3-O-isopropylidene-4,6-O-benzylidene-7-carba-D- mannopyranoside (25).

Acetal protected compound **13** (319 mg, 1.0 mmol, 1 eq) was dissolved in dry EtOAc (20 mL). IBX (1.4 g, 5.0 mmol, 5 eq) was added to the solution and the reaction mixture was refluxed overnight. The reaction mixture was then cooled to RT, filtered over celite and concentrated *in vacuo*. Compound **25** was obtained after silicagel chromatography (Pentane/EtOAc 9:1→1:1; DCM loading of crude; silica was neutralized with Et_3N) as a white solid (250 mg, 0.82 mmol, 82%). Note: this compound readily degrades in non-neutralized $CDCl_3$. $[\alpha]_D^{20}$= -3.2 °(c = 0.010, DCM). ^{1}H NMR (400 MHz, $CDCl_3$) δ: 7.56 – 7.49 (m, 2H, H-arom), 7.42 – 7.31 (m, 3H, H-arom), 5.57 (s, 1H, CH-Ph), 4.73 (dd, J = 8.5, 6.7 Hz, 1H, H-2), 4.63 (d, J = 8.6 Hz, 1H, H-3), 4.33 (dd, J = 11.3, 4.8 Hz, 1H, H-6a), 3.76 (dd, J = 11.3, 6.8 Hz, 1H, H-4), 3.61 (dd, J = 11.4, 10.4 Hz, 1H, H-6b), 2.56 (ddd, J = 17.6, 6.9, 1.0 Hz, 1H, H-7a), 2.52 – 2.40 (m, 1H, H-5), 2.03 (dd, J = 17.5, 11.0 Hz, 1H, H-7b), 1.54 (s, 3H, CH_3-isopr), 1.40 (s, 3H, CH_3-isopr). ^{13}C-APT NMR (101 MHz, $CDCl_3$) δ: 204.7 (C-1), 137.5 (C-arom), 129.4 (C-arom), 128.4 (C-arom), 126.4 (C-arom), 111.9 (C-isopr), 101.6 (CH-Ph), 80.7 (C-4), 79.3 (C-3), 78.5 (C-2), 71.3 (C-6), 36.7 (C-7), 30.8 (C-5), 27.2 (CH_3-isopr), 25.3 (CH_3-isopr). HRMS $[M+Na]^+$: 327.12039 found, 327.12029 calculated.

2,3-O-isopropylidene-4,6-O-benzylidene-7-carba-β-D-mannopyranoside (14).

Ketone **25** (250 mg, 0.82 mmol, 1 eq) was dissolved in a mixture of DCM/MeOH 20:1 (16.5 mL). The solution was cooled to 0°C and $NaBH_4$ (155 mg, 4.1 mmol, 5 eq) was added in portions. After stirring for 30 minutes the reaction was quenched with the addition of water and transferred to a separatory funnel. The water layer was extracted (3x) with DCM and the combined organic layers were washed (1x) with brine, dried over $MgSO_4$, filtered and concentrated *in vacuo*. Compound **14** was obtained after silicagel chromatography

(Pentane/EtOAc 7:3→3:7; DCM loading of crude; silica was neutralized with Et_3N) as a white solid (193 mg, 0.63 mmol, 77%) with an axial to equatorial ratio of 1:32. Note: this compound readily degrades in non-neutralized $CDCl_3$. $[\alpha]_D^{20}$= -70.7 °(c = 0.010, DCM). ^{1}H NMR (400 MHz, $CDCl_3$) δ: 7.54 – 7.46 (m, 2H, H-arom), 7.38 – 7.30 (m, 3H, H-arom), 5.55 (s, 1H, CH-Ph), 4.39 (dd, J = 6.0, 3.8 Hz, 1H, H-2), 4.25 – 4.15 (m, 2H, H-3, H-6a), 4.06 – 3.96 (m, 1H, H-1), 3.84 (dd, J = 10.7, 7.6 Hz, 1H, H-4), 3.65 (pt, J = 10.8 Hz, 1H, H-6b), 2.29 (d, J = 6.6 Hz, 1H, OH), 1.81 – 1.66 (m, 2H, H-7a, H-5), 1.59 (s, 3H, CH_3-isopr), 1.46 – 1.34 (m, 4H, CH_3-isopr, H-7b). ^{13}C-APT NMR (101 MHz, $CDCl_3$) δ: 138.1 (C-arom), 129.0 (C-arom), 128.3 (C-arom), 126.4 (C-arom), 109.8 (C-isopr), 101.9 (CH-Ph), 81.9 (C-4), 77.9 (C-3), 76.6 (C-2), 71.4 (C-6), 67.7 (C-1), 32.5 (C-5), 28.6 (C-7), 28.0 (CH_3-isopr), 25.7 (CH_3-isopr). HRMS $[M+Na]^+$: 329.13596 found, 329.13594 calculated.

1-O-naphthyl-2,3-O-isopropylidene-4,6-O-benzylidene-7-carba-β-D-mannopyranoside (26).

Acetal protected pseudo-mannoside **14** (2.23 g, 7.28 mmol, 1 eq) was co-evaporated with toluene and dissolved in dry DMF (38 mL). The solution was cooled to 0°C and TBAI (269 mg, 0.728 mmol, 0.1 eq) and naphthyl bromide (3.22 g, 14.6 mmol, 2 eq) were added. Then a 60% suspension in mineral oil of NaH (43.7 mg, 10.9 mmol, 1.5 eq) was added in multiple portions to the reaction mixture. After the addition of NaH was complete, the solution was stirred at RT for 2 hours and then quenched with the addition of MeOH. The reaction mixture was then diluted in Et_2O and water and transferred to a separatory funnel. The water layer was extracted (3x) with Et_2O and the combined organic layers were washed (1x) with brine, dried over $MgSO_4$, filtered and concentrated *in vacuo*. Compound **26** was obtained after silicagel chromatography (Pentane/EtOAc 4:1→0:1; DCM loading of crude; silica was neutralized with Et_3N) as a white solid (2.85 g, 6.41 mmol, 88%). Note: this compound readily degrades in non-neutralized $CDCl_3$. $[\alpha]_D^{20}$= -35.5 °(c = 0.010, DCM). ^{1}H NMR (400 MHz, $CDCl_3$) δ: 7.89 – 7.77 (m, 4H, H-arom), 7.56 – 7.43 (m, 5H, H-arom), 7.36 – 7.26 (m, 3H, H-arom), 5.52 (s, 1H, CH-Ph), 4.92 – 4.78 (m, 2H, CH_2-Nap), 4.51 – 4.42 (m, 1H, H-2), 4.15 (dd, J = 11.0, 4.4 Hz, 1H, H-6a), 4.08 (dd, J = 7.8, 5.0 Hz, 1H, H-3), 3.81 – 3.72 (m, 1H, H-1), 3.72 – 3.59 (m, 2H, H-4, H-6b), 1.77 – 1.67 (m, 1H, H-7), 1.67 – 1.45 (m, 5H, CH_3-isopr, H-5, H-7), 1.41 (s, 3H, CH_3-isopr). ^{13}C-APT NMR (101 MHz, $CDCl_3$) δ: 138.0 (C-arom), 135.6 (C-arom), 133.3 (C-arom), 133.2 (C-arom), 129.0 (C-arom), 128.5 (C-arom), 128.2 (C-arom), 128.0 (C-arom), 127.9 (C-arom), 126.8 (C-arom), 126.4 (C-arom), 126.4 (C-arom), 126.2 (C-arom), 125.9 (C-arom), 110.1 (C-isopr), 102.0 (CH-Ph), 82.8 (C-4), 78.2 (C-3), 75.3 (C-2), 74.0 (C-1), 71.3 (CH_2-Nap), 71.1 (C-6), 33.3 (C-5), 28.7 (CH_3-isopr), 26.4 (CH_3-isopr), 26.0 (C-7). HRMS $[M+Na]^+$: 469.19828 found, 469.19855 calculated.

1-O-naphthyl-7-carba-β-D-mannopyranoside (27).

The naphthyl protected **26** (89.3 mg, 0.2 mmol, 1 eq) was dissolved in DCM/MeOH 1:1 (5 mL) and pTsOH (11.4 mg, 0.06 mmol, 0.3 eq) was added. The reaction mixture was stirred at RT for 2 hours, then quenched with the ad- dition of Et_3N and concentrated *in vacuo*. Compound **27** was obtained after silicagel chromatography (EtOAc/MeOH 1:0→4:1; EtOAc loading of crude) as a white solid (58.5 mg, 0.184 mmol, 92%). $[\alpha]_D^{20}$= + 20.5 °(c = 0.010, MeOH). ^{1}H NMR (400 MHz, MeOD) δ: 7.91 – 7.82 (m, 4H, H-arom), 7.58 – 7.44 (m, 3H, H-arom), 4.86 – 4.72 (m, 2H, CH_2-Nap), 4.30 – 4.19 (m, 1H, H-2), 3.84 (dd, J = 10.7, 4.3 Hz, 1H, H-6a), 3.64 – 3.50 (m, 3H, H-1, H-6, H-4), 3.30 (dd, J = 9.4, 2.8 Hz, 1H, H-3), 2.03 – 1.87 (m, 1H, H-7a), 1.73 (pq, J = 12.5

Hz, 1H, H-7b), 1.53 – 1.38 (m, 1H, H-5). ^{13}C-APT NMR (101 MHz, MeOD) δ: 137.5 (C-arom), 134.8 (C-arom), 134.5 (C-arom), 129.1 (C-arom), 128.9 (C-arom), 128.7 (C-arom), 127.5 (C-arom), 127.1 (C-arom), 126.9 (C-arom), 126.9 (C-arom), 78.1 (C-4), 76.4 (C-3), 72.3 (C-1), 72.0 (C-2), 71.4 (CH_2-Nap), 64.8 (C-6), 42.5 (C-5), 28.3 (C-7). HRMS $[M+Na]^+$: 341.13583 found, 341.13594 calculated.

1-O-naphthyl-2,3,4,6-tetra-O-benzyl-7-carba-β-D- mannopyranoside (28).

Naphthyl protected carba-mannoside **27** (726.4 mg, 2.28, 1 eq) was co-evaporated with toluene and dissolved in dry DMF (25 mL). The solution was cooled to 0°C and benzyl bromide (2.171 mL, 18.25 mmol, 8 eq) and TBAI (84 mg, 0.228 mmol, 0.1 eq) were added. Then a 60% suspension in mineral oil of NaH (456 mg, 11.41 mmol, 5 eq) was added in multiple portions to the reaction mixture. After the addition of NaH was complete, the solution was stirred at RT overnight and then quenched with the addition of MeOH. The reaction mixture was then diluted in Et_2O and water and transferred to a separatory funnel. The water layer was extracted (3x) with Et_2O and the combined organic layers were washed (1x) with brine, dried over $MgSO_4$, filtered and concentrated *in vacuo*. Compound **28** was obtained after silicagel chromatography (Pentane/Et_2O 20:1→4:1; DCM loading of crude) as a pale syrup (1.36 g, 1.96 mmol, 86%). ^{1}H NMR (400 MHz, $CDCl_3$) δ: 7.86 – 7.72 (m, 4H, H-arom), 7.52 – 7.39 (m, 5H, H-arom), 7.37 – 7.17 (m, 19H, H-arom), 4.96 – 4.88 (m, 3H, CH_2-Nap, CH_2-Bn), 4.70 (d, J = 12.2 Hz, 1H, CH_2-Bn), 4.66 – 4.59 (m, 3H, CH_2-Bn), 4.53 – 4.46 (m, 3H, CH_2-Bn), 4.21 – 4.14 (m, 1H, H-2), 3.83 (dd, J = 10.6, 9.3 Hz, 1H, H-4), 3.64 (dd, J = 8.8, 3.0 Hz, 1H, H-6a), 3.48 (dd, J = 8.8, 6.9 Hz, 1H, H-6b), 3.43 (ddd, J = 11.2, 5.1, 2.1 Hz, 1H, H-1), 3.37 (dd, J = 9.4, 2.4 Hz, 1H, H-3), 2.15 – 1.99 (m, 2H, H-7), 1.74 – 1.61 (m, 1H, H-5). ^{13}C-APT NMR (101 MHz, $CDCl_3$) δ: 139.7 (C-arom), 139.0 (C-arom), 138.8 (C-arom), 138.7 (C-arom), 136.3 (C-arom), 133.4 (C-arom), 133.0 (C-arom), 128.5 (C-arom), 128.4 (C-arom), 128.2 (C-arom), 128.2 (C-arom), 128.0 (C-arom), 127.9 (C-arom), 127.8 (C-arom), 127.7 (C-arom), 127.7 (C-arom), 127.6 (C-arom), 127.6 (C-arom), 127.4 (C-arom), 127.3 (C-arom), 126.2 (C-arom), 126.0 (C-arom), 125.9 (C-arom), 125.6 (C-arom), 84.5 (C-3), 78.4 (C-4), 78.2 (C-1), 75.6 (C-2), 75.4 (CH_2-Bn), 73.8 (CH_2-Bn), 73.2 (CH_2-Bn), 72.3 (CH_2-Bn), 71.1 (C-6), 70.9 (CH_2-Nap), 39.9 (C-5), 28.4 (C-7). HRMS $[M+Na]^+$: 701.32288 found, 701.32375 calculated.

2,3,4,6-tetra-O-benzyl-7-carba-β-D-mannopyranoside (15).

Fully protected carba-mannoside **28** (505 mg, 0.744 mmol, 1 eq) was dissolved in an emulsion of DCM/water 9:1 (7.5 mL). The solution was stirred in the dark and then DDQ (169 mg, 0.744 mmol, 1 eq) was added. After 2 hours the reaction mixture was diluted with DCM and transferred to a separatory funnel. The organic layer was washed (1x) with (1x) a saturated solution of $NaHCO_3$(aq), (1x) with a saturated solution of $Na_2S_2O_3$(aq), and again (1x) a saturated solution of $NaHCO_3$(aq) until both the organic and the water layer turned clear. The organic layer was then washed (1x) with brine, dried over $MgSO_4$, filtered and concentrated *in vacuo*. Compound **15** was obtained after silicagel chro- matography (Pentane/Et_2O 4:1→3:7; DCM loading of crude) as a light-yellow solid (292 mg, 0.542 mmol, 73%). $[\alpha]_D^{20}$= + 10.2 °(c = 0.010, DCM). ^{1}H NMR (400 MHz, $CDCl_3$) δ: 7.43 – 7.19 (m, 20H, H-arom), 5.16 (d, J = 11.7 Hz, 1H, CH_2-Bn), 4.89 (d, J = 10.8 Hz, 1H, CH_2-Bn), 4.75 (s, 2H, CH_2-Bn), 4.65 (d, J = 11.6 Hz, 1H, CH_2-Ph), 4.52 (d, J = 10.9 Hz, 1H, CH_2-Ph), 4.47 (d, J = 3.1 Hz, 2H, CH_2-Ph), 4.05 – 3.98 (m, 1H, H-2), 3.82 (pt, J = 9.8 Hz, 1H, H-4), 3.62 – 3.50 (m, 3H, H-1, H-6), 3.47 (dd, J = 9.4, 2.3 Hz, 1H, H-3), 2.02 (s, 1H, OH), 1.94 – 1.84 (m, 1H, H-7a), 1.78 (pq, J = 12.1 Hz, 1H, H-7b), 1.72

– 1.61 (m, 1H, H-5). ^{13}C-APT NMR (101 MHz, $CDCl_3$) δ: 139.2 (C-arom), 138.9 (C-arom), 138.7 (C-arom), 138.6 (C-arom), 128.6 (C-arom), 128.6 (C-arom), 128.5 (C-arom), 128.2 (C-arom), 128.0 (C-arom), 127.8 (C-arom), 127.8 (C-arom), 127.7 (C-arom), 127.7 (C-arom), 127.6 (C-arom), 127.6 (C-arom), 85.0 (C-3), 79.4 (C-2), 78.0 (C-4), 75.3 (CH_2-Bn), 74.6 (CH_2-Bn), 73.1 (CH_2-Bn), 73.0 (CH_2-Bn), 70.6 (C-6), 69.6 (C-1), 39.5 (C-5), 32.2 (C-7). HRMS $[M+Na]^+$: 561.26071 found, 561.26115 calculated.

1-O-([N,N-diisopropylamino]-2-O-benzyl-phosphite)-2,3,4,6-tetra-O-benzyl-7-carba-β-D-mannopyranoside (16).

Carba-mannoside **15** (182.4 mg, 0.339 mmol, 1eq) was co-evaporated (2x) with toluene, dissolved in dry DCM (2 ml). DIPEA (0.089 mL, 0.51 mmol, 1.5 eq) and activated 4Å molecular sieves were added and the solution was stirred for 15 minutes under an Argon atmosphere. Then 2-cyanoethyl N,N-diisopropylchlorophosphoramidite (0.406 mmol, 0.091 mL, 1.2 eq) was added to the solution. After stirring for 45 minutes, the reaction was quenched with the addition of water. The following workup and purification were performed as quickly as possible: the reaction mixture was diluted in DCM and transferred to a separatory funnel. The organic layer was washed (1x) with a mixture containing a saturated solution of $NaHCO_3$(aq) and brine 1:1. The organic layer was then dried over Na_2SO_4, filtered and concentrated *in vacuo*. Compound **16** was obtained after silicagel chromatography (Pentane/Et_2O 9:1→1:1; DCM loading of crude; silica was neutralized with Et_3N) as a colorless syrup (170 mg, 0.229 mmol, 68%). ^{1}H NMR (500 MHz, CD_3CN) δ: 7.59 – 7.07 (m, 20H, H-arom), 4.99 – 4.79 (m, 3H, CH_2-Bn), 4.78 – 4.68 (m, 1H, CH_2-Bn), 4.67 – 4.59 (m, 1H, CH_2-Bn), 4.53 – 4.41 (m, 3H, CH_2-Bn), 4.20 (pd, J = 70.87 Hz, 1H, H-2), 4.01 – 3.87 (m, 1H, H-1), 3.87 – 3.59 (m, 5H, CH-N, H-4, OCH_2), 3.59 – 3.48 (m, 3H, H-3, H-6), 2.73 – 2.59 (m, 2H, CH_2CN), 2.05 (pq, J = 12.5 Hz, 1H, H-7a), 1.99 – 1.81 (m, 1H, H-7b), 1.73 – 1.61 (m, 1H, H-5), 1.28 – 1.11 (m, 12H, CH_3). ^{31}P-NMR (202 MHz, CD_3CN) δ: 147.49, 148.66.

2,3,4,6-tetra-O-benzyl-7-carba-β-D-mannopyranosyl-1-(2-O-cyanoethylphosphate)-(4S,8S,12S,16S,20S)-4,8,12,16,20- pentamethylheptacosyl (29).

Lipid **4** (46.3 mg, 0.099 mmol, 1 eq) was co-evaporated (3x) with toluene and then dissolved in a 0.25 M solution of DCI in acetonitrile (0.60 mL, 0.15 mmol, 1.5 eq). Then an additional portion of dry acetonitrile (0.6 mL) was added to dissolve the lipid. 4Å Molecular sieves were added and the solution was stirred for 15 minutes under an Argon atmosphere. A 0.1 M solution of phosphoramidite **16** (2.2 mL, 0.22 mmol, 2.2 eq) in dry acetonitrile was then added slowly to the reaction mixture. The reaction mixture was stirred for 3 hours and upon complete coupling, a 0.25 M solution of CSO (1.2 mL, 0.31 mmol, 3 eq) in dry acetonitrile was added to the reaction mixture. After stirring for 15 minutes, water was added and the reaction mixture was diluted in EtOAc. The organic layer was washed with with a mixture containing a saturated solution of $NaHCO_3$(aq) and brine 1:1 and the water layer was extracted (2x) with EtOAc. The combined organic layers were dried over Na_2SO_4, filtered and concentrated *in vacuo*. Compound **29** was obtained after silicagel chromatography (Pentane/EtOAc 5:1→1:1; DCM loading of crude; silica was neutralized with Et_3N) followed by size exclusion (LH-20, DCM/MeOH, 1/1, v/v) as a colorless syrup (78 mg, 0.070 mmol, 70%). $[\alpha]_D^{20}$ = + 1.2 °(c = 0.005, DCM). ^{1}H NMR (400 MHz, $CDCl_3$) δ: 7.45 – 7.38 (m, 2H, H-arom), 7.36 – 7.25 (m, 16H, H-arom), 7.22 – 7.16 (m, 2H, H-arom), 5.03 – 4.92 (m, 1H, CH_2-Bn), 4.92 – 4.84 (m, 1H, CH_2-Bn), 4.80 (d, J = 12.1 Hz, 1H, CH_2-Bn), 4.74 – 4.61 (m, 2H, CH_2-Bn), 4.53 – 4.42 (m, 3H, CH_2-Bn), 4.42 – 4.33

(m, 1H, H-1), 4.26 – 4.18 (m, 1H, H-2), 4.18 – 4.10 (m, 1H, OCH_2-lipid), 4.10 – 3.95 (m, 3H, OCH_2-lipid, CH-N), 3.90 – 3.78 (m, 1H, H-4), 3.61 – 3.50 (m, 2H, H-6), 3.49 – 3.41 (m, 1H, H-3), 2.67 (t, J = 6.3 Hz, 1H, CH_2CN), 2.61 (td, J = 6.3, 2.7 Hz, 1H, CH_2CN), 2.29 – 2.14 (m, 1H, H-7a), 2.07 – 1.95 (m, 1H, H-7b), 1.76 – 1.55 (m, 3H, H-5, CH_2-lipid), 1.44 – 0.97 (m, 45H, CH_2-lipid, CH-lipid), 0.92 – 0.78 (m, 18H, CH_3-lipid). ^{13}C-APT NMR (101 MHz, $CDCl_3$) δ: 139.3 (C-arom), 139.2 (C-arom), 138.8 (C-arom), 138.6 (C-arom), 138.5 (C-arom), 138.5 (C-arom), 128.5 (C-arom), 128.4 (C-arom), 128.3 (C-arom), 128.2 (C-arom), 127.7 (C-arom), 127.7 (C-arom), 127.7 (C-arom), 127.6 (C-arom), 127.6 (C-arom), 127.6 (C-arom), 127.5 (C-arom), 127.5 (C-arom), 127.4 (C-arom), 127.4 (C-arom), 116.5 (CN), 116.4 (CN'), 84.0 (C-3), 77.6, 77.6, 77.5, 77.5, 77.4, 77.4, 77.3, 77.2, 77.1, 75.4 (CH_2-Bn), 74.6 (CH_2-Bn), 74.5 (CH_2-Bn'), 73.1 (CH_2-Bn), 72.6 (CH_2-Bn), 72.6 (CH_2-Bn'), 70.3 (C-6), 69.1 (d, J = 2.69 Hz, OCH_2-lipid), 69.0 (d, J = 2.61 Hz, OCH_2'-lipid), 61.7 (pt, J = 5.56 Hz, OCH_2-cyanoethyl), 39.2 (CH_2-lipid), 37.6, 37.5, 37.4, 37.2, 32.9 (CH-lipid), 32.9 (CH-lipid), 32.9 (CH-lipid), 32.7, 32.6 (CH-lipid), 32.6 (CH-lipid), 32.1, 30.1, 29.6, 29.5, 28.01 (d, J = 3.50 Hz, C-10, one diastereoisomer), 27.9 (d, J = 3.16 Hz, C-10, one diastereoisomer), 27.2, 24.6, 24.6, 22.8, 19.9 (CH_3-lipid), 19.9 (CH_3-lipid), 19.9 (CH_3-lipid), 19.7 (d, J = 1.15 Hz, CH_2CN), 19.7 (d, J = 1.36 Hz, CH_2CN'), 19.6 (CH_3-lipid), 19.6 (CH_3-lipid), 14.3 (CH_3-lipid). ^{31}P-NMR (162 MHz, $CDCl_3$) δ: -1.70, -1.65. HRMS $[M+Na]^+$: 1142.75454 found, 1142.75483 calculated.

Sodium 2,3,4,6-tetra-O-benzyl-7-carba-β-D-mannopyranosyl-1-phosphoryl-(4S,8S,12S,16S,20S)-4,8,12,16,20-pentamethylheptacosyl (30).

Cyanoethyl protected **29** (36.1 mg, 0.031 mmol, 1 eq) was co-evaporated (2x) with toluene and dissolved in dry acetonitrile (3 mL). The reaction was cooled to 0°C, then Et_3N (0.36 mL, 2.6 mmol, 80 eq) was added and the reaction was stirred at RT for 5 days. Upon completion, the reaction mixture was diluted in dry distilled toluene and concentrated. Purification by size exclusion chromatography (LH-20, DCM/MeOH, 1/1, v/v) yielded the triethylammonium salt of the product. The triethylammonium salt was converted to the sodium salt by dissolving it in MeOH and passing through a small reaction syringe containing amberlite Na^+. Compound **30** was obtained after concentration of the eluate as a colorless oil (25,8 mg, 0.024 mmol, 74%). $[a]_D^{20}$= - 1.4 °(c = 0.008, DCM). ^{1}H NMR (400 MHz, $CDCl_3$) δ: 7.47 – 7.37 (m, 2H, H-arom), 7.35 – 7.20 (m, 16H, H-arom), 7.20 – 7.13 (m, 2H, H-arom), 4.92 – 4.80 (m, 3H, CH_2-Bn), 4.58 (pq, J = 11.7 Hz, 2H, CH_2-Bn), 4.49 – 4.36 (m, 3H, CH_2-Bn), 4.34 – 4.25 (m, 1H, H-1), 4.25 – 4.19 (m, 1H, H-2), 3.93 (pq, J = 6.7 Hz, 2H, OCH_2-lipid), 3.87 – 3.75 (m, 1H, H-4), 3.58 – 3.45 (m, 2H, H-6), 3.40 (dd, J = 9.4, 2.4 Hz, 1H, H-3), 2.20 (pq, J = 12.6 Hz, 1H, H-7a), 2.04 (dt, J = 12.7, 4.5 Hz, 1H, H-7b), 1.73 – 1.48 (m, 3H, H-5, CH_2-lipid), 1.46 – 0.95 (m, 45H, CH_2-lipid, CH-lipid), 0.93 – 0.75 (m, 18H, CH_3-lipid). ^{13}C-APT NMR (101 MHz, $CDCl_3$) δ: 139.3 (C-arom), 138.9 (C-arom), 138.6 (C-arom), 138.6 (C-arom), 128.5 (C-arom), 128.5 (C-arom), 128.4 (C-arom), 128.3 (C-arom), 128.2 (C-arom), 127.7 (C-arom), 127.6 (C-arom), 127.6 (C-arom), 127.4 (C-arom), 84.0 (C-3), 77.2 (C-4), 77.2 (C-2), 76.9 (C-1), 75.3 (CH_2-Bn), 74.7 (CH_2- Bn), 73.1 (CH_2-Bn), 72.3 (CH_2-Bn), 70.4 (C-6), 68.3 (d, J = 5.46 Hz, OCH_2-lipid), 39.3 (C-5), 37.6 (CH_2-lipid), 37.6 (CH_2-lipid), 37.5 (CH_2-lipid), 37.2 (CH_2-lipid), 33.0 (CH-lipid), 33.0 (CH-lipid), 33.0 (CH-lipid), 32.9 (CH-lipid), 32.9 (CH_2-lipid), 32.7 (CH-lipid), 32.1 (CH_2-lipid), 30.2 (CH_2-lipid), 29.9 (CH_2-lipid), 29.6 (C-7), 28.0 (d, J = 7.42 Hz, CH_2-lipid), 27.2 (CH_2-lipid), 24.6 (CH_2-lipid), 24.6 (CH_2-lipid), 22.9 (CH_2-lipid), 20.0 (CH_3-lipid), 19.9 (CH_3-lipid), 19.9 (CH_3-lipid), 19.6 (CH_3-lipid), 14.3 (CH_3-lipid). ^{31}P-NMR (162 MHz, $CDCl_3$) δ: 1.04. HRMS $[M+Na]^+$: 1088.72064 found, 1088.72045 calculated.

Sodium 7-carba-β-D-mannopyranosyl-1-phosphoryl-(4S,8S,12S,16S,20S)-4,8,12,16,20-pentamethylheptacosyl (1).

Benzyl protected **30** (25.6 mg, 0.024 mol, 1 eq) was dissolved in a mixture of $CHCl_3$:MeOH (1:1, v:v, 2.4 mL) and the solution was purged and bubbled through with a flow of Argon. Then Pd/C (12 mg) was added and the solution was purged and bubbled through with Argon once more. The suspension was bubbled through with Hydrogen and subsequently stirred vigorously under a Hydrogen atmosphere. After 6 hours, the reaction mixture was purged of Hydrogen and filtered over a celite pad. The filtrate was concentrated and suspended in acetone. The suspension was filtered over another celite pad. The product was then eluted by washing the celite pad with a mixture of $CHCl_3$/MeOH/water 9.5:9.5:1 and the filtrate was concentrated *in vacuo*. Compound **1** was obtained after size exclusion chromatography (LH-20, DCM/MeOH, 1/1, v/v) as a white solid (8.0 mg, 0.024 mmol, 47%). $[a]_D^{20}$= + 6.0 °(c = 0.003, DCM). ^{1}H NMR (500 MHz, $CDCl_3$/MeOD/D_2O 95:95:10) δ: 4.26 – 4.10 (m, 2H, H-1, H-2), 3.92 – 3.78 (m, 2H, OCH_2-lipid), 3.77 – 3.65 (m, 2H, H-6), 3.65 – 3.56 (m, 1H, H-4), 3.45 – 3.38 (m, 1H, H-3), 1.88 – 1.70 (m, 2H, H-7), 1.70 – 1.57 (m, 2H, CH_2-lipid), 1.57 – 1.48 (m, 1H, H-5), 1.48 – 1.16 (m, 36H, CH_2-lipid, CH-lipid), 1.16 – 1.01 (m, 9H, CH_2-lipid, CH-lipid), 0.97 – 0.78 (m, 18H, CH_3-lipid). ^{13}C-APT NMR (126 MHz, $CDCl_3$/MeOD/D_2O 95:95:10) δ: 74.0 (C-3), 73.3 (d, J = 5.76 Hz, C-1), 72.0 (d, J = 3.12 Hz, C-2), 70.4 (C-4), 65.6 (d, J = 5.52 Hz, OCH_2-lipid), 63.1 (C-6), 40.1 (C-5), 36.9 (CH_2-lipid), 36.8 (CH_2-lipid), 36.8 (CH_2-lipid), 36.7 (CH_2-lipid), 36.4 (CH_2-lipid), 32.6 (CH_2-lipid), 32.3 (CH-lipid), 32.2 (CH-lipid), 32.2 (CH-lipid), 32.1 (CH-lipid), 31.4 (CH_2-lipid), 29.4 (CH_2-lipid), 29.0 (CH_2-lipid), 28.8 (CH_2-lipid), 27.9 (CH_2-lipid), 27.8 (C8), 27.6 (C-7), 26.5 (CH_2-lipid), 23.9 (CH_2-lipid), 23.9 (CH_2-lipid), 23.8 (CH_2-lipid), 22.1 (CH_2-lipid), 19.1 (CH_3-lipid), 19.0 (CH_3-lipid), 18.9 (CH_3-lipid), 18.7 (CH_3-lipid), 13.2 (CH_3-lipid). ^{31}P-Hdec NMR (202 MHz, $CDCl_3$/MeOD/D_2O 95:95:10) δ: 1.28. HRMS $[M+H]^+$: 707.55744 found, 707.55413 calculated.

Mannose-1-C-phosphonate mycoketide

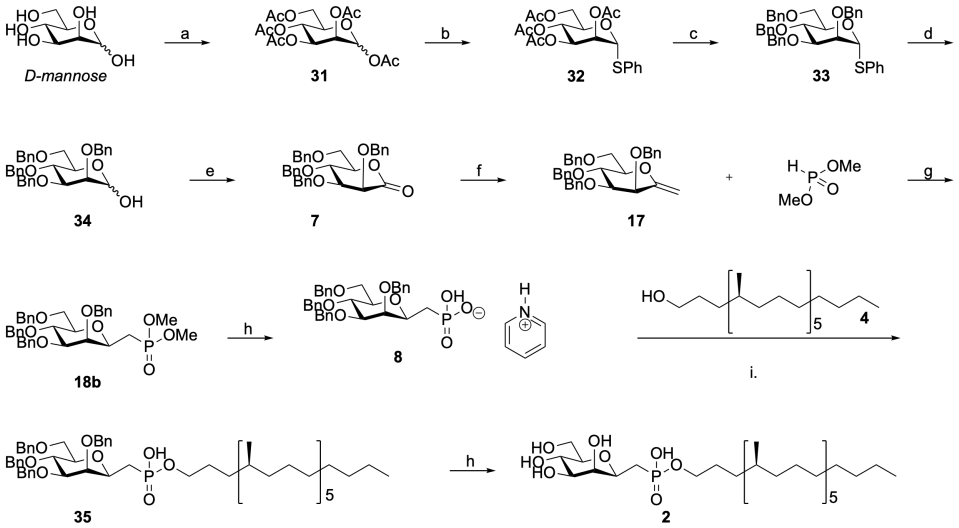

S2 Figure - Synthetic scheme for the generation of C-mannoside 2. a) Ac_2O, pyridine, 77%, b) PhSH, $BF_3{\cdot}Et_2O$, DCM, 74%, c) i. NaOMe, MeOH, ii. BnBr, NaH, TBAI, DMF, 96%, d) NBS, acetone/H_2O 9:1, 30°C quant., e) DMSO, Ac_2O, 77%, f) Cp_2TiMe_2, toluene, 60°C, 79%, g) $(MeO)_2P(=O)H$, DPAP, neat, hν = 375 nm, 59%, h) TMSBr, pyridine, CH_3CN, 85%, i) iPr$_3$PhSO$_2$Cl, pyridine, 50°C, 50%, j) Pd/C, H_2, THF/H_2O (1:1, v/v), 80%.

1,2,3,4,6-penta-O-acetyl-D-mannopyranoside (31).

D(+)-mannose (27.02 g, 150 mmol, 1 eq) was dissolved in pyridine (250 ml). The solution was cooled to 0°C and then Ac_2O (102 ml, 1.08 mol, 7.2 eq) was added. The reaction mixture was stirred at RT overnight. The reaction was quenched with the addition of MeOH, diluted with Et_2O and transferred to a separatory funnel. The organic layer was washed (2x) with a 1 M HCl solution, (1x) with brine, dried over $MgSO_4$, filtered and concentrated *in vacuo*. Compound **31** was obtained as a yellow syrup (45.38 g, 116.3 mmol, 77%) without any further purification. NMR analysis confirmed purity of the product, whose ^{1}H NMR and ^{13}C NMR spectra were in agreement with published literature.[35]

1-thiophenyl-2,3,4,6-tetra-O-acetyl-α-D-mannopyranoside (32).

Compound **31** (45.3 g, 116 mmol, 1 eq) was co-evaporated (3x) with toluene and dissolved in dry DCM (130 ml). Then thiophenol (18 ml, 175 mmol, 1.5 eq) was added and the solution was cooled to 0°C. $BF_3{\cdot}Et_2O$ (72 ml, 581 mmol, 5 eq) was added via dropping funnel and the reaction mixture was stirred overnight at RT. Et_3N (80 ml, 581 mmol, 5 eq) and a saturated solution of $NaHCO_3$ were subsequently added before transferring the mixture to a separatory funnel. The water layer was extracted (2x) with DCM and the combined organic layers were dried with $MgSO_4$, filtered and concentrated *in vacuo*. Compound **32** was obtained after crystallization from Et_2O as a white crystal (37.87 g, 86 mmol, 74%). NMR analysis confirmed

purity of the product, whose ^{1}H NMR and ^{13}C NMR spectra were in agreement with published literature.[36]

1-thiophenyl-2,3,4,6-tetra-O-benzyl-α-D-mannopyranoside (33).

Compound **32** (22 g, 50 mmol, 1 eq) was dissolved in dry MeOH and cooled to 0°C. NaOMe (1.62 g, 30 mmol, 0.6 eq) was added to the solution, which was gradually warmed up to RT and stirred for 2 hours. The reaction mixture was then diluted with MeOH, quenched with amberlite H^+ until neutral pH, filtered and concentrated. The crude was dissolved in dry DMF (370 ml) and the solution was cooled to 0°C. After the careful addition of NaH (60% in oil) (12 g, 300 mmol, 6 eq), the reaction mixture was stirred for 2 hours. Benzyl bromide (35.7 ml, 300 mmol, 6 eq) and TBAI (1.55 g, 6.6 mmol, 0.13 eq) were added and the reaction mixture was stirred overnight at RT. The reaction was then quenched with MeOH and diluted with Et_2O and water and transferred to a separatory funnel. The water layer was extracted (4x) with Et_2O, the combined organic layers were washed (1x) with brine, dried over $MgSO_4$, filtered and concentrated *in vacuo*. Compound **33** was obtained after silicagel chromatography (Pentane/EtOAc 20:1→9:1; DCM loading of crude) as a white solid (30.36 g, 48 mmol, 96%). NMR analysis confirmed purity of the product, whose ^{1}H NMR and ^{13}C NMR spectra were in agreement with published literature.[37]

2,3,4,6-tetra-O-benzyl-D-mannopyranoside (34).

Compound **33** (30.36 g, 48 mmol, 1 eq) was dissolved in a mixture of acetone/water 9:1 (800 ml) and cooled to 0°C. NBS (25 g, 140 mmol, 2.9 eq) was added and the reaction mixture was stirred for 4 hours at room temperature. The reaction mixture was diluted with water and Et_2O and transferred to a separatory funnel. The water layer was extracted (3x) with Et_2O and the combined organic layers were washed (1x) with a saturated solution of $NaHCO_3$ and (1x) with brine. The organic layer was then dried over Na_2SO_4, filtered and concentrated *in vacuo*. Compound **34** was obtained after silicagel chromatography (Petroleum ether/EtOAc 9:1→1:1; DCM loading of crude) as a colorless oil (26 g, 48 mmol, quant). NMR analysis confirmed purity of the product, whose ^{1}H NMR and ^{13}C NMR spectra were in agreement with published literature.[38]

1-one-2,3,4,6-tetra-O-benzyl-D-mannopyranoside (7).

Compound **34** (23.34 g, 43 mmol, 1 eq) was dissolved in dry DMSO (430 ml) and heated to 30°C. Then Ac_2O (81 ml, 860 mmol, 20 eq) was added and the reaction mixture was stirred overnight at 30°C. The reaction mixture was diluted with water and Et_2O and transferred to a separatory funnel. The water layer was extracted (4x) with Et_2O and the combined organic phases dried over dried over $MgSO_4$, filtered and concentrated *in vacuo*. Compound **7** was obtained after crystallization from Et_2O/pentane as a white crystal (17.85 g, 33 mmol, 77%). NMR analysis confirmed purity of the product, whose ^{1}H NMR and ^{13}C NMR spectra were in agreement with published literature.[39]

2,3,4,6-tetra-O-benzyl-1-deoxy-D-manno-hept-1-enitol (17).

Compound **7** (2.6 g, 4.8 mmol, 1 eq) was co-evaporated (2x) with toluene and dissolved in toluene (24 ml). After protecting the reaction vessel from light, a 5% solution of dimethyltitanocene (44 ml, 9.4 mmol, 1.95 eq) in THF/toluene was added, the reaction

mixture was heated to 60°C and stirred overnight. Since the reaction was not complete, an additional portion of dimethyltitanocene (20 ml, 4.6 mmol, 0.96 eq) was added and the reaction mixture stirred for an additional day. At this point the volatiles were removed *in vacuo*. Compound **17** was obtained after silicagel chromatography (Pentane/Et_2O 24:1→6:1; DCM loading of crude) as a colorless oil (2.03 g, 3.8 mmol, 79%). NMR analysis confirmed purity of the product, whose ^1H NMR and ^{13}C NMR spectra were in agreement with published literature.[40]

Dimethyl 2,3,4,6-tetra-O-benzyl-β-D-manno-heptulopyranose-1- phosphonate (18b).

Focused UV irradiation: A mixture of compound **17** (139 mg, 0.25 mmol, 1 eq), 2,2-dimethoxy-2-phenylacetophenone (27 mg, 0.13 mmol, 0.5 eq) and dimethyl phosphite (2.3 ml, 25 mmol, 100 eq) was stirred and irradiated for 3 hours and 30 minutes using UV light (375 nm). Volatiles were removed *in vacuo*. Compound **18b** was obtained after silicagel chromatography (DCM/acetone 15:1→8:2; DCM/acetone loading of crude) as a colorless oil (385 mg, 0.59 mmol, 59%).

Unfocused sunlight:

A mixture of compound **17** (47 mg, 0.08 mmol, 1 eq), 2,2-dimethoxy-2-phenylacetophenone (10 mg, 0.04 mmol, 0.5 eq) and dimethyl phosphite (0.7 ml, 8 mmol, 100 eq) was stirred for 1 day at RT in the absence of additional UV irradiation. Volatiles were removed *in vacuo*. Compound **18b** was obtained after silicagel chromatography (DCM/acetone 15:1→8:2; DCM/acetone loading of crude) as a colorless oil (22 mg, 0.034 mmol, 43%). ^1H NMR (300 MHz, $CDCl_3$) δ: 7.39 – 7.15 (m, 20H, H-arom), 5.07 (d, J = 11.5 Hz, 1H, CH_2-Bn), 4.87 (d, J = 10.8 Hz, 1H, CH_2-Bn), 4.84 – 4.71 (m, 2H, CH_2-Bn), 4.67 (d, J = 11.5 Hz, 1H, CH_2-Bn), 4.62 – 4.45 (m, 4H, CH_2-Bn), 3.95 – 3.84 (m, 2H, H-4, H-2), 3.84 – 3.71 (m, 2H, H-1, H-3), 3.71 – 3.56 (m, 8H, CH_3-O, H-6), 3.50 (ddd, J = 9.8, 5.1, 2.4 Hz, 1H, H-5), 2.21 (ddd, J = 18.1, 15.4, 6.9 Hz, 1H, CH_2-P), 1.98 (ddd, J = 18.3, 15.4, 6.1 Hz, 1H, CH_2-P). ^{13}C-APT NMR (101 MHz, $CDCl_3$) δ: 138.7 (C-arom), 138.4 (C-arom), 128.6 (C-arom), 128.5 (C-arom), 128.4 (C-arom), 128.4 (C-arom), 128.3 (C-arom), 128.2 (C-arom), 128.0 (C-arom), 127.9 (C-arom), 127.8 (C-arom), 127.7 (C-arom), 127.7 (C-arom), 85.0 (C-3), 79.6 (C-5), 75.94 (d, J = 8.3 Hz, C-2), 75.3 (CH_2-Bn), 75.0 (C-4), 74.7 (CH_2-Bn), 73.5 (CH_2-Bn), 73.4 (C-1), 72.8 (CH_2-Bn), 69.6 (C-6), 52.57 (d, J = 74.0 Hz, CH_3-O), 27.76 (d, J = 140.8 Hz, CH_2-P). ^{31}P-Hdec NMR (121 MHz, $CDCl_3$) δ: 30.7. HRMS $[M+H]^+$: 647.2794 found, 647.2768 calculated.

2,3,4,6-tetra-O-benzyl-β-D-manno-heptulopyranose-1- benzyl ketone (18a).

^1H NMR (300 MHz, $CDCl_3$) δ: 7.88 – 7.78 (m, 2H, H-arom), 7.62 – 7.50 (m, 1H, H-arom), 7.47 – 7.02 (m, 22H, H-arom), 4.99 (d, J = 11.8 Hz, 1H, CH_2-Bn), 4.94 – 4.71 (m, 3H, CH_2-Bn), 4.63 – 4.46 (m, 4H, CH_2-Bn), 4.07 – 3.98 (m, 2H, H-3, H-1), 3.93 (t, J = 9.5 Hz, 1H, H-4), 3.80 – 3.73 (m, 1H, H-2), 3.73 – 3.62 (m, 2H, H-6), 3.51 (ddd, J = 9.7, 5.3, 2.1 Hz, 1H, H-5), 3.28 (dd, J = 6.3, 4.1 Hz, 2H, CH_2-C=O). ^{13}C-bbdec NMR (75 MHz, $CDCl_3$) δ: 138.5 (C-arom), 133.4 (C-arom), 128.6 (C-arom), 128.5 (C-arom), 128.5 (C-arom), 128.4 (C-arom), 128.4 (C-arom), 128.3 (C-arom), 128.2 (C-arom), 128.1 (C-arom), 127.8 (C-arom), 127.7 (C-arom), 127.6 (C-arom), 85.3, 79.8, 75.4, 74.6, 74.5, 74.5, 73.6, 72.7, 69.7 (C-6), 40.0 (CH_2-C=O).

Pyridinium 2,3,4,6-tetra-O-benzyl-β-D-manno-heptulopyranose-1-phosphonate (8).

Compound **18b** (385 mg, 0.59 mmol, 1 eq) was co-evaporated (3x) with toluene, dissolved in dry CH_3CN (39 ml) and cooled to 0°C. A glass stopper was used to seal the reaction vessel and a glass covered stirring rod was used to stir the reaction. Pyridine (0.55 ml, 6.8 mmol, 11.5 eq) and TMSBr (1.56 ml, 11.8 mmol, 20 eq) were added dropwise via syringe. The reaction was heated up to RT and stirred for 2 hours. Volatiles were removed *in vacuo*, with water bath temperature of 15°C under fume hood. Ice cold milli-q water and acetonitrile were added and after stirring the mixture for 20 minutes, the volatiles were removed *in vacuo*. Compound **8** was obtained as a white solid (349 mg, 0.5 mmol, 85%) without any further purification. ^{1}H NMR (400 MHz, MeOD/$CDCl_3$ 3:1) δ: 8.81 – 8.62 (m, 6H, H-pyr), 8.48 – 8.36 (m, 3H, H-pyr), 7.97 – 7.81 (m, 7H, H-pyr), 7.29 – 7.06 (m, 20H, H-arom), 4.91 (d, J = 10.6 Hz, 1H, CH_2-Bn), 4.76 (d, J = 11.3 Hz, 2H, CH_2-Bn), 4.61 (d, J = 11.1 Hz, 2H, CH_2-Bn), 4.48 (d, J = 10.9 Hz, 1H, CH_2-Bn), 4.35 – 4.26 (m, 2H, CH_2-Bn), 4.11 (d, J = 2.7 Hz, 1H, H-2), 3.90 – 3.77 (m, 2H, H-4, H-1), 3.68 (dd, J = 9.5, 2.8 Hz, 1H, H-3), 3.60 (dd (2X), J = 10.8, 3.1 Hz, 2H, H-6), 3.37 (ddd, J = 9.7, 4.3, 2.0 Hz, 1H, H-5), 2.09 (ddd (2X), J = 15.1, 11.0, 7.5 Hz, 2H, CH_2-P). ^{13}C-APT NMR (101 MHz, MeOD) δ: 148.1 (C-arom), 143.3 (C-arom), 140.3 (C-arom), 139.9 (C-arom), 139.9 (C-arom), 139.4 (C-arom), 130.8 (C-arom), 129.5 (C-arom), 129.5 (C-arom), 129.5 (C-arom), 129.4 (C-arom), 129.4 (C-arom), 129.4 (C-arom), 129.4 (C-arom), 129.3 (C-arom), 129.3 (C-arom), 129.2 (C-arom), 129.0 (C-arom), 128.9 (C-arom), 128.8 (C-arom), 128.8 (C-arom), 128.8 (C-arom), 128.8 (C-arom), 86.0 (C-3), 80.5 (C-5), 77.70 (d, J = 7.3 Hz, C-2), 76.3 (CH_2-Bn), 76.1 (CH_2-Bn), 75.9 (C-4), 75.5 (C-1), 74.5 (CH_2-Bn), 73.3 (CH_2-Bn), 70.6 (C-6), 31.00 (d, J = 137.6 Hz, CH_2-P). 31P-Hdec NMR (202 MHz, MeOD) δ: 26.5. HRMS $[M+H]^+$: 619.2466 found, 619.2455 calculated.

1-phosphoryl-(4S,8S,12S,16S,20S)-4,8,12,16,20-pentamethylheptacosyl-2,3,4,6-tetra-O-benzyl-β-D-manno- heptulopyranose (35).

Compound **8** (100 mg, 0.1 mmol, 2 eq) and lipid 10 (20 mg, 0.04 mmol, 1 eq) were co-evaporated (2x) in toluene and dissolved in dry pyridine (1.4 ml). TIPPSCl (45 mg, 0.15 mmol, 3 eq) was added and the reaction mixture was stirred at 50°C overnight. The reaction was quenched with milli-q water and stirred for 2 hours, then EtOAc was added and the reaction mixture was transferred to a separatory funnel. The water layer was extracted (1x) with EtOAc and (2x) with DCM, dried over Na_2SO_4 and concentrated *in vacuo*. Compound **35** was obtained after silicagel chromatography (DCM/MeOH 20:1→1:1; DCM/MeOH loading of crude; ultrapure silica) and size exclusion (LH-20, DCM/MeOH, 1/1, v/v) as a colorless oil (20 mg, 0.02 mmol, 50%). The pyridinium salt was converted to the sodium salt by dissolving the product in MeOH and treating it with amberlite Na^+. ^{1}H NMR (600 MHz, $CDCl_3$/MeOD 9:1) δ: 7.38 – 7.21 (m, 18H, H-arom), 7.10 – 6.97 (m, 2H, H-arom), 4.98 (d, J = 11.1 Hz, 1H, CH_2-Bn), 4.83 – 4.72 (m, 2H, CH_2-Bn), 4.70 (d, J = 11.6 Hz, 1H, CH_2-Bn), 4.63 (d, J = 11.1 Hz, 1H, CH_2-Bn), 4.60 – 4.47 (m, 2H, CH_2-Bn), 4.36 (d, J = 10.8 Hz, 1H, CH_2-Bn), 3.85 – 3.77 (m, 2H, H-1, H-2), 3.77 – 3.67 (m, 3H, CH_2-O, H-6a), 3.66 – 3.55 (m, 2H, H-3, H-4), 3.55 – 3.45 (m, 2H, H-6b, H-5), 2.09 – 1.94 (m, 2H, CH_2-P), 1.65 – 1.47 (m, 3H, CH_2-lipid, CH-lipid), 1.37 – 1.17 (m, 33H, CH_2-lipid, CH-lipid), 1.10 – 1.01 (m, 9H, CH_2-lipid, CH-lipid), 0.88 (t, J = 7.0 Hz, 3H, CH_3-lipid), 0.86 – 0.76 (m, 15H, CH_3-lipid). ^{13}C-APT NMR (151 MHz, $CDCl_3$/MeOD 9:1) δ: 138.2 (C-arom), 138.1 (C-arom), 138.0 (C-arom), 137.9 (C-arom), 137.8 (C-arom), 137.0 (C-arom), 128.6 (C-arom), 128.5 (C-arom), 128.5 (C-arom), 128.4 (C-arom), 128.4 (C-arom), 128.4 (C-arom), 128.3 (C-arom), 128.3 (C-arom), 128.2 (C-arom), 128.1 (C-arom), 128.0 (C-arom), 128.0 (C-arom),

127.9 (C-arom), 127.9 (C-arom), 127.8 (C-arom), 127.8 (C-arom), 127.8 (C-arom), 127.7 (C-arom), 127.7 (C-arom), 84.5 (C-3), 78.1 (C-5), 77.3 (C-2), 75.2 (CH_2-Bn), 75.2 (CH_2-Bn), 75.0 (C-1), 74.8 (C-4), 72.9 (CH_2-Bn), 72.5 (CH_2-Bn), 68.6 (C-6), 64.8 (CH_2-O), 37.5 (CH_2-lipid), 37.5 (CH_2-lipid), 37.5 (CH_2-lipid), 37.5 (CH_2-lipid), 37.4 (CH_2-lipid), 37.4 (CH_2-lipid), 37.4 (CH_2-lipid), 37.1 (CH_2-lipid), 33.2 (CH_2-lipid), 32.9 (CH-lipid), 32.9 (CH-lipid), 32.8 (CH-lipid), 32.8 (CH-lipid), 32.8 (CH_3-lipid), 32.0 (CH_2-lipid), 30.0 (CH_2-P), 29.7 (CH_2-lipid), 29.5 (CH_2-lipid), 29.5 (CH_2-lipid), 29.4 (CH_2-P), 29.1 (CH_2-lipid), 28.9 (CH_2-lipid), 28.8 (CH_2-lipid), 28.7 (CH_2-lipid), 28.6 (CH_2-lipid), 28.2 (CH_2-lipid), 27.1 (CH_2-lipid), 24.6 (CH_2-lipid), 24.5 (CH_2-lipid), 24.5 (CH_2-lipid), 24.5 (CH_2-lipid), 22.7 (CH_2-lipid), 19.8 (CH_3-lipid), 19.8 (CH_3-lipid), 19.7 (CH_3-lipid), 19.5 (CH_3-lipid), 19.5 (CH_3-lipid), 14.1 (CH_3-lipid). ^{31}P-Hdec NMR (162 MHz, $CDCl_3$/MeOD 9:1) δ: 25.6, 24.9. HRMS $[M+H]^+$: 1067.74611 found, 1067.74633 calculated.

1-phosphoryl-(4S,8S,12S,16S,20S)-4,8,12,16,20-pentamethylheptacosyl-β-D-manno-heptulopyranose (2).

Compound **35** (20 mg, 0.02 mmol, 1 eq) was dissolved in a mixture of THF/H_2O 1:1 and the solution was purged and bubbled through with a flow of Argon. Then Pd/C (10 mg) was added and the solution was purged and bubbled through with Argon once more. The suspension was bubbled through with Hydrogen and subsequently stirred vigorously under a Hydrogen atmosphere. After 16 hours, the reaction mixture was purged of Hydrogen and filtered over a Whatman filter. Compound **2** was obtained after *in vacuo* removal of volatiles as an amorphous solid (12 mg, 0.016 mmol, 80%). ^{1}H NMR (850 MHz, $CDCl_3$/MeOD/D_2O 95:95:10) δ: 3.91 (d, J = 2.5 Hz, 1H, H-2), 3.88 – 3.78 (m, 4H, H-6a, CH_2-O, H-1), 3.71 (dd, J = 12.0, 5.6 Hz, 1H, H-6b), 3.60 – 3.53 (m, 2H, H-3, H-4), 3.28 (ddt, J = 8.0, 5.6, 2.3 Hz, 1H, H-5), 2.01 – 1.96 (m, 1H, CH_2-P), 1.95 – 1.92 (m, 1H, CH_2-P), 1.69 – 1.56 (m, 4H, CH_2-lipid), 1.43 – 1.15 (m, 43H, CH_2-lipid, CH-lipid), 1.12 – 1.04 (m, 8H, CH_2-lipid), 0.92 – 0.81 (m, 18H, CH_3-lipid). ^{13}C-APT NMR (214 MHz, $CDCl_3$/MeOD/D_2O 95:95:10) δ: 79.8 (C-5), 74.4 (C-1), 74.3 (C-3), 71.19 (d, J = 7.5 Hz, C-2), 66.7 (C-4), 64.32 (d, J = 5.6 Hz, CH_2-O), 60.9 (C-6), 37.0 (CH_2-lipid), 36.9 (CH_2-lipid), 36.9 (CH_2-lipid), 36.9 (CH_2-lipid), 36.9 (CH_2-lipid), 36.8 (CH_2-lipid), 36.8 (CH_2- lipid), 36.5 (CH_2-lipid), 32.7 (CH_2-lipid), 32.3 (CH-lipid), 32.3 (CH-lipid), 32.3 (CH-lipid), 32.2 (CH-lipid), 32.2 (CH-lipid), 31.4 (CH_2-lipid), 29.4 (CH_2-lipid), 29.2 (CH_2-lipid), 29.2 (CH_2-lipid), 28.9 (CH_2-lipid), 28.8 (CH_2-lipid), 28.2 (CH_2- lipid), 28.1 (CH_2-lipid), 26.5 (CH_2-lipid), 24.0 (CH_2-lipid), 24.0 (CH_2-lipid), 23.9 (CH_2-lipid), 23.9 (CH_2-lipid), 23.1 (CH_2-lipid), 22.2 (CH_2-lipid), 19.2 (CH_3-lipid), 19.1 (CH_3-lipid), 19.1 (CH_3-lipid), 19.0 (CH_3-lipid), 18.8 (CH_3-lipid), 13.3 (CH_3-lipid). ^{31}P-Hdec NMR (202 MHz, $CDCl_3$/MeOD/D_2O 95:95:10) δ: 23.0, 22.5. HRMS $[M+H]^+$: 707.5596 found, 707.5585 calculated.

Mannose-1-C-difluorophosphonate mycoketide

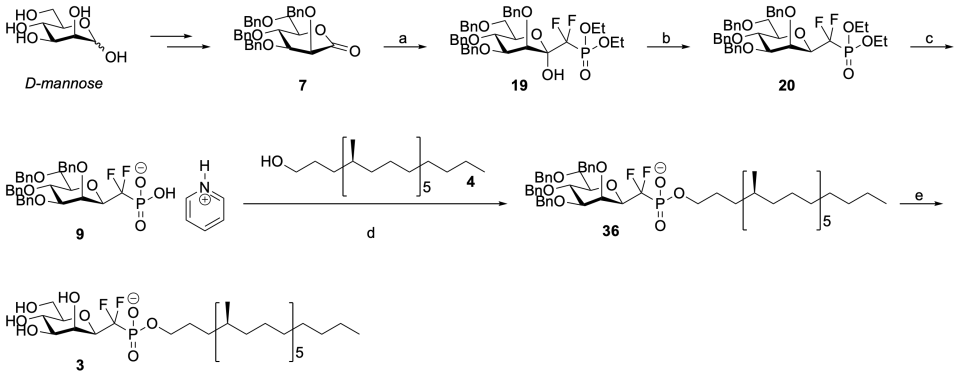

S3 Figure - Synthetic scheme for the generation of difluoro-C-mannoside 3. a) LDA, $(EtO)_2P(=O)CHF_2$, THF, 98%, b) i. $MeO_2CC(=O)Cl$, DCM, ii. AIBN, Bu_3SnH, toluene, 30%, c) TMSBr, pyridine, CH_3CN, quant., d) iPr$_3$PhSO$_2$Cl, toluene:DMF:pyridine (1.25:1:0.5, v/v/v), 50°C, 64%, 6) Pd/C, H_2, THF:H_2O (2:1, v/v), 82%.

Diethyl 1-hydroxy-2,3,4,6-tetra-O-benzyl-β-D-manno-heptulopyranose-1-(difluoro)phosphonate (19).

A solution of DIPA (1.6 ml, 11 mmol, 2 eq) in THF (30 ml) was cooled to -78°C. After the addition of n-BuLi (6.9 ml, 11 mmol, 2 eq) dropwise via syringe, the reaction mixture was rapidly brought to 0°C for 10 minutes and then cooled again to -78°C. A solution of diethyl (difluoromethyl)phosphonate (1.4 ml, 9.3 mmol, 1.7 eq) in THF (10 ml) was cooled to -78°C and added dropwise via cannula to the first solution. After 1 hour and 30 minutes, a solution of lactone **7** (2.96 g, 5.5 mmol, 1 eq) in THF (10 ml) was cooled to -78°C and added dropwise via cannula to the reaction mixture. After 10 minutes from the addition of the last drop of lactone the reaction was stirred for additional 10 minutes with a saturated solution of NH_4Cl(aq) and finally diluted with EtOAc and transferred to a separatory funnel. The water layer was extracted (3x) with EtOAc and the combined organic layers were washed (1x) with water and (1x) with brine, dried over Na_2SO_4 and concentrated *in vacuo*. Compound **19** was obtained after silicagel chromatography (Pentane/EtOAc 10:1→2:1; DCM loading of crude) as a colorless syrup (3.95 g, 5.4 mmol, 98%). ^{1}H NMR (500 MHz, $CDCl_3$) δ: 7.40 – 7.17 (m, 20H, H-arom), 6.00 (s, 1H, -OH), 4.87 (d, J = 10.9 Hz, 1H, CH_2-Bn), 4.82 (d, J = 11.0 Hz, 1H, CH_2-Bn), 4.78 – 4.66 (m, 3H, CH_2-Bn), 4.60 – 4.51 (m, 2H, CH_2-Bn), 4.42 (d, J = 11.8 Hz, 1H, CH_2-Bn), 4.34 – 4.23 (m, 4H, CH_2-O), 4.20 (bs, 1H, H-2), 4.17 – 4.09 (m, 2H, H-3, H-5), 3.99 (t, J = 9.7 Hz, 1H, H-4), 3.79 (dd, J = 11.2, 5.9 Hz, 1H, H-6a), 3.69 (dd, J = 11.4, 1.7 Hz, 1H, H-6b), 1.38 (t, J = 7.1 Hz, 3H, CH_3), 1.17 (t, J = 7.1 Hz, 3H, CH_3). ^{13}C NMR (126 MHz, $CDCl_3$) δ: 138.6 (C-arom), 138.5 (C-arom), 138.4 (C-arom), 138.3 (C-arom), 128.5 (C-arom), 128.4 (C-arom), 128.4 (C-arom), 128.2 (C-arom), 128.1 (C-arom), 128.1 (C-arom), 127.8 (C-arom), 127.7 (C-arom), 127.6 (C-arom), 127.6 (C-arom), 127.6 (C-arom), 127.4 (C-arom), 116.56 (ddd, J = 286.9, 265.2, 194.0 Hz, CF2), 96.61 (ddd, J = 30.6, 19.1, 11.1 Hz, C-1), 81.08 (d, J = 2.6 Hz, C-3), 75.2 (C-2), 75.2

(CH_2-Bn), 74.7 (CH_2-Bn), 74.6 (C-4), 73.1 (CH_2-Bn), 73.1 (C-5), 72.4 (CH_2-Bn), 69.5 (C-6), 65.71 (dd, J = 50.5, 6.3 Hz, CH_2-O), 16.35 (dd, J = 15.2, 5.9 Hz, CH_3). ^{19}F NMR (471 MHz, $CDCl_3$) δ: -118.38 (dd, J = 304.5, 96.1 Hz), -119.83 (dd, J = 304.5, 100.1 Hz). ^{31}P NMR (202 MHz, $CDCl_3$) δ: 8.14 (dd, J = 100.0, 96.0 Hz). HRMS $[M+Na]^+$: 749.26594 found, 749.26615 calculated.

Diethyl 2,3,4,6-tetra-O-benzyl-β-D-manno-heptulopyranose-1-(difluoro)phosphonate (20).

Compound **19** (3.6 g, 5 mmol, 1 eq) was co-evaporated with toluene and dissolved in a dry mixture of DCM/pyridine 5:1 (25 ml) before being cooled to 0°C. Methyl oxalyl chloride (0.92 ml, 10 mmol, 2 eq) was dissolved in DCM (2.5 ml) and slowly added to the first solution via syringe before an extra portion of pyridine was added (2.5 ml). The reaction mixture was warmed up to RT and stirred for 10 minutes before quenching it with EtOH over 10 minutes. Then a saturated solution of $NaHCO_3$ and DCM were used to dilute the reaction mixture before it was transferred to a separatory funnel. The organic layer was concentrated *in vacuo* and the reaction intermediate was dissolved in dry toluene (250 ml) without further purification. This solution was purged and bubbled through with Argon before the addition of Bu_3SnH and AIBN. The reaction mixture was heated up to reflux and stirred overnight. After removal of volatiles *in vacuo*, the crude was purified via silicagel chromatography (Pentane/EtOAc 9:1→3:1), followed by treatment with a 1 M KF(aq) solution and silicagel/KCO_3 9:1 chromatography (Pentane/EtOAc 3:2). Compound **20** was obtained after silicagel chromatography as a colorless syrup (1.05 g, 1.48 mmol, 30% over two steps). ^{1}H NMR (500 MHz, $CDCl_3$) δ: 7.44 – 7.39 (m, 2H, H-arom), 7.35 – 7.23 (m, 16H, H-arom), 7.20 – 7.17 (m, 2H, H-arom), 4.91 – 4.84 (m, 2H, CH_2-Bn), 4.79 (d, J = 11.2 Hz, 1H, CH_2-Bn), 4.70 (d, J = 11.7 Hz, 1H, CH_2-Bn), 4.64 (d, J = 11.8 Hz, 1H, CH_2-Bn), 4.60 – 4.54 (m, 2H, CH_2-Bn), 4.47 (d, J = 11.8 Hz, 1H, CH_2-Bn), 4.30 – 4.18 (m, 5H, CH_2-O, H-2), 3.98 (t, J = 9.6 Hz, 1H, H-4), 3.91 (dt, J = 22.3, 3.4 Hz, 1H, H-1), 3.78 – 3.69 (m, 2H, H-6), 3.63 – 3.56 (m, 2H, H-3, H-5), 1.36 – 1.31 (m, 3H, CH_3), 1.21 – 1.16 (m, 3H, CH_3). ^{13}C NMR (126 MHz, $CDCl_3$) δ: 138.6 (C-arom), 138.3 (C-arom), 138.2 (C-arom), 138.1 (C-arom), 128.5 (C-arom), 128.5 (C-arom), 128.4 (C-arom), 128.3 (C-arom), 128.2 (C-arom), 128.2 (C-arom), 128.1 (C-arom), 127.9 (C-arom), 127.8 (C-arom), 127.8 (C-arom), 127.7 (C-arom), 127.6 (C-arom), 127.5 (C-arom), 117.40 (ddd, J = 280.4, 257.0, 209.8 Hz, CF2), 84.05 (d, J = 1.9 Hz, C-3), 80.6 (C-5), 75.74 (ddd, J = 31.4, 18.8, 13.6 Hz, C-1), 75.3 (CH_2-Bn), 74.7 (C-4), 74.4 (CH_2-Bn), 73.3 (CH_2-Bn), 72.34 (dd, J = 6.1, 2.1 Hz, C-2), 72.2 (CH_2-Bn), 69.5 (C-6), 64.96 (dd, J = 30.3, 6.5 Hz, CH_2-O), 16.43 (dd, J = 9.5, 5.7 Hz, CH_3). ^{31}P NMR (162 MHz, $CDCl_3$) δ: 6.73 (dd, J = 101.2, 99.2 Hz). ^{19}F NMR (471 MHz, $CDCl_3$) δ: -116.13 (dd, J = 312.3, 100.9 Hz), -124.45 (ddd, J = 312.4, 99.0, 22.3 Hz). HRMS $[M+Na]^+$: 733.27157 found, 733.27123 calculated.

Pyridinium 2,3,4,6-tetra-O-benzyl-β-D-manno-heptulopyranose-1-(difluoro)phosphonate (9).

Compound **20** (71 mg, 0.1 mmol, 1 eq) was co- evaporated (3x) with toluene, dissolved in dry CH_3CN (6.7 ml) and cooled to 0°C. A glass stopper was used to seal the reaction vessel and a glass covered stirring rod was used to stir the reaction. Pyridine (0.1 ml, 1.2 mmol, 12 eq) and TMSBr (0.26 ml, 2 mmol, 20 eq) were added dropwise via syringe. The reaction was heated up to RT and stirred overnight. Volatiles were removed *in vacuo*, with water bath temperature of 20°C under fume hood. Ice cold milli-q water and acetonitrile were added and after stirring the mixture for 2 hours and 30 minutes, the volatiles were removed *in vacuo*. Compound **9** was obtained as a white solid (70 mg, 0.1 mmol, quant.) without any further purification. ^{1}H

NMR (500 MHz, MeOD) δ: 8.95 – 8.85 (m, 12H, H-pyr), 8.69 – 8.62 (m, 6H, H-pyr), 8.11 – 8.03 (m, 12H, H-pyr), 7.50 – 7.45 (m, 2H, H-arom), 7.39 – 7.24 (m, 15H, H-arom), 7.22 – 7.17 (m, 3H, H-arom), 7.11 – 7.06 (m, 2H, H-arom), 4.97 – 4.91 (m, 3H, CH_2-Bn), 4.79 – 4.74 (m, 2H, CH_2-Bn), 4.66 (d, J = 11.0 Hz, 2H, H-2, CH_2-Bn), 4.29 – 4.11 (m, 4H, CH_2-Bn, H-4, H-1), 3.89 (dd, J = 9.4, 2.7 Hz, 1H, H-3), 3.81 (dd, J = 11.0, 1.9 Hz, 1H, H-6a), 3.74 (dd, J = 11.0, 3.5 Hz, 1H, H-6b), 3.64 (ddd, J = 9.9, 3.6, 1.9 Hz, 1H, H-5). ^{13}C NMR (126 MHz, MeOD) δ: 148.5 (C-arom), 147.0 (C-arom), 143.0 (C-arom), 140.2 (C-arom), 140.0 (C-arom), 140.0 (C-arom), 139.2 (C-arom), 138.9 (C-arom), 129.9 (C-arom), 129.8 (C-arom), 129.8 (C-arom), 129.8 (C-arom), 129.7 (C-arom), 129.7 (C-arom), 129.7 (C-arom), 129.7 (C-arom), 129.6 (C-arom), 129.6 (C-arom), 129.5 (C-arom), 129.5 (C-arom), 129.4 (C-arom), 129.3 (C-arom), 129.2 (C-arom), 129.2 (C-arom), 129.1 (C-arom), 129.0 (C-arom), 129.0 (C-arom), 129.0 (C-arom), 128.9 (C-arom), 128.9 (C-arom), 85.7 (C-3), 81.4 (C-5), 78.12 (ddd, J = 27.8, 11.8, 4.7 Hz, C-1), 76.2 (CH_2-Bn), 76.1 (CH_2-Bn), 75.9 (C-4), 74.7 (C-2), 74.3 (CH_2-Bn), 73.4 (CH_2-Bn), 70.1 (C-6). ^{19}F NMR (471 MHz, MeOD) δ: -118.58 (ddd, J = 302.1, 88.8, 8.1 Hz), -123.20 (ddd, J = 302.2, 94.6, 19.9 Hz). ^{31}P NMR (202 MHz, MeOD) δ: 3.36 (dd, J = 94.7, 89.0 Hz). HRMS $[M+Na]^+$: 655.22681 found, 655.22669 calculated.

1-(difluoro)phosphoryl-(4S,8S,12S,16S,20S)-4,8,12,16,20-pentamethylheptacosyl-2,3,4,6-tetra-O-benzyl-β-D-manno- heptulopyranose (36).

Compound **9** (7 mg, 0.01 mmol, 1 eq) and lipid **4** (16 mg, 0.018 mmol, 3 eq) were co-evaporated (2x) in toluene and dissolved in a mixture of dry DMF/pyridine 2:1 (0.24 ml) and dry toluene (0.20 ml) respectively. This solution was heated up to 60°C before the addition of TIPPSCl (5.6 mg, 0.018 mmol, 1.8 eq). The reaction mixture was then stirred overnight at this temperature and then concentrated. Compound **36** was obtained after silicagel chromatography ($CHCl_3$/MeOH 40:1→9:1; $CHCl_3$/MeOH 40:1 loading of crude; ultrapure silica, neutralized with 1% Et_3N) as a colorless oil (7 mg, 0.0064 mmol, 64%). ^{1}H NMR (500 MHz, MeOD) δ: 7.64 – 6.96 (m, 20H, H-arom), 4.87 (d, J = 10.9 Hz, 2H, CH_2-Bn), 4.81 (d, J = 11.6 Hz, 1H, CH_2-Bn), 4.74 (d, J = 10.7 Hz, 1H, CH_2-Bn), 4.71 (d, J = 11.6 Hz, 1H, CH_2-Bn), 4.59 (d, J = 11.4 Hz, 2H, CH_2-Bn), 4.50 (d, J = 11.7 Hz, 1H, CH_2-Bn), 4.41 (bs, 1H, H-2), 4.06 – 3.93 (m, 2H, H-1, H-4), 3.93 – 3.81 (m, 6H, -OCH_3), 3.80 – 3.70 (m, 3H, H-3, H-6), 3.66 – 3.56 (m, 1H, H-5). ^{13}C NMR (126 MHz, MeOD) δ: 140.2 (C-arom), 140.0 (C-arom), 140.0 (C-arom), 139.8 (C-arom), 129.7 (C-arom), 129.6 (C-arom), 129.6 (C-arom), 129.5 (C-arom), 129.5 (C-arom), 129.4 (C-arom), 129.4 (C-arom), 129.2 (C-arom), 129.0 (C-arom), 129.0 (C-arom), 128.9 (C-arom), 128.8 (C-arom), 85.4 (d, J = 2.1 Hz, H-3), 81.8 (C-5), 77.6 – 77.0 (m, C-1), 76.4 (CH_2-Bn), 76.1 (C-4), 76.0 (CH_2-Bn), 74.5 (CH_2-Bn), 74.22 – 74.12 (m, C-2), 73.5 (CH_2-Bn), 70.7 (C-6), 56.3 (d, J = 6.4 Hz, -OCH_3), 56.0 (d, J = 6.7 Hz, -OCH_3). ^{31}P NMR (202 MHz, MeOD) δ: 9.85 (pt, J = 102.0 Hz). ^{19}F NMR (471 MHz, MeOD) δ: -114.97 (ddd, J = 313.6, 101.5, 4.3 Hz), -123.23 (ddd, J = 313.5, 102.7, 21.8 Hz). HRMS $[M+H]^+$: 1103.72789 found, 1103.72749 calculated.

1-(difluoro)phosphoryl-(4S,8S,12S,16S,20S)-4,8,12,16,20-pentamethylheptacosyl-β-D-manno-heptulopyranose (3).

Compound **36** (12 mg, 0.011 mmol, 1 eq) was dissolved in a mixture of THF/H_2O 2:1 (5 ml) and the solution was purged and bubbled through with a flow of Argon. Then Pd/C (10 mg) was added and the solution was purged and bubbled through with Argon once more. The suspension was bubbled through with Hydrogen and subsequently stirred vigorously under a Hydrogen atmosphere. After 16 hours, the reaction mixture was purged of Hydrogen and

filtered over celite. Compound **3** was obtained after *in vacuo* removal of volatiles as an amorphous solid (7 mg, 0.009 mmol, 82%). ^{1}H NMR (500 MHz, MeOD) δ: 4.28 (d, J = 3.1 Hz, 1H, H-2), 4.10 – 3.94 (m, 2H, OCH_2), 3.89 (pd, J = 12.3 Hz, 1H, H-6a), 3.87 – 3.61 (m, 4H, H-1, H-6b, H-4), 3.57 – 3.49 (m, 1H, H-3), 3.31 – 3.26 (m, 1H, H-5), 3.18 (q, J = 7.3 Hz, 4H, CH_2-triethylamonium), 1.77 – 1.54 (m, 4H, CH_2-lipid), 1.45 – 1.17 (m, 54H, CH_2-lipid, CH-lipid, CH_3-triethylamonium), 1.12 – 1.02 (m, 9H, CH_2-lipid, CH-lipid), 0.90 – 0.84 (m, 18H, CH_3-lipid). ^{13}C NMR (126 MHz, MeOD) δ: 81.0 (C-5), 79.0 (C-1), 74.2 (C-3), 67.3 (C-4), 67.0 (OCH_2), 66.4 (C-4), 60.8 (C-6), 46.2 (CH_2-triethylammonium), 36.9 (CH_2-lipid), 36.8 (CH_2-lipid), 36.7 (CH_2-lipid), 36.4 (CH_2-lipid), 32.4 (CH_2-lipid), 32.3 (CH-lipid), 32.2 (CH-lipid), 32.2 (CH-lipid), 31.4 (CH_2-lipid), 29.4 (CH_2-lipid), 29.1 (CH_2-lipid), 28.8 (CH_2-lipid), 26.5 (CH_2-lipid), 23.9 (CH_2-lipid), 23.9 (CH_2-lipid), 23.8 (CH_2-lipid), 22.1 (CH_2-lipid), 19.1 (CH_3-lipid), 19.1 (CH_3-lipid), 19.1 (CH_3-lipid), 19.0 (CH_3-lipid), 18.7 (CH_3-lipid), 13.3 (CH_3-lipid), 7.9 (CH_3-triethylammonium). ^{31}P NMR (202 MHz, MeOD) δ: 2.84 (t, J = 85.4 Hz). ^{19}F NMR (471 MHz, MeOD) δ: -115.15 (dd, J = 305.6, 86.7 Hz), -117.29 (dd, J = 305.5, 84.5 Hz). HRMS $[M+H]^+$: 683.25772 found, 683.25799 calculated.

References

1. Moody DB, Ulrichs T, Mühlecker W, Young DC, Gurcha SS, Grant E, et al. CD1c-mediated T-cell recognition of isoprenoid glycolipids in *Mycobacterium tuberculosis* infection. Nature. 2000 Apr;404(6780):884–8.

2. Ly D, Kasmar AG, Cheng T-Y, de Jong A, Huang S, Roy S, et al. CD1c tetramers detect ex vivo T cell responses to processed phosphomycoketide antigens. J Exp Med. 2013 Apr 8;210(4):729–41.

3. de Jong A, Arce EC, Cheng T-Y, van Summeren RP, Feringa BL, Dudkin V, et al. CD1c Presentation of Synthetic Glycolipid Antigens with Foreign Alkyl Branching Motifs. Chem Biol. 2007 Nov;14(11):1232–42.

4. Roy S, Ly D, Li N-S, Altman JD, Piccirilli JA, Moody DB, et al. Molecular basis of mycobacterial lipid antigen presentation by CD1c and its recognition by T cells. Proc Natl Acad Sci. 2014 Oct 28;111(43):E4648–57.

5. Van Rhijn I, Moody DB. CD1 and mycobacterial lipids activate human T cells. Immunol Rev. 2015 Mar;264(1):138–53.

6. Weller S. Human blood IgM 'memory' B cells are circulating splenic marginal zone B cells harboring a prediversified immunoglobulin repertoire. Blood. 2004 Dec 1;104(12):3647–54.

7. Allan LL, Stax AM, Zheng D-J, Chung BK, Kozak FK, Tan R, et al. CD1d and CD1c Expression in Human B Cells Is Regulated by Activation and Retinoic Acid Receptor Signaling. J Immunol. 2011 May 1;186(9):5261–72.

8. Roura-Mir C, Catálfamo M, Cheng T-Y, Marqusee E, Besra GS, Jaraquemada D, et al. CD1a and CD1c Activate Intrathyroidal T Cells during Graves' Disease and Hashimoto's Thyroiditis. J Immunol. 2005 Mar 15;174(6):3773–80.

9. Dzionek A, Fuchs A, Schmidt P, Cremer S, Zysk M, Miltenyi S, et al. BDCA-2, BDCA-3, and BDCA-4: Three Markers for Distinct Subsets of Dendritic Cells in Human Peripheral Blood. J Immunol. 2000 Dec 1;165(11):6037–46.

10. Moody DB, Zajonc DM, Wilson IA. Anatomy of CD1–lipid antigen complexes. Nat Rev Immunol. 2005 May;5(5):387–99.

11. Mansour S, Tocheva AS, Cave-Ayland C, Machelett MM, Sander B, Lissin NM, et al. Cholesteryl esters stabilize human CD1c conformations for recognition by self-reactive T cells. Proc Natl Acad Sci. 2016 Mar 1;113(9):E1266–75.

12. Haig NA, Guan Z, Li D, McMichael A, Raetz CRH, Xu X-N. Identification of Self-lipids Presented by CD1c and CD1d Proteins*. J Biol Chem. 2011 Oct;286(43):37692–701.

13. Adams EJ. Lipid presentation by human CD1 molecules and the diverse T cell populations that respond to them. Curr Opin Immunol. 2014 Feb;26:1–6.

14. Green AM, DiFazio R, Flynn JL. IFN-γ from CD4 T Cells Is Essential for Host Survival and Enhances CD8 T Cell Function during *Mycobacterium tuberculosis* Infection. J Immunol. 2013 Jan 1;190(1):270–7.

15. Kaufmann SHE. How can immunology contribute to the control of tuberculosis? Nat Rev Immunol. 2001 Oct;1(1):20–30.

16. MacMicking JD. Immune Control of Tuberculosis by IFN- -Inducible LRG-47. Science. 2003 Oct 24;302(5645):654–9.

17. Zechel DL, Withers SG. Glycosidase Mechanisms: Anatomy of a Finely Tuned Catalyst. Acc Chem Res. 2000;33(1):11–8.

18. Xu B, Unione L, Sardinha J, Wu S, Ethève-Quelquejeu M, Pilar Rauter A, et al. *gem* -Difluorocarbadisaccharides: Restoring the *exo* -Anomeric Effect. Angew Chem. 2014 Sep 1;126(36):9751–6.

19. Blackburn GM, Kent DE, Kolkmann F. The synthesis and metal binding characteristics of novel, isopolar phosphonate analogues of nucleotides. J Chem Soc Perkin 1. 1984;1119.

20. van Summeren RP, Moody DB, Feringa BL, Minnaard AJ. Total Synthesis of Enantiopure β- D -Mannosyl Phosphomycoketides from *Mycobacterium tuberculosis*. J Am Chem Soc. 2006 Apr;128(14):4546–7.

21. Arjona O, Gómez AM, López JC, Plumet J. Synthesis and Conformational and Biological Aspects of Carbasugars. Chem Rev. 2007 May;107(5):1919–2036.

22. Sugimura H, Hosogai N. Studies toward Stable Analogues of Guanofosfocins. Synthesis of the Protected Derivative of 8-(5a-Carba-α-D-mannopyranosyloxy)purine Nucleoside. Chem Lett. 2007 Jan;36(1):36–7.

23. Tsunoda H, Ogawa S. Pseudosugars, 33. Synthesis of some 5a-carbaglycosylamides, glycolipid analogs of biological interests. Liebigs Ann Chem. 1994 Feb 14;1994(2):103–7.

24. Gao Q, Zaccaria C, Tontini M, Poletti L, Costantino P, Lay L. Synthesis and preliminary biological evaluation of carba analogues from Neisseria meningitidis A capsular polysaccharide. Org Biomol Chem. 2012;10(33):6673.

25. Yang Y, Yu B. Recent Advances in the Chemical Synthesis of *C* -Glycosides. Chem Rev. 2017 Oct 11;117(19):12281–356.

26. Dondoni A, Staderini S, Marra A. Efficiency of the Free-Radical Hydrophosphonylation of Alkenes: The Photoinduced Reaction of Dimethyl *H* -Phosphonate with Enopyranoses as an Exemplary Case: Efficiency of the Free-Radical Hydrophosphonylation of Alkenes. Eur J Org Chem. 2013 Aug;2013(24):5370–5.

27. Vasella A, Baudin G, Panza L. Synthesis of glycosyl phosphonates and related compounds. Heteroat Chem. 1991 Feb;2(1):151–61.

28. Fortuna A, Xavier NM. Recent developments in synthetic methods for sugar phosphate analogs. In: Recent Trends in Carbohydrate Chemistry. Elsevier; 2020. p. 301–29.

29. Romanenko VD, Kukhar VP. Fluorinated Phosphonates: Synthesis and Biomedical Application. Chem Rev. 2006 Sep;106(9):3868–935.

30. Forget SM, Bhattasali D, Hart VC, Cameron TS, Syvitski RT, Jakeman DL. Synthesis and enzymatic evaluation of ketose phosphonates: the interplay between mutarotation, monofluorination and acidity. Chem Sci. 2012;3(6):1866.

31. Bouwman S, Orru RVA, Ruijter E. Stereoselective synthesis of fluorinated aminoglycosyl phosphonates. Org Biomol Chem. 2015;13(5):1317–21.

32. Kovensky J, McNeil M, Sinaÿ P. D -Galactofuranosylphosphonates. First Synthesis of UDP- *C* - D -galactofuranose. J Org Chem. 1999 Aug;64(17):6202–5.

33. Akai S, Tanaka R, Hoshi H, Sato K. Selective Deprotection Method of *N* -Phenylcarbamoyl Group. J Org Chem. 2013 Sep 6;78(17):8802–8.

34. Stick R, Stubbs K. The Synthesis of a New Class of Potential Inhibitors for Glycoside Hydrolases. J Carbohydr Chem. 2005 Aug 1;24(4–6):529–47.

35. Frihed TG, Walvoort MTC, Codée JDC, van der Marel GA, Bols M, Pedersen CM. Influence of O6 in Mannosylations Using Benzylidene Protected Donors: Stereoelectronic or Conformational Effects? J Org Chem. 2013 Mar 15;78(6):2191–205.

36. Gratien J, Heck M-P, Mioskowski C. C-2 Epimerization of aldonolactones promoted by magnesium iodide: a new way towards non-enzymatic epimerization. Carbohydr Res. 2008 Jan;343(1):18–30.

37. Kumar V, Taxak N, Jangir R, Bharatam PV, Kartha KPR. In(III) Triflate-Mediated Solvent-Free Synthesis and Activation of Thioglycosides by Ball Milling and Structural Analysis of Long Chain Alkyl Thioglycosides by TEM and Quantum Chemical Methods. J Org Chem. 2014 Apr 18;79(8):3427–39.

38. Matwiejuk M, Thiem J. New Method for Regioselective Glycosylation Employing Saccharide Oxyanions. Eur J Org Chem. 2011 Oct;2011(29):5860–78.

39. Rauschenberg M, Fritz E-C, Schulz C, Kaufmann T, Ravoo BJ. Molecular recognition of surface-immobilized carbohydrates by a synthetic lectin. Beilstein J Org Chem. 2014 Jun 16;10:1354–64.

40. Waschke D, Thimm J, Thiem J. Highly Efficient Synthesis of Ketoheptoses. Org Lett. 2011 Jul 15;13(14):3628–31.

3

Design and immunological evaluation of peptide-conjugates containing Mincle ligands

Laura Marino [1], Susan J.F. van den Eeden [2], Krista E. van Meijgaarden [2], Nico J. Meeuwenoord [1], Fabrizio Chiodo[3,4], Dmitri V. Filippov[1], Annemieke Geluk [2], Ferry A. Ossendorp [5], Gijs A. van der Marel [1], Jeroen D.C. Codée [1], Tom H.M. Ottenhoff [2]

[1] Department of Bio-organic Synthesis, Leiden University, Leiden, The Netherlands

[2] Department of Infectious Diseases, Leiden University Medical Center, Leiden, The Netherlands

[3] Department of Molecular Cell Biology and Immunology, Amsterdam UMC, Vrije Universiteit Amsterdam, Amsterdam, The Netherlands

[4] Institute of Biomolecular Chemistry, National Research Council (CNR), Pozzuoli, Napoli, Italy

[5] Department of Immunology, Leiden University Medical Center, Leiden, The Netherlands

3

Abstract

Mycobacterium tuberculosis (*Mtb*), the etiological agent of tuberculosis (TB), is one of the most successful pathogens on earth with an estimated 10 million newly infected people and 1.4 million deaths worldwide in 2019 only. Subunit vaccines containing proteins or peptide-epitopes combined with well-defined adjuvants can be attractive tools in the fight against *Mtb*. The glycolipids glucose monomycolate (GMM) and trehalose dimycolate (TDM) are promising immune adjuvants showing affinity for the murine and human C-type lectin receptor Mincle. In this Chapter the synthesis of four simplified GMM and TDM analogues is described and their ability to stimulate murine and human immune cells is tested. During the synthesis, the analogues were successfully equipped with a ligation handle to allow for further conjugation to an *Mtb*-derived peptide epitope. After verifying the ability of the novel synthetic glycolipids to interact with Mincle two TDM analogues were conjugated to an HLA-DR3 presented *Mtb* peptide antigen. An HLA-DR3 transgenic mouse model was then used to investigate the vaccine potential of one of these constructs. Although there was an absence of detectable $CD4^+$ T-cell responses, the self-adjuvanting peptide induced significant systemic humoral immune responses. Interestingly immunisation with this construct induced a reduction of the bacterial load in the spleen of intranasally *Mtb* challenged mice in the absence of detectable T-cell responses in the circulation. Further *in vitro* experiments to translate the findings to human DCs suggested that this compound was not able to activate these cells. A second self-adjuvanting peptide, carrying a very similar TDM analogue, however, was able to do so. The present study provides the first example of self-adjuvanting peptides capable of interacting with the C-type lectin receptor Mincle, provides insights in their immune-stimulatory potential in the context of *Mtb* infection, and shows that protection against *Mtb* challenge can be obtained in the presence of humoral responses.

Introduction

Tuberculosis (TB), an infectious disease caused by *Mycobacterium tuberculosis* (*Mtb*), is responsible for the death of approximately 1.4 million people worldwide in 2019 alone.[1] It is estimated that one quarter to one third of the population is latently infected with *Mtb* and 5-10% of these will develop active disease during their lifetime.[2] In most cases, TB can be treated with antibiotic combinations, but multidrug-resistant strains are emerging, which limit treatment options.[3] In countries with a high incidence of active TB, the World Health Organization (WHO) recommends vaccination of infants with *Mycobacterium bovis* Bacille Calmette-Guérin (BCG), which is the only commercially available vaccine against TB.[1]

The BCG vaccine is an attenuated live mycobacterium derived from *M. bovis*. It can be formulated using different protocols and using (six) different original bacterial inocula-derived strains, with reports indicating that strain variability may influence efficacy.[4] Although there is evidence supporting the utility of this vaccine, especially when administered in the first months of a human's life, epidemiological studies indicate inadequate protection against pulmonary TB in adults and the occurrence of disseminating BCG infection in immunocompromised infants.[5,6] A novel prevention strategy is required to reduce TB burden and possibly eradicate the pathogen.[1,7]

An alternative to attenuated bacteria is the use of subunit vaccines, where antigenic fragments of the pathogen are presented together with molecular adjuvants to increase immunogenicity. Subunit vaccines present a better safety profile compared to whole-cell mycobacteria as they are usually more stable and can be modified at the molecular level to achieve the desired effect.[8] The efficacy of subunit vaccines against *Mtb* infection is suggested through the exemplary case of the M72/AS01 vaccine, consisting of two proteins, Rv1196 (PPE18) and Rv0125 (serine protease, pepA), in liposome and used as a booster to BCG in latently infected individuals. The results of a phase 2b clinical trial indicated 49.7% protection in immunized individuals at 36 months after vaccination.[9,10] However, at the moment, a lack of detailed understanding of the molecular mechanisms governing a successful immune response and clearance of *Mtb,* and the consequent lack of definitive immune markers to protection, hinders the further development of synthetic subunit vaccines from reaching their full potential. In the context of *Mtb* and the use of subunit vaccines, significant effort is placed in exploiting pathogen-associated molecular patterns (PAMPs) to increase the immunogenicity of protein and peptide antigens.[11]

The work reported in this Chapter describes the generation of a prototype synthetic *Mtb*-vaccine, formed by linking a PAMP glycolipid adjuvant and a *Mtb*-derived peptide antigen. Chemically linking an antigen and an adjuvant to generate a

conjugate is a method employed to ensure co-delivery of these two essential components of subunit vaccines. Co-delivery through a single-molecule vaccine usually results in the induction of strong immune-responses.[12] For example, Huang *et al.* have previously reported that co-delivery of the Ag85B-HspX fusion protein with arabinogalactan and the TLR3 ligand Poly(I:C) through chemical conjugation successfully induced humoral and cellular responses against *Mtb in vivo*, while the antigenic protein alone induced only marginal levels of inflammation.[13]

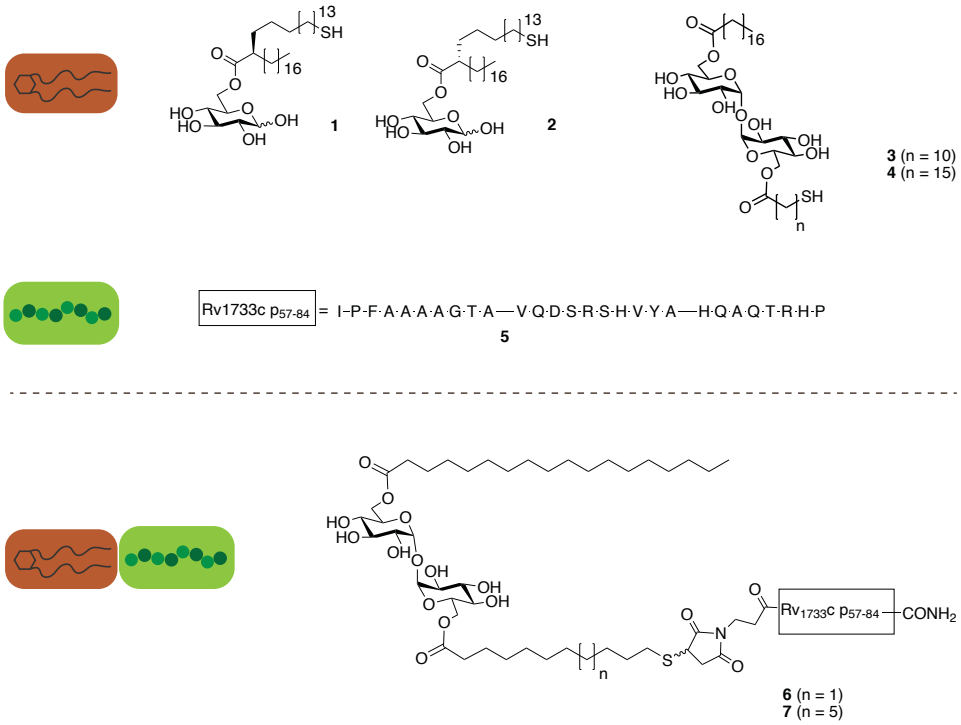

Figure 1 – Synthetic compounds designed and described in this Chapter. GMM analogues (compounds **1** and **2**) TDM analogues (compounds **3** and **4**) equipped with a thiol ligation handle for further conjugation synthetic long peptide p57 (compound **5**). Self-adjuvanting peptides **6** and **7** were synthesized from maleimide functionalized peptide **5**.

A suitable candidate for the generation of the self-adjuvanting peptides described in this Chapter is the Rv1733c peptide **5**, depicted in Figure 1. This peptide, derived from a latency protein, was previously shown by Coppola *et al.* to have antigenic properties and to be presented through the human HLA-DR3 molecule to T-cells *in vivo* using a transgenic HLA-DR3/Ab^0 murine model.[14]

With the idea of chemically coupling this peptide antigen to a relevant synthetic adjuvant, a series of four glycolipids designed to bind to the macrophage inducible C-type lectin (Mincle) receptor was generated (see Figure 1 for their chemical structure). To date, no reports have been published on synthetic conjugates containing ligands for Mincle, although there is ample evidence that this receptor performs important roles in immunity against pathogens: recognition of mycobacterial glycolipids and production of pro-inflammatory cytokines through a signalling cascade that results in activation of nuclear factor kappa-light-chain-enhancer of activated B cells (NF-κB).[15] Finally, it has been shown that Mincle activation enhances the transcription of inflammatory genes, while it also inhibits the late-stage NLRP3-inflammasome activation, preventing excessive inflammation.[16] Because of these desirable characteristics, Mincle represents an interesting target to exploit for the development of vaccines against TB.

Mincle is a transmembrane pattern recognition receptor (PRR) expressed on macrophages, monocytes and dendritic cells, that is able to recognize glycolipids from fungi and mycobacteria. The first ligands for Mincle, trehalose dimycolate (TDM) (pictured in Figure 2a) and its analogue trehalose dibehenate (TDB), were identified in 2009 by Ishikawa *et al.*[17] Recognition of TDB and TDM by Mincle is mediated through its carbohydrate recognition domain in the extracellular region.[18] Measurement of the direct interaction of TDM and its analogues is limited by their poor solubility limiting crystallography studies to analogues containing short alkyl chains. However, a general pattern has been suggested that binding affinity increases for longer alkyl chains.[15] Binding of a ligand to Mincle has been shown to activate the adapter protein Fc receptor ɣ-chain (FcRɣ) which is required for the recruitment of spleen tyrosine kinase (SYK). SYK recruitment is followed by a cascade of signaling events which culminate in NF-κB activation.[15]

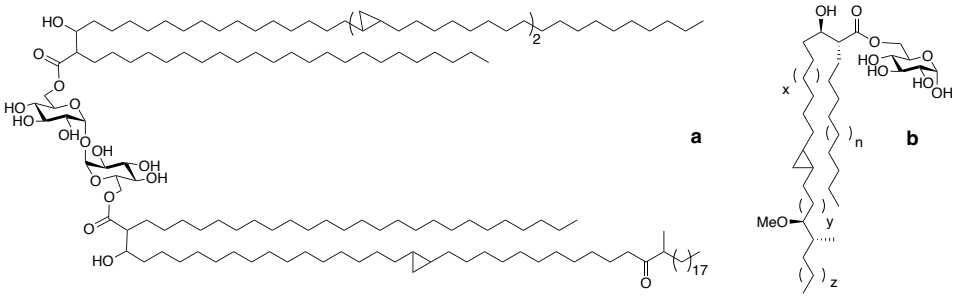

Figure 2 – Chemical structures of natural glycolipids that have been shown to interact with the Mincle receptor. a) Trehalose dimycolate (TDM); b) glucose monomycolate (GMM).

Since 2009, the year of first discovery of TDM/Mincle interaction, several groups have designed simplified synthetic analogues of known Mincle ligands to study their immune-stimulatory potential and reduce toxicity to cells. For example, a series of synthetic TDM analogues was designed by Kallerup *et al.* and Huber *et al.*, and their results indicated that the compounds are able to bind to Mincle and induce G-CSF and NO production in murine macrophages, suggesting that these compounds might also function as adjuvants.[19,20] Other ligands belonging to glycolipid families other than TDM have been discovered and shown to bind to Mincle. Glucose monomycolate (GMM) is one such ligand (chemical structure of GMM shown in Figure 2b).

The present study describes the synthesis of two TDM and two GMM simplified analogues, equipped with simple saturated linear lipid chains and a ligation handle with the ultimate goal being the incorporation of a Mincle ligand in a self-adjuvanting peptide construct. At a later stage this construct could be further expanded to include an additional adjuvant.

The design of the synthetic route of the two TDM analogues described in this Chapter was inspired by the research of Toubiana *et al.,* Johnson, Datta *et al.*,[21–23] using a TMS-protecting group based strategy, advantageous in comparison to the benzyl protecting group strategy used by Nishizawa *et al.* in the ease of scaling up the final deprotection reaction.[24] The choice of lipids for coupling to the carbohydrate core was based on: 1) structural studies suggesting increased binding interaction of trehalose 6-OH mono-substituted compounds with increasing alkyl chain length and the requirement for interaction between the 3-OH and 4-OH positions of trehalose to the carbohydrate recognition domain on the receptor;[25,26] 2) experimental evidence that biological activity in symmetrically substituted trehaloses increased with increasing chain length, with C18 showing little to no difference as compared to C22 (length of alkyl chain in the well-studied analogue TDB);[19,27,28] 3) no evidence was found suggesting the requirement of the two alkyl chains having the same number of carbon atoms. Based on these considerations, the new TDM analogues were designed to contain: a C18 alkyl chain on the 6-OH position of the trehalose and a C11 or C16 alkyl chain on the 6'-OH position, with this latter lipid chemically modified to present a thiol ligation handle for further conjugation.

The design of the two GMM analogues was inspired by a publication by Decout *et al.* reporting of a synthetic GMM analogue, produced as racemic mixture, and named GlcC14C18. This compound exhibited a stronger adjuvant effect than TDB, when formulated in liposomes and it induced protective immunity in a mouse model of *Mtb* infection.[29] Separately, it was shown for multiple TLR2 ligands that different stereoisomers can elicit different biological responses.[30,31] Based on these results, the two GMM analogues containing the enantiomerically pure C14C18 lipids equipped with a thiol ligation handle were designed and synthesised using a similar TMS-protecting group approach as the one selected for the synthesis of the TDM analogues.

To probe the ability of the four synthetic glycolipids to interact with the C-type lectin receptor Mincle, *in vitro* assays using the human embryonic kidney 293 (HEK-293) expressing murine Mincle reporter cell line were performed. The glycolipids showing the best binding affinity for Mincle were conjugated to the *Mtb*-derived peptide. These were evaluated *in vitro* in murine and human cell systems for their immunomodulatory activity. An HLA-DR3/Ab^0 transgenic mouse model was used to investigate the vaccine potential of one of these constructs *in vivo* and their effect on the bacterial load when challenged with live *Mtb*.

Results

Synthesis of GMM and TDM analogues

The synthetic strategy for the generation of the four glycolipids depicted in Figure 1 is based on a protecting group strategy using trimethyl silyl ethers (TMS) and a Steglich esterification approach to introduce the lipid chains. The enantiomeric fatty acids contained in the two GMM analogues, compounds **1** and **2,** were synthesized starting from the same pseudoephedrine derivative **9** (see Figure 3A) via two stereo-divergent approaches.

Starting from compound **9**, a Myers alkylation with diisopropyl amine (DIPA) and allyl bromide delivered the *R*-isomer of α-allyl stearic acid **10**. The *S*-configured lipid **14** was obtained by an O-allylation with sodium hydride and allyl bromide followed by a Claisen rearrangement using triflic anhydride and 2-fluoropyridine.[1] A cross metathesis with *S*-(dodec-11-en-1-yl) ethanethioate then delivered the enantiomeric branched acids **12** and **15**, which were obtained in 46% and 38% yield over 5 steps starting from stearic acid, respectively. The two GMM analogues **1** and **2** were obtained from α-D-glucose, as shown in Figure 3B. α-D-Glucose **16** was first protected as the TMS ethers using TMS chloride, hexamethyldisilazane (HMDS) and pyridine which was followed by deprotection of the primary alcohol with ammonium acetate. The lipids **12** and **15** were then installed by esterification utilizing 1-ethyl-3-(3-dimethylaminopropyl)carbodiimide (EDCI) and DMAP. Afterwards, a simultaneous reduction of the alkyl double bond and thioester with *p*-nitrosulfonyl hydrazide was carried out. Finally, removal of the TMS-protecting groups with amberlite resin and treatment with tris(2-carboxyethyl)phosphine (TCEP) to reduce the disulfide resulted in compounds **1** and **2** with 24% and 14% yield over 6 steps, respectively.

Next, the attention was shifted to the synthesis of TDM analogues **3** and **4** (see Figure 4). Lipid thioester **21**, required for the generation of the conjugation ready TDM analogue **3**, was synthesized in one step via nucleophilic substitution of

[1] A schematic depiction of the suggested mechanism of the reaction and intermediates can be found in the supporting information (Figure S5).

commercially available 11-bromoundecanoic acid with potassium ethanethioate in 91% yield.

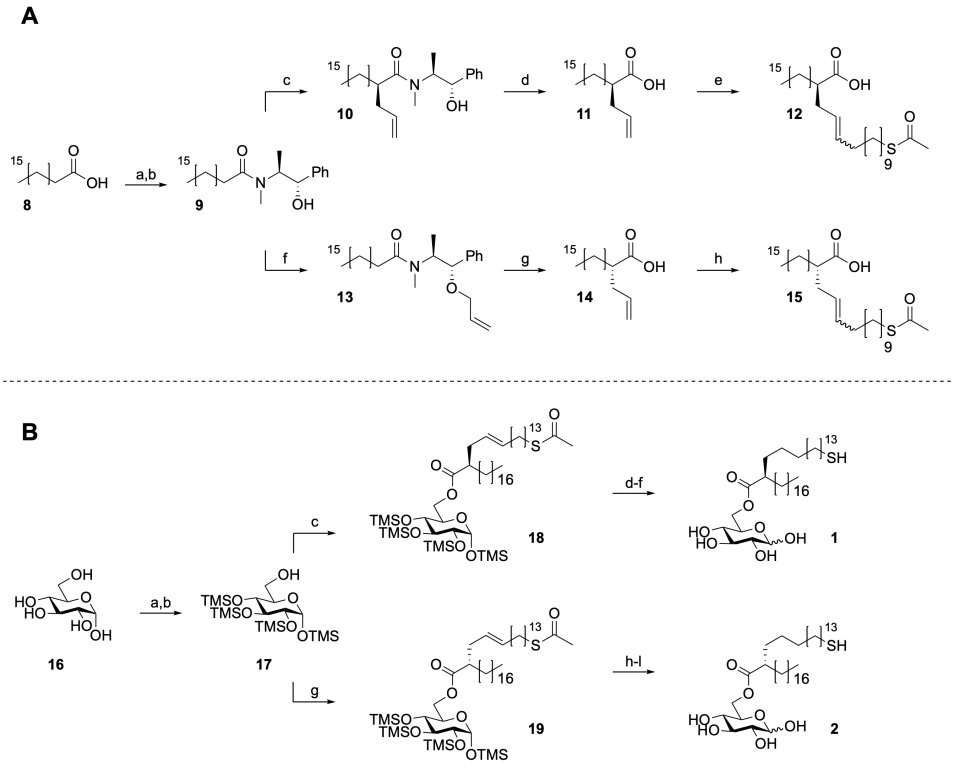

Figure 3 - Synthetic route optimized to generate GMM analogues and enantiomeric lipids. (A) Reaction scheme for the synthesis of lipids. a) oxalyl chloride, DMF, toluene, y: 99%, b) pseudoephedrine, Et_3N, DCM, y: 99%, c) DIPA, LiCl, allyl bromide, THF, y: 84%, d) H_2SO_4 (5N)/dioxane 1:1, y: 73%, e) S-(dodec-11-en-1-yl) ethanethioate, Grubbs 1st generation, DCM, reflux, y: 76%, f) NaH, allyl bromide, DCM, y: 86%, g) i. Tf_2O, 2-fluoropyridine, DCM, 0◦C, ii. H_2SO_4 (2.5 N)/dioxane 1:1, 100◦C, y: 60%, h) S-(dodec-11-en-1-yl) ethanethioate, Grubbs 1st generation, DCM, reflux, y: 76%. **(B)** Reaction scheme for the synthesis of glycolipids. a) TMSCl, HMDS, pyridine, y: quant. b) NH_4OAc, DCM/MeOH 1:1, y: 73%, c) lipid, EDCI, DMAP, y: 52%, d) p-nitrosulfonyl hydrazide, Et_3N, DCM, e) amberlite H^+, DCM/MeOH 1:1, f) TCEP.HCl, PBS, MeOH/CH_3CN 1:1, y: 62% over 3 steps, g) lipid, EDCI, DMAP, y: 50%, h) *p*-nitrosulfonyl hydrazide, Et_3N, DCM, i) amberlite H^+, DCM/MeOH 1:1, l) TCEP.HCl, PBS, MeOH/CH_3CN 1:1, y: 73% over three steps.

For the synthesis of thioester **24,** the chosen reaction sequence consisted of the opening of cyclohexadecanolide with NaOMe, subsequent bromination to replace the hydroxyl moiety, saponification of the ester and nucleophilic substitution of the bromide with potassium thioacetate to obtain lipid **24** in 43% overall yield. In line

with the assembly of **1** and **2**, the alcohols of trehalose were protected as TMS-ethers except this time the reaction was carried out using *N*,*O*-bis(trimethylsilyl)acetamide and TBAF. After the primary hydroxyl groups were deprotected with potassium carbonate in methanol, stearic acid was installed with EDCI and DMAP to provide the monoesters (Figure 4B). Next, a condensation with lipid thioesters **21** and **24** provided the fully protected TDM analogues **27** and **28**. Removal of the silyl ethers under acidic conditions and conversion of thioester to free thiol with hydrazine then provided compounds **3** and **4** in 26% and 27% yield, respectively, over 5 steps starting from trehalose.

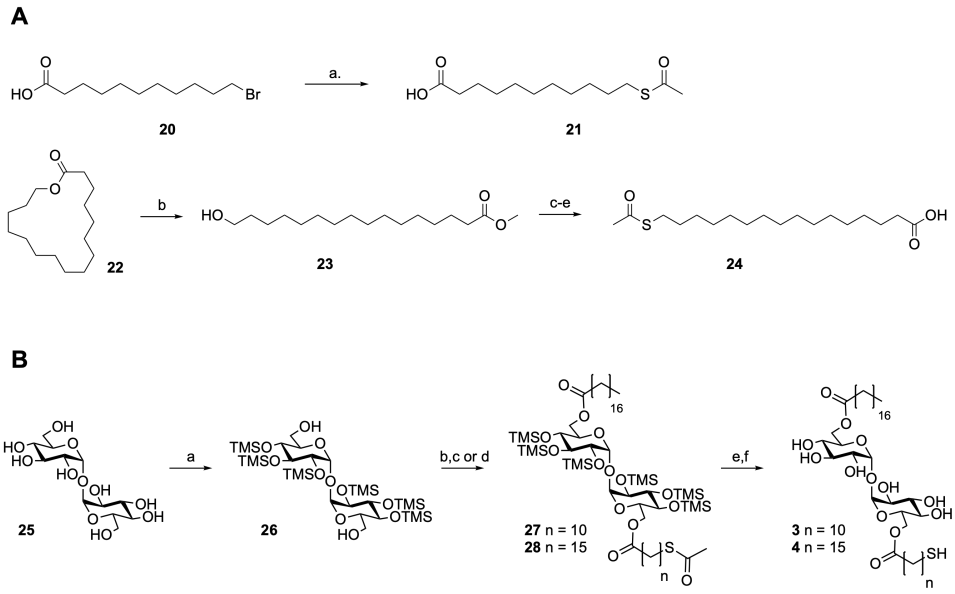

Figure 4 - Synthetic route optimized to generate TDM analogues and lipids with different chain length. (A) Reaction scheme for the synthesis of lipids. a) potassium thioacetate, DMF, y: 91%, b) NaOMe, MeOH, y: 85%, c) PPh_3, $NaHCO_3$, NBS, y: 88%, d) LiOH, THF, y: 91%, e) potassium thioacetate, DMF, y: 63%. **(B)** Reaction scheme for the synthesis of glycolipids. a) i. *N*,*O*-bis(trimethylsilyl)acetamide, TBAF, DMF, ii. K_2CO_3, MeOH, y: 79%, b) stearic acid, EDCI, DMAP, toluene, y: 47%, c) 11-(acetylthio)undecanoic acid, EDCI, DMAP, toluene, y: 70%, d) amberlite H^+, DCM/MeOH 1:1, y: quant., e) $NH_2NH_2CH_3{\cdot}COOH$, DCM/MeOH 1:1, y: quant., f) 11-(acetylthio)hexadecanoic acid, EDCI, DMAP, toluene, y: 85%, g) amberlite H^+, DCM/MeOH 1:1, y: 87%, h) $NH_2NH_2{\cdot}H_2O$, DCM/MeOH 1:1, y: quant. (isolated as mixture of oxidized and reduced thiol).

In vitro evaluation of Mincle ligand-peptide conjugates

With the simplified GMM and TDM analogues in hand, the HEK-Blue mMincle reporter cell line was used to probe the binding of these constructs. HEK-Blue mMincle is a commercially available cell line transfected to overexpress murine

Mincle. Functional binding of a ligand to Mincle in this cellular system results in release of secreted alkaline phosphatase (SEAP) in the cells supernatant, which induces a colour change in the QUANTI-blue medium proportional to the amount of secreted SEAP. The colour change is detectable by eye and can be measured quantitatively using a spectrophotometer at 620-655 nm. The synthetic TLR2 ligand UPam, known immune stimulator for human and murine antigen presenting cells (APCs),[30] was used as negative control to validate the assay's specificity.

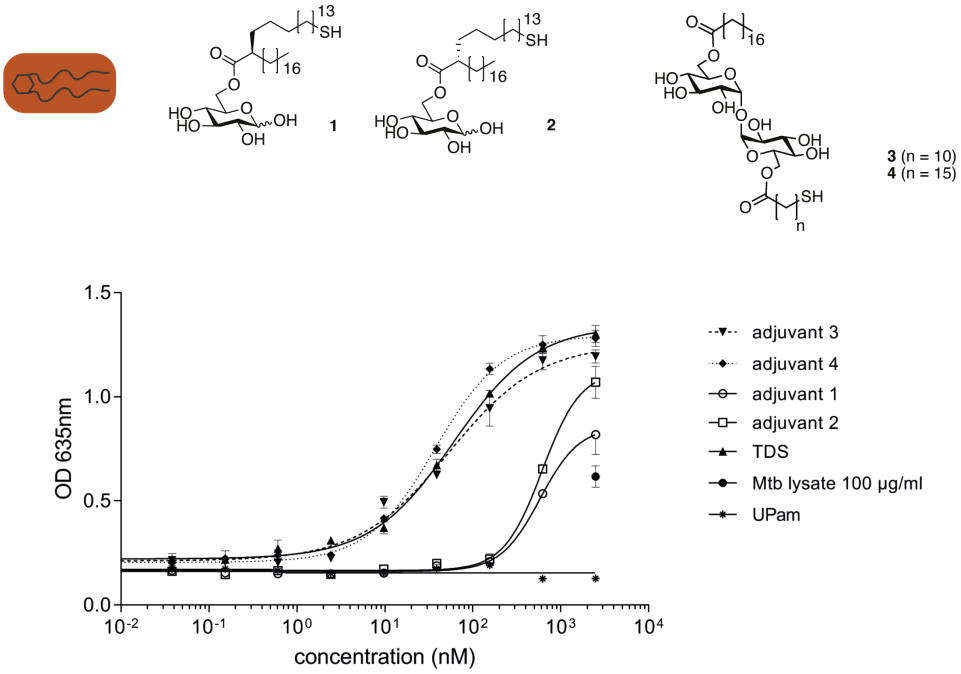

Figure 5 - Dose-response curves for HEK-293 mMincle activation. HEK-293 cells expressing murine Mincle and a NF-κB-inducible reporter system were stimulated with plate-bound glycolipids for 16h. NF-κB activation was determined by measuring secreted embryonic alkaline phosphatase (SEAP) activity and reading O.D. at 635 nm after mixing of 20 µl of the culture supernatant with 180 µl of Quanti-BlueTM (InvivoGen). TDS and Mtb lysate (expected to contain TDM) were used as positive controls. UPam, a TLR2 ligand, was used as negative control. Dots represent mean + SEM of duplicates from one experiment. Curves were interpolated using a non-linear regression model with 4 parameters as calculated using GraphPad Prism software.

Cells stimulated with each analogue responded to the stimulation by releasing SEAP in the cell supernatant, indicating that all four analogues are able to bind to and activate the murine Mincle receptor (see Figure 5). The two TDM analogues,

compounds **3** and **4**, bound the receptor with higher potency than the two GMM analogues, compounds **1** and **2**, and were therefore chosen for the generation of the two self-adjuvanting peptides described in the next section.

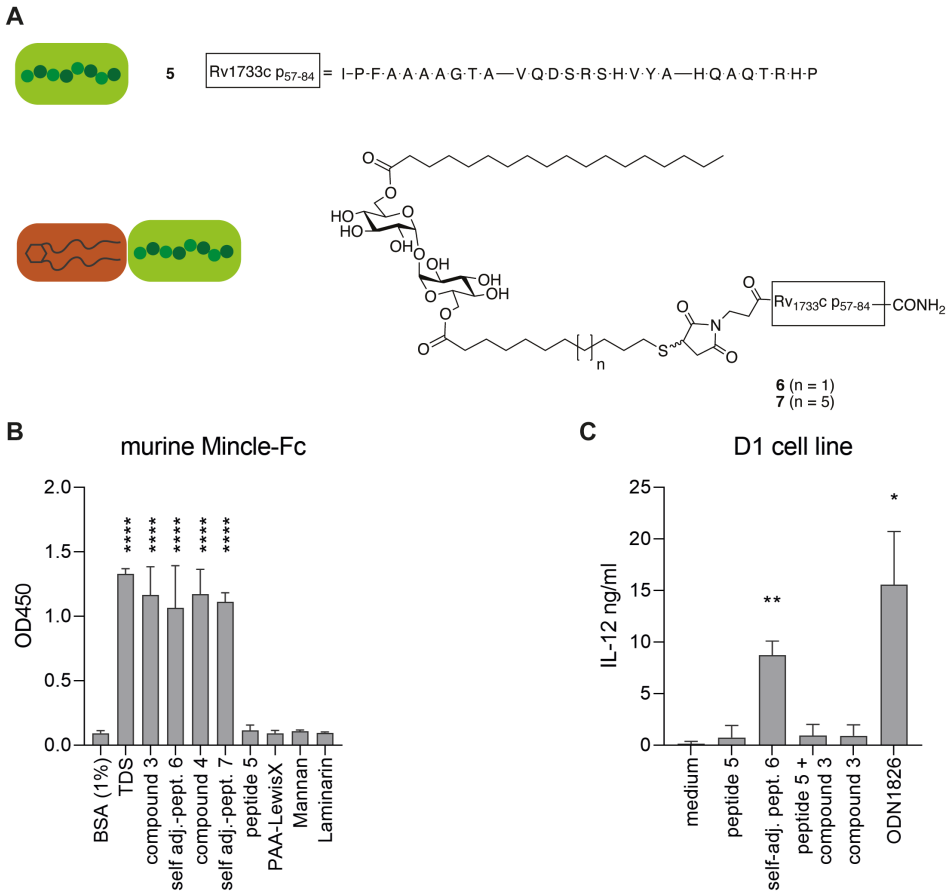

Figure 6 - Binding experiment using soluble murine Mincle (B) and stimulation experiment using murine D1 dendritic cells (C). (A) Chemical structures of synthetic long peptide p57 (compound **5**) and self-adjuvanting peptides **6** and **7. (B)** ELISA experiment was performed using plate-bound glycolipids (5 nmol/well), self-adjuvanted peptides (5 nmol/well) and control compounds. TDS = Trehalose distearate (5 nmol/well) was used as positive control. PAA-LewisX (10 μg/ml), Mannan (10 μg/ml) and Laminarin (3 μg/ml) known to bind other CLRs, and the reference peptide p57 (5 nmol/well) were chosen as negative controls. Soluble recombinant murine Mincle Fc chimera protein was used for assaying binding interaction. **(C)** IL-12p40 production by murine D1 DC cells stimulated for 20 hours using synthetic compounds (50 µM) or ODN1826 control (1 µg/ml), as measured by ELISA. Bars represent mean + SD of duplicates from two independent experiments. Statistical significance with reference to the negative control group, BSA (1%) in buffer (plot a) and DMSO (0.1%) in medium (plot b), was determined by one-way ANOVA with Tukey's multiple comparisons test (****$p < 0.0001$, **$p < 0.01$, *$p < 0.05$).

Peptide **5** (amino acid sequence shown in Figure 6A) was functionalized with an N-terminal maleimide ligation handle for conjugation to the thiol-functionalized TDM analogues. It was synthesized using an automatic solid phase synthesizer and obtained in 6.7% yield after purification. The conjugation of the glycolipids to the synthetic long peptide was performed via thiol-maleimide addition. Self-adjuvanting peptides **6** and **7** (chemical structures shown in Figure 6A) were obtained with, respectively, 73% and 25% yield after HPLC purification. Partial precipitation and low solubility of self-adjuvanting peptide **7** in many organic solvents rendered isolation and purification of the product difficult resulting in a lower yield.

The two self-adjuvanting peptides were tested for their binding to murine Mincle. An ELISA assay was performed using the commercially available Mincle-Fc-chimera recombinant soluble receptor. This assay, as shown in Figure 6B, indicated that the two self-adjuvanting peptides had a fully preserved ability to interact with this receptor. As expected, no binding between soluble Mincle receptor and peptide **5** was observed. This result confirmed that the interaction between the self-adjuvanting peptides and Mincle is mediated by the glycolipid moiety. As additional negative controls, known CLRs ligands, such as Lewis X polyacrylamide conjugate (PAA-LewisX), Mannan and Laminarin,[32] were selected and none of them bound to Mincle. The synthetic compound TDS was used as positive control in all binding assays.[2]

Next, the functional effect of self-adjuvanting peptide **6** was studied using the well-defined, immature murine D1 dendritic cell line. As shown in Figure 6C, stimulation using self-adjuvanting peptide **6** resulted in production of significant amounts of IL-12p40, although no increase in CD40 or CD86 activation markers could be observed (data not shown). Somewhat unexpectedly, this was not the case for the mixture of separate peptide **5** and compound **3**, where neither activation nor production of the pro-inflammatory cytokine IL-12p40 was observed. ODN1826, potent immune-stimulatory agent able to interact with dendritic cells via TLR9, was used as positive control.[33]

To functionally characterise the synthetic TDM analogues and derived self-adjuvanting peptides, human dendritic cells and macrophages were generated starting from monocytes. Changes in activation or T cell co-stimulatory markers and released pro-inflammatory/anti-inflammatory cytokines were used as a measure of immunogenicity of novel constructs. Immature monocyte-derived dendritic cells (moDCs) and macrophages were differentiated as described in the Materials and Methods section of this Chapter, and their cell surface marker phenotype was characterised by CD1a, CD14, CD11b, CD163 expression.[34,35] Flow cytometry analysis of the CD83 activation marker for dendritic cells showed that little or no activation

[2] Studies performed using an HEK-Blue mMincle reporter assay resulted in absence of detectable amounts of SEAP when stimulating cells with the two self-adjuvanting peptides.

was induced by treatment with the compounds containing the shorter alkyl chains, namely compound **3** and self-adjuvanting peptide **6**, while the compounds containing the longer alkyl chain, compound **4** and self-adjuvanting peptide **7**, did induce up-regulation of this activation marker to a comparable extent to that induced by LPS (Figure 7). In the case of the CD86 marker, compound **4** induced a 5-fold increase in marker expression as compared to the negative control. The self-adjuvanting peptide **7** was responsible for a more modest up-regulation of CD86, with a 3-fold increase, comparable to the increase induced by self-adjuvanting peptide **6**. Up-regulation of the CD80 marker in human moDCs was induced only by stimulation with self-adjuvanting peptide **7**. A two-fold increase in MHC class II expression as compared to unstimulated control is observed for moDCs treated with compounds **3** and **4**, peptide **5** and the self-adjuvanting peptides. Cell supernatants were analysed via ELISA to quantify production of IL-12p40 and IL-10 (see supporting Figure S6). The anti-inflammatory cytokine IL-10 was only detected in the LPS control. On the other hand, a ten-fold increase of IL-12p40 was detected in supernatants of cells treated with the self-adjuvanting peptide **7**. Luminex analysis of the same supernatants allowed for the identification of IL-6 and TNF-α as two additional pro-inflammatory cytokines released upon treatment with self-adjuvanting peptide **7**. However, the increase in cytokine production for this compound did not show statistical significance.

Macrophage differentiation by GM-CSF, which leads to pro-inflammatory M1-type cells, and M-CSF, leading to anti-inflammatory M2-type macrophages was studied next, and the results are summarised in Figure 8. The CD80 marker was significantly upregulated on M1 and M2 macrophages upon stimulation with self-adjuvanting peptides **6** and **7**. The latter was also shown to induce CD83 upregulation on both macrophage types. Interestingly, stimulation using the unconjugated TDM analogues **3** and **4** did not promote expression of CD80. However, analogue **4** caused upregulation of CD83 to a similar extent to self-adjuvanting peptide **7** and LPS control.

Analysis of cell supernatants via ELISA for the quantification of IL-12p40 and IL-10 indicates that IL-10 is released by M-CSF/M2 macrophages upon stimulation with both self-adjuvanting peptides (Figure 9). No IL-10 nor IL-12p40 was detected in supernatants of GM-CSF/M1 macrophages.

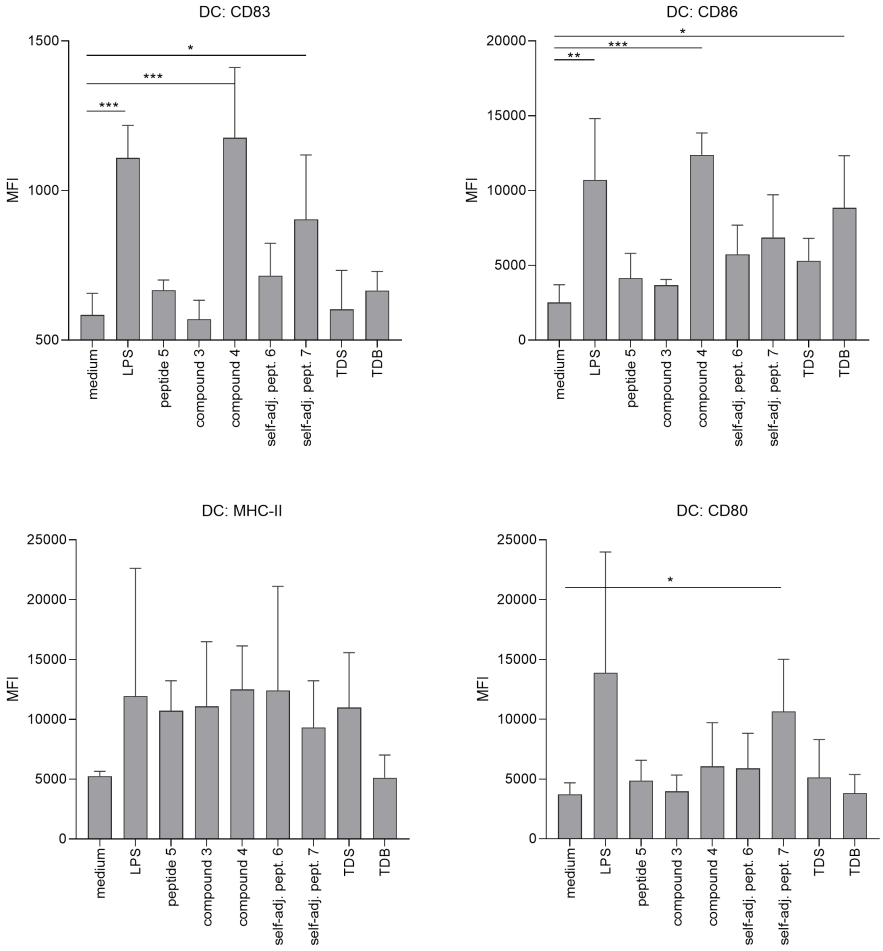

Figure 7 - Bar plots depicting the mean expression of selected surface markers on monocyte-derived dendritic cells from 3 different donors as measured by flow cytometry. All synthetic compounds were used at a final concentration of 20 μM in medium. LPS (100 ng/ml) is used as a positive control. Statistical significance with reference to cells exposed to medium + DMSO was calculated through one-way ANOVA method (***$p < 0.001$, **$p < 0.01$, *$p < 0.05$). Bars indicate the mean value + SD of the MFI dataset for each condition as calculated using GraphPad Prism.

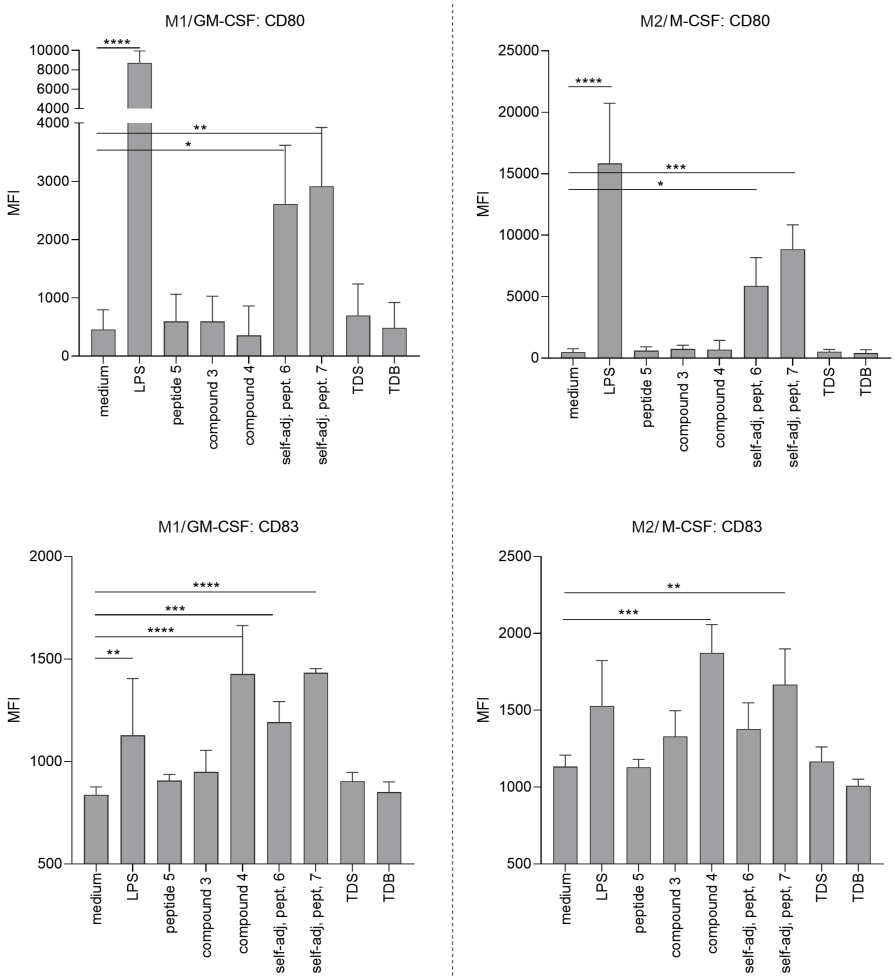

Figure 8 - Bar plots depicting the mean expression of CD80 and CD83 markers on GM-CSF/M1 and M-CSF/M2 macrophages cells from 3 different donors as measured by flow cytometry. All synthetic compounds were used at a final concentration of 20 μM in medium. LPS (100 ng/ml) is used as a positive control. Statistical significance with reference to cells exposed to medium + DMSO (0.1%) was calculated through one-way ANOVA method (****p < 0.0001, ***p < 0.001, **p < 0.01, *p < 0.05). Bars indicate the mean value + SD of the MFI dataset for each condition as calculated using GraphPad Prism.

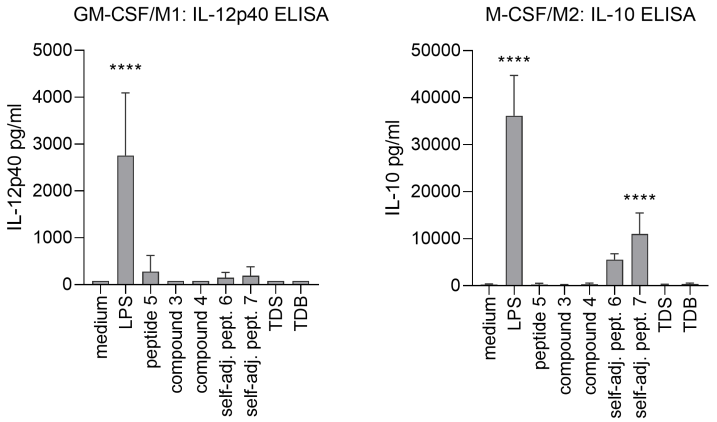

Figure 9 - Cytokine production profile of human macrophages stimulated for 20 hours using TDM analogues 3 and 4, and self-adjuvanting peptides 6 and 7, as measured by ELISA (IL-12p40 and IL-10) or Luminex (IL-6 and TNF-α). All synthetic compounds were used at a final concentration of 20 μM in medium. LPS (100 ng/ml) is used as a positive control. Bars indicate the mean value + SD of duplicates from three donors as calculated using GraphPad Prism. Statistical significance with reference to cells exposed to medium + DMSO was calculated through one-way ANOVA method (***$p < 0.001$, **$p < 0.01$, *$p < 0.05$).

3

In vivo evaluation of Mincle ligand-peptide conjugate

An HLA-DR3 transgenic mouse model lacking murine MHC class II system (HLA-DR3/Ab^0), previously shown to be suitable for the *in vivo* study of peptide p57 HLA-DR3 restricted T-cell immunity, [14] was used to evaluate the *in vivo* immunogenicity of self-adjuvanting peptide **6**. In this model, mice were immunised subcutaneously three times with either peptide **5** in admixture with ODN1826 as positive control, peptide **5** in admixture with compound **3**, self-adjuvanting peptide **6** or injected with PBS as negative control. Intracellular IFN-γ, TNF-α and IL-17 production by CD4$^+$ T-cells was measured via flow-cytometry after *in vitro* stimulation of splenocytes with either the peptide antigen or recombinant protein. The control mixture of the peptide with ODN1826 induced strong Th1 responses, as previously reported, [28] a result which was confirmed also by analysis of the cell supernatants by IFN-γ ELISA (see supporting information S7). Immunisation with either the mixture of peptide **5** with **3** or with self-adjuvanting peptide **6** did not induce detectable CD4$^+$ T-cell responses.

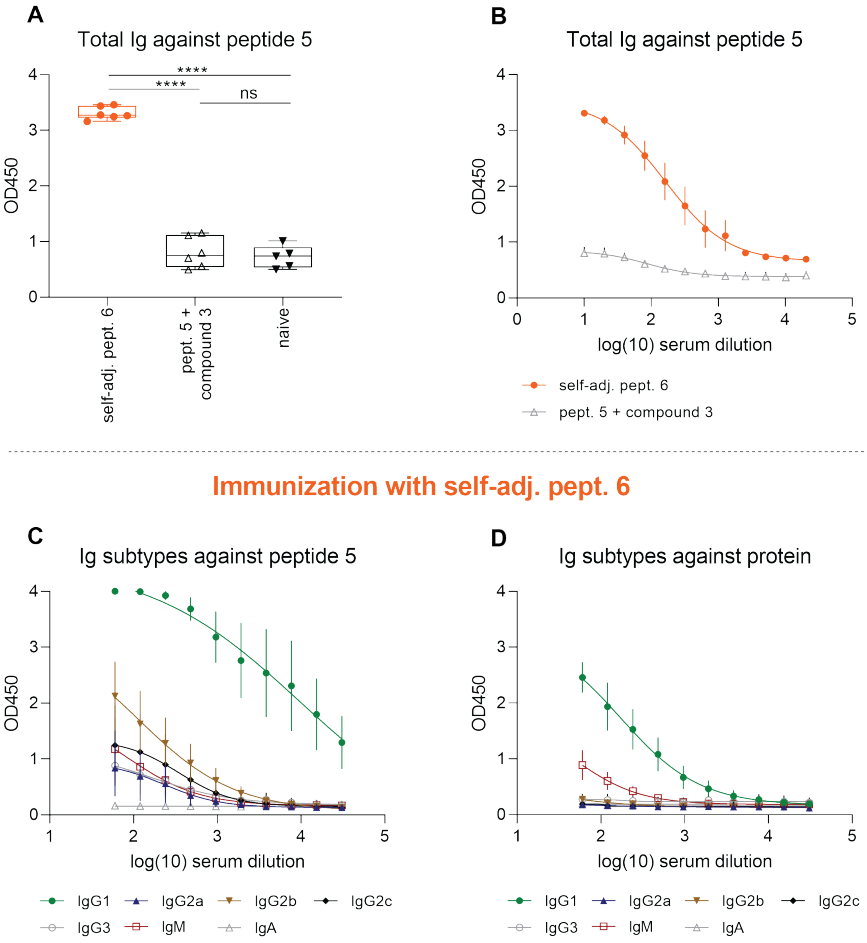

Figure 10 - Measurement of antigen-specific antibodies from sera of mice (n=6) immunized with self-adjuvanting peptide 6 (40 nmol), peptide 5 (40 nmol) in admixture with UPam adjuvant (40 nmol) or treated with PBS only (naïve group). Plate-bound peptide p57 antigen was used for the Total Ig antibodies assay. **(A)** Box plots representing absorbance (OD450) corresponding to amount of Total Ig antibodies and measured for sera diluted 10 times (n = 5 for naïve, n = 6 for the other groups). Statistical significance was calculated using one-way ANOVA as calculated with GraphPad Prism software (****p < 0.0001, ns > 0.05). **(B)** Dose-response dot plots representing mean + SEM of absorbance measurements from 5 or 6 mice as calculated using GraphPad Prism. **(C)** Measurement of antigen-specific antibody isotypes from sera of mice (n=6) immunised with self-adjuvanted peptide **6**. Plate-bound peptide 5 antigen was used for the Ig subtypes antibodies assay. Dots represent mean + SEM of single measurements from 6 mice as calculated using GraphPad Prism. **(D)** Measurement of antigen-specific antibody isotypes from sera of mice (n=6) immunised with self-adjuvanted peptide **6**. Plate-bound Rv1733c recombinant protein antigen was used for the Ig subtypes antibodies assay. Dots represent mean + SEM of single measurements from 6 mice as calculated using GraphPad Prism.

To verify if humoral responses were induced by the chosen treatments, sera were analysed for the presence of antigen-specific antibodies (see Figure 10). The mixture of antigen plus adjuvant did not stimulate production of antigen-specific antibodies. In striking contrast, self-adjuvanting peptide **6** consistently induced production of antibodies able to bind peptide **5**, indicating the importance of antigen-adjuvant co-delivery. Analysis of antibody subtypes lead to the identification of high titers of antigen-specific IgG1, associated with Th2 activation in mice, able to recognize both peptide **5** and its source, Rv1733c protein. In addition, IgG2b antibodies, associated with T-cell independent responses, that were able to recognize the peptide antigen were also found.[36–38]

To further assess the vaccine potential of the self-adjuvanting peptide **6**, its prophylactic effect was evaluated using a live *Mtb* challenge model. Here enumeration of the colony forming units (CFU) in the lung and spleen of infected mice was used as a measure of protection.

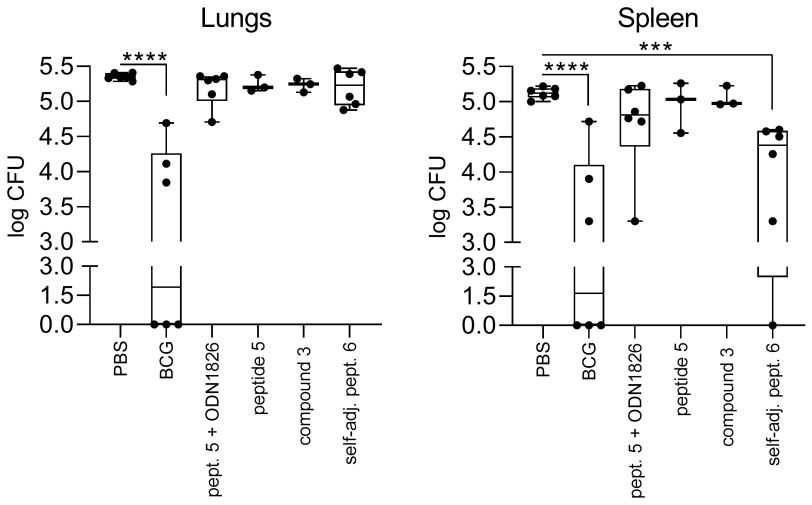

Figure 11 - Protective efficacy against *Mtb* infection in the spleen of mice that were immunised s.c. for 3 times with 2 weeks interval. Mice (n=6) were immunised with a mixture of peptide 5 (40 nmol) with ODN1826 (50 µg/ml) as positive control, with self-adjuvanted peptide 6 (40 nmol) or mice (n=3) were treated with TDM analogue 3 (40 nmol) or with peptide 5 (40 nmol). Six weeks later, the mice were challenged with intranasal *Mtb* H37Rv (10^5 CFU). Alternatively, the mice received 10^6 CFU BCG s.c. 10 weeks before challenge. Colonies in lungs and spleen were counted after 3 weeks of incubation at 37 °C. Statistical significance with reference to the naive group was calculated through one-way ANOVA method (****$p < 0.0001$, ***$p < 0.001$). Box plots were generated using GraphPad Prism.

The following groups were included in the study: mice immunised with a mixture of peptide **5** with ODN1826, mice immunised with the standard BCG1331 vaccine, mice immunised with peptide **5** only, mice immunised with TDM analogue **3** and mice immunised the self-adjuvanting peptide **6**. As shown in Figure 11, analysis of infection progression in the lungs of immunised mice indicated that only the BCG control was able to cause a reduction of the bacterial load locally in the lungs at the time of organ isolation. Nevertheless, signs of a protective systemic immune response were evident when analysing the spleen of mice immunised with the self-adjuvanting peptide **6**, as the latter significantly reduced the number of CFU in the spleen of vaccinated mice (Figure 11). This reduction is present only in the case of vaccination with the self-adjuvanting peptide, and not following vaccination with the unconjugated peptide or compound **3**. Vaccination with the self-adjuvanting peptide led to a lower bacterial count than vaccination with the mixture of the peptide with ODN1826.

Discussion

The study discussed in this Chapter shows that conjugation of the latency antigen Rv1733c p57 peptide to synthetic compound **3**, a novel Mincle ligand, induces stronger immune responses *in vivo* than the simple admixture of adjuvant-antigen. This study provides the first evidence that a self-adjuvanting peptide containing a TDM analogue can induce protection against TB in an *in vivo* model.

Considerations on the design rationale of the TDM and GMM analogues containing a ligation handle for conjugation to the Rv1733c p57 peptide antigen were detailed in the introduction section of this Chapter. Binding of TDM analogues **3** and **4** to the murine Mincle receptor did not seem to be affected by the introduction of a thiol ligation handle, which was purposefully located on the 6' O-alkyl chain. Comparison of the dose-response curves for compounds **3**, **4** and the structurally similar experimental control TDS, lacking the thiol ligation handle, indicated comparable activation of the HEK-Blue mMincle reporter cell line upon stimulation with the aforementioned compounds.

Using the same HEK-Blue mMincle reporter assay, it was observed that the two GMM synthetic adjuvants also activated this reporter cell line. A difference was, however, recognized when comparing the two TDM analogues to the two GMM analogues, with the GMM analogues inducing significantly lower activation.

For this reason, the TDM analogues were used to generate the two single molecule subunit vaccines. The synthesis of the trehalose conjugates was achieved by reacting the thiol-functionalised glycolipids with a maleimide functionalised peptide. This reaction required judicious solvent optimization, to meet the different solubility requirements of the two reagents. A mixture of DMF/chloroform/water 4:3:1 was

identified to allow for optimal solubilization of both reagents and by adjusting the pH of the mixture to 8 by addition of N-methyl-morpholine.

The conjugates, composed of the peptide antigen and TDM analogues, were assayed for their ability to activate HEK-Blue mMincle cells. Unexpectedly, the responses were very low for both self-adjuvanting peptides. Aggregation of the conjugates was observed experimentally at the highest concentrations, and this could explain the reduced binding of the conjugates in the HEK-Blue mMincle cells.[3] Further research into the specific cause of the unexpected result would be required to shed light on the significance of these results. To verify if this result was connected to the model or it would indicate disrupted binding of the glycolipid moiety to the Mincle receptor, an additional model was selected to qualitatively assess the interaction to the murine receptor. Following the steps of Decout *et al.* and Chinthamani *et al.*,[29,40] an ELISA assay was performed using the commercially available murine Mincle-Fc-chimera receptor. This assay indicated that the two self-adjuvanting peptides preserved the ability to interact with Mincle.[4]

The functional effect of the synthetic glycolipids and self-adjuvanting peptides was studied using human monocyte-derived dendritic cells and macrophages. Changes in expression of CD80, CD83and CD86 molecules were monitored via flow cytometry as an indication of stimulatory activity of the synthetic compounds. CD80 and CD86 are type I glycoproteins expressed on the surface of APCs, with the ability to interact with CD28 and with cytotoxic T lymphocyte antigen-4 (CTLA-4) expressed on activated T cells.[41] They are therefore conventionally considered co-stimulatory molecules for T cells, and their upregulation is associated with APC activation.[42] CD83 is a member of the immunoglobulin family and is conventionally used as a marker for mature dendritic cells, although it is expressed on the cell surface of several APCs.[43]

The results here described clearly indicate that human monocyte-derived dendritic cells respond differently to the two synthetic TDM analogues and that the response depends on the difference in alkyl chain length. Flow cytometry analysis of the CD83 and CD86 activation markers for dendritic cells showed that little or no activation is induced by treatment with the compounds containing the shorter C11-alkyl chain (compounds **3** and **6**), while the compounds containing the longer C16-alkyl chain (compounds **4** and **7**) induced up-regulation of these activation markers to an extent comparable to that induced by LPS. As previously mentioned, several reports have suggested that biological activity depends on the lipid chain length in trehalose mono- and di-esters. However, those studies focused on murine bone-marrow derived macrophages and employed plate-bound glycolipids. It is not possible to

[3] An alternative hypothesis could be endoplasmatic reticulum stress, which has been previously shown to cause critical interference in secreted protein-based reporter assays. [39]

[4] The use of human Mincle-Fc-chimera in a preliminary ELISA assay indicated that the novel adjuvants and self-adjuvanting peptides are also capable of binding to the human receptor (see Chapter 6).

directly compare the results obtained using dissolved/suspended compounds to those referring to experiments performed using plate-bound glycolipids.[19,28]. With the goal of incorporating a Mincle ligand in a self-adjuvanting peptide construct, and, at a later stage, further expand the self-adjuvanting construct to include an additional adjuvant, the use of plate-bound lipid was avoided in the evaluation of the *in vitro* functional studies reported in this Chapter. Furthermore, the supernatants from moDCs were analysed via ELISA and Luminex for the quantification of pro-inflammatory cytokines, and it was observed that only the self-adjuvanting peptide **7** induced release of IL-12p40, IL-6 and TNF-α. These cytokines were not released upon stimulation with the stand-alone trehalose adjuvant nor the peptide, suggesting either a synergistic effect of the two or, possibly, formation of supramolecular structures which results in improved immunogenicity for the self-adjuvanting peptide.

Analysis of the activation markers for GM-CSF/M1 and M-CSF/M2 macrophages further indicated that the self-adjuvanting peptides more strongly activated human antigen-presenting cells than the TDM analogues alone, as exemplified by expression of CD80 for M1 and M2 and cytokine production by M2 macrophages. However, activation of macrophages seems to be less sensitive to the alkyl chain length of the TDM analogue linked to the peptide. Further structure-activity relationship studies to identify how the chain length influences response in human monocyte-derived dendritic cells are warranted.

To compare the vaccine potential of the self-adjuvanting peptide **6** to that of a mixture of adjuvant **3** and peptide **5**, an *in vivo* experiment was performed to assess both cellular and humoral responses in class II-deficient mice, transgenic for HLA-DRA/B1*0301 (DR3) allele. The expected responses were found in the group of mice immunised subcutaneously with positive control, where IFN-γ TNF-α double positive $CD4^+$ T-cell responses were detected. The IFN-γ production by restimulated splenocytes in the control group was confirmed by ELISA assay performed on splenocytes supernatant. On the contrary, no $CD4^+$ T-cell responses were detected for either the mixture of antigen plus compound **3** nor self-adjuvanting peptide **6**. Splenocytes supernatants were also assayed using a Luminex kit for the identification of cytokine increase upon restimulation. Also in this case, no increase in quantity of cytokines was observed upon restimulation. To verify if humoral responses were induced by the self-adjuvanting peptide, sera were analysed for the presence of antigen-specific antibodies. The mixture of antigen plus compound **3** did not stimulate production of antigen-specific antibodies. On the contrary, high titers of IgG1 and IgG2b antibodies were induced by immunisation with the self-adjuvanting peptide **6**. Murine IgG1 antibodies are usually associated with a Th2 type response and their production is shown to increase in the presence of IL-4.[36,37] Switching to IgG2b antibodies seems to be mediated by transforming-growth factor-β and it has been associated with a T-independent immune response.[38]

The majority of TB vaccine candidates currently in clinical trials have been selected on the basis of pre-clinical studies focused on inducing a $CD4^+$ Th1/Th17 cellular response.[44] The paradigm of protection that revolved around the induction of polyfunctional $CD4^+$ T-cells in response to immunisation is only very recently shifting towards a broader interest in the interplay between innate, cellular and humoral immunity to tackle the challenge of developing an effective TB vaccine.[44–46] To further assess if the self-adjuvanting peptide could effectively counteract *Mtb* infection, even though only humoral responses were detected, a challenge experiment with live *Mtb* was performed. Following the same immunisation protocol described above, and using BCG immunisation as positive control, it was determined that the self-adjuvanting peptide **6** was able to reduce hepatic bacterial load in vaccinated mice, although no effect was observed in the lungs of the same mice. This adds to the growing body of evidence that significant protective effects against mycobacterial infection can be observed in the presence of humoral responses.[47,48]

Conclusion

Subunit vaccines comprised of fully-synthetic antigens and adjuvants represent a promising strategy to overcome safety-related issues connected to BCG immunisation against *Mtb*, and co-delivery of antigen and adjuvant in single-molecule vaccines allows for the induction of strong immune-responses. The work reported in this Chapter describes the generation of a prototype synthetic *Mtb*-vaccine, formed by linking a glycolipid adjuvant and a *Mtb* derived peptide. For that purpose, four novel simplified analogues of immune adjuvants TDM and GMM were designed and successfully synthesized already equipped with a thiol ligation handle for conjugation to antigenic peptides. The TDM analogues, the most potent Mincle binders identified in the present study, were chosen for the generation of two self-adjuvanting peptides. This study provides a proof of principle that fully synthetic self-adjuvanting peptides containing a Mincle ligand are immunogenic and can induce protection against *Mtb* infection, in association with humoral (including IgG1 and IgG2b) but unexpectedly, no detectable cellular ($CD4^+$ T cell) responses. The results from the murine experiments here described indicate the presence of antigen-specific IgG1 and IgG2b antibodies in the sera of mice immunised with self-adjuvanting peptide **6** and a reduced bacterial load in their spleen, which is indicative of a systemic and protective immune response induced by this construct. Further research is required to determine if the observed protection can be generalised to other antigens and whether this solely depends on humoral immune responses.

Materials and methods

General synthetic methods

General synthetic methods and description of analytical instrumentation are provided in the materials and methods section of Chapter 2.

Glucose monomycolate analogues

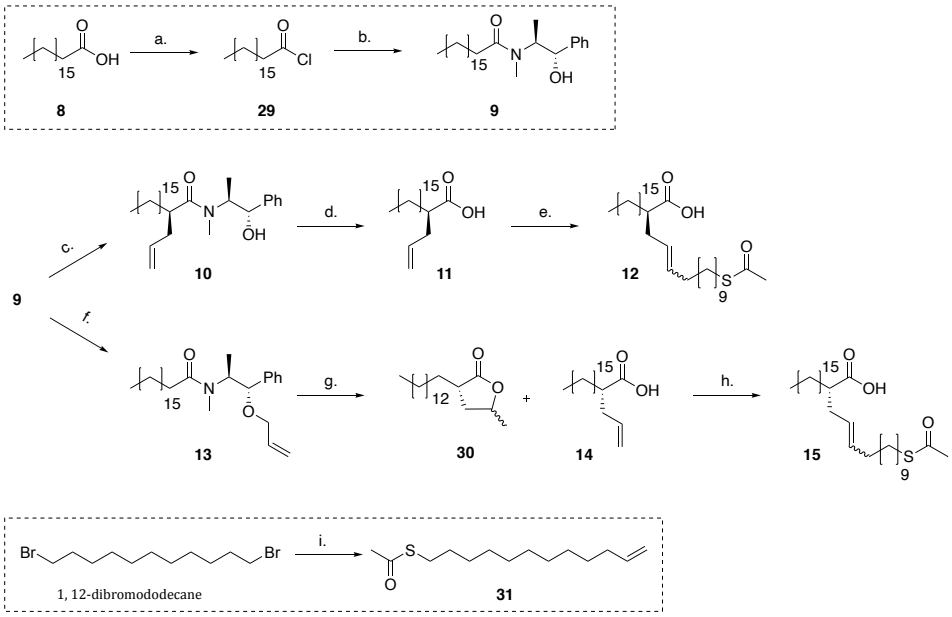

S1 Figure - Synthetic scheme for the generation of lipid moieties of glucose monomycolate analogues. a) oxalyl chloride, DMF, toluene, y: 99%, b) pseudoephedrine, Et_3N, DCM, y: 99%, c) DIPA, LiCl, allyl bromide, THF, y: 84%, d) H_2SO_4 (5N)/dioxane 1:1, y: 73%, e) *S*-(dodec-11-en-1-yl) ethanethioate, Grubbs 1st generation, DCM, reflux, y: 76%, f) NaH, allyl bromide, DCM, y: 86%, g) i. Tf_2O, 2-fluoropyridine, DCM, 0 °C, ii. H_2SO_4 (2.5 N)/dioxane 1:1, 100, y of **14**: 60%, h) *S*-(dodec-11-en-1-yl) ethanethioate, Grubbs 1st generation, DCM, reflux, y: 76%, i) i. Potassium tert-butoxide, THF/toluene 2:1, 5 °C, ii. Potassium thioacetate, DMF, 80 °C, y: 19%.

S-(dodec-11-en-1-yl) ethanethioate (31).

A solution of 1, 12-dibromododecane (39.4 g, 120 mmol, 1 eq) in THF/toluene 2:1 (80 ml) was cooled to 0 °C. Potassium tert-butoxide (20.2 g, 180 mmol, 1.5 eq) was added to the solution in portions of about 2 g over 30 minutes. After addition of the last portion of potassium tert-butoxide, the reaction mixture was stirred at 5 °C for 1 hour. The reaction was then quenched with water and HCl (1 M) and transferred to a separatory funnel. The water layer was extracted (3x) with toluene and the combined organic layers were washed (1x) with HCl (1 M) and (2x) with brine. The toluene layer was dried over $MgSO_4$, filtered and concentrated in vacuo. The crude from the elimination reaction was dissolved in DMF (800 ml) for the subsequent reaction. Potassium thioacetate (25 g, 219 mmol, 1.8 eq) was added to this solution and heated to 80 °C for 2 hours. The reaction was then quenched with water, diluted with Et_2O and transferred to a separatory funnel. The water layer was extracted (3x) with Et_2O, then the combined organic layers were washed (1x) with water and (1x) with brine. The organic layer was dried over $MgSO_4$, filtered and concentrated in vacuo. Compound **31** was obtained after silicagel chromatography (Pentane/Et_2O 95:5; DCM loading of crude) as a transparent oil (5.6 g, 23.1 mmol, 19% over two steps). ^{1}H NMR (300 MHz, $CDCl_3$) δ: 5.80 (ddt, *J* = 16.9, 10.2, 6.7 Hz, 1H, CH=), 5.07 – 4.80 (m, 2H, CH_2=), 2.86 (t, *J* = 7.3 Hz, 2H, CH_2-S), 2.31 (s, 3H, CH_3-thioacetyl), 2.10 – 1.94 (m, 2H, CH_2-allylic), 1.63 – 1.47 (m, 2H, CH_2-lipid), 1.44 – 1.12 (m, 16H, CH_2-lipid). ^{13}C-APT NMR (75 MHz, $CDCl_3$) δ: 195.9 (S-C=O), 139.2 (CH=), 114.2 (CH_2=), 33.9 (CH_2-allylic), 30.6 (CH_3-thioacetyl), 29.6 (CH_2-lipid), 29.5 (CH_2-lipid), 29.2 (CH_2-lipid), 29.1 (CH_2-lipid), 29.0 (CH_2-lipid), 28.9 (CH_2-lipid). HRMS $[M+H]^+$: 243.17762 found, 243.17771 calculated.

Stearoyl chloride (29).

Stearic acid (17.71 g, 60 mmol, 1 eq) and DMF (0.6 ml, 7.8 mmol, 0.13 eq) were dissolved in toluene (600 ml) and cooled to 0 °C. Oxalyl chloride (21 ml, 240 mmol, 4 eq) was added dropwise to the solution via cannula over 15 minutes. The resulting solution was slowly allowed to heat up to room temperature. After stirring for 20 hours at RT, the solution was heated to reflux to complete the reaction. Solvents and volatiles were removed by rotatory evaporation under fume hood. Compound **29** was obtained as a white solid (18.02 g, 59.5 mmol, 99%) without any further purification. NMR analysis confirmed purity of the product, whose ^{1}H NMR and ^{13}C NMR spectra were in agreement with published literature.[49]

N-((1S,2S)-1-hydroxy-1-phenylpropan-2-yl)-N-methylstearamide (9).

Pseudoephedrine (3.3 g, 20 mmol, 1 eq) was dissolved in DCM (70 ml). Triethylamine (5.6 ml, 40 mmol) was added and this solution was cooled to 0 °C. A solution of compound **29** in DCM (30 ml) was added dropwise to the pseudoephedrine solution via cannula over 20 minutes. The reaction mixture was then heated up to room temperature and stirred overnight. The reaction mixture was quenched with a saturated solution of NH_4Cl (aq), diluted in EtOAc and transferred to a separatory funnel. The water layer was extracted (3x) with EtOAc and the combined organic layers were dried over $MgSO_4$, filtered and concentrated in vacuo. Compound **9** was obtained after silicagel chromatography (Pentane/EtOAc 5:1→1:1; DCM loading of crude; Et_3N neutralization of silica) as a white solid (8.57 g, 19.8 mmol, 99%). Rotamer a: ^{1}H NMR (400 MHz, $CDCl_3$) δ: 7.42 – 7.14 (m, 5H, H-arom), 4.73 – 4.51 (m, 2H, CH-Bn, OH), 4.51 – 4.34 (m, 1H, CH-N), 2.79 (s, 3H, CH_3-N), 2.33 – 2.17 (m, 2H, CH_2-C=O), 1.66 – 1.49 (m, 2H, CH_2-lipid), 1.36 – 1.16 (m, 28H, CH_2-lipid), 1.08 (d, J = 6.9 Hz, 3H, CH_3-lipid), 0.92

– 0.82 (m, 3H, CH_3-lipid). ^{13}C-APT NMR (101 MHz, $CDCl_3$) δ: 175.5 (C=O), 142.6 (C-arom), 128.3 (C-arom), 127.6 (C-arom), 126.4 (C-arom), 76.5 (CH-Bn), 58.4 (CH-N), 34.4 (CH_2-C=O), 32.9 (CH_3-N), 32.0 (CH_2-lipid), 29.7 (CH_2-lipid), 29.7 (CH_2-lipid), 29.7 (CH_2-lipid), 29.7 (CH_2-lipid), 29.6 (CH_2-lipid), 29.6 (CH_2-lipid), 29.5 (CH_2-lipid), 29.5 (CH_2-lipid), 29.5 (CH_2-lipid), 29.4 (CH_2-lipid), 25.1 (CH_2-lipid), 22.7(CH_2-lipid), 14.5 (CH_3-lipid), 14.2 (CH_3-lipid). Rotamer b: ^{1}H NMR (400 MHz, $CDCl_3$) δ: 7.42 – 7.14 (m, 5H, H-arom), 4.73 – 4.51 (m, 1H, CH-Bn), 3.97 (dq, J = 8.7, 6.8 Hz, 1H, CH-N), 3.52 (s, 1H, OH), 2.88 (s, 3H, CH_3-N), 2.38 (t, J = 7.8 Hz, 2H, CH_2-C=O), 1.66 – 1.49 (m, 2H, CH_2-lipid), 1.36 – 1.16 (m, 28H, CH_2-lipid), 0.96 (d, J = 6.7 Hz, 3H, CH_3-lipid), 0.92 – 0.82 (m, 3H, CH_3-lipid). ^{13}C-APT NMR (101 MHz, $CDCl_3$) δ: 174.4 (C=O), 141.7 (C-arom), 128.6 (C-arom), 128.2 (C-arom), 127.0 (C-arom), 75.4 (CH-Bn), 58.4 (CH-N), 33.8 (CH_2-C=O), 32.0 (CH_2-lipid), 29.7 (CH_2-lipid), 29.7(CH_2-lipid), 29.7 (CH_2-lipid), 29.7 (CH_2-lipid), 29.6 (CH_2-lipid), 29.6 (CH_2-lipid), 29.5 (CH_2-lipid), 29.5 (CH_2-lipid), 29.5 (CH_2-lipid), 29.4 (CH_2-lipid), 26.8 (CH_3-N), 25.5 (CH_2-lipid), 22.7 (CH_2-lipid), 15.4 (CH_3-lipid), 14.2 (CH_3-lipid). HRMS $[M+Na]^+$: 454.3652 found, 454.3655 calculated.

(R)-2-allyl-N-((1S,2S)-1-hydroxy-1-phenylpropan-2-yl)-N-methyloctadecanamide (10).

Diisopropylamine (1.39 ml, 9.9 mmol, 4.4 eq) and LiCl (1.14 g, 27 mmol, 12 eq) were suspended in dry THF (45 ml) and the suspension was cooled to -78 °C. A solution of *n*-BuLi (1.6 M in hexanes) (5.6 ml, 9 mmol, 4 eq) was added dropwise via syringe to the THF solution. The reaction mixture was quickly warmed to 0 °C, stirred at this temperature for 10 minutes, then cooled again to -78 °C. Compound **9** (1.94 g, 4.5 mmol, 2 eq) was co-evaporated (3x) with dry toluene, then dissolved in THF (10 ml) and slowly added to the freshly made LDA solution. The reaction mixture was stirred at -78 °C for 1 hour and 30 minutes before being heated up to 0 °C and stirred at this temperature for 15 minutes. The reaction mixture was then heated up further to RT for 5 minutes and cooled again at 0 °C for the addition of allyl bromide (195 µL, 2.25 mmol, 1 eq). After 2 hours, the reaction was quenched by the addition of a saturated solution of NH_4Cl (aq) (100 ml, 10 minutes stirring at 0 °C), diluted with EtOAc and transferred to a separatory funnel. The water layer was extracted (3x) with EtOAc and the combined organic layers were dried over $MgSO_4$, filtered and concentrated in vacuo. Compound **10** was obtained after silicagel chromatography (Pentane/EtOAc 8:1→4:1; DCM loading of crude; Et_3N neutralization of silica) as a white solid (0.90 g, 1.9 mmol, 84%). Rotamer a:^{1}H NMR (400 MHz, $CDCl_3$) δ: 7.45 – 7.17 (m, 5H, H-arom), 5.64 (ddt, J = 17.2, 10.1, 7.0 Hz, 1H, CH=), 5.00 – 4.90 (m, 2H, CH_2=), 4.70 – 4.53 (m, 1H, CH-Bn), 4.41 (s, 1H, CH-N), 2.84 (bs, 3H, CH_3-N), 2.63 (tt, J = 8.4, 5.6 Hz, 1H, CH-C=O), 2.27 (dtt, J = 26.6, 13.6, 6.6 Hz, 1H, CH_2-allylic), 2.19 – 2.07 (m, 1H, CH_2-allylic), 1.70 – 1.52 (m, 1H, CH_2-lipid), 1.52 – 1.35 (m, 1H, CH_2-lipid), 1.34 – 1.17 (m, 28H, CH_2-lipid), 1.14 (d, J = 7.0 Hz, 3H, CH_3-lipid), 0.92 – 0.79 (m, 3H, CH_3-lipid). ^{13}C-APT NMR (101 MHz, $CDCl_3$) δ: 178.0 (C=O), 142.6 (C-arom), 136.1 (CH=), 128.4 (C-arom), 127.6 (C-arom), 126.4 (C-arom), 116.6 (CH_2=), 76.4 (CH-Bn), 58.4 (CH-N), 42.4 (CH-C=O), 37.2 (CH_2-allylic), 33.7(CH_3-N), 32.7 (CH_2-lipid), 32.0 (CH_2-lipid), 29.9 (CH_2-lipid), 29.9 (CH_2-lipid), 29.8 (CH_2-lipid), 29.8 (CH_2-lipid), 29.8 (CH_2-lipid), 29.8 (CH_2-lipid), 29.7 (CH_2-lipid), 29.7 (CH_2-lipid), 29.6 (CH_2-lipid), 29.5 (CH_2-lipid), 27.5 (CH_2-lipid), 27.1 (CH_2-lipid), 22.8 (CH_2-lipid), 14.7 (CH_3-lipid), 14.3 (CH_3-lipid). Rotamer b: ^{1}H NMR (400 MHz, $CDCl_3$) δ: 7.45 – 7.17 (m, 5H, H-arom), 5.95–5.71 (m, 1H, CH=), 5.19 – 5.00 (m, 2H, CH_2=), 4.70 – 4.53 (m, 1H, CH-Bn), 4.21 – 4.04 (m, 1H, CH-N), 2.91 (s, 3H, CH_3-N), 2.89 – 2.77 (m, 1H, CH-C=O), 2.53 – 2.42 (m, 1H, CH_2-allylic), 2.42 – 2.19 (m, 1H, CH_2-allylic), 1.70 – 1.52 (m, 1H, CH_2-lipid), 1.52 – 1.35 (m, 1H, CH_2-lipid), 1.34 – 1.17 (m, 28H, CH_2-lipid), 0.99 (d, J = 6.7 Hz, 3H, CH_3-lipid), 0.92 – 0.79 (m, 3H, CH_2-lipid). ^{13}C-APT NMR (101 MHz, $CDCl_3$) δ: 176.8 (C=O), 141.2 (C-arom), 137.0 (CH=), 128.8 (C-arom),

128.5 (C-arom), 127.1 (C-arom), 116.8 (CH_2=), 116.7 (CH_2=), 76.3 (CH-Bn), 75.5 (CH-Bn), 58.4 (CH-N), 41.5 (CH-C=O), 37.4 (CH_2-allylic), 32.9 (CH_2-lipid), 32.0 (CH_2-lipid), 29.9 (CH_2-lipid), 29.9 (CH_2-lipid), 29.8 (CH_2-lipid), 29.8 (CH_2-lipid), 29.8 (CH_2-lipid), 29.8 (CH_2-lipid), 29.7 (CH_2-lipid), 29.7(CH_2-lipid), 29.6 (CH_2-lipid), 29.5 (CH_2-lipid), 27.7 (CH_2-lipid), 27.1 (CH_3-N), 22.8 (CH_2-lipid), 15.7 (CH_3-lipid), 14.3 (CH_3-lipid). HRMS $[M+Na]^+$: 494.3971 found, 494.3968 calculated.

(R)-2-allyl octadecanoic acid (11).

Compound **10** (192 mg, 0.41 mmol, 1 eq) was dissolved in dioxane (2 ml). A solution of H_2SO_4 in water (5 N, 2 ml) was added and the reaction mixture was stirred at reflux over the weekend. After cooling the reaction mixture to RT, water (40 ml) and DCM (20 ml) were added before transferring to a separatory funnel. The water layer was extracted (3x) with DCM. The combined organic layers were dried over $MgSO_4$, filtered and concentrated in vacuo. Compound **11** was obtained after silicagel chromatography (Pentane/EtOAc 8:1→1:1; Pentane/EtOAc 8:1 + a drop of DCM for loading of crude) as a white solid (103 mg, 0.3 mmol, 73%). ^{1}H NMR (400 MHz, $CDCl_3$) δ: 5.77 (ddt, J = 16.8, 10.1, 6.8 Hz, 1H, CH=), 5.19 – 4.93 (m, 2H, CH_2=), 2.51 – 2.32 (m, 2H, CH-C=O, CH_2-allylic), 2.32 – 2.18 (m, 1H, CH_2-allylic), 1.73 – 1.57 (m, 1H, CH_2-lipid), 1.57 – 1.45 (m, 1H, CH_2-lipid), 1.32 – 1.23 (m, 28H, CH_2-lipid), 0.93 – 0.83 (m, 3H, CH_3-lipid). ^{13}C-APT NMR (101 MHz, $CDCl_3$) δ: 182.6 (C=O), 135.4 (CH=), 117.1 (CH_2=), 45.4 (CH-C=O), 36.3 (CH_2-lipid), 32.1 (CH_2-lipid), 31.7 (CH_2-lipid), 29.9 (CH_2-lipid), 29.8 (CH_2-lipid), 29.8 (CH_2-lipid), 29.8 (CH_2-lipid), 29.7 (CH_2-lipid), 29.6 (CH_2-lipid), 29.5 (CH_2-lipid), 27.3 (CH_2-lipid), 22.9 (CH_2-lipid), 14.3 (CH_3-lipid). HRMS $[M+H]^+$: 325.3105 found, 325.3101 calculated.

(R)-2-(13-(acetylthio)tridec-2-en-1-yl)octadecanoic acid (12).

Compound **11** (227 mg, 0.7 mmol, 1 eq) was co-evaporated with toluene (2x) and dissolved in dry DCM (15 ml). Compound **31** (970 mg, 4 mmol, 5.7 eq) was also co-evaporated with toluene (2x) before being dissolved in DCM (5 ml) and added to the carboxylic acid solution. After addition of Grubbs 1st generation catalyst (41 mg, 0.05 mmol, 0.07 eq), the solution was heated to reflux overnight. Compound **12** was obtained after removal of volatiles followed by silicagel chromatography (Pentane/EtOAc 20:1→5:1; DCM for loading of crude) and size exclusion (LH-20, DCM/MeOH, 1/1, v/v) as a white solid (308 mg, 0.53 mmol, 76%). ^{1}H NMR (400 MHz, $CDCl_3$) δ: 5.47 (dt, J = 14.9, 6.6 Hz, 1H, CH=), 5.41– 5.28 (m, 1H, CH=), 2.86 (t, J = 7.3 Hz, 2H, CH_2S), 2.51 – 2.09 (m, 6H, CH_3-thioacetyl, CH_2-allylic, CH-C=O), 1.99 (dq, J = 20.9, 7.6, 7.0 Hz, 2H, CH_2-allylic), 1.61 – 1.44 (m, 4H, CH_2-lipid), 1.36 – 1.19 (m, 42H, CH_2-lipid), 0.93 – 0.82 (m, 3H, CH_3-lipid). ^{13}C NMR (101 MHz, $CDCl_3$) 196.2 (S-C=O), 182.5 (C=O), 133.5 (CH=), 126.5 (CH=), 45.7 (CH-C=O), 35.2 (CH_2-allylic), 32.7 (CH_2-allylic), 32.1 (CH_2-lipid), 31.6 (CH_2-lipid), 30.8 (CH_3-thioacetyl), 29.9 (CH_2-lipid), 29.8 (CH_2-lipid), 29.8 (CH_2-lipid), 29.8 (CH_2-lipid), 29.7 (CH_2-lipid), 29.6 (CH_2-lipid), 29.6 (CH_2-lipid), 29.6 (CH_2-lipid), 29.6 (CH_2-lipid), 29.5 (CH_2-lipid), 29.3 (CH_2-lipid), 29.3 (CH_2-lipid), 29.2 (CH_2-lipid), 29.0 (CH_2-lipid), 27.4 (CH_2-lipid), 22.8 (CH_2-lipid), 14.3 (CH_3-lipid). HRMS $[M+Na]^+$: 561.4315 found, 561.4312 calculated.

N-((1S, 2S)-1-(allyloxy)-1-phenylpropan-2-yl)-N-methylstearamide (13).

Compound **9** (3.44 g, 7.98 mmol, 1 eq) was co-evaporated (2x) with toluene and dissolved in a mixture of dry DCM/DMF 1:1 (80 ml) and CH_3CN (1 ml). Allylbromide (1 ml, 11.97 mmol, 1.5 eq) was added and the reaction mixture was cooled to 0 °C. After the addition of NaH (478 mg,

11.97 mmol, 1.5 eq) the solution was slowly heated to RT and stirred overnight. The reaction was quenched with water on ice, diluted with EtOAc and transferred to a separatory funnel. The organic layer was washed (2x) with brine, dried over $MgSO_4$, filtered and concentrated in vacuo. Compound **13** was obtained as a white solid (3.22 g, 6.83 mmol, 86%) without the need for further purification. Rotamer a: ^{1}H NMR (400 MHz, $CDCl_3$) δ: 7.41 – 7.24 (m, 5H, H-arom), 5.81 (dddd, J = 16.8, 10.6, 6.1, 4.7 Hz, 1H, CH=), 5.25 – 5.06 (m, 2H, CH_2=), 4.20 (d, J = 8.3 Hz, 1H, CH-Bn), 4.09 – 3.99 (m, 1H, CH-N), 3.88 (dddd, J = 17.7, 13.0, 4.7, 1.6 Hz, 1H, CH_2-allylic), 3.65 (dddd, J = 14.5, 12.9, 6.1, 1.5 Hz, 1H, CH_2-allylic), 2.87 (s, 3H, CH_3-N), 2.34 (dd, J = 8.1, 7.6 Hz, 2H, CH_2-C=O), 1.71– 1.48 (m, 2H, CH_2-lipid), 1.38 – 1.16 (m, 28H, CH_2-lipid), 0.99 (d, J = 6.6 Hz, 3H, CH_3-lipid), 0.88 (t, J = 6.8 Hz, 3H, CH_3-lipid). ^{13}C-APT NMR (101 MHz, $CDCl_3$) δ: 174.4 (C=O), 139.4 (C-arom), 134.5 (CH=), 128.8 (C-arom), 128.4 (C-arom), 127.6 (C-arom), 116.9 (CH_2=), 82.1 (CH-Bn), 69.5 (CH_2-allylic), 57.3 (CH-N), 33.6 (CH_2-C=O), 32.0 (CH_2-lipid), 29.8 (CH_2-lipid), 29.8 (CH_2-lipid), 29.7 (CH_2-lipid), 29.7 (CH_2-lipid), 29.7 (CH_2-lipid), 29.6 (CH_2-lipid), 29.6 (CH_2-lipid), 29.5 (CH_2-lipid), 29.4 (CH_2-lipid), 29.3 (CH_2-lipid), 27.2 (CH_3-N), 25.5 (CH_2-lipid), 25.2 (CH_2-lipid), 25.0 (CH_2-lipid), 22.8 (CH_2-lipid), 14.3 (CH_3-lipid), 14.2 (CH_3-lipid). Rotamer b: ^{1}H NMR (400 MHz, $CDCl_3$) δ: 7.41 – 7.24 (m, 5H, H-arom), 5.81 (dddd, J = 16.8, 10.6, 6.1, 4.7 Hz, 1H, CH=), 5.25 – 5.06 (m, 2H, CH_2=), 5.03 –4.83 (m, 1H, CH-N), 4.34 (bs, 1H, CH-Bn), 3.88 (dddd, J = 17.7, 13.0, 4.7, 1.6 Hz, 1H, CH_2-allylic), 3.65 (dddd, J = 14.5, 12.9, 6.1, 1.5 Hz, 1H, CH_2-allylic), 2.87 (s, 3H, CH_3-N), 2.25 (td, J = 7.3, 1.9 Hz, 1H, CH_2-C=O), 1.71 – 1.48 (m, 2H, CH_2-lipid), 1.38 – 1.16 (m, 28H, CH_2-lipid), 0.99 (d, J = 6.6 Hz, 3H, CH_3-lipid), 0.88 (t, J = 6.8 Hz, 3H, CH_3-lipid). ^{13}C-APT NMR (101 MHz, $CDCl_3$) δ: 173.8 (C=O), 139.6 (C-arom), 134.9 (CH=), 128.4 (C-arom), 128.0 (C-arom), 127.7 (C-arom), 116.5 (CH_2=), 82.3 (CH-Bn), 69.6 (CH_2-allylic), 57.3 (CH-N), 34.2 (CH_2-C=O), 32.0 (CH_2-lipid), 29.8 (CH_2-lipid), 29.8 (CH_2-lipid), 29.7 (CH_2-lipid), 29.7 (CH_2-lipid), 29.7 (CH_2-lipid), 29.6 (CH_2-lipid), 29.6 (CH_2-lipid), 29.5 (CH_2-lipid), 29.4 (CH_2-lipid), 29.3 (CH_2-lipid), 27.2 (CH_3-N), 25.5 (CH_2-lipid), 25.2 (CH_2-lipid), 25.0 (CH_2-lipid), 22.8 (CH_2-lipid), 15.8 (CH_3-lipid), 14.2 (CH_3-lipid). HRMS $[M+H]^+$: 472.4142 found, 472.4149 calculated.

(S)-2-allyloctadecanoic acid (14).

Compound **13** (377 mg, 0.8 mmol, 1 eq) was co-evaporated (3x) with toluene and dissolved in dry DCM (10 ml). 2-fluoropyridine (179 µL, 2.08 mmol, 2.6 eq) was added and the solution was cooled to 0 °C. Triflic anhydride (262 µL, 1.56 mmol, 1.95 eq) was added and the reaction mixture was stirred at 0 °C overnight. The day after the mixture was concentrated, dioxane (5 ml) and H_2SO_4 (2.5 N, 5 ml) were added and this reaction mixture was heated up to 100 °C and stirred overnight. The day after the reaction was diluted in water (50 ml) and DCM (25 ml) and transferred to a separatory funnel. The water layer was extracted (3x) with DCM and the combined organic layers were dried over $MgSO_4$, filtered and concentrated in vacuo. Compound **14** was obtained after silicagel chromatography (Petroleum ether/EtOAc 20:1→9:1; DCM for loading of crude) as a white solid (155 mg, 0.48 mmol, 60%). ^{1}H NMR (400 MHz, $CDCl_3$) δ: 11.80 (s, 1H, COOH), 5.76 (ddt, J = 16.8, 10.2, 6.8 Hz, 1H, CH=), 5.12 – 4.98 (m, 2H, CH_2=), 2.50 – 2.31 (m, 2H, CH-C=O, CH_2-allylic), 2.24 (dt, J = 13.4, 6.1 Hz, 1H, CH_2-allylic), 1.62 (ddd, J = 14.0, 8.6, 5.0 Hz, 1H, CH_2-lipid), 1.49 (ddd, J = 13.5, 8.3, 5.3 Hz, 1H, CH_2-lipid), 1.34 – 1.22 (m, 28H, CH_2-lipid), 0.88 (t, J = 6.8 Hz, 3H, CH_3-lipid). ^{13}C-APT NMR (101 MHz, $CDCl_3$) δ: 182.1 (C=O), 135.4 (CH=), 117.1 (CH_2=), 45.3 (CH-C=O), 36.3 (CH_2-lipid), 32.1 (CH_2-lipid), 31.7 (CH_2-lipid), 29.8 (CH_2-lipid), 29.8 (CH_2-lipid), 29.7 (CH_2-lipid), 29.7 (CH_2-lipid), 29.6 (CH_2-lipid), 29.5 (CH_2-lipid), 27.3 (CH_2-lipid), 22.8 (CH_2-lipid), 14.3 (CH_3-lipid). HRMS $[M+H]^+$: 325.31015 found, 325.31011 calculated.

(3S)-5-methyl-3-tetradecyldihydrofuran-2 (3H)-one (side product 30).

In addition to the desired product also the cyclized side product **30** (41 mg, 0.13mmol, 16%) was isolated and characterized. Diastereoisomer a: ^{1}H NMR (850 MHz, $CDCl_3$) δ: 4.85 – 4.76 (m, 1H, CH-O), 2.81 – 2.70 (m, 1H, CH-C=O), 2.26 – 2.19 (m, 1H, CH_2-ring), 2.15 (ddd, J = 12.8, 9.0, 5.0 Hz, 1H, CH_2-ring), 2.12 – 2.03 (m, 1H, CH_2-lipid), 2.01 – 1.93 (m, 1H, CH_2-lipid), 1.90 – 1.66 (m, 1H, CH_2-lipid), 1.65 – 1.58 (m, 1H, CH_2-lipid), 1.58 –1.53 (m, 1H, CH_2-lipid), 1.51 (d, J = 6.4 Hz, 3H, CH_3-ring), 1.50 – 1.46 (m, 2H, CH_2-lipid), 1.46 - 1.27 (m, 21H, CH_2-lipid), 1.02 (t, J = 7.1 Hz, 3H, CH_3-lipid). ^{13}C-APT NMR (214 MHz, $CDCl_3$) δ: 179.3 (C=O), 75.3 (CH-O), 41.7 (CH-C=O), 35.2 (CH_2-ring), 32.1 (CH_2-lipid), 30.8 (CH_2-lipid), 30.5 (CH_2-lipid), 29.9 (CH_2-lipid), 29.8 (CH_2-lipid), 29.8 (CH_2-lipid), 29.8 (CH_2-lipid), 29.8 (CH_2-lipid), 29.8 (CH_2-lipid), 29.7 (CH_2-lipid), 29.7 (CH_2-lipid), 29.6 (CH_2-lipid), 29.6 (CH_2-lipid), 29.5 (CH_2-lipid), 29.5 (CH_2-lipid), 27.5 (CH_2-lipid), 27.5 (CH_2-lipid), 22.8 (CH_2-lipid), 21.2 (CH_3-ring), 14.3 (CH_3-lipid). Diastereoisomer b:^{1}H NMR (850 MHz, $CDCl_3$) δ: 4.67 – 4.57 (m, 1H, CH-O), 2.81 – 2.70 (m, 1H, CH-C=O), 2.61 (ddd, J = 12.4, 8.5, 5.5 Hz, 1H, CH_2-ring), 1.90 – 1.66 (m, 2H, CH_2-lipid), 1.65 – 1.58 (m, 2H, CH_2-ring, CH_2-lipid), 1.58 –1.53 (m, 4H, CH_3-ring, CH_2-lipid), 1.50 – 1.46 (m, 2H, CH_2-lipid), 1.46 - 1.27 (m, 22H, CH_2-lipid), 1.02 (t, J = 7.1 Hz, 3H, CH_3-lipid). ^{13}C-APT NMR (214 MHz, $CDCl_3$) δ: 179.6 (C=O), 75.1 (CH-O), 39.5 (CH-C=O), 37.2 (CH_2-ring), 32.1 (CH_2-lipid), 30.8 (CH_2-lipid), 30.5 (CH_2-lipid), 29.9 (CH_2-lipid), 29.8 (CH_2-lipid), 29.8 (CH_2-lipid), 29.8 (CH_2-lipid), 29.8 (CH_2-lipid), 29.8 (CH_2-lipid), 29.7 (CH_2-lipid), 29.7 (CH_2-lipid), 29.6 (CH_2-lipid), 29.6 (CH_2-lipid), 29.5 (CH_2-lipid), 29.5 (CH_2-lipid), 27.5 (CH_2-lipid), 27.5 (CH_2-lipid), 22.8 (CH_2-lipid), 21.4 (CH_3-ring), 14.3 (CH_3-lipid). HRMS $[M+H]^+$: 325.30999 found, 325.31011 calculated.

(S)-2-(13-(acetylthio)tridec-2-en-1-yl)octadecanoic acid (15).

Compound **14** (630 mg, 1.94 mmol, 1 eq) was co-evaporated with toluene (2x) and dissolved in dry DCM (30 ml). Compound **31** (1.88 g, 7.76 mmol, 4 eq) was also co-evaporated with toluene (2x) before being dissolved in DCM (9 ml) and added to the carboxylic acid solution. After addition of Grubbs 1st generation catalyst (80mg, 0.1 mmol, 0.05 eq), the solution was heated to reflux for 2 days. Compound10was obtained after removal of volatiles followed by silicagel chromatography(Pentane/EtOAc 95:5→5:1; DCM for loading of crude) and size exclusion (LH-20, DCM/MeOH, 1/1, v/v) as a white solid (855 mg, 1, 46 mmol, 76%). ^{1}H NMR (400 MHz, $CDCl_3$) δ: 5.58 – 5.22 (m, 2H, CH=), 2.86 (t, J = 7.3 Hz, 2H, CH_2S), 2.52 - 2.09 (m, 6H, CH_3-thioacetyl, CH_2-allylic, CH-C=O), 1.98 (dt, J= 21.0, 7.0 Hz, 2H, CH_2-allylic), 1.71 – 1.42 (m, 4H, CH_2-lipid), 1.25 (d, J = 2.4Hz, 42H, CH_2-lipid), 0.92 – 0.82 (m, 3H, CH_3-lipid). ^{13}C-APT NMR (101 MHz, $CDCl_3$) δ: 196.2 (S-C=O), 182.5 (C=O), 133.4 (CH=), 132.4 (CH=), 126.6 (CH=), 126.0 (CH=), 45.9 (CH-C=O), 35.2 (CH_2-allylic), 32.7 (CH_2-allylic), 32.1 (CH_2-lipid), 31.7 (CH_2-lipid), 31.6 (CH_2-lipid), 30.7 (CH_3-thioacetyl), 29.8 (CH_2-lipid), 29.8 (CH_2-lipid), 29.8 (CH_2-lipid), 29.8 (CH_2-lipid), 29.7 (CH_2-lipid), 29.7 (CH_2-lipid), 29.6 (CH_2-lipid), 29.6 (CH_2-lipid), 29.6 (CH_2-lipid), 29.6 (CH_2-lipid), 29.5 (CH_2-lipid), 29.5 (CH_2-lipid), 29.3 (CH_2-lipid), 29.3 (CH_2-lipid), 29.2 (CH_2-S), 29.0 (CH_2-lipid), 27.5 (CH_2-lipid), 27.4 (CH_2-lipid), 27.4 (CH_2-lipid), 22.8 (CH_2-lipid), 14.3 (CH_3-lipid). HRMS $[M+Na]^+$: 561.4315 found, 561.4312 calculated.

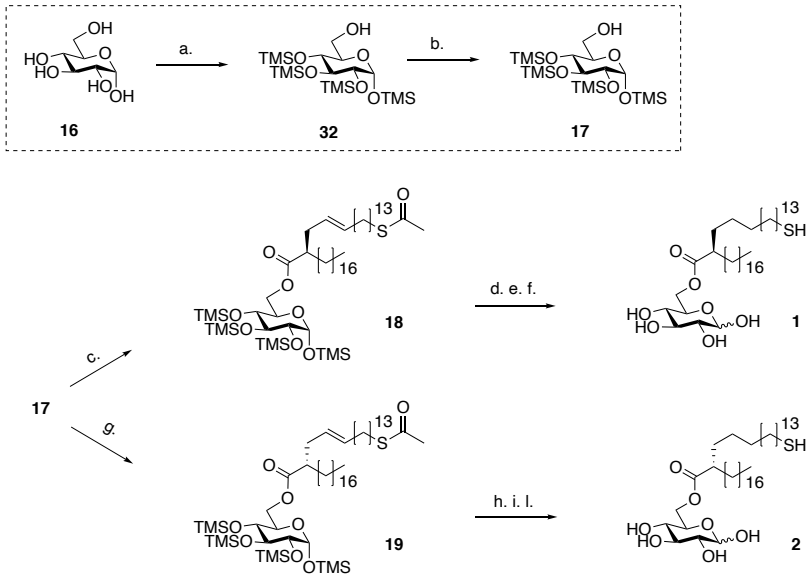

S2 Figure - Synthetic scheme for the generation of glucose monomycolate analogues. a) TMSCl, HMDS, pyridine, y: quant. b) NH_4OAc, DCM/MeOH 1:1, y: 73%, c) lipid, EDCI, DMAP, y: 52%, d) 2-nitrobenzenesulfonyl hydrazide, Et_3N, DCM, e) amberlite H^+, DCM/MeOH 1:1, f) TCEP.HCl, PBS, MeOH/CH_3CN 1:1, y: 62% over 3 steps, g) lipid, EDCI, DMAP, y: 50%, h) 2-nitrobenzenesulfonyl hydrazide, Et_3N, DCM, i) amberlite H^+, DCM/MeOH 1:1, l) TCEP.HCl, PBS, MeOH/CH_3CN 1:1, y: 73% over three steps.

1, 2, 3, 4, 6-penta-trimethylsilyl-α-glucopyranoside (32).

α-D-glucose (1.8 g, 10 mmol, 1 eq) was dissolved in pyridine (100 ml). HMDS (18 ml, 86 mmol, 8.6 eq) and TMSCl (8.9 ml, 70 mmol, 7 eq) were added to this solution and heated up to 75 °C for 1 hour. The reaction mixture was allowed to cool to RT and ice-water (100 ml) was added to it. The mixture was then diluted with pentane and transferred to a separatory funnel. The water layer was extracted (3x) with pentane, then the combined organic layers were washed (3x) with water, dried over $MgSO_4$, filtered and concentrated in vacuo. Compound **32** was obtained as a white solid (5.5 g, 10 mmol, 100%) without any further purification. NMR analysis confirmed purity of the product, whose ^1H NMR and ^{13}C NMR spectra were in agreement with published literature.[50]

1, 2, 3, 4-tetra-trimethylsilyl-6-hydroxy-α-glucopyranoside (17).

Compound **32** (5.5 g, 10 mmol, 1 eq) was dissolved in a mixture of DCM/MeOH 1:1 (83 ml) and NH_4OAc (1.54 g, 20 mmol, 2 eq) was added. When TLC showed complete consumption of the starting material, the volatiles were removed by evaporation, the crude was dissolved in pentane and the mixture transferred to a separatory funnel. The organic layer was washed

(3x) with water, (1x) with brine, dried over $MgSO_4$, filtered and concentrated in vacuo. Compound **17** was obtained after silicagel chromatography (Pentane/EtOAc 15:1; DCM for loading of crude) as a white solid (3.43 g, 7.31 mmol, 73%). ^{1}H NMR (400 MHz, $CDCl_3$) δ: 5.00 (d, J = 3.0 Hz, 1H, H-1), 3.87 – 3.59 (m, 4H, H-3, H-5, H-6), 3.45 (dd, J = 9.5, 8.6 Hz, 1H, H-4), 3.34 (dd, J = 9.1, 3.0 Hz, 1H, H-2), 1.76 (t, J = 6.1 Hz, 1H, -OH), 0.20 – 0.12 (m, 36H, CH_2-TMS). ^{13}C-APT NMR (101 MHz, $CDCl_3$) δ: 94.0 (C-1), 74.1 (C-2), 73.6 (C-3), 72.0 (C-5), 71.8 (C-4), 61.9 (C-6), 1.2 (CH_3-TMS), 0.9 (CH_3-TMS), 0.4 (CH_3-TMS), 0.2 (CH_3-TMS). HRMS $[M+Na]^+$: 491.21040 found, 491.21072 calculated.

6-((R)-2-(13-(acetylthio)tridec-2-en-1-yl)octadecanoyl)-1, 2, 3, 4-tetra-trimethylsilyl-α-glucopyranoside (18).

Compound **17** (260 mg, 0.55 mmol, 1.26 eq) and compound **12** (260 mg, 0.44mmol, 1 eq) were co-evaporated (3x) with toluene before being dissolved in dry toluene (8.8 ml). After addition of DMAP (54 mg, 0.44 mmol, 1 eq), the solution was cooled to 0 °C. EDCI (169 mg, 0.88 mmol, 2 eq) was added and the reaction mixture was heated up to 70 °C. After 4 hours the reaction was cooled to RT, diluted with water and EtOAc and transferred to a separatory funnel. The organic layer was washed (2x) with brine and the combined water layers were extracted (1x) with EtOAc. The combined organic layers were washed (1x) with brine, dried over $MgSO_4$, filtered and concentrated in vacuo. Compound **18** was obtained after silicagel chromatography (Pentane/EtOAc 100:3→9:1; DCM for loading of crude) as a white solid (228 mg, 0.22 mmol, 50%). ^{1}H NMR (400 MHz, $CDCl_3$) δ: 5.47 – 5.27 (m, 2H, CH=), 4.98 (d, J = 3.0Hz, 1H, H-1), 4.59 – 4.46 (m, 1H, H-6a), 3.97 – 3.85 (m, 2H, H-6b, H-4), 3.79 (pt, J = 8.8 Hz, 1H, H-3), 3.40 (td, J = 8.9, 2.6 Hz, 1H, H-5), 3.33 (dd, J = 9.1, 3.1Hz, 1H, H-2), 2.86 (t, J = 7.4 Hz, 2H, CH_2-S), 2.44 – 2.30 (m, 5H, CH_3-thioacetyl, CH_2-allylic, CH-C=O), 2.29 – 2.08 (m, 1H, CH_2-allylic), 2.08 – 1.89 (m, 2H, CH_2-allylic), 1.64 – 1.41 (m, 5H, CH_2-lipid), 1.38 – 1.16 (m, 49H, CH_2-lipid), 0.90 – 0.86 (m, 3H, CH_3-lipid), 0.18 – 0.12 (m, 36H, CH_3-TMS). ^{13}C-APT NMR (101 MHz, $CDCl_3$) δ: 196.2 (S-C=O), 175.9 (a C=O), 175.8 (b C=O), 133.1 (a CH=), 132.2 (b CH=), 126.9 (a CH=), 126.4 (b CH=), 94.0 (C-1), 74.2 (C-2), 74.2 (C-3), 73.9 (a C-5), 73.9 (b C-5), 72.8 (C-4), 70.3 (a C-6), 70.2 (b C-6), 63.5 (a CH-C=O), 63.4 (b CH-C=O), 46.0 (a CH_2-allylic), 45.8 (b CH_2-allylic), 35.3 (CH_2-allylic), 32.8 (CH_2-lipid), 32.1 (CH_2-lipid), 31.9 (CH_2-lipid), 31.9 (CH_2-lipid), 30.8 (CH_3-thioacetyl), 29.9 (CH_2-lipid), 29.8 (CH_2-lipid), 29.8 (CH_2-lipid), 29.7 (CH_2-lipid), 29.6 (CH_2-lipid), 29.5 (CH_2-lipid), 29.5 (CH_2-lipid), 29.3 (CH_2-lipid), 29.3 (CH_2-lipid), 29.3 (CH_2-lipid), 29.0 (CH_2-lipid), 27.5 (CH_2-lipid), 27.4 (CH_2-lipid), 27.4 (CH_2-lipid), 22.8 (CH_2-lipid), 14.3 (CH_3-lipid), 1.4 (CH_3-TMS), 1.1 (CH_3-TMS), 0.6 (CH_3-TMS), 0.3 (CH_3-TMS), 0.2 (CH_3-TMS). HRMS $[M+Na]^+$: 1011.6424 found, 1011.6421 calculated.

6-((R)-2-(13-(mercapto)tridec-2-en-1-yl)octadecanoyl)-α-glucopyranoside (1).

Compound **18** (52 mg, 0.05 mmol, 1 eq) was co-evaporated (2x) with toluene and dissolved in dry DCM (0.25 ml). To this solution, Et_3N (0.25 ml) and 2-nitrobenzenesulfonohydrazide (22 mg, 0.1 mmol, 2 eq) were added and the reaction was stirred overnight. The morning after TLC showed that the reaction was not complete and therefore an extra portion of 2-nitrobenzenesulfonohydrazide (22 mg, 0.1 mmol, 2 eq) was added and the reaction was stirred for another day. After that the reaction mixture was diluted with EtOAc and brine and transferred to a separatory funnel. The organic layer was washed (2x) with brine, dried over $MgSO_4$, filtered and concentrated in vacuo. This reaction intermediate was then dissolved in a mixture of DCM/MeOH 1:1 (9 ml) and a spatula of amberlite H^+ was added. The TMS-removal

reaction was complete after 30 minutes as verified by TLC. Amberlite H^+ was removed from the solution by means of filtration and the volatiles were removed in vacuo. The crude was then dissolved in a mixture of MeOH/CH_3CN 1:1 (7 ml) and a solution of TCEP·HCl (143 mg, 0.5 mmol, 10 eq) in PBS (0.7 ml) was added. The reaction mixture was stirred for 15 minutes, then the volatiles were removed in vacuo. Compound **1** was obtained after silicagel chromatography ($CHCl_3$/MeOH 14:1; eluent used for loading of crude; N_2 flow was used for purification) as a white solid (24 mg, 0.036mmol, 73%). α-anomer: ^{1}H NMR (600 MHz, MeOD/$CDCl_3$ 1:1) δ: 5.03 (d, J = 3.7 Hz, 1H, H-1), 4.40 – 4.36 (m, 1H, H-6a), 4.14 – 4.05 (m, 1H, H-6b), 3.88 (ddd, J = 10.1, 5.0, 2.2 Hz, 1H, H-5), 3.60 (t, J = 9.3 Hz, 1H, H-3), 3.32 – 3.27 (m, 1H, H-2), 3.27– 3.19 (m, 1H, H-4), 2.46 – 2.38 (m, 2H, CH_2-S), 2.35 – 2.22 (m, 1H, CH-C=O), 1.68 – 1.45 (m, 4H, CH_2-lipid), 1.45 – 1.26 (m, 5H, CH_2-lipid), 1.26 – 1.13 (m, 43H, CH_2-lipid), 0.80 (t, J = 7.0 Hz, 3H, CH_3-lipid). β-anomer: ^{1}H NMR (600 MHz, MeOD/$CDCl_3$1:1) δ: 4.41 (d, J = 7.8 Hz, 1H, H-1), 4.37 – 4.33 (m, 1H, H-6a), 4.14 – 4.05 (m, 1H, H-6b), 3.40 (ddd, J =9.8, 6.4, 2.0 Hz, 1H, H-5), 3.32 – 3.27 (m, 1H, H-3), 3.27 – 3.19 (m, 1H, H-4), 3.09 (dd, J = 9.3, 7.8 Hz, 1H, H-2), 2.46 – 2.38 (m, 2H, CH_2-S), 2.35 – 2.22 (m, 1H, CH-C=O), 1.68 – 1.45 (m, 4H, CH_2-lipid), 1.45 – 1.26 (m, 5H, CH_2-lipid), 1.26 –1.13 (m, 43H, CH_2-lipid), 0.80 (t, J = 7.0 Hz, 3H, CH_3-lipid). α-anomer: ^{13}C-APT NMR (151 MHz, MeOD/$CDCl_3$1:1) δ: 176.8 (C=O), 92.0 (C-1), 76.1 (C-2), 73.0 (C-3), 69.9 (C-4), 68.9 (C-5), 62.7 (C-6), 45.2 (CH-C=O), 33.5 (CH_2-lipid), 33.4 (CH_2-lipid), 31.7 (CH_2-lipid), 31.7 (CH_2-lipid), 31.6 (CH_2-lipid), 31.6 (CH_2-lipid), 31.5 (CH_2-lipid), 31.3 (CH_2-lipid), 29.1 (CH_2-lipid), 29.0 (CH_2-lipid), 29.0 (CH_2-lipid), 29.0 (CH_2-lipid), 29.0 (CH_2-lipid), 29.0 (CH_2-lipid), 29.0 (CH_2-lipid), 29.0 (CH_2-lipid), 29.0 (CH_2-lipid), 29.0 (CH_2-lipid), 28.9 (CH_2-lipid), 28.9 (CH_2-lipid), 28.9 (CH_2-lipid), 28.8 (CH_2-lipid), 28.8 (CH_2-lipid), 28.8 (CH_2-lipid), 28.8 (CH_2-lipid), 28.7 (CH_2-lipid), 28.5 (CH_2-lipid), 27.7 (CH_2-lipid), 26.7 (CH_2-lipid), 26.7 (CH_2-lipid), 26.7 (CH_2-lipid), 26.7 (CH_2-lipid), 23.5 (CH_2-S), 22.0 (CH_2-lipid), 13.1 (CH_3-lipid). β-anomer: ^{13}C-APT NMR (151 MHz, MeOD/$CDCl_3$1:1) δ: 176.8 (C=O), 96.2 (C-1), 74.2 (C-2), 73.6 (C-5), 71.9 (C-3), 69.9 (C-4), 63.2 (C-6), 45.1 (CH-C=O), 33.5 (CH_2-lipid), 33.4 (CH_2-lipid), 31.7 (CH_2-lipid), 31.7 (CH_2-lipid), 31.612 (CH_2-lipid), 31.6 (CH_2-lipid), 31.5 (CH_2-lipid), 31.3 (CH_2-lipid), 29.1 (CH_2-lipid), 29.0 (CH_2-lipid), 29.0 (CH_2-lipid), 29.0 (CH_2-lipid), 29.0 (CH_2-lipid), 29.0 (CH_2-lipid), 29.0 (CH_2-lipid), 29.0 (CH_2-lipid), 29.0 (CH_2-lipid), 28.9 (CH_2-lipid), 28.9 (CH_2-lipid), 28.9 (CH_2-lipid), 28.8 (CH_2-lipid), 28.8 (CH_2-lipid), 28.8 (CH_2-lipid), 28.8 (CH_2-lipid), 28.7 (CH_2-lipid), 28.5 (CH_2-lipid), 27.7 (CH_2-lipid), 26.7 (CH_2-lipid), 26.7 (CH_2-lipid), 26.7 (CH_2-lipid), 26.7 (CH_2-lipid), 23.5 (CH_2-S), 22.0, 13.1 (CH_3-lipid). HRMS $[M+Na]^+$: 683.4882 found, 683.4891 calculated.

6-((S)-2-(13-(acetylthio)tridec-2-en-1-yl)octadecanoyl)-1, 2, 3, 4-tetra-trimethylsilyl-α-glucopyranoside (19).

Compound **17** (105 mg, 0.23 mmol, 1 eq) and compound **15** (157 mg, 0.27mmol, 1.2 eq) were co-evaporated (3x) with toluene before being dissolved in dry toluene (4.5 ml). After addition of DMAP (28 mg, 0.225 mmol, 1 eq), the solution was cooled to 0 °C. EDCI (86 mg, 0.45 mmol, 2 eq) was added and the reaction mixture was heated up to 70 °C. After 1 hour another portion of EDCI (43 mg, 0.23 mmol, 1 eq) was added to the reaction mixture and after 3 hours the reaction was cooled to RT, diluted with water and EtOAc and transferred to a separatory funnel. The organic layer was washed (2x) with brine and the combined organic layers were dried over $MgSO_4$, filtered and concentrated in vacuo. Compound **19** was obtained after silicagel chromatography (Pentane/EtOAc 100:3→9:1; DCM for loading of crude) as a white solid (122 mg, 0.12 mmol, 52%). ^{1}H NMR (400 MHz, $CDCl_3$) δ: 5.49 – 5.38 (m, 1H, CH=), 5.37 – 5.25 (m, 1H, CH=), 4.99 (d, J = 3.1 Hz, 1H, H-1), 4.55 – 4.40 (m, 1H, H-6a), 3.99 – 3.84 (m, 2H, H-6b, H-4), 3.79 (pt, J = 8.9 Hz, 1H, H-3), 3.44 – 3.36 (m, 1H, H-5), 3.36 – 3.30 (m, 1H, H-2), 2.86

(t, J = 7.4 Hz, 2H, CH_2-S), 2.46 – 2.29 (m, 5H, CH_3-thioacetyl, CH_2-allylic, CH-C=O), 2.28 – 2.12 (m, 1H, CH_2-allylic), 2.07 – 1.90 (m, 2H, CH_2-allylic), 1.76 – 1.51 (m, 5H, CH_2-lipid), 1.49 – 1.14 (m, 49H, CH_2-lipid), 0.91 – 0.85 (m, 3H, CH_3-lipid), 0.18 – 0.13 (m, 36H, CH_3-TMS). ^{13}C-APT NMR (101 MHz, $CDCl_3$) δ: 196.2 (S-C=O), 175.9 (a C=O), 175.8 (b C=O), 133.1 (a CH=), 132.2 (b CH=), 126.8 (a CH=), 126.3 (b CH=), 94.0 (C-1), 74.2 (C-2), 74.0 (C-3), 73.9 (C-5), 72.8 (C-4), 70.3 (a C-6), 70.2 (b C-6), 63.5 (CH-C=O), 46.0 (a CH_2-allylic), 45.9 (b CH_2-allylic), 35.5 (CH_2-allylic), 32.8 (CH_2-lipid), 32.1 (CH_2-lipid), 31.6 (CH_2-lipid), 31.5 (CH_2-lipid), 30.8 (CH_3-thioacetyl), 30.1 (CH_2-lipid), 29.9 (CH_2-lipid), 29.8 (CH_2-lipid), 29.8 (CH_2-lipid), 29.7 (CH_2-lipid), 29.7 (CH_2-lipid), 29.7 (CH_2-lipid), 29.6 (CH_2-lipid), 29.5 (CH_2-lipid), 29.3 (CH_2-lipid), 29.3 (CH_2-lipid), 29.3 (CH_2-lipid), 29.0 (CH_2-lipid), 27.6 (CH_2-lipid), 27.5 (CH_2-lipid), 27.4 (CH_2-lipid), 22.8 (CH_2-lipid), 14.3 (CH_3-lipid), 1.4 (CH_3-TMS), 1.1 (CH_3-TMS), 0.6 (CH_3-TMS), 0.6 (CH_3-TMS), 0.3 (CH_3-TMS). HRMS $[M+Na]^+$: 1011.64176 found, 1011.64212 calculated.

6-((S)-2-(13-(mercapto)tridec-2-en-1-yl)octadecanoyl)-α-glucopyranoside (2).

Compound **19** (100 mg, 0.1 mmol, 1 eq) was co-evaporated (2x) with toluene and dissolved in dry DCM (0.5 ml). To this solution, Et_3N (0.5 ml) and 2-nitrobenzenesulfonohydrazide (84 mg, 0.39 mmol, 4 eq) were added and the reaction was stirred overnight. The morning after TLC showed that the reaction was not complete and therefore an extra portion of 2-nitrobenzenesulfonohydrazide (22 mg, 0.1 mmol, 1 eq) was added and the reaction was stirred for 4 hours. After that the reaction mixture was diluted with EtOAc and brine and transferred to a separatory funnel. The organic layer was washed (2x) with brine, dried over $MgSO_4$, filtered and concentrated in vacuo. This reaction intermediate was then dissolved in a mixture of DCM/MeOH 1:1 (18 ml) and a spatula of amberlite H^+ was added. The TMS-removal reaction was complete after 30 minutes as verified by TLC. Amberlite H^+ was removed from the solution by means of filtration and the volatiles were removed in vacuo. A mixture of reduced and oxidised forms of the desired product was isolated after silicagel chromatography ($CHCl_3$/MeOH 14:1; eluent used for loading of crude; N_2 flow was used for purification) as a white solid (55 mg, 0.083 mmol, 85%). The product was then dissolved in a mixture of MeOH/CH_3CN 1:1 (12 ml) and a solution of TCEP·HCl (238 mg, 0.83 mmol, 10 eq) in PBS (1.2 ml) was added. The reaction was complete after 15 minutes and the volatiles were removed in vacuo. Compound **2** was obtained after silicagel chromatography ($CHCl_3$/MeOH 14:1; eluent used for loading of crude; N_2 flow was used for purification) as a white solid (41 mg, 0.062 mmol, 62% over 3 steps). α-anomer: ^{1}H NMR (400 MHz, MeOD/$CDCl_3$1:1) δ: 5.14 (d, J = 3.7 Hz, 1H, H-1), 4.50 – 4.45 (m, 1H, H-6a), 4.26 – 4.20 (m, 1H, H-6b), 3.98 (ddd, J =10.0, 5.0, 2.2 Hz, 1H, H-5), 3.70 (pt, J = 9.3 Hz, 1H, H-3), 3.44 – 3.36 (m, 2H, H-2, H-4), 2.75 – 2.63 (m, 2H, CH_2-S), 2.43 – 2.34 (m, 1H, CH-C=O), 1.80 – 1.54 (m, 4H, CH_2-lipid), 1.54 – 1.36 (m, 4H, CH_2-lipid), 1.36 – 1.06 (m, 48H, CH_2-lipid), 0.89 (t, J = 6.7 Hz, 3H, CH_3-lipid). β-anomer: ^{1}H NMR (400 MHz, MeOD/$CDCl_3$1:1) δ: 4.51 (d, J = 7.8 Hz, 1H, H-1), 4.44 (d, J = 2.1 Hz, 1H, H-6a), 4.20 – 4.15 (m, 1H, H-6b), 3.57 – 3.47(m, 1H, H-5), 3.44 – 3.36 (m, 2H, H-3, H-4), 3.24 – 3.15 (m, 1H, H-2), 2.75 – 2.63 (m, 2H, CH_2-S), 2.43 – 2.34 (m, 1H, CH-C=O), 1.80 – 1.54 (m, 4H, CH_2-lipid), 1.54 – 1.36 (m, 4H, CH_2-lipid), 1.36 – 1.06 (m, 48H, CH_2-lipid), 0.89 (t, J = 6.7Hz, 3H, CH_3-lipid). α-anomer: ^{13}C-APT NMR (101 MHz, MeOD/$CDCl_3$1:1) δ: 176.9 (C=O), 92.1 (C-1), 76.1 (C-2), 73.1 (C-3), 70.0 (C-4), 69.0 (C-5), 62.8 (C-6), 45.2 (CH-C=O), 33.5 (CH_2-lipid), 31.7 (CH_2-lipid), 31.4 (CH_2-lipid), 29.1 (CH_2-lipid), 29.1 (CH_2-lipid), 29.1 (CH_2-lipid), 29.0 (CH_2-lipid), 29.0 (CH_2-lipid), 29.0 (CH_2-lipid), 28.9 (CH_2-lipid), 28.8 (CH_2-lipid), 28.5 (CH_2-lipid), 27.8 (CH_2-lipid), 26.8 (CH_2-lipid), 23.7 (CH_2-S), 22.1 (CH_2-lipid), 13.2 (CH_3-lipid). β-anomer: ^{13}C-APT NMR (101 MHz, MeOD/$CDCl_3$1:1) δ: 176.9 (C=O), 96.3 (C-1), 74.3 (C-2), 73.7 (C-5), 71.9 (C-3), 70.0 (C-4), 63.3

(C-6), 45.3 (CH-C=O), 33.5 (CH_2-lipid), 31.7 (CH_2-lipid), 31.4 (CH_2-lipid), 29.1 (CH_2-lipid), 29.1 (CH_2-lipid), 29.1 (CH_2-lipid), 29.0 (CH_2-lipid), 29.0 (CH_2-lipid), 29.0 (CH_2-lipid), 28.914 (CH_2-lipid), 28.8 (CH_2-lipid), 28.5 (CH_2-lipid), 27.8 (CH_2-lipid), 26.8 (CH_2-lipid), 23.7 (CH_2-S), 22.1 (CH_2-lipid), 13.2 (CH_3-lipid). HRMS $[M+Na]^+$: 683.48900 found, 683.48910 calculated.

Trehalose dimycolate analogues

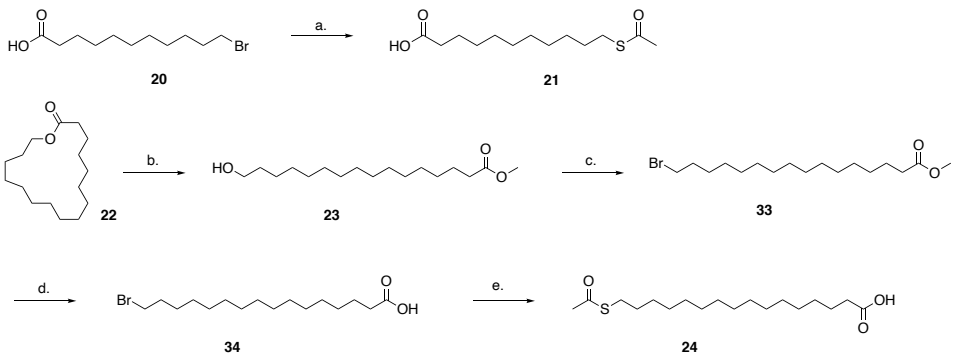

S3 Figure - Synthetic scheme for the generation of lipid moieties of trehalose dimycolate analogues. a) potassium thioacetate, DMF, y: 91%, b) NaOMe, MeOH, y: 85%, c) PPh_3, $NaHCO_3$, NBS, y: 88%, d) LiOH, THF, y: 91%, e) potassium thioacetate, DMF, y: 63%.

11-(acetylthio)undecanoic acid (21).

1-Bromoundecanoic acid (398 mg, 1.5 mmol, 1 eq) was dissolved in DMF (10ml) and cooled to 0 °C. Potassium ethanethioate (308 mg, 2.7 mmol, 1.8 eq) was added to the solution and the mixture was stirred at RT for 1 h and 30 minutes. At this point the reaction mixture was diluted with DCM and the organic layer was washed (3x) with water, dried over $MgSO_4$, filtered and concentrated in vacuo. Compound **21** was obtained as a brown solid (352 mg, 1.35 mmol, 91%) without any further purification. ^{1}H NMR (400 MHz, $CDCl_3$) δ: 2.86 (t, J = 7.3 Hz, 2H, CH_2-S), 2.42 –2.24 (m, 5H, CH_2-C=O, CH_3-thioacetyl), 1.70 – 1.51 (m, 4H, CH_2-lipid), 1.36– 1.21 (m, 12H, CH_2-lipid). ^{13}C-APT NMR (101 MHz, $CDCl_3$) δ: 196.3 (S-C=O), 179.7 (C=O), 34.1 (CH_2-C=O), 30.8 (CH_3-thioacetyl), 29.6 (CH_2-lipid), 29.5 (CH_2-lipid), 29.4 (CH_2-lipid), 29.3 (CH_2-lipid), 29.3 (CH_2-lipid), 29.2 (CH_2-lipid), 29.1 (CH_2-S), 28.9 (CH_2-lipid), 28.9 (CH_2-lipid), 24.8 (CH_2-lipid). HRMS $[M+Na]^+$: 283.1339 found, 283.1338 calculated.

methyl 16-hydroxyhexadecanoate (23).

Cyclohexadecanolide (3.61 g, 15 mmol, 1 eq) was co-evaporated with toluene and dissolved in dry MeOH (88 ml). After addition of NaOMe (4.05 g, 75 mmol, 5eq) the reaction mixture was heated up to reflux for 1 hour and 30 minutes. The reaction was quenched with a 1 M solution of HCl until pH 11, then brine and EtOAc were added and the mixture was transferred to a separatory funnel. The water layer was extracted (2x) with EtOAc. Compound **23** was obtained as a white solid (3.68 g, 12.8 mmol, 85%) without any further purification.^{1}H NMR (400 MHz, $CDCl_3$) δ: 3.73 – 3.58 (m, 5H, CH_3-O, CH_2-OH), 2.30 (t, J = 7.6 Hz, 2H, CH_2-C=O), 1.65 – 1.52 (m,

4H, CH_2-lipid), 1.33 – 1.23 (m, 20H, CH_2-lipid). ^{13}C-APT NMR (101 MHz, $CDCl_3$) δ: 174.5 (C=O), 63.2 (CH_2-OH), 51.6 (CH_3-O), 34.3 (CH_2-C=O), 32.9 (CH_2-lipid), 29.8 (CH_2-lipid), 29.8 (CH_2-lipid), 29.7 (CH_2-lipid), 29.7 (CH_2-lipid), 29.6 (CH_2-lipid), 29.4 (CH_2-lipid), 29.3 (CH_2-lipid), 25.9 (CH_2-lipid), 25.1 (CH_2-lipid). HRMS $[M+H]^+$: 287.2572 found, 287.2586 calculated.

methyl 16-bromohexadecanoate (33).

Compound **23** (3.44 g, 12 mmol, 1 eq) was co-evaporated with toluene and dissolved in DCM (60 ml). Triphenylphospine (3.93 g, 15.6 mmol, 1.3 eq) and $NaHCO_3$ (90 mg, 1.08 mmol, 0.09 eq) were added and the solution was cooled to 0 °C. Subsequently, NBS (2.55 g, 21.6 mmol, 1.8 eq) was added in portions over 20 minutes and the reaction mixture was stirred for 2 hours at RT. Compound **33** was obtained after silicagel chromatography (Pentane/EtOAc 9:1→8:2; DCM loading of crude) as a white solid (3.69 g, 10.56 mmol, 88%). ^{1}H NMR (400 MHz, $CDCl_3$) δ: 3.67 (s, 3H, CH_3-O), 3.41 (t, J = 6.9 Hz, 2H, CH_2-Br), 2.30 (t, J = 7.5 Hz, 2H, CH_2-C=O), 1.90 – 1.81 (m, 2H, CH_2-lipid), 1.65– 1.57 (m, 2H, CH_2-lipid), 1.46 – 1.38 (m, 2H, CH_2-lipid), 1.31 – 1.22 (m, 20H, CH_2-lipid). ^{13}C-APT NMR (101 MHz, $CDCl_3$) δ: 174.5 (C=O), 51.6 (CH_3-O), 34.2 (CH_2-Br), 34.2 (CH_2-C=O), 33.0 (CH_2-lipid), 29.8 (CH_2-lipid), 29.7 (CH_2-lipid), 29.7 (CH_2-lipid), 29.7 (CH_2-lipid), 29.6 (CH_2-lipid), 29.4 (CH_2-lipid), 29.3 (CH_2-lipid), 28.9 (CH_2-lipid), 28.3 (CH_2-lipid), 25.1 (CH_2-lipid). HRMS $[M+Na]^+$: 371.1563 found, 371.1556 calculated.

16-bromohexadecanoic acid (34).

Compound **33** (3.49 g, 10 mmol, 1 eq) was dissolved in THF (100 ml). Subsequently a 1 M solution of LiOH (25 ml) was added and the reaction mixture was stirred overnight at RT. The reaction was quenched with a 1 M HCl solution until pH 2, after which this mixture was diluted with DCM and water and transferred toa separatory funnel. The water layer was extracted (3x) with DCM and the combined organic layers were dried over $MgSO_4$, filtered and concentrated in vacuo. Compound **34** was obtained as a brown solid (352 mg, 1.35 mmol, 91%) without any further purification. ^{1}H NMR (400 MHz, $CDCl_3$) δ: 3.41 (t, J = 6.9 Hz, 2H, CH_2-Br), 2.35 (t, J = 7.5 Hz, 2H, CH_2-C=O), 1.85 (dt, J = 14.5, 6.9 Hz, 2H, CH_2-lipid), 1.68 – 1.58 (m, 2H, CH_2-lipid), 1.46 – 1.39 (m, 2H, CH_2-lipid), 1.33– 1.23 (m, 20H, CH_2-lipid). ^{13}C-APT NMR (101 MHz, $CDCl_3$) δ: 180.4 (C=O), 34.2 (CH_2-Br), 34.2 (CH_2-C=O), 33.0 (CH_2-lipid), 29.8 (CH_2-lipid), 29.7 (CH_2-lipid), 29.7 (CH_2-lipid), 29.7 (CH_2-lipid), 29.6 (CH_2-lipid), 29.6 (CH_2-lipid), 29.4 (CH_2-lipid), 29.2 (CH_2-lipid), 28.9 (CH_2-lipid), 28.3 (CH_2-lipid), 24.8 (CH_2-lipid). HRMS $[M+H]^+$: 319.1283 found, 319.1278 calculated.

16-(acetylthio)hexadecanoic acid (24).

Compound **34** (36 mg, 0.11 mmol, 1 eq) was dissolved in DMF (0.73 ml) and cooled to 0 °C. Potassium ethanethioate (22 mg, 0.19 mmol, 1.8 eq) was added to the solution and the mixture was stirred at RT for 4 hours. The reaction mixture was then diluted with DCM, the organic layer was washed (5x) with water, dried over $MgSO_4$, filtered and concentrated in vacuo. Compound **24** was obtained as a brown solid (22.8 mg, 0.07 mmol, 63%) without any further purification. ^{1}H NMR (400 MHz, $CDCl_3$) δ: 2.86 (t, J = 7.3 Hz, 2H, CH_2-S), 2.36 (t, J= 3.8 Hz, 2H, CH_2-C=O), 2.32 (s, 3H, CH_3-thioacetyl), 1.72 – 1.50 (m, 4H, CH_2-lipid), 1.35 – 1.23 (m, 20H, CH_2-lipid). ^{13}C-APT NMR (101 MHz, $CDCl_3$) δ: 196.4 (S-C=O), 179.4 (C=O), 34.1 (CH_2-C=O), 30.8 (CH_3-thioacetyl), 29.8 (CH_2-lipid), 29.7 (CH_2-lipid), 29.6 (CH_2-lipid), 29.6 (CH_2-lipid), 29.6 (CH_2-lipid), 29.4 (CH_2-lipid), 29.3 (CH_2-lipid), 29.3 (CH_2-S), 29.2 (CH_2-lipid), 29.0 (CH_2-lipid), 24.8 (CH_2-lipid). HRMS $[M+H]^+$: 331.2310 found, 331.2307 calculated.

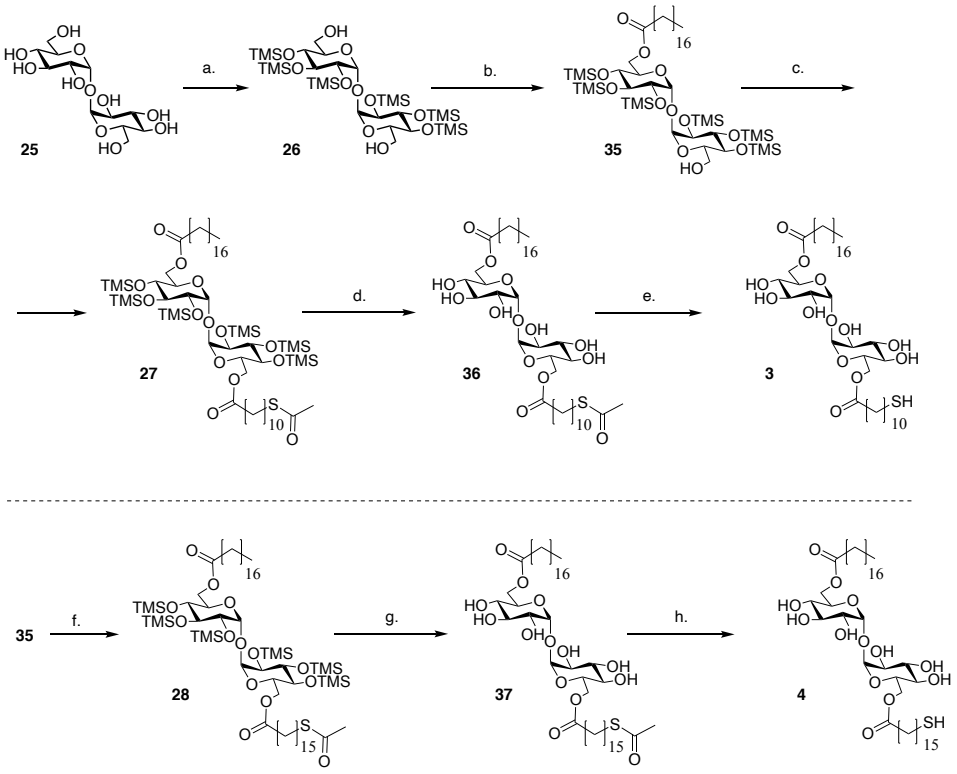

S4 Figure - Synthetic scheme for the generation of trehalose dimycolate analogues. a) i. N,O-bis(trimethylsityl)acetamide, TBAF, DMF, ii. K_2CO_3, MeOH, y: 79%, b) stearic acid, EDCI, DMAP, toluene, y: 47%, c) 11-(acetylthio)undecanoic acid, EDCI, DMAP, toluene, y: 70%, d) amberlite H^+, DCM/MeOH 1:1, y: quant., e) $NH_2NH_2CH_3COOH$, DCM/MeOH 1:1, y: quant., f) 11-(acetylthio)hexadecanoic acid, EDCI, DMAP, toluene, y: 85%, g) amberlite H^+, DCM/MeOH 1:1, y: 87%, h) $NH_2NH_2H_2O$, DCM/MeOH 1:1, y: quant. (isolated as mixture of oxidized and reduced thiol).

2, 3, 4, 2', 3', 4'-hexaakis-O-(trimethylsilyl)-α, α'-trehalose (26).

D(+)-Trehalose dihydrate (684 mg, 2 mmol, 1 eq) was co-evaporated (2x) with toluene and dissolved in dry DMF (3 ml). Bis(trimethylsilyl)acetamide (3.56 g, 17mmol, 8.7 eq) and a 1 M solution of TBAF (0.12 mmol, 0.06 eq) in THF were added and the reaction mixture was stirred for 2 hours at RT. The solution was cooled to0 °C and quenched with i-propanol (1.2 ml). After diluting the mixture with MeOH (45 ml), K_2CO_3 (138 mg, 1 mmol, 0.5 eq) in MeOH (60 ml) was added and the reaction mixture was stirred for 2 hours at 0 °C. The solution was warmed up to room temperature, diluted with brine and EtOAc and transferred to a separatory funnel. The water layer was extracted (3x) with EtOAc. The combined organic layers were dried over $MgSO_4$, filtered and concentrated in vacuo. Compound **26** was obtained after silicagel chromatography (Pentane/EtOAc 4:1; DCM loading of crude) as a white solid (1.22 g, 1.58

mmol, 79%). NMR analysis confirmed purity of the product, whose ^{1}H NMR and ^{13}C NMR spectra were in agreement with published literature.[20]

6-O-stearoyl-2, 3, 4, 2', 3', 4'-hexaakis-O-(trimethylsilyl)-α, α'-trehalose (35).

Compound **26** (533 mg, 0.69 mmol, 1.2 eq) and stearic acid (163 mg, 0.57 mmol, 1eq) were co-evaporated (2x) with toluene and dissolved in toluene (1.9 ml). After the solution was cooled to 0 °C, DMAP (7 mg, 0.057 mmol, 0.1 eq) and EDCI (132 mg, 0.69 mmol, 1.2 eq) were added and the reaction mixture was warmed first to room temperature over 1 hour and then to 70 °C. After 4 hours, the reaction mixture was diluted with EtOAc and transferred to a separatory funnel. The organic layer was washed (2x) with brine, dried over $MgSO_4$, filtered and concentrated in vacuo. Compound **35** was obtained after silicagel chromatography (Pentane/EtOAc 20:1→9:1; DCM loading of crude) as a transparent oil (279 mg, 0.27 mmol, 47%). ^{1}H NMR (400 MHz, $CDCl_3$) δ: 4.95 – 4.88 (d (2x), J = 2.9, 2H, H-1, H-1'), 4.30 (dd, J = 11.8, 2.2 Hz, 1H, H-6a), 4.06 (dd, J = 11.8, 4.5 Hz, 1H, H-6b), 4.01 (ddd, J = 9.6, 4.4, 2.2 Hz, 1H, H-5), 3.94 – 3.87 (dd (2x), J = 9.0, 4.2 Hz, 2H, H3, H3'), 3.87 – 3.81 (dd (2x), J = 9.5, 3.4 Hz, 1H, H-5'), 3.75 – 3.63 (m, 2H, H-6'), 3.52 – 3.39 (m, 4H, H-4, H-4', H-2, H-2'), 2.35 (td, J = 7.4, 3.1 Hz, 2H, CH_2-C=O), 1.84 – 1.51 (m, 4H, CH_2-lipid), 1.25 (m, 28H, CH_2-lipid), 0.90 – 0.85 (m, 3H, CH_3-lipid), 0.19 – 0.09 (m, 54H, CH_3-TMS). ^{13}C-APT NMR (101 MHz, $CDCl_3$) δ: 173.9 (C=O), 94.6 (C-1), 94.5 (C-1'), 73.6 (C-5), 73.4 (C-4), 73.1 (C-4'), 72.9 (C-2), 72.7 (C-2'), 72.0 (C-5'), 71.5 (C-3), 70.9 (C-3'), 63.4 (C-6), 61.8 (C-6'), 34.3 (CH_2-C=O), 32.1 (CH_2-lipid), 29.9 (CH_2-lipid), 29.8 (CH_2-lipid), 29.8 (CH_2-lipid), 29.6 (CH_2-lipid), 29.5 (CH_2-lipid), 29.5 (CH_2-lipid), 29.3 (CH_2-S), 25.0 (CH_2-lipid), 22.9 (CH_2-lipid), 14.3 (CH_3-lipid), 1.2 (CH_3-TMS), 1.2 (CH_3-TMS), 1.0 (CH_3-TMS), 1.0 (CH_3-TMS), 0.3 (CH_3-TMS), 0.3 (CH_3-TMS). HRMS $[M+Na]^+$: 1063.6024 found, 1063.6036 calculated.

6-O-stearoyl-6'-11-(acetylthio)undecanoyl-2, 3, 4, 2', 3', 4'-hexaakis-O-(trimethylsilyl)-α, α'-trehalose (27).

Compound **35** (97 mg, 0.1 mmol, 1 eq) was co-evaporated (2x) with toluene and dissolved in dry toluene (1.8 ml). Therefore, compound **21** (48.5 mg, 0.19 mmol, 2 eq) and DMAP (5.7 mg, 0.05 mmol, 0.5 eq) were added and the solution was cooled to 0 °C. EDCI (44.6 mg, 0.23 mmol, 2.5 eq) was finally added. The reaction mixture was warmed first to room temperature and then to 70 °C. After 2 days, the reaction mixture was diluted with EtOAc and transferred to a separatory funnel. The organic layer was washed (2x) with brine, dried over $MgSO_4$, filtered and concentrated in vacuo. Compound **27** was obtained after silicagel chromatography (Pentane/EtOAc 18:1→9:1; DCM loading of crude) as a transparent oil (83 mg, 0.07 mmol, 70%). ^{1}H NMR (400 MHz, $CDCl_3$) δ: 4.92 (d, J = 3.1 Hz, 2H, H-1, H-1'), 4.27 (dd, J= 11.9, 2.2 Hz, 2H, H-6a, H-6a'), 4.06 (dd, J = 11.8, 4.4 Hz, 2H, H-6b, H-6b'), 4.00 (ddd, J = 9.6, 4.4, 2.2 Hz, 2H, H-5, H-5'), 3.90 (pt, J = 8.9 Hz, 2H, H-3, H-3'), 3.54– 3.39 (m, 4H, H-4, H-4', H-2, H-2'), 2.86 (t, J = 7.3 Hz, 2H, CH_2-S), 2.38 – 2.30 (m, 7H, CH_2-C=O, CH_3-thioacetyl), 1.65 – 1.53 (m, 6H, CH_2-lipid), 1.32 – 1.23 (m, 40H, CH_2-lipid), 0.88 (t, J = 6.7 Hz, 3H, CH_3-lipid), 0.18 – 0.09 (m, 54H, CH_3-TMS). ^{13}C-APT NMR (101 MHz, $CDCl_3$) δ: 207.9 (S-C=O), 173.9 (C=O), 94.5 (C-1, C-1'), 73.6 (C-3, C-3'), 72.8 (C-2, C-2'), 72.0 (C-4, C-4'), 70.8 (C-5, C-5'), 63.4 (C-6, C-6'), 34.3 (CH_2-C=O), 32.1 (CH_2-lipid), 30.8 (CH_3-thioacetyl), 29.8 (CH_2-lipid), 29.8 (CH_2-lipid), 29.6 (CH_2-lipid), 29.6 (CH_2-lipid), 29.5 (CH_2-lipid), 29.5 (CH_2-lipid), 29.4 (CH_2-S), 29.3 (CH_2-lipid), 29.2 (CH_2-lipid), 28.9 (CH_2-lipid), 24.9 (CH_2-lipid), 22.8 (CH_2-lipid), 14.3 (CH_3-lipid), 1.2 (CH_3-TMS), 1.0 (CH_3-TMS), 0.3 (CH_3-TMS). HRMS $[M+Na]^+$: 1305.7379 found, 1305.7376 calculated.

6-O-stearoyl-6'-(11-(acetylthio)undecanoyl)-α, α'-trehalose (36).

Compound **27** (932 mg, 0.72 mmol, 1 eq) was dissolved in a mixture of DCM/MeOH 1:1 (140 ml). Amberlite H^+ was added until methanolysis of the TMS groups could be observed via TLC. The reaction was followed every 5 minutes, until after 30 minutes no starting material and only one lower running spot could be observed. The resin was removed via filtration and washed with DCM/MeOH 1:1. The filtered solution was concentrated and compound **36** was obtained as a white solid (620 mg, 0.72 mmol, quant.) without any further purification. ^{1}H NMR (400 MHz, $CDCl_3$) δ: 5.10 (d, J = 3.7 Hz, 2H, H-1, H-1'), 4.38 –4.24 (m, 4H, H-6, H-6'), 4.08 (bs, 6H, OH), 3.99 (ddd, J = 10.2, 4.6, 2.5 Hz, 2H, H-5, H-5'), 3.88 (pt, J = 9.4 Hz, 2H, H-3, H-3'), 3.54 (dd, J = 9.8, 3.7 Hz, 2H, H-2, H-2'), 3.37 (dd, J = 10.2, 8.8 Hz, 2H, H-4, H-4'), 2.86 (t, J = 7.3 Hz, 2H, CH_2-S), 2.43 – 2.29 (m, 7H, CH_2-C=O, CH_3-thioacetyl), 1.65 – 1.53 (m, 6H, CH_2-lipid), 1.31 – 1.25 (m, 40H, CH_2-lipid), 0.90 – 0.86 (m, 3H, CH_3-lipid). ^{13}C-APT NMR (101 MHz, $CDCl_3$) δ: 196.9 (S-C=O), 174.6 (C=O), 174.5 (C=O), 93.5 (C-1, C-1'), 72.9 (C-3, C-3'), 71.6 (C-2, C-2'), 70.2 (C-4, C-4'), 70.0 (C-5, C-5'), 63.1 (C-6, C-6'), 34.1 (CH_2-C=O), 31.9 (CH_2-lipid), 30.5 (CH_2-S), 29.7 (CH_2-lipid), 29.6 (CH_2-lipid), 29.5 (CH_2-lipid), 29.4 (CH_2-lipid), 29.4 (CH_2-lipid), 29.3 (CH_2-lipid), 29.3 (CH_2-lipid), 29.3 (CH_2-lipid), 29.2 (CH_2-lipid), 29.1 (CH_2-lipid), 29.1 (CH_2-lipid), 29.0 (CH_2-S), 28.7 (CH_2-lipid), 24.8 (CH_2-lipid), 24.8 (CH_2-lipid), 22.6 (CH_2-lipid), 14.0 (CH_3-lipid). HRMS $[M+Na]^+$: 873.5020 found, 873.5005 calculated.

6-O-stearoyl-6'-(11-mercaptoundecanoyl)-α, α'-trehalose (3).

Compound **36** (51 mg, 0.06 mmol, 1 eq) was dissolved in a degassed solution of DCM/MeOH 1:1 (0.6 ml) and hydrazine monoacetate (14 mg, 0.15 mmol, 2.5eq) was added. After 5 hours an extra portion of hydrazine monoacetate (14 mg, 0.15 mmol, 2.5 eq) was added and the reaction mixture was stirred overnight. The morning after a white precipitate formed that was filtered and rinsed with a solution of degassed DCM/MeOH 9:1. The filtrate was dried in vacuo and compound **3** was obtained after silicagel chromatography ($CHCl_3$/MeOH 9:1→8:2; $CHCl_3$/MeOH9:1 loading of crude; N_2 flow was used for purification) as a white solid (48 mg, 0.06 mmol, quant.). Reduced form: ^{1}H NMR (300 MHz, $CDCl_3$/MeOD 9:1) δ: 5.11 (d, J = 3.8 Hz, 2H, H-1, H-1'), 4.35 – 4.26 (m, 4H, H-6, H-6'), 4.00 – 3.92 (m, 2H, H-5, H-5'), 3.77 (pt, J = 9.3 Hz, 2H, H-3, H-3'), 3.53 (dd, J = 9.7, 3.7 Hz, 2H, H-2, H-2'), 3.40 – 3.32 (m, 7H, H-4, H-4', MeOH), 2.52 (t, J = 7.5 Hz, 2H, CH_2-SH), 2.39 – 2.31 (m, 4H, CH_2-C=O), 1.68 – 1.55 (m, 6H, CH_2-lipid), 1.43 – 1.19 (m, 40H, CH_2-lipid), 0.92 – 0.83 (m, 3H, CH_3-lipid). ^{13}C-APT NMR (75 MHz, $CDCl_3$/MeOD 9:1) δ: 174.6 (C=O), 93.5 (C-1, C1'), 72.9 (C-3, C-3'), 71.6 (C-2, C-2'), 70.2 (C-4, C-4'), 70.0 (C-5, C-5'), 63.1 (C-6, C-6'), 34.1 (CH_2-C=O), 31.9 (CH_2-lipid), 29.7 (CH_2-lipid), 29.6 (CH_2-lipid), 29.5 (CH_2-lipid), 29.4 (CH_2-lipid), 29.3 (CH_2-lipid), 29.2 (CH_2-lipid), 29.1 (CH_2-lipid), 29.0 (CH_2-lipid), 28.3 (CH_2-lipid), 24.8 (CH_2-lipid), 24.4 (CH_2-SH), 22.7 (CH_2-lipid), 14.0 (CH_3-lipid). HRMS $[M+Na]^+$: 831.4907 found, 831.4899 calculated. Oxidized form: ^{1}H NMR (400 MHz, $CDCl_3$/MeOD 9:1) δ: 5.11 (d, J = 3.6 Hz, 2H, H-1, H-1'), 4.39 – 4.21 (m, 14H, H-6, H-6', OH), 4.05 – 3.94 (m, 2H, H-5, H-5'), 3.85 (pt, J =9.4 Hz, 2H, H-3, H-3'), 3.55 (dd, J = 9.8, 3.7 Hz, 2H, H-2, H-2'), 3.43 – 3.31 (m, 3H, H-4, H-4', MeOH), 2.69 (t, J = 7.3 Hz, 2H, CH_2-S), 2.35 (t, J = 7.6 Hz, 4H, CH_2-C=O), 1.76 – 1.53 (m, 6H, CH_2-lipid), 1.43 – 1.24 (m, 40H, CH_2-lipid), 0.89 (t, J = 6.6 Hz, 3H, CH_3-lipid). ^{13}C-APT NMR (101 MHz, $CDCl_3$/MeOD 9:1) δ:174.5 (C=O), 93.5 (C-1, C-1'), 72.9 (C-3, C-3'), 71.5 (C-2, C-2'), 70.1 (C-4, C-4'), 69.9 (C-5, C-5'), 63.0 (C-6, C-6'), 39.0 (CH_2-S), 34.0 (CH_2-C=O), 31.8 (CH_2-lipid), 29.5 (CH_2-lipid), 29.4 (CH_2-lipid), 29.3 (CH_2-lipid), 29.3 (CH_2-lipid), 29.2 (CH_2-lipid), 29.1 (CH_2-lipid), 29.1 (CH_2-lipid), 29.0 (CH_2-lipid), 28.9 (CH_2-lipid), 28.3 (CH_2-lipid), 24.7 (CH_2-lipid), 22.5 (CH_2-lipid), 13.8 (CH_3-lipid).

6-O-stearoyl-6'-(16-(acetylthio)hexadecanoyl)-2, 3, 4, 2', 3', 4'-hexaakis-O-(trimethylsilyl)-α, α'-trehalose (28).

Compound **35** (211 mg, 0.2 mmol, 1 eq) was co-evaporated (2x) with toluene and dissolved in dry toluene (4 ml). Therefore, compound **24** (99 mg, 0.3 mmol, 1.5 eq) and DMAP (24 mg, 0.2 mmol, 1 eq) were added and the solution was cooled to 0 °C. EDCI (77 mg, 0.4 mmol, 2 eq) was finally added. The reaction mixture was warmed first to room temperature and then to 70 °C. The day after, the reaction mixture was diluted with EtOAc and transferred to a separatory funnel. The organic layer was washed (2x) with brine, dried over $MgSO_4$, filtered and concentrated in vacuo. Compound **28** was obtained after silicagel chromatography (Pentane/EtOAc 20:1→9:1; DCM loading of crude) as a transparent oil (232 mg, 0.17 mmol, 85%). ^{1}H NMR (400 MHz, $CDCl_3$) δ: 4.92 (d, J = 3.1 Hz, 2H, H-1, H-1'), 4.28 (dd, J = 11.8, 2.2 Hz, 2H, H-6a, H-6a'), 4.06 (dd, J = 11.8, 4.4 Hz, 2H, H-6b, H-6b'), 4.00 (ddd, J = 9.5, 4.4, 2.2 Hz, 2H, H-5, H-5'), 3.90 (pt, J = 9.0 Hz, 2H, H-3, H-3'), 3.53 – 3.39 (m, 4H, H-4, H-4', H-2, H-2'), 2.86 (t, J = 7.3 Hz, 2H, CH_2-SH), 2.38– 2.31 (m, 7H, CH_2-C=O, CH_3-thioacetyl), 1.66 – 1.53 (m, 6H, CH_2-lipid), 1.31– 1.22 (m, 50H, CH_2-lipid), 0.90 – 0.85 (m, 3H, CH_3-lipid), 0.17 – 0.12 (m, 54H, CH_3-TMS). ^{13}C-APT NMR (101 MHz, $CDCl_3$) δ: 196.2 (S-C=O), 173.9 (C=O), 94.5 (C-1, C-1'), 73.6 (C-3, C-3'), 72.8 (C-2, C-2'), 72.0 (C-4, C-4'), 70.9 (C-5, C-5'), 63.4 (C-6, C-6'), 34.3 (CH_2-C=O), 32.1 (CH_2-lipid), 30.8 (CH_3-thioacetyl), 29.8 (CH_2-lipid), 29.8 (CH_2-lipid), 29.8 (CH_2-lipid), 29.7 (CH_2-lipid), 29.6 (CH_2-lipid), 29.6 (CH_2-lipid), 29.5 (CH_2-lipid), 29.5 (CH_2-lipid), 29.3 (CH_2-lipid), 29.3 (CH_2-lipid), 29.0 (CH_2-S), 24.9 (CH_2-lipid), 22.8 (CH_2-lipid), 14.3 (CH_3-lipid), 2.1 (CH_3-TMS), 1.2 (CH_3-TMS), 1.0 (CH_3-TMS), 0.4 (CH_3-TMS), 0.3 (CH_3-TMS). HRMS $[M+Na]^+$: 1375.81640 found, 1375.81586 calculated.

6-O-stearoyl-6'-(16-(acetylthio)hexadecanoyl)-α, α'-trehalose (37).

Compound **28** (230 mg, 0.17 mmol, 1 eq) was dissolved in a mixture of DCM/MeOH 1:1 (36 ml). Amberlite H^+ was added until methanolysis of the TMS groups could be observed via TLC. The reaction was followed every 5 minutes, until after 30 minutes no starting material and only one lower running spot could be observed. The resin was removed via filtration and washed with DCM/MeOH 1:1. The filtered solution was concentrated and compound **37** was obtained as a white solid (138mg, 0.15 mmol, 87%) without any further purification. ^{1}H NMR (400 MHz, $CDCl_3$/MeOD 3:1) δ: 5.11 (d, J = 3.7 Hz, 2H, H-1, H-2), 4.37 – 4.28 (m, 4H, H-6, H-6'), 3.98 (ddd, J = 10.2, 4.8, 2.5 Hz, 2H, H-5, H-5'), 3.83 (pt, J = 9.3 Hz, 2H, H-3, H-3'), 3.53 (dd, J = 9.8, 3.7 Hz, 2H, H-2, H-2'), 3.41– 3.32 (m, 3H, H-4, H4', MeOH), 2.87 (t, J = 7.3 Hz, 2H, CH_2-S), 2.39 – 2.30 (m, 7H, CH_2-C=O, CH_3-thioacetyl), 1.67 – 1.54 (m, 6H, CH_2-lipid), 1.34 – 1.24 (m, 50H, CH_2-lipid), 0.88 (t, J = 6.7 Hz, 3H, CH_3-lipid). ^{13}C-APT NMR (214 MHz, $CDCl_3$/MeOD 9:1) δ: 197.1 (S-C=O), 174.6 (C=O), 93.5 (C-1, C-1'), 77.3 (C-3, C-3'), 71.6 (C-2, C-2'), 70.2 (C-4, C-4'), 70.0 (C-5, C-5'), 63.1 (C-6, C-6'), 34.1 (CH_2-C=O), 34.1 (CH_2-C=O), 31.9 (CH_2-lipid), 30.5 (CH_2-lipid), 29.6 (CH_2-lipid), 29.6 (CH_2-lipid), 29.6 (CH_2-lipid), 29.6 (CH_2-lipid), 29.6 (CH_2-lipid), 29.6 (CH_2-lipid), 29.5 (CH_2-lipid), 29.5 (CH_2-lipid), 29.4 (CH_2-lipid), 29.4 (CH_2-lipid), 29.4 (CH_2-lipid), 29.4 (CH_2-lipid), 29.3 (CH_2-lipid), 29.2 (CH_2-lipid), 29.1 (CH_2-lipid), 29.1 (CH_2-lipid), 29.0 (CH_2-S), 28.7 (CH_2-lipid), 24.9 (CH_2-lipid), 24.8 (CH_2-lipid), 22.6 (CH_2-lipid), 14.0 (CH_3-lipid). HRMS $[M+Na]^+$: 943.5804 found, 943.5787 calculated.

6-O-stearoyl-6'-(16-mercaptohexadecanoyl)-α, α'-trehalose (4).

Compound **37** (46 mg, 0.05 mmol, 1 eq) was dissolved in a degassed solution of DCM/MeOH 1:1 (0.5 ml) and hydrazine monohydrate (13 µL, 0.25 mmol, 5 eq) was added. After 5 hours an

extra portion of hydrazine monohydrate (13 µL, 0.25 mmol, 5 eq) was added and the reaction mixture was stirred overnight. The morning after the volatiles were removed in vacuo and compound **4** was obtained after silicagel chromatography ($CHCl_3$/MeOH 9:1→8:2; $CHCl_3$/MeOH 9:1 loading of crude; N_2 flow was used for purification) as a white solid (26 mg, 0.03 mmol, 50%). The remaining 50% was recovered as a mixture of free thiol and disulfide as confirmed by NMR analysis. ^{1}H NMR (300 MHz, $CDCl_3$/MeOD 1:1) δ: 5.10 (d, J = 3.7 Hz, 2H, H-1, H-1'), 4.43 – 4.20 (m, 4H, H-6, H-6'), 4.00 (ddd, J = 10.1, 5.0, 2.4 Hz, 2H, H-5, H-5'), 3.81 (pt, J = 9.3 Hz, 2H, H-3, H-3'), 3.53 (dd, J = 9.8, 3.8 Hz, 2H, H-2, H-2'), 3.46 – 3.29 (m, 3H, H-4, H-4', MeOH), 2.60 – 2.45 (m, 2H, CH_2-SH), 2.36 (t, J = 7.5 Hz, 4H, CH_2-C=O), 1.71 – 1.53 (m, 6H, CH_2-lipid), 1.41 – 1.21 (m, 50H, CH_2-lipid), 0.89 (t, J = 6.3 Hz, 3H, CH_3-lipid). ^{13}C-APT NMR (75 MHz, $CDCl_3$/MeOD 3:1) δ:174.4 (C=O), 93.3 (C-1, C1'), 73.1 (C-3, C-3'), 71.5 (C-2, C-2'), 70.2 (C-4, C-4'), 69.8 (C-5, C-5'), 63.0 (C-6, C-6'), 33.9 (CH_2-C=O), 31.6 (CH_2-lipid), 29.4 (CH_2-lipid), 29.4 (CH_2-lipid), 29.2 (CH_2-lipid), 29.0 (CH_2-lipid), 28.9 (CH_2-lipid), 28.8 (CH_2-lipid), 28.1 (CH_2-lipid), 24.6 (CH_2-SH), 24.1 (CH_2-lipid), 22.4 (CH_2-lipid), 13.6 (CH_3-lipid). HRMS $[M+Na]^+$: 901.56788 found, 901.56813 calculated.

6, 6'-O-distearoyl-2, 3, 4, 2', 3', 4'-hexaakis-O-(trimethylsilyl)-α, α'-trehalose (38).

Compound **26** (311 mg, 0.4 mmol, 1 eq) and stearic acid (228 mg, 0.8 mmol, 2 eq) were co-evaporated (2x) with toluene and dissolved in toluene (1.3 ml). After the solution was cooled to 0 °C, DMAP (49 mg, 0.04 mmol, 0.1 eq) and EDCI (75 mg, 0.5 mmol, 1.2 eq) were added and the reaction mixture was warmed first to room temperature over 1 hour and then to 70 °C. After 4 hours, the reaction mixture was diluted with EtOAc and transferred to a separatory funnel. The organic layer was washed (2x) with brine, dried over $MgSO_4$, filtered and concentrated in vacuo. Compound **38** was obtained after silicagel chromatography (Pentane/EtOAc 20:1→9:1; DCM loading of crude) as a transparent oil (433 mg, 0.33 mmol, 82%). ^{1}H NMR (300 MHz, $CDCl_3$) δ: 4.99 (d, J = 3.1 Hz, 2H, H-1, H-1'), 4.35 (dd, J = 11.7, 2.0 Hz, 2H, H-6a, H-6b), 4.19 – 4.03 (m, 4H, H-6a', H-6b', H-5, H-5'), 3.98 (pt, J = 8.9 Hz, 2H, H-3, H-3'), 3.60 – 3.45 (m, 4H, H-2, H-2', H-4, H-4'), 2.41 (t, J = 7.3 Hz, 4H, CH_2-C=O), 1.69 (p, J = 7.4 Hz, 4H, CH_2-lipid), 1.43– 1.25 (m, 56H, CH_2-lipid), 0.93 (t, J = 7.0 Hz, 6H, CH_3-lipid), 0.27 – 0.16 (m, 54H, CH_3-TMS). ^{13}C-bbdec. NMR (101 MHz, $CDCl_3$) δ: 173.9 (C=O), 94.5 (C-1, C-1'), 73.6 (C-3, C-3'), 72.8 (C-2, C-2'), 72.0 (C-4, C-4'), 70.8 (C-5, C-5'), 63.4 (C-6, C-6'), 34.3 (CH_2-C=O), 32.1 (CH_2-lipid), 30.4 (CH_2-lipid), 29.8 (CH_2-lipid), 29.8 (CH_2-lipid), 29.8 (CH_2-lipid), 29.6 (CH_2-lipid), 29.5 (CH_2-lipid), 29.5 (CH_2-lipid), 29.3 (CH_2-lipid), 24.9 (CH_2-lipid), 22.8 (CH_2-lipid), 14.3 (CH_3-lipid), 1.6 (CH_3-TMS), 1.2 (CH_3-TMS), 1.0 (CH_3-TMS), 0.7 (CH_3-TMS), 0.3 (CH_3-TMS), -0.1 (CH_3-TMS). HRMS $[M+Na]^+$: 1329.6190 found, 1329.8645 calculated.

Trehalose-6, 6'-distearate (39).

Compound **38** (1.6 g, 1.23 mmol, 1 eq) was dissolved in a mixture of DCM/MeOH1:1 (200 ml). Amberlite H^+ was added until methanolysis of the TMS groups could be observed via TLC. After 2 hours, the resin was removed via filtration and washed with MeOH. The filtered solution was concentrated and compound **39** was obtained as a white solid (864 mg, 0.96 mmol, 78%) without any further purification. ^{1}H NMR (400 MHz, $CDCl_3$/MeOD 2:1) δ: 5.09 (d, J = 3.7 Hz, 2H, H-1, H-2), 4.32 (dd, J = 12.1, 2.4 Hz, 2H, H-6a, H-6b), 4.26 (dd, J = 12.0, 4.9 Hz, 2H, H-6a', H-6b'), 3.97 (ddd, J = 10.2, 4.9, 2.4 Hz, 2H, H-5, H-5'), 3.78 (pt, J = 9.3Hz, 2H, H-3, H-3'), 3.52 (dd, J = 9.7, 3.7 Hz, 2H, H-2, H-2'), 3.39 – 3.30 (m, 3H, H-4, H-4', MeOH), 2.34 (t, J = 7.6 Hz, 4H, CH_2-C=O), 1.61 (p, J = 7.5 Hz, 4H, CH_2-lipid), 1.31 – 1.22 (m, 56H, CH_2-lipid), 0.87 (t, J = 6.8 Hz, 6H,

CH_3-lipid). ^{13}C-APT NMR (101 MHz, $CDCl_3$/MeOD 2:1) δ: 174.4 (C=O), 93.4 (C-1, C-1'), 73.03 (C-3, C-3'), 71.4 (C-2, C-2'), 70.1 (C-4, C-4'), 69.8 (C-5, C-5'), 63.0 (C-6, C-6'), 33.9 (CH_2-C=O), 31.7 (CH_2-lipid), 29.4 (CH_2-lipid), 29.4 (CH_2-lipid), 29.36 (CH_2-lipid), 29.2 (CH_2-lipid), 29.2 (CH_2-lipid), 29.1 (CH_2-lipid), 29.0 (CH_2-lipid), 28.9 (CH_2-lipid), 24.6 (CH_2-lipid), 22.4 (CH_2-lipid), 13.6 (CH_3-lipid). HRMS $[M+H]^+$: 897.62662 found, 897.62736 calculated.

Peptide conjugates

Materials for the synthesis of peptides and conjugates

All reagents and solvents used in the solid phase peptide synthesis were purchased from Novabiochem (San Diego, CA, USA) and Biosolve (Valkenswaard, The Netherlands), with the exception of 3-maleimido-propionic acid (Bachem, Torrance, CA, USA), palmitoyl-Cys((RS)-2, 3-di(palmitoiloxy)-propyl)-OH (Bachem, Torrance, CA, USA) and tetradecyl isocyanate (Sigma-Aldrich, St.Louis, MO, USA). Tentagel resins were purchased from Rapp Polymere (Tuebingen, Germany). All chemicals were used as received. Analytical LC-MS was performed using an Agilent 1260 LC system (215 and 254 nm UV sensors included) coupled to Agilent 6120 single quadrupole mass analyzer. This LC-MS system was equipped with one of the following columns: Macherey-Nagel NUCLEODUR® C18 5 µm, 4.6 x 50 mm; Hichrom Vydac® 219TP Diphenyl 5 µm, 4.6 x 150 mm; Cosmosil 5C4-MS 120˚A 5µm, 4.6 x 150 mm. Ternary solvent system: A - 100% water; B - 100% acetonitrile; C - 1% TFA in water. Gradients of B in A were employed in combination with 10% C. Purifications were performed on a Preparative HPLC system from Gilson equipped with one of the following columns: Macherey-Nagel NUCLEODUR® C18 5 µm, 10 x 250 mm; Hichrom Vydac® 219TP Diphenyl 5 µm, 10 x 250 mm; Cosmosil 5C4-MS 120˚A 5µm, 10 x 250 mm. Binary solvent system: A - 1% TFA in water; B - 100% acetonitrile. Gradients of B in A were employed over 3 CV unless stated otherwise. MALDI-TOF spectra were recorded on an Ultraflextreme MALDI-TOF or a 15T MALDI-FT-ICR MS system.

General methods for the synthesis of peptides

The solid phase peptide synthesis was performed on a Liberty Blue™ Automated Microwave Peptide Synthesizer. TentaGel® S RAM resin and Fmoc based protocols were employed for the synthesis of the peptides, unless stated otherwise. The steps performed for each amino acid coupling were: a) DMF washes (2 times) and subsequent nitrogen purge of the solvent; b) Fmoc protecting group removal using 4 ml of a solution containing 20% piperidine in DMF (3 times 1.5 minutes) at 90 °C; c) DMF washes (3 times) and subsequent nitrogen purge of the solvent; d) Fmoc protected amino acid (5 eq) coupling in the presence of oxyma pure (1 M, 1 eq) and DIC (0.5 M, 1 eq), performed at 90 °C for 2.5 minutes; e) DMF washes (3 times) and subsequent nitrogen purge; f) washing of the resin with DMF (3 times), DCM (3 times), Et_2O (2 times) and subsequent nitrogen purge. After completion of all synthetic cycles, the resin was transferred to a polypropylene syringe equipped with a porous polypropylene disc at the bottom and treated for 1 hour and 30 minutes with a TFA/TIS/H_2O (38:1:1, v/v/v) cleavage cocktail (5 mL/100 µmol scale reaction). The reaction mixture containing the cleaved peptide was filtered into cold Et_2O/pentane (1:1, v/v) (50 ml/5 ml cleavage cocktail) and the resin was washed with 1 ml TFA (2 times) into the cold Et_2O/pentane solution. The solution was stored in a -20 °C freezer for 2 hours, then centrifuged (10 minutes, 4400 rpm, 3 x g); finally, the

supernatant was discarded and the precipitate was purified via RP-HPLC. Synthetic compounds were tested using LAL assay to exclude the possibility of LPS contamination.

***Rv1733c p57-84 peptide: Ile-Pro-Phe-Ala-Ala-Ala-Ala-Gly-Thr-Ala-Val-Gln-Asp-Ser-Arg-Ser-His-Val-Tyr-Ala-His-Gln-Ala-Gln-Thr-Arg- His-Pro-*NH_2 (5)**

The p57 peptide (compound **5**) was synthesized according to the general procedure for peptide synthesis described above. Pseudoproline dipeptides Fmoc-Asp(OtBu)-Ser (ψMe, Mepro)-OH and Fmoc-Gly-Thr (ψMe, Mepro)-OH were employed to enhance synthetic efficiency. Purification by RP-HPLC (linear gradient 20→30% B in 10 min) followed by lyophilization yielded compound **5** as a white powder (90.4 mg, 30.26 µmol, 12.1% yield based on theoretical resin loading of 0.23 mmol/g). LC-MS analysis (C18 column, linear gradient 10→90% B, 11 min): Rt = 3.571 min, ESI-MS $[M+H]^{2+}$ = 1494.3 found, 1493.8 calculated. MALDI-TOF $[M+H]^{+}$: 2986.4517 found, 2986.5143 calculated.

Rv1733c p57-84 maleimido-peptide: Maleimido-Ile-Pro-Phe-Ala-Ala-Ala-Ala-Gly-Thr-Ala-Val-Gln-Asp-Ser-Arg-Ser-His-Val-Tyr-Ala-His-Gln-Ala-Gln-Thr-Arg-His-Pro-*NH_2 *(40)

Compound **40** was synthesised according to the general procedure for peptide synthesis described above. Pseudoproline dipeptides Fmoc-Asp(OtBu)-Ser (ψMe, Mepro)-OH and Fmoc-Gly-Thr (ψMe, Mepro)-OH were employed to enhance synthetic efficiency. Purification by RP-HPLC (linear gradient 20→35% B in 10 min) followed by lyophilisation yielded **40** as a white powder (20.99 mg, 6.68µmol, 6.7%yield based on theoretical resin loading of 0.23 mmol/g). LC-MS analysis (C18 column, linear gradient 10→50% B, 11 min): Rt = 6.395 min, ESI-MS $[M+H]^{2+}$= 1570.0 found, 1569.3 calculated.

3-(3-(trehalose-6-stearoyl-6'-undecanoylthio)-2, 5-dioxopyrrolidin-1-yl) propanoate-Ile-Pro-Phe-Ala-Ala-Ala-Ala-Gly-Thr-Ala-Val-Gln-Asp-Ser-Arg-Ser-His-Val-Tyr-Ala-His-Gln-Ala-Gln-Thr-Arg-His-Pro-*NH_2 *(6)

Trehalose glycolipid **3** (12 mg, 14.4µmol, 3 eq) was dissolved in degassed $CHCl_3$ (0.9 ml) and added to a mixture of Rv1733c p57-84 maleimido-peptide **40** (15 mg, 4.7µmol, 1 eq) in degassed DMF (1.2 ml) and H_2O (0.3 ml). The reaction was stirred overnight under Argon atmosphere. Compound **6** was obtained after purification by RP-HPLC (C18 column, linear gradient 25→75% B, 12 min) as a white powder (14.8 mg, 3.7µmol, 79%). LC-MS analysis (C18 column, linear gradient 10→90%B, 11 min): Rt = 7.906 min, ESI-MS $[M+H]^{2+}$= 1974.5 found, 1973.5 calculated. MALDI-TOF $[M+H]^{+}$: 3946.121 found, 3946.038 calculated.

3-(3-(trehalose-6-stearoyl-6'-palmitoylthio)-2, 5-dioxopyrrolidin-1-yl) propanoate-Ile-Pro-Phe-Ala-Ala-Ala-Ala-Gly-Thr-Ala-Val-Gln-Asp-Ser-Arg-Ser-His-Val-Tyr-Ala-His-Gln-Ala-Gln-Thr-Arg-His-Pro-*NH_2 *(7)

Trehalose glycolipid **4** (0.9 mg, 1.02µmol, 1 eq) was dissolved in degassed $CHCl_3$ (0.19 ml) and added to a mixture of Rv1733c p57-84 maleimido-peptide **40** (8 mg, 2.5µmol, 2.5 eq) in degassed DMF (0.25 ml) and H_2O (0.06 ml). The reaction was stirred overnight under Argon atmosphere. A precipitate formed, which was separated after centrifuging from the mother liquor, and redissolved in a 3:3:1 mixture of t-BuOH/CH_3CN/H_2O (500µl) with addition of TFA (50µl) to improve solubility. Compound **7** was obtained after purification by RP-HPLC (C18 column, linear gradient 30→100% B, 15 min) as a white powder (0.9 mg, 3.7µmol, 22%).LC-MS analysis (C18 column, linear gradient 10→90% B, 11 min): Rt = 9.081min, ESI-MS

$[M+H]^{3+}$= 1339.9 found, 1339.4 calculated. MALDI-TOF $[M+H]^{+}$: 4016.0244 found, 4016.1202 calculated.

Immunological methods

Culturing and stimulation of HEK-Blue mMincle cell line

The HEK-Blue mMincle cell line was purchased from InvivoGen (San Diego, United States) and cultured according to manufacturer's instructions in Dulbecco's Modified Eagle Medium DMEM (Gibco, PAA, Linz, Austria) + 4.5 g/l glucose, 10% (v/v) heat-inactivated fetal calf serum (FCS) (HyClone, GE Healthcare Life Sciences, Eindhoven, the Netherlands), 50 U/ml penicillin, 50 mg/ml streptomycin, 100 mg/ml Normocin and 2 mM L-glutamine (Life Technologies-Invitrogen, Bleiswijk, the Netherlands). All compounds used for stimulation were dissolved in iso-propanol and transferred to 96 well plates (Microlon high binding, Greiner Bio-One International). The solvent was evaporated completely at 50 °C. HEK-293 cells were suspended in Quantiblue (InvivoGen, San Diego, United States) medium and approximately 50.000 cells/well were transferred to 96 well plate. Reference peptide and UPam were used as negative controls. After overnight stimulation with novel adjuvants and conjugates, sample absorbance at 635 nm was measured using a Spectramax i3x (Molecular Devices, CA, USA) spectrometer.

ELISA using murine Mincle-Fc receptor

Recombinant Murine CLEC4E Fc Chimera Protein was purchased from RD systems (Minneapolis, MN, USA) and used at concentrations of 0.83 µg/ml. Control compound PAA-Lewis X was purchased from Lectinity (MW approx. 20 KDa, Carbohydrate content around 20% mol). Laminarin (from *Laminaria digitata*) and Mannan (from *Saccharomyces cerevisiae*) were purchased from Sigma-Aldrich (St.Louis, MO, USA). All synthetic compounds were dissolved in iso-propanol and were transferred to 96 well plates (Nunc MaxiSorp, Biolegend, London, UK) at three different concentrations (5 - 1 - 0.2 nmol/well) for a total volume of 50 µL/well. The solvent was evaporated at 50 °C. Control compounds Laminarin (3 µg/ml), PAA-Lewis X (1 µg/ml) and Mannan (1 µg/ml) were diluted in PBS and used to coat remaining wells for a total volume of 50 µL/well. After coating for 2 hours at room temperature, all the wells were washed twice with TMS (20 mM tris(hydroxymethyl)aminomethane (Tris)-HCl, pH 8.0; 150 mM NaCl; 1 mM $CaCl_2$; 2 mM $MgCl_2$) (150µL) and blocked with 100 µL TMS with 1% of BSA (Fraction *V*, Merk Millipore, Burlington, MA, USA) for 30 minutes at room temperature. The plates were then incubated for 1 hour at room temperature with 50 µL soluble receptor in TMS with 1% of BSA. The wells were washed two times with TMS (150µL) and incubated at room temperature with 50 µL of Goat-anti human HRP (0.8 µg/mL, Jackson Immuno Research, Germany) in TMS with 1% of BSA for 30 minutes. After two washes with TMS (150µL), 50 µL of substrate solution (3, 3, 5, 5-Tetramethylbenzidine, TMB, in citric/acetate buffer, pH=4, and H_2O_2) were added and after 2 minutes at room temperature the reaction was stopped with 50 µL of H_2SO_4 (0.8M). Sample absorbance at 450 nm was measured using a Spectramax i3x (Molecular Devices, CA, USA) spectrometer.

Culturing and stimulation of murine D1 DC cell line

The D1 cell line[51] was obtained from the department of Immunohematology and Blood Transfusion of the Leiden University Medical Centre. The cells were cultured in IMDM medium (Lonza, Belgium) containing 10% heat inactivated FCS (HyClone, GE Healthcare Life Sciences, Eindhoven, the Netherlands), 2 mM GlutaMAX™ (Gibco, PAA, Linz, Austria), 50 μM β-mercaptoethanol (Sigma, St.Louis, MO, USA) and 30% supernatant from R1 cells (mouse fibroblast NIH/3T3 cells transfected with mouse GM-CSF gene), which was collected from confluent cultures and filtered. Cells were harvested using PBS containing 2 mM EDTA, counted and transferred to 96 well plates (round bottom, Corning Costar TC-Treated Microplates, Corning, NY) at approximately 50.000 cells/well. Immediately after plating, the cells were stimulated at a concentration of 50 μM of trehalose 6-6'-distearate and synthetic compounds. Synthetic compounds were dissolved in DMSO (Sigma, St.Louis, MO, USA) at a concentration of 5 nmol/μL, further diluted and premixed in culture medium. ODN1826 (1 μg/ml; 5′-TCCATGACGTTCCTGACGTT-3′; InvivoGen, San Diego, CA) was used as positive control for stimulated cells. Supernatants were harvested 20 hours after the addition of stimuli for subsequent analysis of cytokines and cells were stained as described below.

Flow cytometric analysis of D1 DC cell line

After 20 h stimulation, murine D1 cells were incubated for 30 minutes at 4 °C with the following dye-labelled antibodies: PE anti-mouse CD40 clone 3/23 (Biolegend, London, UK) and FITC anti-mouse CD86 clone B7-2 (eBioscience, San Diego, CA). Samples containing the stained cells were characterized on a BD FACSLyric™ flow cytometer and analysed using FlowJo v10 software (Treestar Inc).

Generation and stimulation of immature human moDCs and macrophages

Buffy coats of healthy human Blood Bank donors were purchased from Sanquin, Amsterdam, The Netherlands. $CD14^+$ monocytes were isolated from whole blood using Ficoll-Paque density gradient followed by purification on autoMACS® Pro Separator instrument using CD14 MicroBeads (MACS, Miltenyi Biotec, Bergisch Gladsbach, Germany). The monocytes were differentiated to monocyte-derived dendritic cells (moDCs) at a concentration of 10^6 cells/mL in RPMI 1640 (Gibco, PAA, Linz, Austria) medium containing 10% FCS (Hyclone, GE Healthcare Life Sciences, Eindhoven, the Netherlands), 2 mM GlutaMAX™ (Gibco, PAA, Linz, Austria), 100 U/ml penicillin, and 100 μg/ml streptomycin and 10 ng/mL GM-CSF (Life Technologies-Invitrogen, Bleiswijk, the Netherlands) and 10 ng/mL IL-4 (Peprotech, Rocky Hill, NJ). Differentiation into macrophages was done in the presence of a final concentration of 5 ng/ml GM-CSF for type 1 macrophages and 50 ng/ml M-CSF (R&D Systems, Abingdon, UK) for type 2 macrophages. On day 3 of culturing, all cultures were replenished with fresh culture media with the appropriate concentrations of GM-CSF and IL-4 for the moDC's and GM-CSF/M-CSF for the different subtypes of macrophages. Cells were incubated for a total of 5 days at 37 °C and in a 5% CO_2 atmosphere incubator. Immature dendritic cells were then harvested, counted and transferred to 96 well plates (round bottom, Corning Costar TC-Treated Microplates, Corning, NY) at approximately 50.000 cells/well; macrophages type 1 and type 2 were harvested, counted and transferred to 96 well plates (flat bottom, Corning Costar TC-Treated Microplates, Corning, NY) at approximately 30.000 cells/well. The next day, cells were stimulated at fixed concentrations (20 – 1 -0.05 μM) of trehalose 6-6'-distearate and synthetic compounds. Synthetic compounds were dissolved in DMSO (Sigma, St.Louis, MO, USA) at a

concentration of 5 nmol/µL, further diluted and premixed in RPMI 1640 medium containing 10% FCS, 2 mM GlutaMAX™, 100 U/ml penicillin, and 100 µg/ml streptomycin. LPS (InvivoGen, San Diego, United States), at a concentration of 100 ng/ml, was used as positive control for stimulated cells. Supernatants were harvested 20 hours after the addition of stimuli for subsequent analysis of cytokines and cells were stained as described below.

Flow cytometric analysis of human moDCs and macrophages

Cells were incubated for 10 minutes at room temperature with 5% human serum (Sigma, Merck, Darmstadt, Germany) in PBS to prevent nonspecific binding of the antibodies. Subsequently, cells were stained for 10 minutes at 4 °C using LIVE/DEAD™ Fixable Violet Dead Cell Stain Kit (Thermo Fisher scientific, Merelbeke, Belgium), followed by surface staining (30 minutes at 4 °C) with CD40 - APC (clone 5C3), CD80 - APC-R700 (clone L307.4), CD83 - PE (clone HB15e), CD86 - BB700 (clone 2331 (FUN-1)), HLA-DR-DP-DQ - BV510 (clone Tu39); all antibodies were purchased from BD Biosciences. All samples were characterized on a BD FACSLyric™ flow cytometer and analysed using FlowJo v10 software (Treestar Inc).

ELISA human cytokines

Human IL-12/IL-23 (p40) and human IL-10 ELISA kits were purchased from Biolegend (ELISA MAX™ Standard Set; London, UK). All supernatants were tested in duplicates according to manufacturer's instructions. Microlon high binding 96 well plates (Greiner Bio-One International) were used for the assays. Sample absorbance was measured using a Spectramax i3x (Molecular Devices, CA, USA) spectrometer.

Luminex human Th1/Th17

Cytokines and chemokines in culture supernatants were measured with the Milliplex magnetic bead kit (Merck, USA) on 96 well multiscreen filter plates (Millipore, USA) using the Bio-Plex-100-suspension-array-system (Bio-Rad Laboratories, Veenendaal, The Netherlands) and analyzed using the Bio-Plex Manager software 6.1 (Bio-Rad Laboratories, Veenendaal, The Netherlands). Cytokines/chemokines included: IL-6, GM-CSF, TNF-α, IFN-γ. After prewetting the filter with assay solution supernatant samples (25 µl) were added to the plates, together with 25 µl assay buffer and 25 µl beads, and the plates were incubated for overnight at 4 °C. After two washing steps with 200 µl wash buffer (Millipore, USA), 25 µl detection Ab mixture was added per well, and plates were incubated at room temperature in the dark for 1 hour on a plate shaker at 300 rpm. Per well 25 µl streptavidin-PE solution was added and incubated for 30 min at room temperature in the dark. After two washes, 150 µl Sheath Fluid was added to each well, and the plates were placed in the Bio-Plex System. From each well, a minimum of 50 analyte-specific beads was analyzed for fluorescence. A curve fit was applied to each standard curve according to the manufacturer's manual. Sample concentrations were interpolated from these standard curves. Analyte concentrations outside the upper or lower limits of quantification were assigned the values of the limits of quantification of the cytokine or chemokine.

Mice

HLA-DRB1*0301/DRA transgenic (tg), murine class II-deficient (HLA-DR3/Ab^0) mice were bred under specific-pathogen-free conditions at the Leiden University Medical Centre (LUMC) animal facility. During breeding, PBMCs of each mouse were typed for expression and

segregation of the transgene by flow cytometry for HLA-DR PE-labelled mouse IgG2a anti-HLA-DR (clone G46-6; BD Biosciences, Franklin Lakes, NJ, USA) and murine CD4 FITC-labelled rat IgG2a, κ anti-mouse CD4 (clone H129.19; BD Biosciences). Littermates lacking HLA-DR expression were excluded from these experiments.

Immunizations

Mice (3 to 6 animals per group; 6 weeks old) were injected subcutaneously (s.c.) in the right flank with conjugate, or mixtures of p57-peptide and trehalose adjuvant, in 200 µl phosphate-buffered saline (PBS) at 2 weeks interval. Two weeks after the last immunization, splenocytes were harvested.

In vitro cultures of splenocytes

Splenocytes were isolated from individual animals by homogenizing spleens through a 70µm cell strainer (Falcon; Fisher Scientific, Loughborough, UK), and were resuspended in Iscove's modified Dulbecco's medium (Invitrogen, Thermo Fisher Scientific, Bleiswijk, the Netherlands) + Glutamax (Gibco, PAA, Linz, Austria), supplemented with 100 U/100 µg/ml penicillin-streptomycin solution (Invitrogen) and 8% FCS (Hyclone, GE Healthcare Life Sciences, Eindhoven, the Netherlands) at 3 x 10^6 cells/ml in a 96-well round-bottom microtiter plates (Costar; Corning Incorporated, Corning, NY). Cells were incubated in quadruplicate with 100 µl of medium, peptide (final concentration 10 µg/ml), or relevant recombinant *Mtb* protein (10 µg/ml). The mitogen concanavalin A (ConA; 2 µg/ml; Sigma, St.Louis, MO, USA) was used as a positive control for cell viability. After 6 days, supernatants were taken from each well and quadruplicates were pooled and frozen at -20°C.

Intracellular cytokine staining

Splenocytes (6 x 10^6/well) were cultured *in vitro* with medium, peptide (5 µg/ml) or protein (5 µg/ml) in a 24 well plate. After 4 h, BrefeldinA (2.5 µg/ml, Sigma, St.Louis, MO, USA) was added and incubated overnight. The following day cells were stained with the following surface markers CD8α-Horizon V500 (clone 53-6.7), CD62L APC (clone MEL-14) (BD Biosciences, San Diego, CA), CD44-BV605 (clone IM7), HLA-DR-AF700 (clone L243), PD-1-PE-Cy7 (clone RMP1-30) (Biolegend, London, UK), KLRG1-V450 (clone 2F1) (ThermoFisher Scientific, Waltham, MA, USA). After fixation cells were permeabilized with Cytofix/Cytoperm reagents (BD Bioscience, San Diego, CA) according to manufacturer's instructions and stained intracellularly with IFN-γ-AlexaFluor488 (clone XMG1.2) (Biolegend, London, UK), TNF-α-PE (clone MP6-XT22). IL-2-APC Cy7 (clone JES6-5H4) (BD Biosciences, San Diego, CA) and IL-17A-PerCP-Cy5.5 (clone eBio17B7) (ThermoFisher Scientific, Waltham, MA, USA).

Antibody detection

Antibodies against the Rv1733c p57 peptide, Rv1733c protein and *Mtb* sonicate in serum from immunized mice were determined by ELISA: High binding 96 well plates (Microlon, Greiner Bio-One International, Alphen a/d Rijn, The Netherlands) were coated overnight at 4 °C with Bovine Serum Albumine (0.4%, BSA, Roche, Woerden, The Netherlands) to determine the non-specific background, peptide (5µg/ml), protein (5µg/ml) or *Mtb* sonicate (5µg/ml) for the specific antibody responses; washed three times with PBS/0.05% Tween-20 and blocked with 1% BSA/1% Tween-20 for 2h at 37 °C. After washing three times, serum dilutions in 1% BSA were incubated at 37 °C for 2h, followed by three times washing and incubated for 2h at 37 °C

with horse radish peroxide (HRP)-labelled Ig antibodies (total Ig, IgG1, IgG2a, IgG2b, IgG2c, IgG3, IgM and IgA (all Dako, Glostrup, Denmark)) in PBS/1% BSA. After incubation, plates were washed five times and TMB substrate (Sigma, St.Louis, MO, USA) was added for 10 minutes at RT, H_2SO_4 (1M) was added to stop the colorimetric reaction and OD450 was determined.

IFN-γ ELISA

Splenocytes (6 x 10^6/well) were cultured *in vitro* with medium, peptide (5 μg/ml) or protein (5 μg/ml) in a 24 well plate. IFN-γ ELISA (BD Bioscience, San Diego, CA) was performed on supernatants according to manufacturer's instructions. Absorbance (OD450) was determined and Microplate Manager software version 5.2.1 (Biorad Laboratories, The Netherlands) was used to convert the values into concentrations using a standard curve.

Cytokine-chemokine analysis

Cytokines and chemokines in supernatants from splenocytes were measured using a Milliplex magnetic bead kit (Merck, USA) on 96 well multiscreen filter plates (Millipore, USA) using the Bio-Plex-100-suspension-array-system (Bio-Rad Laboratories, Veenendaal, The Netherlands) and analyzed using the Bio-Plex Manager software 6.1 (Bio-Rad Laboratories, Veenendaal, The Netherlands). Cytokines/chemokines included: IL-2, IL-6, IL-15, IFN-γ, IL-1β, IL-4, IL-5, IL-10, IL-13, IL-17A, IL-17F, IL-21, IL-22, CD40L, TNF-α, TNF-β, MIP-3α, GM-CSF. After prewetting the filter with assay solution supernatant samples (25 μl) were added to the plates, together with 25 μl assay buffer and 25 μl beads, and the plates were incubated for overnight at 4 °C. After two washing steps with 200 μl wash buffer (Millipore, USA), 25 μl detection Ab mixture was added per well, and plates were incubated at room temperature in the dark for 1 hour on a plate shaker at 300 rpm. Streptavidin-PE solution (25 μl/well) was added and incubated for 30 min at room temperature in the dark. After two washes, 150 μl Sheath Fluid was added to each well, and the plates were placed in the Bio-Plex System. From each well, a minimum of 50 analyte-specific beads was analyzed for fluorescence. A curve fit was applied to each standard curve according to the manufacturer's manual. Sample concentrations were interpolated from these standard curves. Analyte concentrations outside the upper or lower limits of quantification were assigned the values of the limits of quantification of the cytokine or chemokine.

BCG immunization

Mice were injected s.c. in the right flank with 10^6 CFU BCG1331 (*M. bovis* bacillus Calmette Guérin; Statens Serum Institut, Copenhagen, Denmark) from glycerol stocks, 12 weeks before *Mtb* challenge.

Intranasal infection of mice with live Mtb

Mice were anesthetized with isofluoran (2-chloro-2-(difluoromethoxy)-1, 1, 1-trifluoro-ethane; Pharmachemie BV, The Netherlands) and intranasally (i.n.) infected with 10^5 CFU live *Mtb* strain H37Rv from glycerol stocks, 2 weeks after the third antigen immunization or 12 weeks after BCG immunization. Mice were daily monitored for ethical requirements, and weighed once a week. They were sacrificed 6 weeks after *Mtb* infection, lungs and splenocytes were aseptically removed. Organs were homogenized using 70 μM cell strainers (Fisher Scientific, Loughborough, UK) and the numbers of *Mtb* bacteria were determined by plating serial dilutions of the homogenates on 7H11 agar plates (BD Bioscience, San Diego, CA),

supplemented with BBL Middlebrook OADC enrichment and PANTA (all BD Bioscience, San Diego, CA). Colonies were counted after 3 weeks of incubation at 37 °C.

Supporting figures

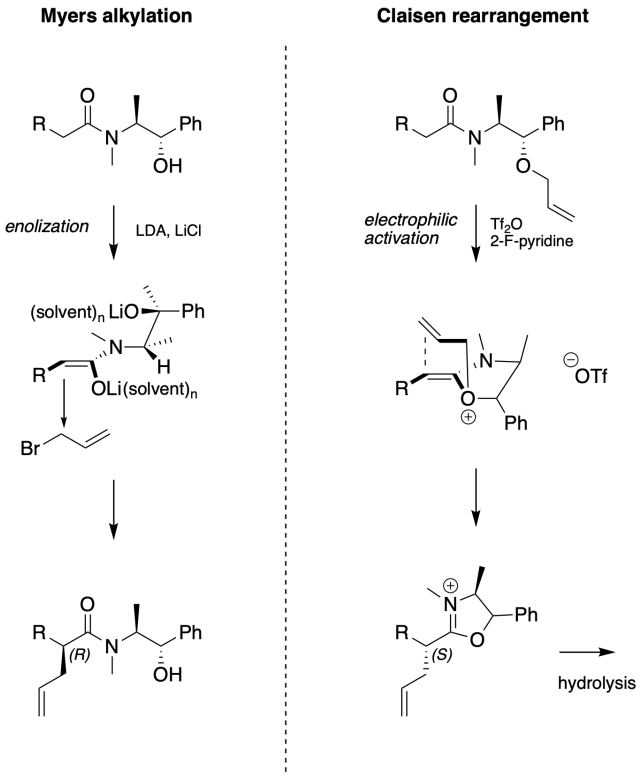

S5 Figure - Schematic comparison of the reaction mechanisms for Myers alkylation and Peng's strategy employing Claisen rearrangement.[52]

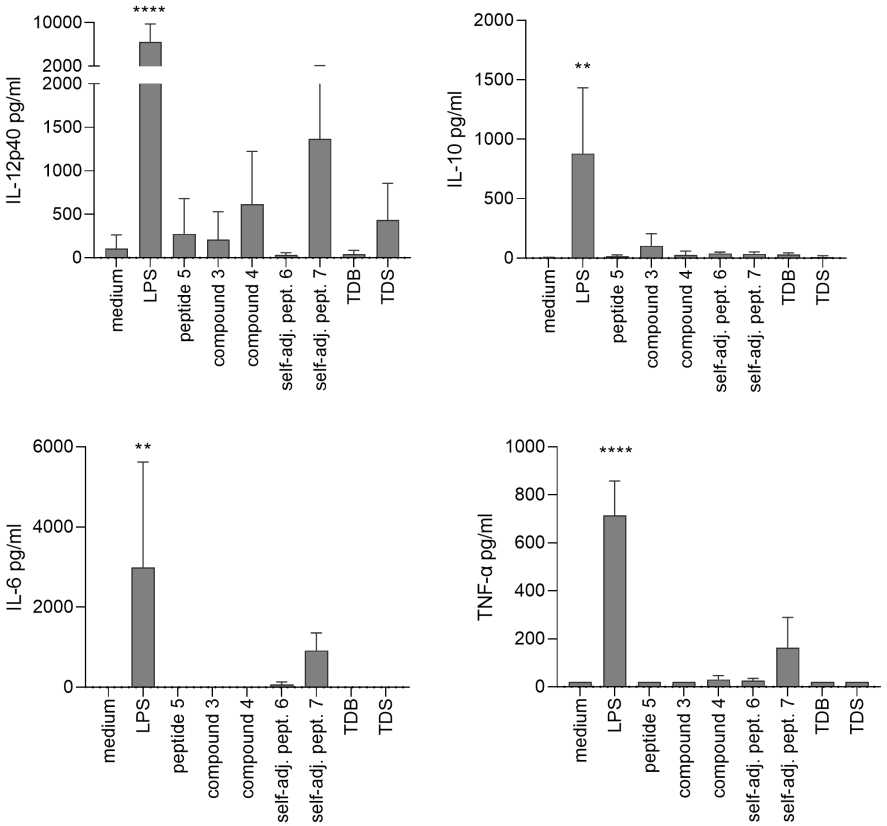

S6 Figure - Cytokine production profile of human moDCs stimulated for 20 hours using TDM analogues 3 and 4, and self-adjuvanting peptides 6 and 7, as measured by ELISA (IL-12p40 and IL-10) or Luminex (IL-6 and TNF-α). All synthetic compounds were used at a final concentration of 20 μM in medium. LPS (100 ng/ml) is used as a positive control. Bars indicate the mean value + SD of duplicates from three donors as calculated using GraphPad Prism.

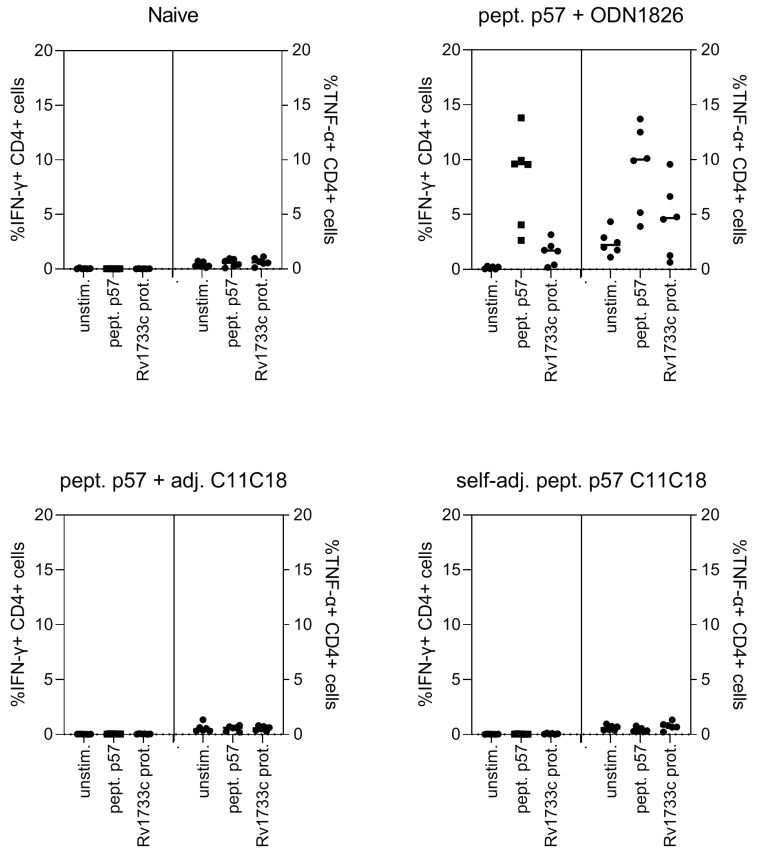

S7 Figure - IFN-γ released in cell supernatant after in vitro stimulation of splenocytes of immunized mice with either purified peptide p57 (5 µg/ml) or recombinant protein (5 µg/ml), as measured by ELISA assay. Mice (n=6) were injected three times with either PBS as negative control, peptide p57 (40 nmol) in admixture with ODN1826 (8 nmol) as positive control, peptide p57 (40 nmol) in admixture with adjuvant C11C18 (40 nmol) or self-adjuvanted peptide p57 C11C18 (40 nmol). Splenocytes were obtained two weeks after the last immunisation.

References

1. Geneva: World Health Organization. Global tuberculosis report 2020. 2020.

2. Ottenhoff THM. Overcoming the global crisis: "Yes, we can", but also for TB … ?: FORUM. Eur J Immunol. 2009 Aug;39(8):2014–20.

3. Kim H-R, Hwang SS, Kim HJ, Lee SM, Yoo C-G, Kim YW, et al. Impact of Extensive Drug Resistance on Treatment Outcomes in Non-HIV-Infected Patients with Multidrug-Resistant Tuberculosis. Clin Infect Dis. 2007 Nov 15;45(10):1290–5.

4. Martin C, Aguilo N, Marinova D, Gonzalo-Asensio J. Update on TB Vaccine Pipeline. Appl Sci. 2020 Apr 10;10(7):2632.

5. Hesseling AC, Marais BJ, Gie RP, Schaaf HS, Fine PEM, Godfrey-Faussett P, et al. The risk of disseminated Bacille Calmette-Guerin (BCG) disease in HIV-infected children. Vaccine. 2007 Jan;25(1):14–8.

6. Andersen P, Doherty TM. The success and failure of BCG — implications for a novel tuberculosis vaccine. Nat Rev Microbiol. 2005 Aug;3(8):656–62.

7. Ottenhoff THM, Kaufmann SHE. Vaccines against Tuberculosis: Where Are We and Where Do We Need to Go? Chitnis CE, editor. PLoS Pathog. 2012 May 10;8(5):e1002607.

8. Young DB. Disease states and vaccines: selected cases. In: The Vaccine Book. Elsevier; 2003. p. 279–89.

9. van Der Meeren O, Hatherill M, Nduba V, Wilkinson RJ, Muyoyeta M, van Brakel E, et al. Phase 2b Controlled Trial of M72/AS01E Vaccine to Prevent Tuberculosis. N Engl J Med. 2018 Oct 25;379(17):1621–34.

10. Tait DR, Hatherill M, van Der Meeren O, Ginsberg AM, van Brakel E, Salaun B, et al. Final Analysis of a Trial of M72/AS01E Vaccine to Prevent Tuberculosis. N Engl J Med. 2019 Dec 19;381(25):2429–39.

11. Pahari S, Kaur G, Aqdas M, Negi S, Chatterjee D, Bashir H, et al. Bolstering Immunity through Pattern Recognition Receptors: A Unique Approach to Control Tuberculosis. Front Immunol. 2017 Aug 2;8:906.

12. Wang Z-B, Xu J. Better Adjuvants for Better Vaccines: Progress in Adjuvant Delivery Systems, Modifications, and Adjuvant–Antigen Codelivery. Vaccines. 2020 Mar 13;8(1):128.

13. Huang Q, Yu W, Hu T. Potent Antigen-Adjuvant Delivery System by Conjugation of *Mycobacterium tuberculosis* Ag85B-HspX Fusion Protein with Arabinogalactan-Poly(I:C) Conjugate. Bioconjug Chem. 2016 Apr 20;27(4):1165–74.

14. Coppola M, van den Eeden SJF, Wilson L, Franken KLMC, Ottenhoff THM, Geluk A. Synthetic Long Peptide Derived from Mycobacterium tuberculosis Latency Antigen Rv1733c Protects against Tuberculosis. Pascual DW, editor. Clin Vaccine Immunol. 2015 Sep;22(9):1060–9.

15. Richardson MB, Williams SJ. MCL and Mincle: C-type lectin receptors that sense damaged self and pathogen-associated molecular patterns. Front Immunol. 2014 Jun;5:288.

16. Lee W-B, Kang J-S, Choi WY, Zhang Q, Kim CH, Choi UY, et al. Mincle-mediated translational regulation is required for strong nitric oxide production and inflammation resolution. Nat Commun. 2016 Apr;7(1):1–14.

17. Ishikawa E, Ishikawa T, Morita YS, Toyonaga K, Yamada H, Takeuchi O, et al. Direct recognition of the mycobacterial glycolipid, trehalose dimycolate, by C-type lectin Mincle. J Exp Med. 2009 Dec 21;206(13):2879–88.

18. Yamasaki S, Ishikawa E, Sakuma M, Hara H, Ogata K, Saito T. Mincle is an ITAM-coupled activating receptor that senses damaged cells. Nat Immunol. 2008 Oct;9(10):1179–88.

19. Huber A, Kallerup RS, Korsholm KS, Franzyk H, Lepenies B, Christensen D, et al. Trehalose diester glycolipids are superior to the monoesters in binding to Mincle, activation of macrophages in vitro and adjuvant activity in vivo. Innate Immun. 2016 Aug;22(6):405–18.

20. Kallerup RS, Madsen CM, Schiøth ML, Franzyk H, Rose F, Christensen D, et al. Influence of trehalose 6,6′-diester (TDX) chain length on the physicochemical and immunopotentiating properties of DDA/TDX liposomes. Eur J Pharm Biopharm. 2015 Feb;90:80–9.

21. Toubiana R, Das BC, Defaye J, Mompon B, Toubiana M-J. Étude du cord-factor et de ses analogues. Carbohydr Res. 1975 Nov;44(2):308–12.

22. Johnson DA. Simple procedure for the preparation of trimethylsilyl ethers of carbohydrates and alcohols. Carbohydr Res. 1992 Dec;237:313–8.

23. Datta AK, Takayama K, Nashed MA, Anderson L. An improved synthesis of trehalose 6-mono and 6,6′-dicorynomycolates and related esters. Carbohydr Res. 1991 Sep;218:95–109.

24. Nishizawa M, Minagawa R, Garcia DM, Hatakeyama S, Yamada H. Syntheses and characterization of four diastereomers of trehalose-6, 6′-dicorynomycolates (TD BH32). Tetrahedron Lett. 1994 Aug;35(32):5891–4.

25. Furukawa A, Kamishikiryo J, Mori D, Toyonaga K, Okabe Y, Toji A, et al. Structural analysis for glycolipid recognition by the C-type lectins Mincle and MCL. Proc Natl Acad Sci. 2013 Oct 22;110(43):17438–43.

26. Feinberg H, Rambaruth NDS, Jégouzo SAF, Jacobsen KM, Djurhuus R, Poulsen TB, et al. Binding Sites for Acylated Trehalose Analogs of Glycolipid Ligands on an Extended Carbohydrate Recognition Domain of the Macrophage Receptor Mincle. J Biol Chem. 2016 Sep;291(40):21222–33.

27. Khan AA, Chee SH, McLaughlin RJ, Harper JL, Kamena F, Timmer MSM, et al. Long-Chain Lipids Are Required for the Innate Immune Recognition of Trehalose Diesters by Macrophages. ChemBioChem. 2011 Nov 25;12(17):2572–6.

28. Stocker BL, Khan AA, Chee SH, Kamena F, Timmer MSM. On One Leg: Trehalose Monoesters Activate Macrophages in a Mincle-Dependent Manner. ChemBioChem. 2014 Feb 10;15(3):382–8.

29. Decout A, Silva-Gomes S, Drocourt D, Barbe S, André I, Cueto FJ, et al. Rational design of adjuvants targeting the C-type lectin Mincle. Proc Natl Acad Sci. 2017 Mar;114(10):2675–80.

30. Willems MM, Zom GG, Khan S, Meeuwenoord N, Melief CJ, van der Stelt M, et al. N-tetradecylcarbamyl lipopeptides as novel agonists for toll-like receptor 2. J Med Chem. 2014 Jul;57(15):6873–8.

31. Wu W, Li R, Malladi SS, Warshakoon HJ, Kimbrell MR, Amolins MW, et al. Structure–Activity Relationships in Toll-like Receptor-2 Agonistic Diacylthioglycerol Lipopeptides. J Med Chem. 2010 Apr 22;53(8):3198–213.

32. Smith AJ, Graves B, Child R, Rice PJ, Ma Z, Lowman DW, et al. Immunoregulatory Activity of the Natural Product Laminarin Varies Widely as a Result of Its Physical Properties. J Immunol. 2018 Jan 15;200(2):788–99.

33. Ballas ZK, Krieg AM, Warren T, Rasmussen W, Davis HL, Waldschmidt M, et al. Divergent Therapeutic and Immunologic Effects of Oligodeoxynucleotides with Distinct CpG Motifs. J Immunol. 2001 Nov 1;167(9):4878–86.

34. Verreck FA, de Boer T, Langenberg DM, Hoeve MA, Kramer M, Vaisberg E, et al. Human IL-23-producing type 1 macrophages promote but IL-10-producing type 2 macrophages subvert immunity to (myco) bacteria. Proc Natl Acad Sci. 2004 Mar;101(13):4560–5.

35. Verreck FA, de Boer T, Langenberg DM, van der Zanden L, Ottenhoff TH. Phenotypic and functional profiling of human proinflammatory type-1 and anti-inflammatory type-2 macrophages in response to microbial antigens and IFN-γ-and CD40L-mediated costimulation. J Leukoc Biol. 2006 Feb;79(2):285–93.

36. Snapper CM, Mond JJ. Towards a comprehensive view of immunoglobulin class switching. Immunol Today. 1993 Jan;14(1):15–7.

37. Mosmann TR, Coffman RL. TH1 and TH2 cells: different patterns of lymphokine secretion lead to different functional properties. Annu Rev Immunol. 1989;7:145–73.

38. Deenick EK, Hasbold J, Hodgkin PD. Switching to IgG3, IgG2b, and IgA is division linked and independent, revealing a stochastic framework for describing differentiation. J Immunol Baltim Md 1950. 1999 Nov 1;163(9):4707–14.

39. Hiramatsu N, Kasai A, Hayakawa K, Nagai K, Kubota T, Yao J, et al. Secreted protein-based reporter systems for monitoring inflammatory events: Critical interference by endoplasmic reticulum stress. J Immunol Methods. 2006 Aug;315(1–2):202–7.

40. Chinthamani S, Settem RP, Honma K, Kay JG, Sharma A. Macrophage inducible C-type lectin (Mincle) recognizes glycosylated surface (S)-layer of the periodontal pathogen Tannerella forsythia. PLoS ONE. 2017 Mar 6;12(3):e0173394.

41. Vasu C. CD80 and CD86 C domains play an important role in receptor binding and co-stimulatory properties. Int Immunol. 2003 Feb 1;15(2):167–75.

42. Mir MA. Introduction to Costimulation and Costimulatory Molecules. In: Developing Costimulatory Molecules for Immunotherapy of Diseases. Elsevier; 2015. p. 1–43.

43. Li Z, Ju X, Silveira PA, Abadir E, Hsu W-H, Hart DNJ, et al. CD83: Activation Marker for Antigen Presenting Cells and Its Therapeutic Potential. Front Immunol. 2019 Jun 7;10:1312.

44. Nunes-Alves C, Booty MG, Carpenter SM, Jayaraman P, Rothchild AC, Behar SM. In search of a new paradigm for protective immunity to TB. Nat Rev Microbiol. 2014 Apr;12(4):289–99.

45. Divangahi M. Are tolerance and training required to end TB? Nat Rev Immunol. 2018 Nov;18(11):661–3.

46. Brazier B, McShane H. Towards new TB vaccines. Semin Immunopathol. 2020 Jun;42(3):315–31.

47. Achkar JM, Casadevall A. Antibody-Mediated Immunity against Tuberculosis: Implications for Vaccine Development. Cell Host Microbe. 2013 Mar;13(3):250–62.

48. Tran AC, Kim M-Y, Reljic R. Emerging Themes for the Role of Antibodies in Tuberculosis. Immune Netw. 2019;19(4):e24.

49. Begam AJJ, Basheer KA, Jubie S, Jupudi S, Azam MA, Dhanabal P. A New Class of Pure Estrogen Alpha Receptor Antagonists; Design, Synthesis and in-vitro Screening. Lett Drug Des Discov. 2018 Nov 1;16(1):66–81.

50. Berthe W, Sevrain CM, Chantôme A, Bouchet AM, Gueguinou M, Fourbon Y, et al. New Disaccharide-Based Ether Lipids as SK3 Ion Channel Inhibitors. ChemMedChem. 2016 Jul 19;11(14):1531–9.

51. Winzler C, Rovere P, Rescigno M, Granucci F, Penna G, Adorini L, et al. Maturation Stages of Mouse Dendritic Cells in Growth Factor–dependent Long-Term Cultures. J Exp Med. 1997 Jan;185(2):317–28.

52. Peng B, Geerdink D, Maulide N. Electrophilic Rearrangements of Chiral Amides: A Traceless Asymmetric α-Allylation. J Am Chem Soc. 2013 Oct 9;135(40):14968–71.

4

Synthesis and immunological evaluation of conjugates containing a TLR2 agonist

Laura Marino [1], Susan J.F. van den Eeden [2], Krista E. van Meijgaarden [2], Nico J. Meeuwenoord [1], Dmitri V. Filippov[1], Annemieke Geluk [2], Ferry A. Ossendorp [3], Gijs A. van der Marel [1], Jeroen D.C. Codée [1], Tom H.M. Ottenhoff [2]

[1] Department of Bio-organic Synthesis, Leiden University, Leiden, The Netherlands

[2] Department of Infectious Diseases, Leiden University Medical Center, Leiden, The Netherlands

[3] Department of Immunology, Leiden University Medical Center, Leiden, The Netherlands

4

Abstract

Despite the availability of the Bacillus Calmette-Guérin vaccine for the prevention of tuberculosis (TB), *Mycobacterium tuberculosis (Mtb)* remains one of the deadliest pathogens in the world. Novel vaccination strategies are required, and synthetic chemistry provides excellent tools to develop highly pure, homogenous and economical vaccines. Antigenic peptide epitopes are the smallest fragments in protein antigens recognized by immune cells. However, they are often poorly immunogenic by themselves. To overcome their poor immunogenicity, peptides can be formulated with adjuvants, or covalently linked to immunostimulatory molecules. Here, a panel of three synthetic peptide-conjugates was generated, with each containing a TLR2 ligand covalently attached to one of three antigenic peptides (p57 from the *Mtb* Rv1733c protein, p31 and p75 from the *Mtb* Rv2034 protein). These synthetic conjugates induced strong innate immune responses *in vitro* using human antigen-presenting cells. Most importantly, it is reported that one conjugate was more immunogenic *in vivo* when compared to the unconjugated admixture of peptide and TLR2 ligand. After subcutaneous vaccination in mice, the synthetic conjugate induced Th17 cellular responses and co-expression of multiple antigen-specific IgG subclasses. Furthermore, the conjugate was effective in reducing the bacterial load in the spleen of humanized, HLA-DR3 transgenic mice that had been intranasally infected with *Mtb* bacilli. These results suggest a promising role for molecularly defined TLR2 ligand-peptide conjugates as novel TB vaccine modalities, and provide additional support to the role of synthetic chemistry in aiding the development of highly pure and versatile vaccines.

Introduction

Tuberculosis (TB) is one of the top ten causes of death worldwide and is caused by aerosol infection with *Mycobacterium tuberculosis (Mtb)*.[1] Novel improved vaccination strategies replacing or complementing current Bacillus Calmette-Guérin (BCG) vaccinations, are required to reduce the TB burden.[2] According to the latest epidemiological studies reported by the World Health Organization, the most affected populations are those in developing countries, with the majority of infection cases in India (26%), Indonesia (8.5%), China (8.4%), the Philippines (6.0%), Pakistan (5.7%) and Nigeria (4.4%).[1] The development of an efficacious and inexpensive vaccine against *Mtb* would accelerate the global efforts to halt the spread of this disease to vulnerable populations.

Fully synthetic compounds, with their economical, versatile and robust manufacturing processes, represent a promising resource which can find application in the field of vaccine development, as illustrated by the fast de novo design and production of SARS-COV2 synthetic vaccines.[3,4] The rational design of such modern synthetic vaccines relies on the identification of suitable antigens to induce selective immunity towards a specific pathogen.[5] Proteins and peptides are the most common antigenic units that are recognized by antigen-presenting cells (APCs) and that are subsequently presented to B and T cells, key players for the development of humoral and cellular immunity.[6]

Usually, such antigens by themselves are poorly immunogenic when injected, and generally only induce weak immune responses if employed as a single entity. The combination of antigenic proteins or peptides with immune-stimulatory molecules, called adjuvants, is a proven successful strategy to circumvent the issue of poor immunogenicity.[7,8] Synthetic long peptides (SLPs) have been successfully employed to design therapeutic vaccines against the *Human Papillomavirus*.[9]

Recently, synthetic conjugates containing antigen(s) covalently attached to the adjuvant(s) of choice in the form of a single molecular construct, have been studied and shown to induce efficient antitumor immunity.[10,11] This Chapter reports on the application of a similar simple approach for the discovery of synthetic vaccines against TB. The novel molecular constructs employed in these studies were designed to include a toll-like receptor 2 (TLR2) ligand which would act as adjuvant, and one of three different synthetic long peptides (SLPs) as *Mtb* antigens. These conjugates were evaluated to determine the robustness of the conjugation strategy and the effect of conjugation on the biological outcome (see Figure 1 for a schematic overview of the study design).

TLR2 is a pattern recognition receptor (PRR) mainly expressed on the cell surface of antigen-presenting cells, such as dendritic cells and macrophages, and it is known to interact with bacterial lipoproteins. Upon agonist engagement with TLR2, a

TIRAP/MyD88 activation pathway is initiated which results in transcription of several inflammatory genes.[12] This receptor is often expressed as a heterodimer in combination with TLR1 or TLR6.[13]

Synthetic vaccines comprising TLR2 ligands have been shown to induce strong immune responses. In 2014, Pam_3CysSK_4, a TLR2/TLR1 ligand, was covalently attached to melanoma or lymphoma tumor derived epitopes and shown to promote $CD4^+$ and $CD8^+$ T cell responses, which correlated with *in vivo* anti-tumor activity.[14] In 2016, the same research group employed UPam (also known as Amplivant), also a TLR2/TLR1 ligand, in the form of a synthetic conjugate to stimulate human monocyte-derived dendritic cells and specifically activate cancer patient-derived T cells.[15] Most importantly, pulmonary immunization of C57BL/6 mice using the TLR2/TLR6 ligand Lipokel (a derivative of Pam_2Cys linked to the Ni^{2+}-chelating entity 3NTA) conjugated to *Mtb*-derived proteins was shown to provide protection after low dose *Mtb* challenge (100 CFU), while inducing IFN-γ^+ T lymphocytes and IgG antibodies.[16]

Given its enhanced immune-stimulatory ability as compared to the more popular Pam_3CysSK_4 adjuvant, UPam was chosen for the construction of the conjugates described in the present chapter.[17] This compound can be easily conjugated to SLPs using a synthetic strategy that involves exclusively the use of solid phase synthesis, which is a common methodology employed for the generation of SLPs. Compared to the more classical wet chemistry methods, solid phase synthesis offers several advantages, including simplicity and speed (since all reactions are carried out in a single reaction vessel), efficiency and cost-effectiveness (since it can easily be automated and the large losses normally encountered during isolation and purification of intermediates are reduced).[18]

The chosen Mtb-derived SLPs used for conjugation to UPam are HLA-DR3 binding peptide sequences, with HLA-DR3 being a major class II allele that is present in about 20% of the human population.[19] The selected peptides were shown to be presented to HLA-DR3 restricted T cells in humans or in transgenic mice.[20–23] They belong to either the Rv1733c or Rv2034 proteins, expressed during latent and inflammatory pulmonary infection, respectively. These two proteins were both shown to be strongly recognized by T cells from mycobacteria-exposed individuals.[24,25] The *in vivo* vaccine potential of Rv1733c- and Rv2034-derived synthetic long peptides, administered subcutaneously to HLA-DR3/Ab^0 mice in admixture with a toll-like receptor 9 (TLR9) agonist, has been previously shown.[21,22]

In the present study, three conjugates containing UPam covalently linked to the p57 peptide (Rv1733c a.a. 57-84), p31 peptide (Rv2034 a.a. 31-60) and the p75 peptide (Rv2034 a.a. 75-105) were synthesized. It was demonstrated that these synthetic compounds induced strong immune responses *in vitro* using human antigen-presenting cells. Most importantly, the vaccine potential of the p57-UPam conjugate

was revealed in a preliminary study following challenge of HLA-DR3 transgenic mice with live *Mtb*, which resulted in a significant reduction of the bacterial load in the spleen of vaccinated mice. This finding correlated with the induction of a Th17 cellular response and strong antibody titers *in vivo*.

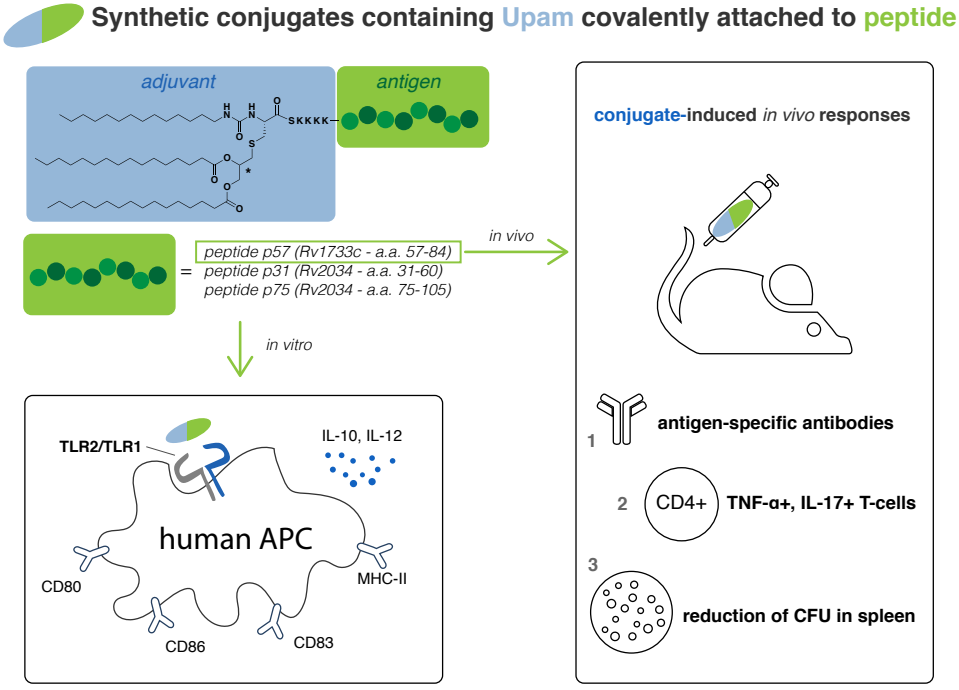

Figure 1 – Visual representation of synthetic conjugates generated and key immunological assays performed. Three conjugates were synthesized using in-line solid phase peptide synthesis, containing a TLR2 ligand (UPam) and one of three peptides contained in either Rv1733c or Rv2034 *Mtb*-derived protein. The three conjugates were assayed for their ability to activate human antigen-presenting cells (monocyte-derived dendritic cells and macrophages type 1 and 2) *in vitro*. One selected conjugate was further studied for its ability to induce humoral and cellular responses *in vivo*, and was shown to significantly reduce the bacterial load in the spleen of immunized mice that were live *Mtb* challenged.

Results

Synthesis of peptides and conjugates

The peptides were synthesized using standard Fmoc automated solid-phase synthesis. The use of pseudoproline derivatives for the generation of the p57 and p75 peptides was chosen to minimize aggregation during the stepwise assembly of these two hydrophobic peptides. The resulting yields after HPLC purification (12.1 and

14.1% for the p57 and p75 peptides, respectively) were comparable to that calculated for the water-soluble p31 peptide (12.0%). Synthesis of the peptide-UPam conjugates was performed according to an inline solid-phase synthetic protocol. In summary, the peptide was generated by Fmoc automated solid-phase synthesis and, without cleavage from the resin, it was immediately elongated with a known cysteine derivative (see materials and methods section) in the presence of oxyma pure and DIC. Subsequent washing and Fmoc-removal steps were followed by treatment with tetradecyl isocyanate to complete synthesis of UPam moiety. The conjugate was then cleaved from the resin and simultaneously deprotected. The p57, p31 and p75 UPam conjugates were obtained with overall yields of 3.3, 7.3 and 2.8%, respectively, after HPLC purification.

Dynamic light scattering measurements

The peptides have different physicochemical properties, including a different net charge at pH 7 and different water solubility. As determined using dynamic light scattering (DLS), the p57 peptide forms nanoparticles with hydrodynamic diameter of 170 nm and very low polydispersity index (PDI), peptide p31 forms nanoparticles with hydrodynamic diameter of 238 nm and intermediate PDI, peptide p75 forms bigger nanoparticles with hydrodynamic diameter of 986 nm and very high PDI.

Table 1 – Dynamic light scattering measurements for peptides in deionized water (20 μM):

	net charge at pH 7*	**particle size (nm)**	**PDI**	**derived count rate (kcps)**
pept. p57	2.3	170	0.062	4658
pept. p31	3.1	238	0.200	52**
pept. p75	-1	986	0.402	705

*calculated using Pepcalc.com prediction software

**The good water solubility of peptide p31, as predicted using Pepcalc.com, may be responsible for the low derived count rate calculated using the zetasizer software v7.13 (Malvern Panalytical).

In vitro evaluation using TLR2 ligand-peptide conjugates

The commercially available HEK-293-hTLR2 and HEK-null cell lines were used to probe binding of p57-UPam, p31-UPam and p75-UPam conjugates. The HEK-293-hTLR2 cell line is a reporter cell line transfected to over-express human TLR2

protein, while the HEK-null cell line is the not-transfected negative control cell line.[1] HEK-293-hTLR2 cells were stimulated with ligands able to engage the TLR2 receptor and responses determined by measuring the release of IL-8 in the cell supernatant by ELISA. The free UPam adjuvant was used as a positive control, and a reference dose-response curve using this compound was generated. After 20 hours of stimulation of HEK-293-hTLR2 cells all three synthetic conjugated peptides induced production of IL-8 in a concentration dependent manner, as shown in Figure 2. The p31-UPam conjugate induced response that closely paralleled the physiological response to free UPam adjuvant. The responses induced by the p57-UPam and p75-UPam conjugates were lower than that of UPam, but significantly higher than the background. The absence of any detectable amount of IL-8 in the cell supernatant of HEK-null cells stimulated with UPam or conjugates (data not shown) confirmed that the responses were strictly TLR2 dependent.

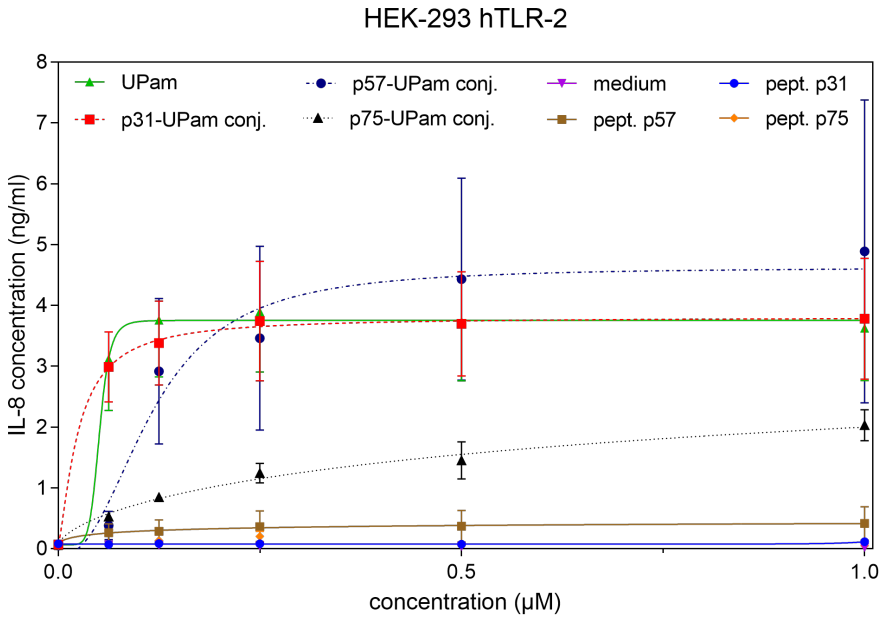

Figure 2 – Amount of IL-8 released by HEK-293 hTLR2 cells as a measure of TLR2 activation. HEK-293 cells expressing human TLR2 were stimulated with soluble UPam adjuvant, free peptides or UPam-conjugated peptides for 20h. HEK-293 null cells, not transfected with human TLR2, were used as negative control cell line and stimulated according to the same protocol as HEK-293 hTLR2 cells. NF-κB activation was determined by measuring secreted IL-8 in the cell supernatants by ELISA. Dots represent mean + SEM of duplicates from two independent experiments. Curves were interpolated using a non-linear regression model with 4 parameters as calculated using GraphPad Prism software.

[1] Both cell lines express TLR1, a receptor which can form heterodimers with TLR2.

To further evaluate the TLR2 ligand-peptide conjugates, monocytes were isolated from healthy human donors, differentiated into dendritic cells (GM-CSF/IL-4), macrophages type 1 (GM-CSF) or macrophages type 2 (M-CSF). As quality control, their archetypical cell surface marker phenotypes were characterized by CD1a, CD14, CD11b and CD163 expression.[26,27] These antigen-presenting cells were then stimulated for 24 hours using synthetic conjugates, free peptides or free UPam adjuvant. Lipopolysaccharide (LPS) was used as positive control. Cells were assayed for the expression of activation markers, T cell co-stimulatory molecules and MHC-II molecules using flowcytometry. Furthermore, cell supernatants were analyzed via ELISA to determine the level of IL-12p40 and IL-10 cytokines.

The three conjugates, the UPam adjuvant and the LPS control were able to activate both dendritic cells and macrophages. The median fluorescence intensity (MFI), as obtained from flow cytometry measurements, displayed in Figure 3 for one selected cell surface marker per cell type, exemplifies the extent of cellular activation (histograms for CD80, CD83, CD86 and MHC-II are shown in the supporting Figures S1, S2 and S3). Free UPam and all conjugates induced upregulation of CD86 on the cell surface of monocyte-derived dendritic cells (moDCs) and upregulation of CD80 on macrophages in a dose dependent manner, while corresponding free peptides neither promoted activation nor enhanced the expression of these markers.

Cell activation induced by UPam and synthetic conjugates was confirmed by analysis of cytokine levels in the supernatant of tested antigen-presenting cells (see Figure 4). In this analysis, it was observed that the p57-UPam and p75-UPam conjugate stimulated dendritic cells to release higher amounts of IL-12p40 (with mean values of 47 and 27 ng/ml respectively) and IL-10 (with mean values of approximately 1.1 ng/ml for both) at their highest experimental concentration (20 μM), when compared to the p31-UPam conjugate (mean values of 1.5 ng/ml IL-12p40 and 0.1 ng/ml IL-10). Cell viability was measured by flow cytometry, and no difference was observed between the p31-UPam conjugate and UPam. Nevertheless, a higher amount of cytokines was detected in the case of cell stimulation using the intermediate concentration of the p31-UPam conjugate as compared to the 20 μM concentration. As expected, the unconjugated peptides did not induce cytokine production.

Stimulation of macrophages type 1 with the UPam adjuvant or the conjugates resulted in production of only IL-12p40, as expected, with mean values ranging from 0.3 to 2.1 ng/ml, while stimulation of macrophages type 2 as expected resulted in production of only IL-10, with mean values ranging from 0.5 to 3.0 ng/ml. Stimulation with unconjugated peptides did not induce any detectable amount of tested cytokines.

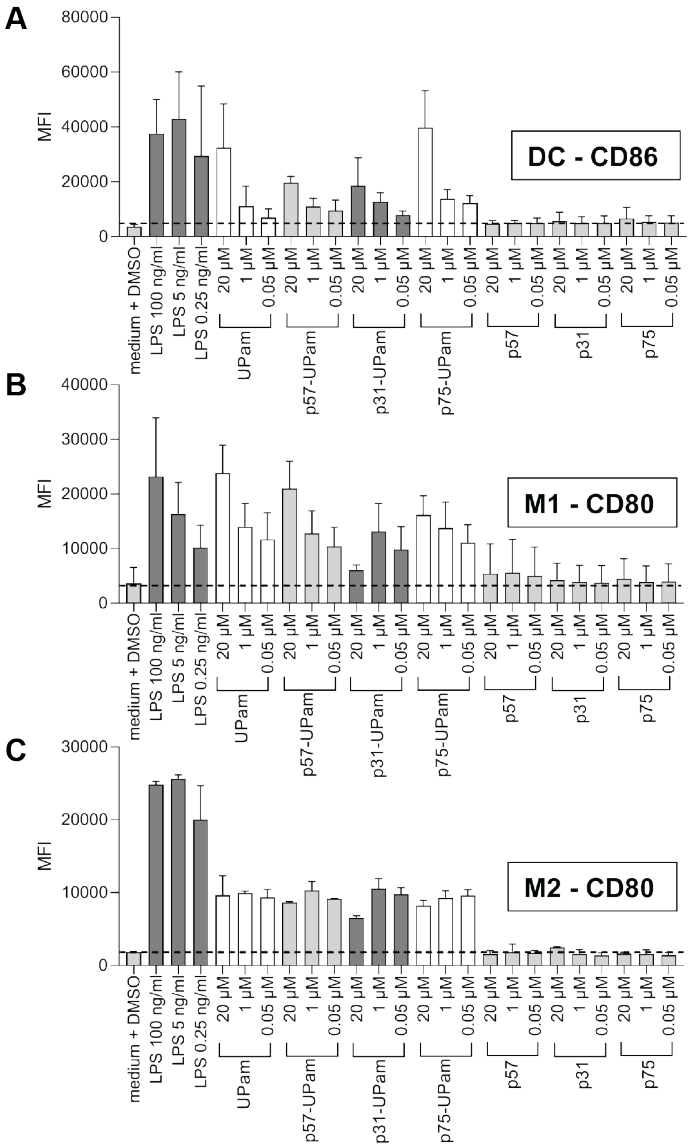

Figure 3 – Expression of selected activation markers by APCs stimulated with UPam conjugates and controls. Human monocyte-derived DCs, M1 and M2 cells were stimulated with soluble UPam adjuvant, free peptides or UPam-conjugated peptides for 24h. Expression levels of activation and T cell co-stimulatory markers were measured by flow cytometry. Bar plots represent the mean value + SD (n = 3 donors) of the median fluorescence intensity (MFI) of selected surface markers, as calculated using GraphPad Prism. LPS was used as a positive control. **(A)** MFI of the CD86 activation marker on human dendritic cells; **(B)** MFI of the CD80 co-stimulatory marker on human macrophages type 1; **(C)** MFI of the CD80 co-stimulatory marker on human macrophages type 2.

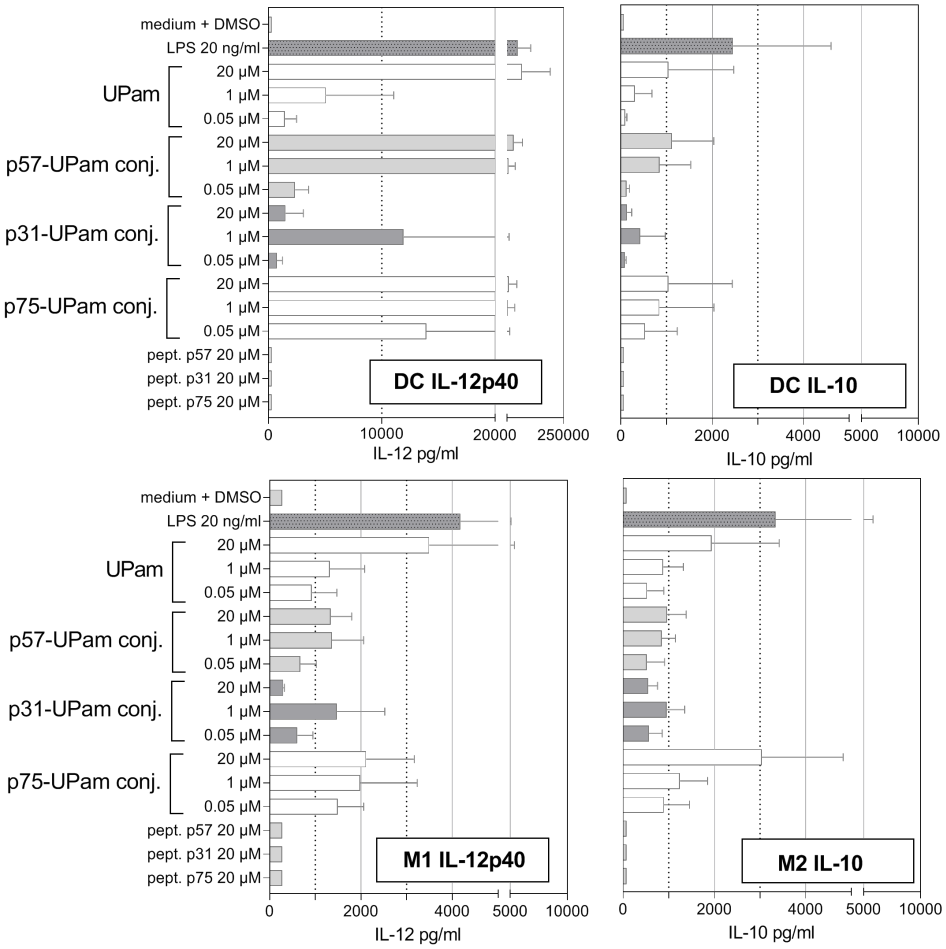

Figure 4 - Cytokine production profile of human monocyte-derived APCs stimulated for 24 hours with single adjuvant, free peptides or UPam-conjugated peptides thereof as measured by ELISA. LPS (20 ng/ml) was used as a positive control. Bar graph indicate the amount of IL-10 and IL-12p40 detected in the supernatant of macrophages and dendritic cells. No IL-10 was detected in the cell supernatant of macrophages type 1, and no IL-12p40 was detected in the cell supernatant of macrophages type 2 (data not shown). Error bars represent mean + SD of duplicates from three donors as calculated using GraphPad Prism.

To study unwarranted possible inhibitory effects of conjugation on antigen-presentation by human antigen presenting cells, on PBMC's or GM-CSF/IL-4 differentiated monocyte-derived dendritic cells, T cell assays were performed, measuring activation through proliferation by [^{3}H]-thymidine incorporation.

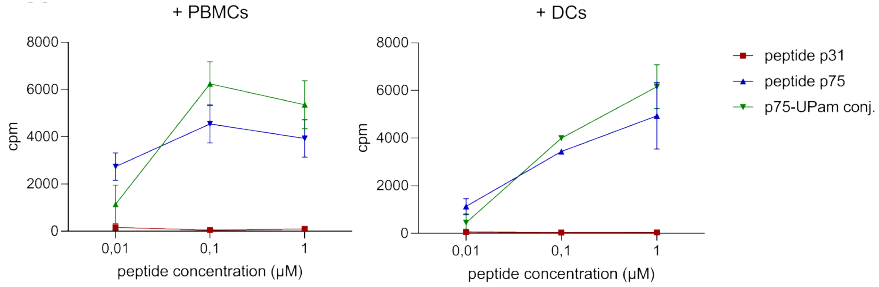

Figure 5 - Antigen-presentation to T cells. The experiment was performed by co-culturing T cells with HLA class II matched moDCs or PBMCs in the presence of the Rv2034 peptide p75 or p75-UPam conjugate. The T cell clone used in this study is specific for the Rv2034 p75 peptide, Rv2034 p31 peptide was used as a negative control. T cell proliferation was measured after 96 hour peptide stimulation using [^{3}H]thymidine incorporation and is expressed as counts per minute (cpm). Values represent mean + SD of triplicate measurements from a representative experiment, as calculated using GraphPad Prism.

The HLA-DR3 restricted CD4$^+$ T cell clone specific for the *Mtb* antigen Rv2034 (peptide 81-100), was cocultured with antigen-presenting cells in the presence of free p75 peptide or UPam-conjugated p75 peptide. Additionally, the p31 peptide originating from the same Rv2034 protein and its UPam conjugate were included in the assay as negative controls (Figure 5).

The p75-UPam conjugate induced a dose-dependent T cell proliferation when presented to the CD4$^+$ T cell clone by HLA-DR matched APCs, as shown in Figure 5. Stimulation with p75-UPam conjugate showed comparable T cell proliferation levels as from p75 peptide stimulation for both PBMCs and DCs as antigen-presenting cells.

In vivo evaluation using TLR2 ligand-peptide

An HLA-DR3 transgenic mouse model, genetically lacking expression of murine MHC class II (I-A) molecules (HLA-DR3/Ab^0) has been previously used for *in vivo* induction of HLA-DR3 restricted Rv1733c derived p57 peptide specific T cell responses using subcutaneous (s.c.) SLP vaccination.[22,28] Here, this model was used to evaluate the *in vivo* immunogenicity of the p57-UPam conjugate compared to an equimolar mixture of unconjugated p57 peptide and UPam adjuvant. Intracellular IFN-γ, TNF-α and IL-17 production by CD4$^+$ CD44$^+$ T cells was measured by flow-cytometry after *in vitro* stimulation of splenocytes with either the p57 peptide antigen or with the original recombinant *Mtb* Rv1733c protein. The expression of CD44 was used as a marker of T cell activation. After antigen encounter, T cells rapidly up-regulate CD44 and its expression is also maintained in memory T cells.[29]

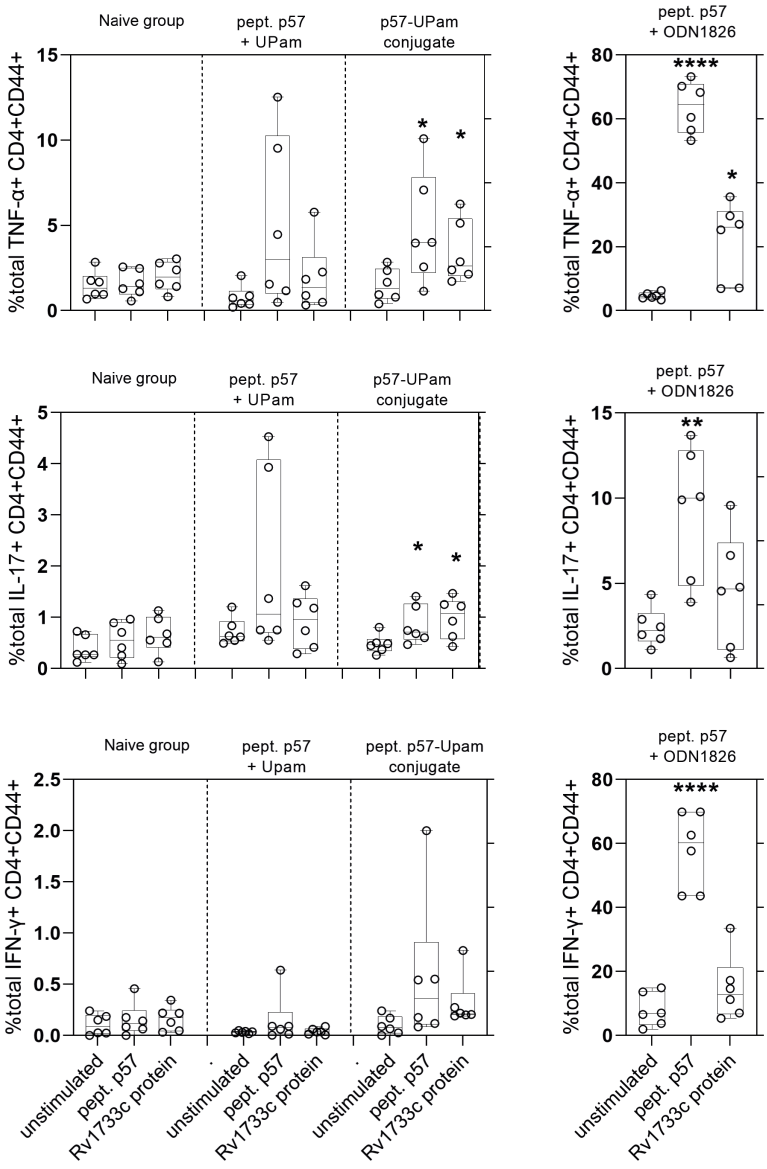

Figure 6 – Intracellular cytokine production by splenic T cells. Intracellular IL-17, TNF-α and IFN-γ production by $CD4^{+}CD44^{+}$ T cells was measured via flow-cytometry after in vitro stimulation of splenocytes with either peptide p57 (5 µg/ml) or Rv1733c recombinant protein (5 µg/ml). Mice (n=6) were injected three times with either PBS as negative control, peptide p57 (40 nmol) in admixture with ODN1826 (8 nmol) as positive control, peptide p57 (40 nmol) in admixture with UPam adjuvant (40 nmol) or peptide p57-UPam conjugate (40 nmol). Splenocytes were obtained two weeks after the last immunization. Statistical significance was calculated using a paired t-test as calculated with GraphPad Prism software (****$p < 0.0001$, **$p < 0.01$, *$p < 0.05$).

T cells from mice immunized with the p57-UPam conjugate were responsive to both the reference peptide p57 and to the Rv1733c recombinant protein *ex vivo*, as indicated by the significant increase in percentage of IL-17$^+$CD4$^+$CD44$^+$ and TNF-α^+CD4$^+$CD44$^+$ T cells (see Figure 6). Although a similar trend could be observed for the group of mice immunized with a mixture of peptide p57 with UPam, the results were not statistically significant. The group immunized with a mixture of peptide p57 with ODN1826 was used as positive control for the experiment, as it has been previously shown this to induce strong Th1 responses. This was here confirmed by the detection of significant numbers of IFN-γ^+CD4$^+$CD44$^+$ T cells by intracellular cytokine staining analysis for spleen of mice immunized with positive control. However, neither of the two UPam treatments induced expansion of IFN-γ positive T cells upon *ex vivo* antigen re-encounter, as shown in Figure 6.

Antigen specific total Ig antibodies were detected in the sera of mice immunized with either p57/adjuvant mixture or p57-UPam conjugate. The results revealed significantly higher antibody titers following vaccination with the conjugate (see Figure 7) compared to the unconjugated mixture, suggesting superior immunogenicity of the conjugated p57.

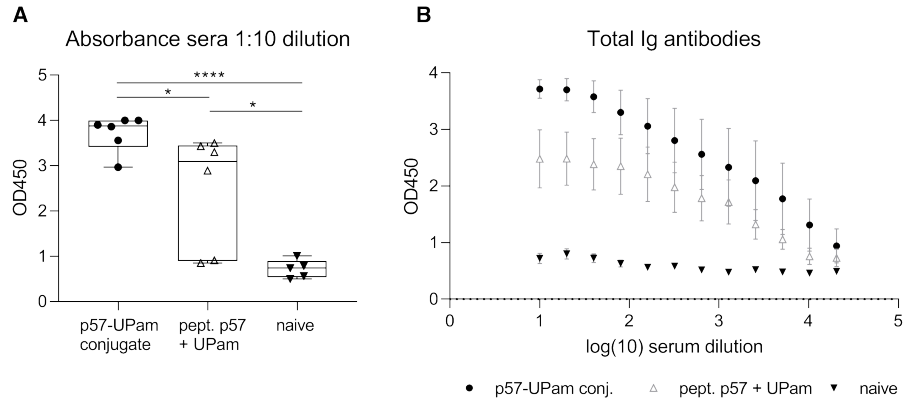

Figure 7 – Antibody production in the sera of immunized mice. Measurement of antigen-specific total Ig antibodies from sera of mice (n=6) immunized with peptide p57-UPam conjugate (40 nmol), peptide p57 (40 nmol) in admixture with UPam adjuvant (40 nmol) or treated with PBS only (naïve group). Plate-bound peptide p57 antigen was used for the Ig antibodies assay. **(A)** Box plots representing absorbance (OD450) corresponding to amount of antigen-specific total Ig antibodies and measured for sera diluted 10 times (n = 5 for naïve, n = 6 for the other groups). Statistical significance was calculated using unpaired t-test as calculated with GraphPad Prism software (****$p < 0.0001$, *$p < 0.05$). **(B)** Dose-response dot plots representing mean + SEM of absorbance measurements of the antigen-specific total Ig antibodies from 5 or 6 mice as calculated using GraphPad Prism.

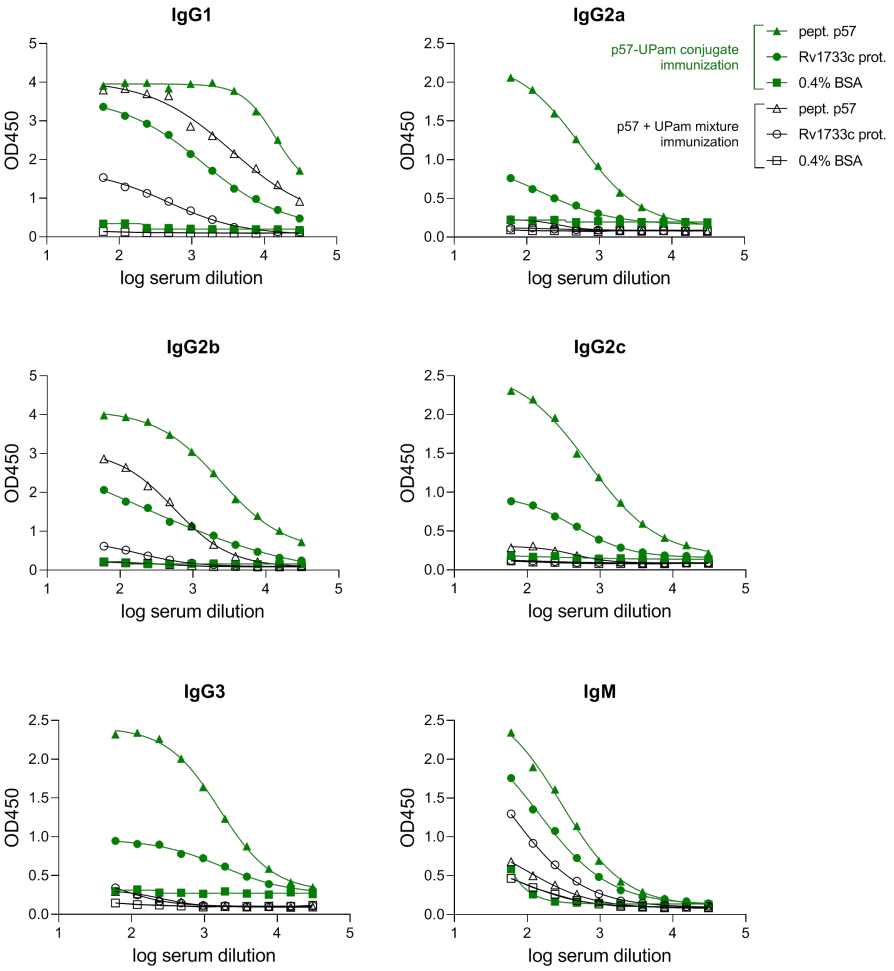

Figure 8 – Antibody subtypes in murine sera. Measurement of antigen-specific antibody isotypes from serum of mice (n=6) immunized with peptide p57-UPam conjugate or peptide p57 plus UPam mixture. Antigen-specific antibodies were measured using plate-bound peptide p57 or recombinant protein (Rv1733c). Mean data from sera of all mice (n=6 for peptide p57-UPam conjugate immunization; n=4 for peptide p57 plus UPam mixture) are shown. Curves were interpolated using a non-linear regression model with 4 parameters as calculated using GraphPad Prism. Data from the sera of each mouse are shown in the supplementary information.

Subsequent comparison of antibody titers between the two groups indicated a highly diversifying response between vaccination with the p57-UPam conjugate and unconjugated p57 with UPam. As shown in Figure 8, p57-UPam conjugate immunization induced antigen-specific IgG1, IgG2a, IgG2b, IgG2c, IgG3 and IgM recognizing not only the synthetic peptide, but also the Rv1733c recombinant

protein. This diversified antibody response was detected for all immunized mice. For comparative purposes, antibody subtypes in mice immunized using the mixture of peptide with adjuvant are also depicted in Figure 8. In this case, only four out of six mice vaccinated with the mixture of peptide with UPam developed antigen-specific Ig antibodies and the response was less diverse, with IgG1, IgG2b and IgM as main subtypes present in sera of mixture immunized mice. Thus, conjugation of p57 to UPam strikingly enhances its immunogenicity and also impacts the quality of the antibody subclass responses.

The vaccine potential of the p57-UPam conjugate was further evaluated in a prophylactic vaccination / *Mtb* challenge model using the same HLA-DR3 transgenic mouse model. Following a vaccination with BCG as positive control, or three times p57 with 2 weeks intervals, as described in the materials and methods section, mice were intranasally infected with 10^5 *Mtb* H37Rv. Six weeks later the spleen and lungs of infected mice were analyzed to determine the bacterial load by enumeration of the colony forming unit (CFU). Immunization with peptide p57 or UPam alone did not significantly reduce the CFU load in the spleen nor in the lungs (see Figure 9). As additional positive control next to BCG, vaccination with peptide p57 and ODN1826 was studied.

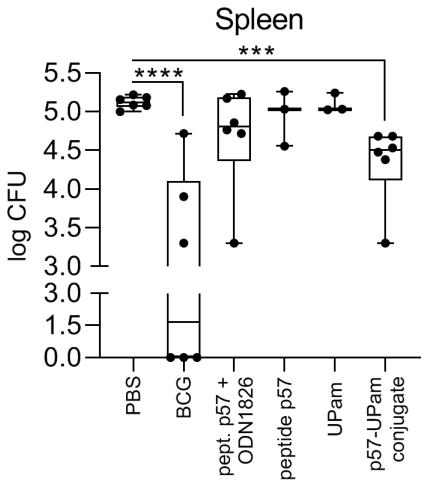

Figure 9 – Bacterial load in the spleen of immunized mice. Protective efficacy against *Mtb* in the spleen of mice that were immunized s.c. for 3 times with 2 weeks interval. Mice (n=6) were immunized with a mixture of peptide p57 (40 nmol) with ODN1826 (50 µg/ml) as adjuvant control, peptide p57-UPam conjugate (40 nmol) or mice (n=3) were treated with UPam adjuvant (40 nmol) or peptide p57 (40 nmol). Six weeks later, the mice were challenged intranasally with *Mtb* H37Rv (10^5 CFU). Alternatively, the mice received 10^6 CFU BCG s.c. 12 weeks before challenge. Colonies in lungs (data not shown) and spleen were counted after 3 weeks of incubation at 37°C. Statistical significance with reference to the naive group was determined by ANOVA with Tukey's multiple comparisons test (****$p < 0.0001$, ***$p < 0.001$). Box plots were generated using GraphPad Prism.

While BCG vaccination induced a significant reduction of the CFU in both the spleen and the lungs, immunization with peptide and ODN1826 did not, despite its impressive induction of T cell immunity (Figures 6A, 6B). In contrast, immunization with the p57-UPam conjugate resulted in a significant decrease in the number of CFU in the spleen of vaccinated mice, indicative of a systemic immune response to this construct that was conjugation dependent (since neither free p57 peptide nor free adjuvant were effective), and involving both T cells as well as strong antibody induction.

Discussion

Mycobacterium tuberculosis remains one of the deadliest pathogens worldwide. The only currently available vaccine, BCG, presents several limitations including its failure to induce robust and consistent protection.[30,31] Additionally, the burden of TB is especially afflicting populations in countries with fragile or developing economies The discovery of efficient synthetic vaccines against TB would hold promise of inexpensive and accessible vaccine for everyone. Despite their ease of manufacturing, versatility and improved safety profile as compared to inactivated or attenuated live vaccines, it was not until 2020 that two synthetic vaccines received their first historic emergency use authorization, with the liposomal mRNA vaccines against SARS-CoV-2 by BioNtech/Pfizer and Moderna.[3,4,32–34] One of the reasons for the delayed commercialization of fully synthetic vaccines is that their development has started later than that of attenuated/inactivated vaccines; another being the modest, yet growing, body of data available on the immune mechanisms of action involved in protection.[35–38] In general terms, rational design of fully synthetic vaccines requires the selection of relevant targets, the definition of a strategy to preserve/enhance immunogenicity of the synthetic molecule which acts on the selected target, and the verification of its mode of action. The present study provides evidence for the potential of rationally designed synthetic vaccines to induce protective immunity within the context of *Mtb* infection.

The conjugates here presented are designed to target human antigen-presenting cells in a TLR2-dependent manner. Previous studies have shown the beneficial effect of using TLR2 agonists to the induction of strong cellular immune responses, correlated to the reduction of tumor growth *in vivo* or protection against *Mtb*.[16,39] In this context, the immune-stimulatory potential of conjugates containing the TLR2/TLR1 ligand UPam covalently linked to one of the three following peptides was assessed: the p57 peptide (Rv1733c a.a. 57-84) for *in vivo* mouse studies, p31 peptide (Rv2034 a.a. 31-60) and the p75 peptide (Rv2034 a.a. 75-105) for *in vitro* human studies. This strategy allowed for co-delivery of antigen and adjuvant, which has been shown to improve immunogenicity as compared to delivering the two

separately, with the possibility to modify the chemical structure by linking additional moieties to increase immunogenicity or modulate solubility.[40] Additionally, synthetic conjugate vaccines can be generated with high purity and homogeneity. However, this strategy presents the risk of loss of immune-stimulatory potential of the adjuvant after conjugation to the peptide, or the impairment of antigen-presentation.

Despite the big differences in physicochemical properties of the three peptides selected in this study[2], it is shown that all generated conjugates retain the ability to interact with the TLR2 receptor. Using a HEK-293 cell line over-expressing human TLR2, the extent of binding of the novel conjugates to the receptor was assessed. Differences in potency and efficacy of binding were observed, possibly reflecting the different physicochemical properties of the three conjugates.

Typically, synthetic long peptides require processing through antigen-presenting cells for presentation to cognate T cell. To verify that conjugation did not affect APC processing, a human Rv2034-specific $CD4^+$ T cell clone that recognizes the epitope within the p75-UPam conjugate was employed for T cell proliferation and activation studies.

Comparable T cell proliferation levels were observed upon stimulation of monocytes, or alternatively dendritic cells, loaded with the p57-UPam conjugate or with the corresponding free SLP peptide. This observation was supported by flow cytometry analysis of the demonstrating increased expression levels of CD154 and IFN-γ by $CD4^+$ T cells. These studies indicated that the efficacy of antigen-presentation was not impaired by conjugation of the p75 peptide to UPam. A similar finding was reported by Zom *et al.* in 2016, where the HPV16-specific $CD4^+$ T cell clones were activated by peptide and UPam-conjugate to a comparable extent.[15]

The immune-stimulatory potential of the three conjugates was assessed *in vitro* by stimulating human monocyte-derived dendritic cells and macrophages (type 1 and type 2), and analyzing activation and T cell costimulatory markers together with production of the IL-12 and IL-10 cytokines.

Previous reports have indicated the presence of both IL-12 and IL-10 in the supernatant from moDCs stimulated with various TLR2 ligands.[15] While the role of IL-12 has been unequivocally defined as pivotal in the induction of pro-inflammatory responses and specific cellular immunity, that of IL-10 mostly confers anti-inflammatory and regulatory activity.[41–43]

As expected, stimulation of moDCs resulted in production of IL-12p40 and IL-10 cytokines. A relatively higher production of IL-12p40 was detected upon stimulation with two of the three conjugates (p57-UPam and p75-UPam) as compared to the other (p31-UPam conjugate), with the highest cytokine levels induced by the

[2] See their diverse predicted net charge, solubility and by the measurement of their hydrodynamic diameter (Table 1).

p57-UPam conjugate. A similar observation was indeed reported for conjugates containing the same adjuvant but different peptides.[15] This was not the case for the level of IL-10, which was produced in similar amounts across conjugate groups. It is additionally reported that IL-12 and IL-10 were released upon stimulation of macrophages type 1 and type 2, respectively, providing further evidence for the ability of these constructs to induce activation of these important cell types.

Interestingly, the p31-UPam conjugate induced an unconventional dose-response effect as compared to the UPam and to the other conjugates. It is highly unlikely that cell death caused the observed difference in response, as cell viability for moDCs treated with this conjugate was not different than with UPam alone. These results could be related, instead, to the different physicochemical properties of the peptides that are included in such constructs.

Additionally, this chapter reports evidence that free UPam and conjugates induced upregulation of CD86 on the cell surface of moDCs and upregulation of CD80 on macrophages in a dose dependent manner, while corresponding free peptides neither promoted activation nor enhanced the expression of these markers.

The *in vivo* immunogenicity of the p57-UPam conjugate was determined using an HLA-DR3/Ab^0 transgenic mouse model. Subcutaneous immunization with the conjugate was compared to immunization with an equimolar mixture of peptide and UPam. Additionally, a mixture of peptide with the TLR9 ligand ODN1826 was used as positive control, with previous work showing that this combination induced a Th1-polarized cellular response *in vivo*.[21,22]

Mice were immunized three times on a two weeks interval schedule, and, two weeks after the last immunization, draining lymph nodes and splenocytes were examined for CD4$^+$ T cell responses both *ex vivo* and after antigen restimulation. Evidence of the beneficial effect of CD4$^+$ T cell responses in containment of *Mtb* have been extensively provided in the last years, with a strong focus on Th1/Th17 polarized cellular responses.[44,45] More recently a renewed interest in the interplay between cellular, humoral and innate immune responses has been leading the scientific discussion in the field of vaccine development.[46–48] Therefore, in addition to the determination of T cell responses, the murine sera from the immunization studies were analyzed for the presence of antigen-specific antibodies.

As expected for the positive control, polyfunctional CD4$^+$ IFN-γ^+ TNF-α^+ T cell responses were detected in mice vaccinated with the reference peptide plus ODN1826 mixture. TNF-α^+ and IL-17$^+$ CD4$^+$ T cell responses were also identified in mice immunized with either p57-UPam conjugate or mixture of p57 peptide plus UPam, indicating the development of a Th17 polarized cellular immune response. The significance of Th17 immunity for protection against *Mtb* is somewhat debated, with studies supporting its beneficial effect during early phases of mycobacterial

infection, and others indicating that it might lead to increased immunopathology and tissue destruction.[49–51]

Nevertheless, in addition to the $CD4^+$ T cell responses, the UPam conjugate induced very strong antibody responses, with multiple antigen-specific IgG subtypes found in sera of vaccinated mice. As opposed to mice vaccinated with the mixture of peptide plus UPam, where only IgG1 and IgG2b antibodies were found, mice vaccinated with the conjugate developed high titer IgG1, IgG2a, IgG2b, IgG2c and IgG3 antigen-specific antibodies. Importantly, high antibody titers against the cell lysate from heat-killed *Mtb* were detected in the case of IgG1 and IgG2b subtypes found in the sera of mice vaccinated with the conjugate. Traditionally, murine IgG1 are associated with a Th2 polarized immune response, while IgG2b antibodies are thought to be derived from T cell independent responses.[52–54] In 2016 Collins suggested a model of murine IgG function, called the quartet model, to integrate the beneficial effect of co-expression of different IgG subclasses. As formulated in Collins' paper, IgG3 and IgG2b antibody subclasses would play an important role in the early immune response, when cellular immune responses are slowly building up. In the specific, Collins underlined that IgG3 antibodies are associated with complement fixation, and IgG2b antibodies with early FcγR-mediated effector functions. On the other hand, IgG2a and IgG1 antibodies, which are defined as two murine T cell-mediated subclasses, would come into play in late immune responses. In fact, IgG2a has been shown to be involved both in complement fixation and late FcγR-mediated effector functions. Although the role of IgG1 in immune protection is currently debated, due to its inability to fix complement and its binding to the inhibitory FcγRIIb receptor, Collins suggested that it could well be involved in limiting inflammation and immunopathology. [55]

Perhaps the most important evidence supporting vaccine efficacy of the UPam conjugate was obtained in the murine *in vivo Mtb* challenge model, in which immunized mice were exposed to a high dose (10^5 CFU) of *Mtb* intranasally. The significant reduction in bacterial load in the spleen of conjugate-immunized mice was indicative of a systemic immune response, with significantly better results obtained for this treatment as compared to both the unconjugated peptide/UPam mixture, as well as the unconjugated peptide mixed with ODN1826. In 2019, Ashhurst *et al.* published a study showing that intranasal immunization using a Pam_2Cys-peptide conjugate was superior to subcutaneous immunization, by inducing stronger Th17 cellular responses and providing better protection against mycobacterial infection.[56] As opposed to the experiments reported in this chapter, which employ a TLR2/TLR1 ligand, their experiments were performed using a TLR2/TLR6 adjuvant, lower dose (10^2 CFU) nasal *Mtb* infection and a different oligopeptide. Nevertheless, their promising results, where protection against *Mtb* is evident also in the lung of vaccinated mice, further supports the potential of synthetic conjugates containing toll-like receptor ligands for the development of novel

vaccines against TB. Their research, published after the execution of the experiments reported in this chapter, combined with the reported observations, provides useful insights for possible next steps such as to assess the vaccine potential of the p57-UPam conjugate as intranasal vaccine and the development of second-generation synthetic conjugates including additional (synergistic) adjuvants and/or epitopes that can be presented by multiple HLA class II cell molecules.

Conclusion

In search for an effective conjugate vaccine against tuberculosis, a panel of three synthetic conjugates containing a TLR2 ligand covalently attached to one of three antigenic peptides was designed (p57 from the *Mtb* Rv1733c protein, p31 and p75 from the Rv2034 protein). In the present study, it is reported that these conjugates induced activation and maturation of human monocyte-derived dendritic cells *in vitro*, with production of IL-12p40 and IL-10 cytokines. Moreover, they were able to activate human monocyte-derived macrophages type 1 and type 2 yielding similar activation profiles to those of the adjuvant alone, an indication that the adjuvanticity of the TLR2 ligand was preserved even when the adjuvant was covalently linked to the peptide. Importantly, peptide antigen processing by monocytes and dendritic cells, and presentation to T lymphocytes were not impaired by conjugation, as determined by *in vitro* T cell antigen presentation experiments with a *Mtb* Rv2034-specific human $CD4^+$ T cell clone. To further assess the vaccine potential of the new conjugates, *in vivo* subcutaneous immunization experiments were performed in mice using one of the three constructs as a proof of concept. Comparison of cellular and humoral immunity elicited in response to this conjugate and in response to the mixture of peptide with adjuvant indicated the superior efficacy of the synthetic conjugate strategy when compared to the mixture. Vaccination with the conjugate resulted in a strong Th17 cellular response and multifunctional T lymphocytes in the spleen, in addition to the presence of several diverse subtypes of peptide-specific IgG antibodies in sera. Finally, immunization with this construct induced a significant reduction of the bacterial load in the spleen of intranasally *Mtb* challenged mice, not seen in response to the unconjugated components. These data suggest a promising role for TLR2 ligand-peptide synthetic conjugates as a novel TB vaccine approach.

Materials and methods

Synthetic methods

Materials and methods for the synthesis of peptides and conjugates

Description of materials, analytical tools and general synthetic methods are provided in the "Materials for the synthesis of peptides and conjugates" and "General methods for the synthesis of peptides" sections of Chapter 3.

p57 peptide: Ile-Pro-Phe-Ala-Ala-Ala-Ala-Gly-Thr-Ala-Val-Gln-Asp-Ser-Arg-Ser-His-Val-Tyr-Ala-His-Gln-Ala-Gln-Thr-Arg- His-Pro-NH_2

The p57 peptide was synthesized according to the general procedure for peptide synthesis described above. Pseudoproline dipeptides Fmoc-Asp(OtBu)-Ser(ψMe,Mepro)-OH and Fmoc-Gly-Thr(ψMe,Mepro)-OH were employed to enhance synthetic efficiency. Purification by RP-HPLC (linear gradient 20→30% B in 10 min) followed by lyophilization yielded the p57 peptide as a white powder (90.4 mg, 30.26 μmol, 12.1% yield based on theoretical resin loading of 0.23 mmol/g). LC-MS analysis (C18 column, linear gradient 10→90% B, 11 min): Rt = 3.571 min, ESI-MS $[M+H]^{2+}$ = 1494.3 found, 1493.8 calculated. MALDI-TOF $[M+H]^{+}$: 2986.4517 found, 2986.5143 calculated.

p31 peptide: Leu-Ala-Val-Gly-Glu-Leu-Ala-Arg-Asp-Leu-Pro-Val-Ser-Arg-Pro-Ala-Val-Ser-Gln-His-Leu-Lys-Val-Leu-Lys-Thr-Ala-Arg-Leu-Val

The p31 peptide was synthesized according to the general procedure for peptide synthesis described above. TentaGel™ S PHB-Val-Fmoc resin was used in place of TentaGel® S RAM. Purification by RP-HPLC (linear gradient 20→35% B in 10 min) followed by lyophilization yielded the p31 peptide as a white powder (3.9 mg, 1.20 μmol, 12.0% yield based on theoretical resin loading of 0.19 mmol/g). LC-MS analysis (C18 column, linear gradient 10 → 50% B, 11 min): Rt = 5.895 min, ESI-MS $[M+H]^{2+}$ = 1619.5 found, 1618.5 calculated. MALDI-TOF $[M+H]^{+}$: 3237.425 found, 3236.932 calculated.

p75 peptide: Thr-Gly-Leu-Ala-Ala-Leu-Arg-Thr-Asp-Leu-Asp-Arg-Phe-Trp-Thr-Arg-Ala-Leu-Thr-Gly-Tyr-Ala-Gln-Leu-Ile-Asp-Ser-Glu-Gly-Asp-NH_2

The p75 peptide was synthesized according to the general procedure for peptide synthesis described above. Pseudoproline dipeptides Fmoc-Asp(OtBu)-Ser(ψMe,Mepro)-OH and Fmoc-Leu-Thr(ψMe,Mepro)-OH were employed to enhance synthetic efficiency. Purification by RP-HPLC (linear gradient 30→45% B in 10 min) followed by lyophilization yielded the p75 peptide as a white powder (11.7 mg, 3.53 μmol, 14.1% yield based on theoretical resin loading of 0.23 mmol/g). LC-MS analysis (C18 column, linear gradient 10→90% B, 11 min): Rt = 5.508 min, ESI-MS $[M+H]^{2+}$ = 1663.4 found, 1662.9 calculated. MALDI-TOF $[M+H]^{+}$: 3325.092 found, 3324.693 calculated.

UPam (Amplivant) synthesis

Compound UPam was synthesized according to published protocol and analytical data were in agreement with those published in the literature.[17]

General methods for UPam-conjugates synthesis

Peptide sequence was synthesized according to the general procedure for peptide synthesis described in Chapter 3. After completion of all the synthetic cycles, the peptide was not cleaved from the resin. Instead, the resin was treated with a 0.1 M stock solution of Fmoc-Cys((RS)-2,3-di(palimitoyloxy)-propyl)-OH (2eq) and in the presence of oxyma pure (1 M, 1 eq) and DIC (0.5 M, 1 eq), with the reaction being performed overnight at RT. After NMP and DCM washes, the resin was swelled in a mixture of DCM/NMP 2:1 and treated with 20% piperidine in NMP (3 times, 5 minutes) to remove Fmoc protecting groups. After NMP wash the resin was suspended in DCM/NMP 1:1 (1 ml per 10 µmol resin) and treated with tetradecyl isocyanate (25 µl per 25 µmol resin). The mixture was reacted for 6 hours at RT, washed with NMP and DCM and air dried. The resin was then treated for 1 hour and 30 minutes with a TFA/TIS/H_2O (38:1:1, v/v/v) cleavage cocktail (5 ml/100 µmol scale reaction). The reaction mixture containing the cleaved peptide was filtered into cold Et_2O/pentane (1/1, v/v) (50 mL/1 ml cleavage cocktail) and the resin was washed with 1 mL TFA (2 times) into the cold Et_2O/pentane solution. The solution was stored in a -20°C freezer for 2 hours, then centrifuged (10 minutes, 4400 rpm, 3 x g); finally, the supernatant was discarded and the precipitate was purified via RP-HPLC.

p57-UPam conjugate: UPam-Ser-Lys-Lys-Lys-Lys-Ile-Pro-Phe-Ala-Ala-Ala-Ala-Gly-Thr-Ala-Val-Gln-Asp-Ser-Arg-Ser-His-Val-Tyr-Ala-His-Gln-Ala-Gln-Thr-Arg-His-Pro-NH_2

Purification by RP-HPLC (C4 column, linear gradient 50→90% B in 10 min) followed by lyophilization yielded p57-UPam conjugate as a white powder (15.1 mg, 3.35 µmol, 3.3% yield based on theoretical resin loading of 0.23 mmol/g). LC-MS analysis (C4 column, linear gradient 25→75% B, 21 min): Rt = 8.737 min, ESI-MS $[M+H]^{3+}$ = 1494.2 found, 1493.9 calculated. MALDI-TOF $[M+H]^{+}$: 4478.5690 found, 4478.6563 calculated.

p31-UPam conjugate: UPam-Ser-Lys-Lys-Lys-Lys-Leu-Ala-Val-Gly-Glu-Leu-Ala-Arg-Asp-Leu-Pro-Val-Ser-Arg-Pro-Ala-Val-Ser-Gln-His-Leu-Lys-Val-Leu-Lys-Thr-Ala-Arg-Leu-Val

TentaGel™ S PHB-Val-Fmoc resin was used in place of TentaGel® S RAM. Purification by RP-HPLC (C4 column, linear gradient 50→90% B in 10 min) followed by lyophilization yielded p31-UPam conjugate as a white powder (34.5 mg,7.27 µmol, 7.3% yield based on theoretical resin loading of 0.19 mmol/g). LC-MS analysis (C4 column, linear gradient 50→90% B, 15 min): Rt = 8.910 min, ESI-MS $[M+H]^{3+}$ = 1577.9 found, 1577.0 calculated. MALDI-TOF $[M+H]^{+}$: 4729.1481 found, 4729.0744calculated.

p75-UPam conjugate: UPam-Ser-Lys-Lys-Lys-Lys-Thr-Gly-Leu-Ala-Ala-Leu-Arg-Thr-Asp-Leu-Asp-Arg-Phe-Trp-Thr-Arg-Ala-Leu-Thr-Gly-Tyr-Ala-Gln-Leu-Ile-Asp-Ser-Glu-Gly-Asp-NH_2

Purification by RP-HPLC (C4 column, linear gradient 50→90% B in 10 min) followed by lyophilization yielded SLP3-UPam as a white powder (7.0 mg, 1.4 µmol, 2.8% yield based on theoretical resin loading of 0.23 mmol/g). LC-MS analysis (C4 column, linear gradient 10→90% B, 21 min): Rt = 12.688 min, ESI-MS $[M+H]^{3+}$ = 1607.0 found, 1606.3 calculated. MALDI-TOF $[M+H]^{+}$: 4816.6670 found, 4816.8392 calculated.

Immunological methods

Culturing of HEK-293 cell line

The HEK-293-h-TLR2 and HEK-293-null cell lines were purchased from InvivoGen (San Diego, United States) and cultured according to manufacturer's instructions. DMEM (Gibco, PAA, Linz, Austria) culture medium contained: 4.5 g/l glucose, 10% (v/v) fetal calf serum (FCS) (HyClone, GE Healthcare Life Sciences, Eindhoven, the Netherlands), 50 U/ml penicillin, 50 mg/ml streptomycin, 100 mg/ml Normocin and 2 mM L-glutamine (Life Technologies-Invitrogen, Bleiswijk, the Netherlands).

Stimulation of HEK-293 cells

Approximately 20.000 cells/well were transferred to 96 well plates (flat bottom, Corning Costar TC-Treated Microplates, Corning, NY, USA). All compounds used for stimulation were pre-dissolved in DMSO (Sigma, St.Louis, MO, USA) at a concentration of 5 nmol/μL and subsequently diluted in culture medium. Reference peptides were used as negative controls. After overnight stimulation with UPam and UPam conjugates, supernatants were harvested for IL-8 cytokine detection.

Generation and stimulation of immature human moDCs and macrophages

Human moDCs and GM-CSF/M-CSF macrophages were generated as described in "Generation and stimulation of immature human moDCs and macrophages" section in Chapter 3. Cells were stimulated using synthetic compounds (at concentrations ranging from 20-1-0.05 μM). The synthetic compounds were dissolved in DMSO at a concentration of 5 nmol/μL, further diluted and premixed in RPMI 1640 medium containing 10% FCS, 2 mM GlutaMAX™, 1% Pen-Strep. LPS (100 ng/ml) was used as positive control for stimulated cells. Supernatants were harvested 20 hours after the addition of stimuli for subsequent analysis of cytokines and cells were stained as described in Flow cytometric analysis of human moDCs and macrophages section in Chapter 3.

Human IL-8, IL-12(p40) and IL-10 ELISA

Human IL-8 Elisa kit was purchased from R&D Systems (Abingdon, UK). Human IL-12/IL-23 (p40) and human IL-10 ELISA kits were purchased from Biolegend (ELISA MAX™ Standard Set; London, UK). All supernatants were tested in duplicates according to manufacturer's instructions. Sample absorbance was measured using a Spectramax i3x (Molecular Devices, CA, USA) spectrometer.

T cell proliferation

T cell proliferation was assessed by coculturing 2500 HLA-DR3 matched monocyte derived dendritic cells or $5x10^4$ irradiated (2000 rad), HLA-DR3 matched PBMC's with 10^4 T cells from an established T cell clone specific for peptide 75-105 of Rv2034 from *M.tuberculosis*, in a 96 well round bottom plate in the absence or presence of serial dilutions of UPam conjugated peptides. Cells were cultured in IMDM supplemented with Glutamax, 100 U/ml penicillin, 100 μg/ml streptomycin (Gibco, Thermo Fisher Scientific, Bleiswijk, the Netherlands) and 10% pooled human serum (Sigma, Merck, Darmstadt, Germany) for a total of 96 hours in a humidified incubator at 37°C and 5% CO_2. After 72 hours [^{3}H]-Thymidine (Perkin Elmer,

Groningen, the Netherlands) was added at 0.5µCi/well. Following an additional 18 hours of incubation cells were harvested with a TomTec cell harvester and measured on a MicroBetaPlate Scintillation counter 1450 (Wallac, Turku, Finland). Data is represented as mean counts per minute from triplicate wells.

Flowcytometric antigen specificity analysis

HLA-DR3$^+$ monocyte derived dendritic cells were cocultured with the different peptides and peptide conjugates and 1x10^5 T cells from the Rv2034 specific T cell clone (recognizing peptide 75-105) in a 5 ml Falcon tube in a total volume of 400 µl IMDM supplemented with Glutamax, 100 U/ml penicillin, 100 µg/ml streptomycin (Gibco, Thermo Fisher Scientific, Bleiswijk, the Netherlands) and 10% pooled human serum (Sigma, Merck, Darmstadt, Germany). After 6 hours Brefeldin-A was added (3 µg/ml) (Sigma, Merck, Darmstadt, Germany) and cells were incubated for an additional 16 hours. Subsequently cells were harvested and stained for flowcytometric analysis with the violet live/dead stain (ViViD, Invitrogen, Thermo Fisher Scientific, Bleiswijk, the Netherlands), surface markers CD3-HorizonV500 (clone UCHT; BD Biosciences, San Diego, CA, USA), CD4-AlexaFluor 700 (clone RPAT4; BD Biosciences), CD8-FITC (clone HIT8a; Biolegend) and after fixation and permeabilization with fix/perm reagents (Nordic MUbio, Susteren, the Netherlands) for IFN-ϒ-PerCP-Cy5.5 (clone B27; BD Biosciences) and CD154-PE (clone TRAP1; BD Biosciences). Cells were acquired on a LSRFortessa with FACSDiva vxx and analyzed with Flowjo v9.7.6 (Treestar Inc, Ashland, OR, USA)

Mice

HLA-DRB1*0301/DRA transgenic, murine class II-deficient (HLA-DR3/Ab^0) mice were bred and PBMCs of each mouse were typed for expression and segregation of the transgene as described in Mice section in Chapter 3.

Immunizations

Mice (3 to 6 animals per group; 6 weeks old) were injected subcutaneously in the right flank with conjugate, or mixtures of p57-peptide and UPam adjuvant, in 200 µl phosphate-buffered saline (PBS) at 2 weeks interval. Two weeks after the last immunization, splenocytes were harvested.

In vitro culture, stimulation and intracellular cytokine staining of splenocytes

Splenocytes were isolated and incubated with medium, peptide, or relevant recombinant *Mtb* protein as described in the "In vitro cultures of splenocytes" section in Chapter 3. Intracellular cytokine staining was performed as described in the Intracellular cytokine staining section in Chapter 3.

Antibody detection

Antibodies against the Rv1733c p57 peptide, Rv1733c protein and *Mtb* sonicate in serum from immunized mice were determined by ELISA as described in "Antibody detection" section in Chapter 3.

BCG immunization and intranasal infection of mice with live Mtb

See section "BCG immunization and intranasal infection of mice with live Mtb" in Chapter 3.

Supporting figures

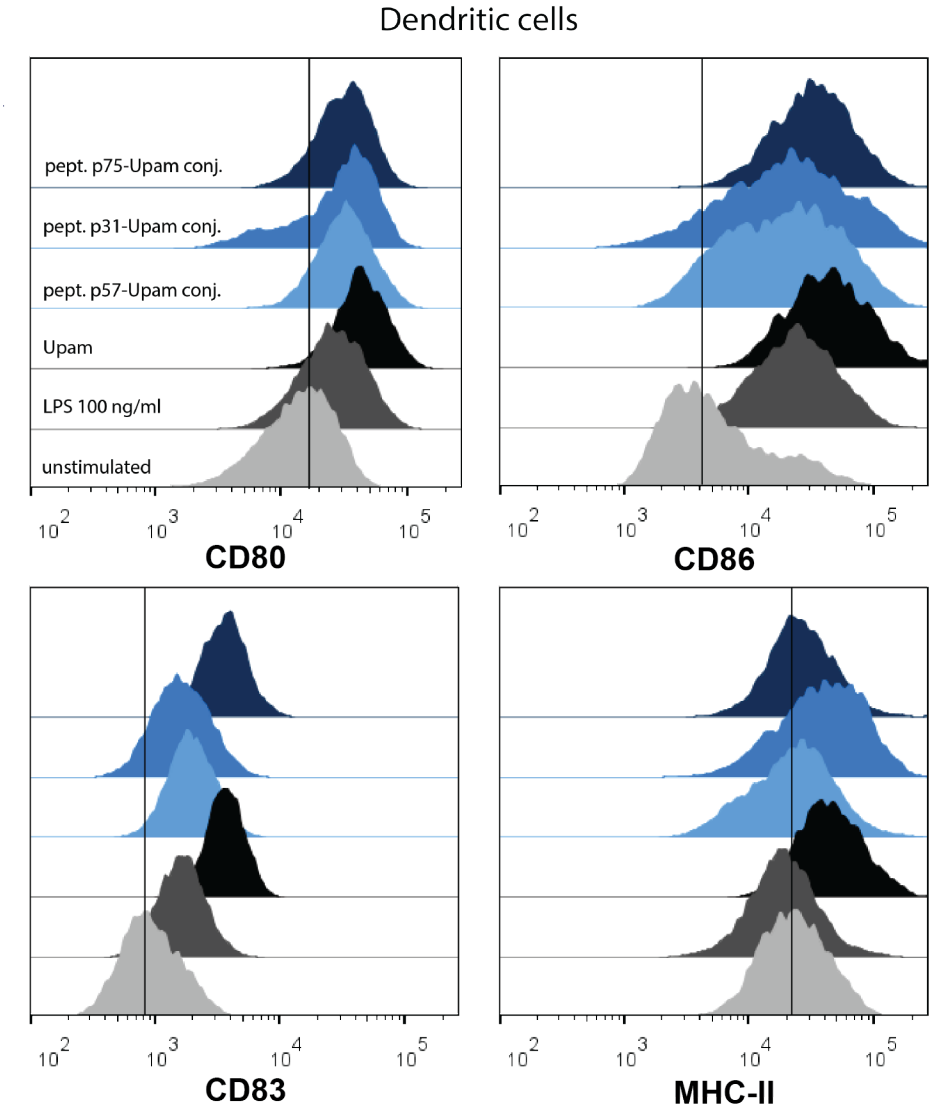

S1 Figure - Expression of activation or T cell costimulatory markers by DCs as measured by flow cytometry. UPam (20 μM) and synthetic conjugates (20 μM) are used to stimulate human monocyte-derived dendritic cells. LPS (100ng/ml) was used as positive control. Representative data from one of three human donors are shown.

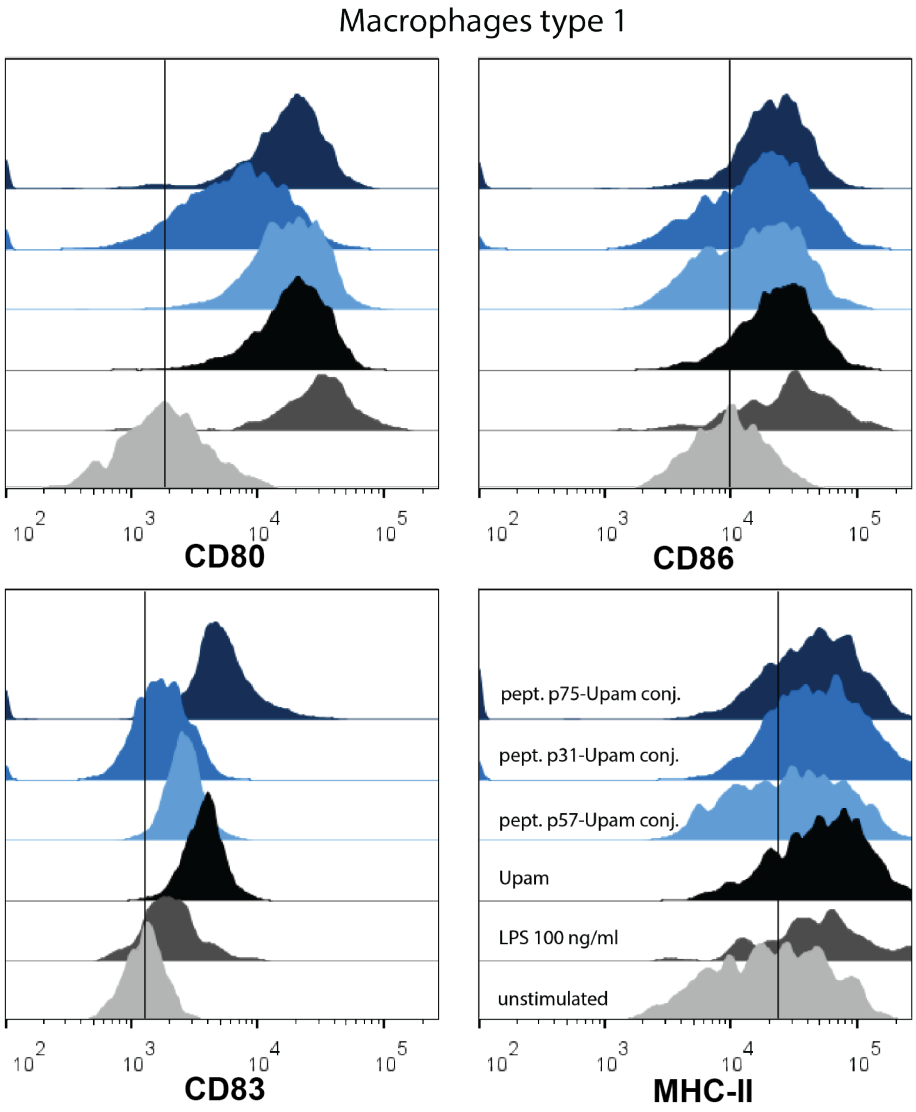

S2 Figure - Expression of activation or T cell costimulatory markers by GM-CSF/M1 macrophages as measured by flow cytometry. UPam (20 µM) and synthetic conjugates (20 µM) are used to stimulate human monocyte-derived macrophages type 1. LPS (100ng/ml) was used as positive control. Representative data from one of three human donors are shown.

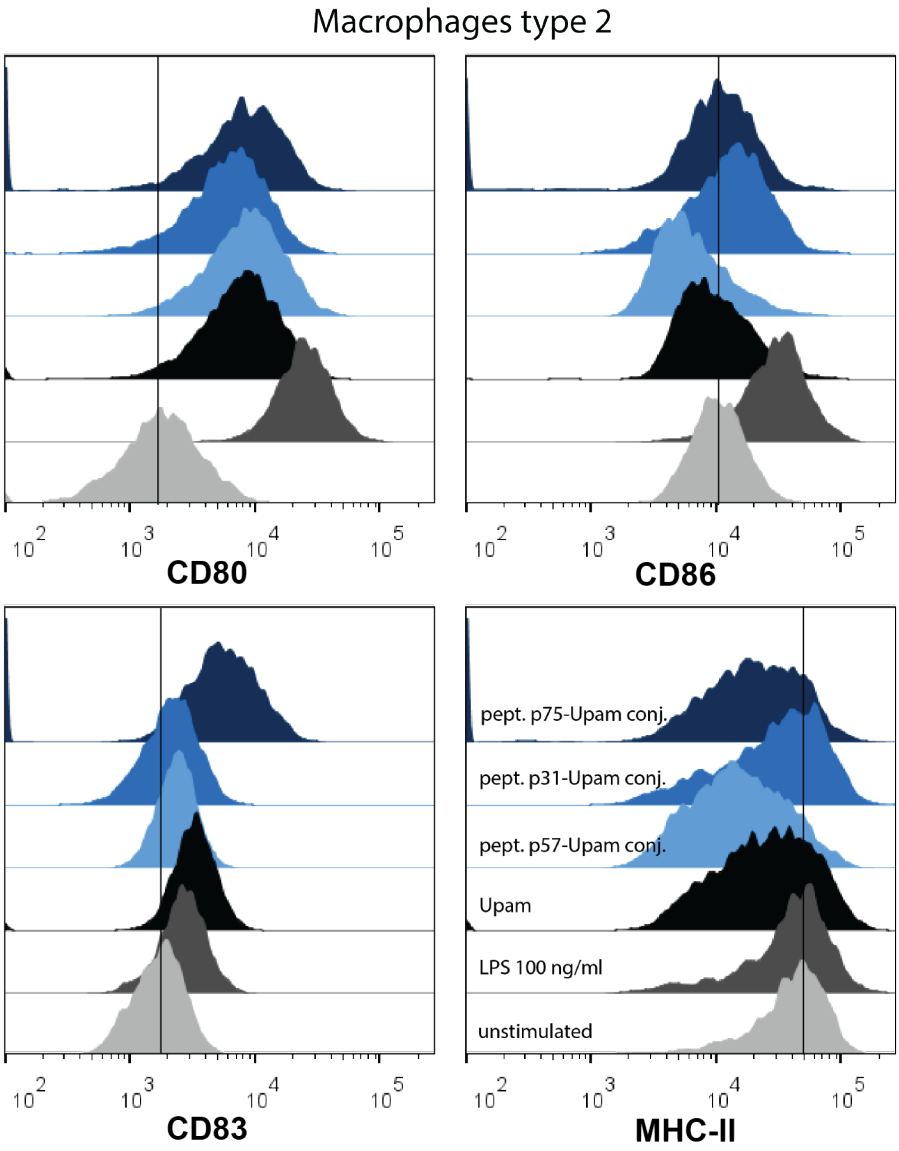

S3 Figure - Expression of activation or T cell costimulatory markers by M-CSF/M2 macrophages as measured by flow cytometry. UPam (20 μM) and synthetic conjugates (20 μM) are used to stimulate human monocyte-derived macrophages type 2. LPS (100ng/ml) was used as positive control. Representative data from one of three human donors are shown.

References

1. Geneva: World Health Organization. Global tuberculosis report 2020. 2020.

2. Andersen P, Kaufmann SHE. Novel Vaccination Strategies against Tuberculosis. Cold Spring Harb Perspect Med. 2014 Jun 1;4(6):a018523–a018523.

3. Rappuoli R, De Gregorio E, Del Giudice G, Phogat S, Pecetta S, Pizza M, et al. Vaccinology in the post–COVID-19 era. Proc Natl Acad Sci. 2021 Jan 19;118(3):e2020368118.

4. Verbeke R, Lentacker I, De Smedt SC, Dewitte H. The dawn of mRNA vaccines: The COVID-19 case. J Controlled Release. 2021 May;333:511–20.

5. Rueckert C, Guzmán CA. Vaccines: From Empirical Development to Rational Design. PLoS Pathog. 2012 Nov 8;8(11):e1003001.

6. Jones LH. Recent advances in the molecular design of synthetic vaccines. Nat Chem. 2015 Dec;7(12):952–60.

7. Jiang Z-H, Koganty R. Synthetic Vaccines: The Role of Adjuvants in Immune Targeting. Curr Med Chem. 2003 Aug 1;10(15):1423–39.

8. Skwarczynski M, Toth I. Peptide-based synthetic vaccines. Chem Sci. 2016;7(2):842–54.

9. Hancock G, Hellner K, Dorrell L. Therapeutic HPV vaccines. Best Pract Res Clin Obstet Gynaecol. 2018 Feb;47:59–72.

10. Ouerfelli O, Warren JD, Wilson RM, Danishefsky SJ. Synthetic carbohydrate-based antitumor vaccines: challenges and opportunities. Expert Rev Vaccines. 2005 Oct;4(5):677–85.

11. Quakkelaar ED, Melief CJM. Experience with Synthetic Vaccines for Cancer and Persistent Virus Infections in Nonhuman Primates and Patients. In: Advances in Immunology. Elsevier; 2012. p. 77–106.

12. Yamamoto M, Sato S, Hemmi H, Sanjo H, Uematsu S, Kaisho T, et al. Essential role for TIRAP in activation of the signalling cascade shared by TLR2 and TLR4. Nature. 2002 Nov;420(6913):324–9.

13. van Bergenhenegouwen J, Plantinga TS, Joosten LAB, Netea MG, Folkerts G, Kraneveld AD, et al. TLR2 & Co: a critical analysis of the complex interactions between TLR2 and coreceptors. J Leukoc Biol. 2013 Nov;94(5):885–902.

14. Zom GG, Khan S, Britten CM, Sommandas V, Camps MGM, Loof NM, et al. Efficient Induction of Antitumor Immunity by Synthetic Toll-like Receptor Ligand–Peptide Conjugates. Cancer Immunol Res. 2014 Aug;2(8):756–64.

15. Zom GG, Welters MJ, Loof NM, Goedemans R, Lougheed S, Valentijn RR, et al. TLR2 ligand-synthetic long peptide conjugates effectively stimulate tumor-draining lymph node T cells of cervical cancer patients. Oncotarget. 2016 Oct;7(41):67087.

16. Tyne AS, Chan JGY, Shanahan ER, Atmosukarto I, Chan H-K, Britton WJ, et al. TLR2-targeted secreted proteins from *Mycobacterium tuberculosis* are protective as powdered pulmonary vaccines. Vaccine. 2013 Sep;31(40):4322–9.

17. Willems MM, Zom GG, Khan S, Meeuwenoord N, Melief CJ, van der Stelt M, et al. N-tetradecylcarbamyl lipopeptides as novel agonists for toll-like receptor 2. J Med Chem. 2014 Jul;57(15):6873–8.

18. Palomo JM. Solid-phase peptide synthesis: an overview focused on the preparation of biologically relevant peptides. RSC Adv. 2014;4(62):32658–72.

19. Ottenhoff THM, Elferink DG, Hermans J, de Vries RRP. HLA class II restriction repertoire of antigen-specific T cells. I. The main restriction determinants for antigen presentation are associated with HLA-D/DR and not with DP and DQ. Hum Immunol. 1985 Jun;13(2):105–16.

20. Commandeur S, van Meijgaarden KE, Prins C, Pichugin AV, Dijkman K, van den Eeden SJF, et al. An Unbiased Genome-Wide *Mycobacterium tuberculosis* Gene Expression Approach To Discover Antigens Targeted by Human T Cells Expressed during Pulmonary Infection. J Immunol. 2013 Feb 15;190(4):1659–71.

21. Commandeur S, van den Eeden SJF, Dijkman K, Clark SO, van Meijgaarden KE, Wilson L, et al. The in vivo expressed *Mycobacterium tuberculosis* (IVE-TB) antigen Rv2034 induces CD4+ T-cells that protect against pulmonary infection in HLA-DR transgenic mice and guinea pigs. Vaccine. 2014 Jun;32(29):3580–8.

22. Coppola M, van den Eeden SJF, Wilson L, Franken KLMC, Ottenhoff THM, Geluk A. Synthetic Long Peptide Derived from *Mycobacterium tuberculosis* Latency Antigen Rv1733c Protects against Tuberculosis. Pascual DW, editor. Clin Vaccine Immunol. 2015 Sep;22(9):1060–9.

23. Coppola M, van Meijgaarden KE, Franken KLMC, Commandeur S, Dolganov G, Kramnik I, et al. New Genome-Wide Algorithm Identifies Novel In-Vivo Expressed *Mycobacterium Tuberculosis* Antigens Inducing Human T-Cell Responses with Classical and Unconventional Cytokine Profiles. Sci Rep. 2016 Dec;6(1):37793.

24. Black GF, Thiel BA, Ota MO, Parida SK, Adegbola R, Boom WH, et al. Immunogenicity of Novel DosR Regulon-Encoded Candidate Antigens of *Mycobacterium tuberculosis* in Three High-Burden Populations in Africa. Clin Vaccine Immunol. 2009 Aug;16(8):1203–12.

25. Commandeur S, Coppola M, Dijkman K, Friggen AH, van Meijgaarden KE, van den Eeden SJF, et al. Clonal Analysis of the T-Cell Response to In Vivo Expressed *Mycobacterium tuberculosis* Protein Rv2034, Using a CD154 Expression Based T-Cell Cloning Method. PLoS ONE. 2014 Jun 6;9(6):e99203.

26. Verreck FA, de Boer T, Langenberg DM, Hoeve MA, Kramer M, Vaisberg E, et al. Human IL-23-producing type 1 macrophages promote but IL-10-producing type 2 macrophages subvert immunity to (myco) bacteria. Proc Natl Acad Sci. 2004 Mar;101(13):4560–5.

27. Verreck FA, de Boer T, Langenberg DM, van der Zanden L, Ottenhoff TH. Phenotypic and functional profiling of human proinflammatory type-1 and anti-inflammatory type-2 macrophages in response to microbial antigens and IFN-γ-and CD40L-mediated costimulation. J Leukoc Biol. 2006 Feb;79(2):285–93.

28. Geluk A, Taneja V, van Meijgaarden KE, Zanelli E, Abou-Zeid C, Thole JER, et al. Identification of HLA class II-restricted determinants of *Mycobacterium tuberculosis*-derived proteins by using HLA-transgenic, class II-deficient mice. Proc Natl Acad Sci. 1998 Sep 1;95(18):10797–802.

29. Budd RC, Cerottini JC, Horvath C, Bron C, Pedrazzini T, Howe RC, et al. Distinction of virgin and memory T lymphocytes. Stable acquisition of the Pgp-1 glycoprotein concomitant with antigenic stimulation. J Immunol. 1987 May 15;138(10):3120.

30. Andersen P, Doherty TM. The success and failure of BCG — implications for a novel tuberculosis vaccine. Nat Rev Microbiol. 2005 Aug;3(8):656–62.

31. Hesseling AC, Marais BJ, Gie RP, Schaaf HS, Fine PEM, Godfrey-Faussett P, et al. The risk of disseminated Bacille Calmette-Guerin (BCG) disease in HIV-infected children. Vaccine. 2007 Jan;25(1):14–8.

32. Martin C, Aguilo N, Marinova D, Gonzalo-Asensio J. Update on TB Vaccine Pipeline. Appl Sci. 2020 Apr 10;10(7):2632.

33. Li J, Zhao A, Tang J, Wang G, Shi Y, Zhan L, et al. Tuberculosis vaccine development: from classic to clinical candidates. Eur J Clin Microbiol Infect Dis. 2020 Aug;39(8):1405–25.

34. Vetter V, Denizer G, Friedland LR, Krishnan J, Shapiro M. Understanding modern-day vaccines: what you need to know. Ann Med. 2018 Feb 17;50(2):110–20.

35. Stewart E, Triccas JA, Petrovsky N. Adjuvant Strategies for More Effective Tuberculosis Vaccine Immunity. Microorganisms. 2019 Aug 12;7(8):255.

36. Del Giudice G, Rappuoli R, Didierlaurent AM. Correlates of adjuvanticity: A review on adjuvants in licensed vaccines. Semin Immunol. 2018 Oct;39:14–21.

37. Mishra A, Akhtar S, Jagannath C, Khan A. Pattern recognition receptors and coordinated cellular pathways involved in tuberculosis immunopathogenesis: emerging concepts and perspectives. Mol Immunol. 2017 Jul;87:240–8.

38. Irvine DJ, Swartz MA, Szeto GL. Engineering synthetic vaccines using cues from natural immunity. Nat Mater. 2013 Nov;12(11):978–90.

39. Zhang Y, Luo F, Cai Y, Liu N, Wang L, Xu D, et al. TLR1/TLR2 Agonist Induces Tumor Regression by Reciprocal Modulation of Effector and Regulatory T Cells. J Immunol. 2011 Feb 15;186(4):1963–9.

40. Wang Z-B, Xu J. Better Adjuvants for Better Vaccines: Progress in Adjuvant Delivery Systems, Modifications, and Adjuvant–Antigen Codelivery. Vaccines. 2020 Mar 13;8(1):128.

41. Ma X, Yan W, Zheng H, Du Q, Zhang L, Ban Y, et al. Regulation of IL-10 and IL-12 production and function in macrophages and dendritic cells. F1000Research. 2015 Dec 17;4:1465.

42. Groux H, Bigler M, de Vries JE, Roncarolo M-G. Inhibitory and Stimulatory Effects of IL-10 on Human $CD8^+$ T Cells. J Immunol. 1998 Apr 1;160(7):3188.

43. Santin AD, Hermonat PL, Ravaggi A, Bellone S, Pecorelli S, Roman JJ, et al. Interleukin-10 Increases Th1 Cytokine Production and Cytotoxic Potential in Human Papillomavirus-Specific $CD8^+$ Cytotoxic T Lymphocytes. J Virol. 2000 May 15;74(10):4729–37.

44. Ottenhoff THM. New pathways of protective and pathological host defense to mycobacteria. Trends Microbiol. 2012 Sep;20(9):419–28.

45. Ottenhoff THM, Kaufmann SHE. Vaccines against Tuberculosis: Where Are We and Where Do We Need to Go? PLoS Pathog. 2012 May 10;8(5):e1002607.

46. Nunes-Alves C, Booty MG, Carpenter SM, Jayaraman P, Rothchild AC, Behar SM. In search of a new paradigm for protective immunity to TB. Nat Rev Microbiol. 2014 Apr;12(4):289–99.

47. Divangahi M. Are tolerance and training required to end TB? Nat Rev Immunol. 2018 Nov;18(11):661–3.

48. Brazier B, McShane H. Towards new TB vaccines. Semin Immunopathol. 2020 Jun;42(3):315–31.

49. Khader SA, Bell GK, Pearl JE, Fountain JJ, Rangel-Moreno J, Cilley GE, et al. IL-23 and IL-17 in the establishment of protective pulmonary CD4+ T cell responses after vaccination and during Mycobacterium tuberculosis challenge. Nat Immunol. 2007 Apr;8(4):369–77.

50. Cruz A, Fraga AG, Fountain JJ, Rangel-Moreno J, Torrado E, Saraiva M, et al. Pathological role of interleukin 17 in mice subjected to repeated BCG vaccination after infection with *Mycobacterium tuberculosis*. J Exp Med. 2010 Aug 2;207(8):1609–16.

51. Torrado E, Robinson RT, Cooper AM. Cellular response to mycobacteria: balancing protection and pathology. Trends Immunol. 2011 Feb;32(2):66–72.

52. Snapper CM, Mond JJ. Towards a comprehensive view of immunoglobulin class switching. Immunol Today. 1993 Jan;14(1):15–7.

53. Mosmann T. TH1 and TH2 cells: different patterns of lymphokine secretion lead to different functional properties. Annu Rev Immunol. 1989 Apr;

54. Deenick EK, Hasbold J, Hodgkin PD. Switching to IgG3, IgG2b, and IgA is division linked and independent, revealing a stochastic framework for describing differentiation. J Immunol Baltim Md 1950. 1999 Nov 1;163(9):4707–14.

55. Collins AM. IgG subclass co-expression brings harmony to the quartet model of murine IgG function. Immunol Cell Biol. 2016 Nov;94(10):949–54.

56. Ashhurst AS, McDonald DM, Hanna CC, Stanojevic VA, Britton WJ, Payne RJ. Mucosal Vaccination with a Self-Adjuvanted Lipopeptide Is Immunogenic and Protective against *Mycobacterium tuberculosis*. J Med Chem. 2019 Sep 12;62(17):8080–9.

5

Mincle/TLR2 co-stimulation using synthetic ligands

Laura Marino [1], Susan J.F. van den Eeden [2], Krista E. van Meijgaarden [2], Nico J. Meeuwenoord [1], Dmitri V. Filippov[1], Gijs A. van der Marel [1], Jeroen D. C. Codée [1], Tom H.M. Ottenhoff [2]

[1] Department of Bioorganic Synthesis, Leiden University, Leiden, The Netherlands

[2] Department of Infectious Diseases, Leiden University Medical Center, Leiden, The Netherlands

Abstract

C-type lectin receptors (CLRs) and Toll-like receptors (TLRs) are proteins expressed on antigen-presenting cells, involved in pathogen recognition by the host. CLRs and TLRs can act in synergy by interacting with different microbial ligands thus inducing amplified immune responses, which may result in the production of pro-inflammatory cytokines to a significantly higher extent than that resulting from interaction with a single ligand. Given the importance of the macrophage inducible C-type lectin receptor (Mincle) and the Toll-like receptor 2 (TLR2) in mycobacterial recognition, with Mincle shown to interact with cell-wall glycolipids and TLR2 interacting with lipoproteins from *Mycobacterium tuberculosis*, the effects of Mincle/TLR2 co-stimulation on murine and human dendritic cells was investigated. Dendritic cells are key players in the induction of innate and adaptive immune responses, and their activation can result in induction of both pro- and anti-inflammatory cytokines. In the present study two synthetic compounds were selected, namely trehalose distearate (TDS, a Mincle ligand) and UPam, a TLR2 ligand, and by using a matrix of concentrations for the two ligands, identified TDS/UPam combinations which resulted in increased production of pro-inflammatory, as well as anti-inflammatory cytokines by human monocyte-derived dendritic cells (moDCs). On the basis of these results, it was investigated whether Mincle/TLR2 co-stimulation would also affect (positively or negatively) adaptive immune responses by studying antigen presentation to human monoclonal $CD4^+$ Th1 T cells specific for peptide epitopes from the mycobacterial Heat shock protein 65. These results showed that, upon stimulation of moDCs in the presence of cognate antigen, the addition of combinations of TDS and UPam did not affect (neither increased nor decreased) the level of T cell proliferative responses compared to single pathogen recognition receptor stimuli.

Introduction

The immune system is able to detect microbial pathogens through pathogen recognition receptors (PRRs), proteins expressed by antigen presenting cells (APCs) such as dendritic cells (DCs) and macrophages, amongst others. It is well established that different PRRs can be simultaneously engaged by infecting pathogens, and several groups have investigated synergistic interactions between different PRRs.[1–3]

Toll-like receptors (TLRs) recognise a plethora of microbial structures and they are arguably the most studied PRRs for their effects of co-stimulation on the induction of inflammatory responses. For example, Napolitani *et al.* measured the induction of several pro-inflammatory cytokines in human and murine DCs via ELISA and RT-PCR, showing that TLR3 and TLR4 activating ligands can act in synergy with ligands for three other receptors, namely TLR7, TLR8 and TLR9.[4] On the other hand, much less is currently known about the interaction of TLRs with C-type lectin receptors (CLRs), a class of PRRs specialized in detection of microbial carbohydrates. The investigation of TLRs/CLRs interactivity is of interest, since it can provide insights into the interaction of two distinct signalling pathways.[5,6]

During mycobacterial infections, host immune cells are exposed to mycobacterial lipoproteins as well as glycolipids. These pathogen-associated molecular patterns (PAMPs) can engage the TLR2 and the macrophage inducible C-type lectin receptor (Mincle), which are expressed on the cell surface of human and murine antigen presenting cells. TLR2 engagement induces pro-inflammatory cytokine production via the MyD-88/TIRAP signalling pathway, while Mincle signals via ITAM/Syk/Card9, and both pathways converge on NF-κB activation.[7–9] Interestingly it has been shown that expression of the Mincle receptor is increased upon TLR2 stimulation. Schick *et al.* have shown that glycolipid extracts of *C. diphtheriae* and of *C. ulcerans*, as well as the commercially available TLR2 ligand lipopeptide Pam_3CSK_4 upregulated Mincle expression by murine bone marrow-derived macrophages (BMMs) in a TLR2-dependent manner.[10] Matsumura *et al.* proposed that TLR2-induced production of IL-6 enhanced Mincle expression on IFN-γ-producing immature myeloid cells.[11] More information on the cooperation between Mincle and TLR2 was provided by Lee *et al.* who stimulated murine BMMs with Pam_3CSK_4 and trehalose 6-6'-dimycolate. Using RNA sequencing they compared the changes in mRNA transcriptional profiles by stimulating BMMs either with the single ligands or the combination of the two, and concluded that Mincle signalling at the initial stage of cell activation synergistically modulated the transcription of most TLR2-regulated genes towards pro-inflammatory anti-mycobacterial responses (*e.g.,* iNOS, IL-12 and CCL2), at least in mice. They also showed that, at this stage, type I interferon responses were selectively inhibited, while at a later stage,

continuous Mincle/TLR2 stimulation inhibited the general translational machinery, possibly leading to inflammation control.[12] These results point to a potential double role of trehalose 6-6'-dimycolate in admixture with TLR2 ligands in initiation and control of host responses to infection.

Given the key role that DCs play in the induction of innate and adaptive immune responses, the effect of co-stimulation of human dendritic cells with well-defined, synthetic TLR2 and Mincle ligands was here investigated. Trehalose-6,6'-distearate (TDS) and 1-tetradecylcarbamyl-Cys((RS)-2,3-di-(palimitoyloxy)propyl)-Ser-Lys-Lys-Lys-Lys-NH_2 (UPam) were used to investigate whether this combination can result in synergistic activation of murine and human dendritic cells (the chemical structures are shown in Figure 1). The ligands used in the present study were selected because of their known ability to interact with murine and human Mincle and TLR2, respectively.[13–15] Moreover, these compounds are readily produced via synthetic pathways and can be easily modified for conjugation to antigens, making them versatile tools for the generation of subunit vaccines.

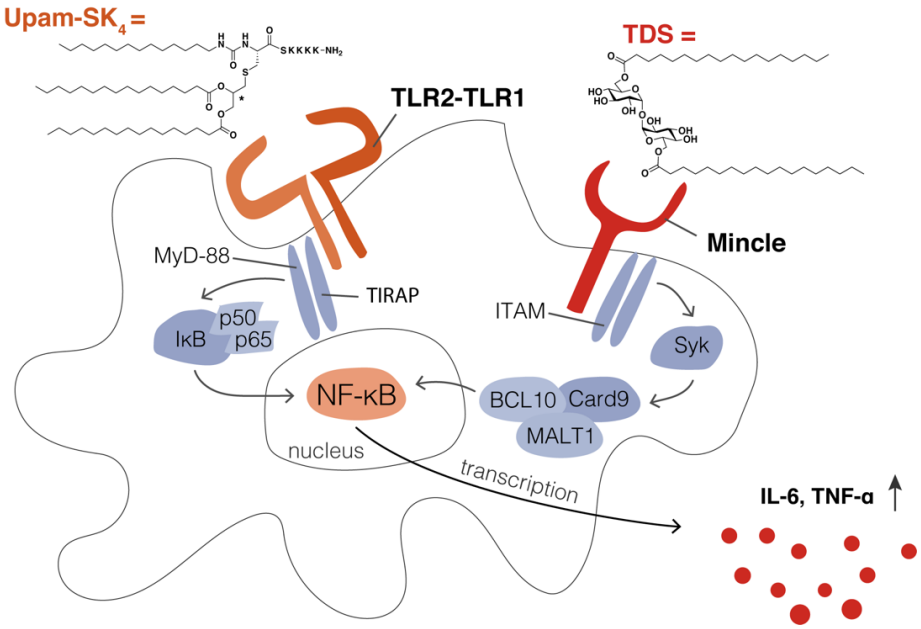

Figure 1 – Visual representation of a dendritic cell and its interaction with UPam and TDS via TLR2/TLR1 and Mincle, respectively. Key proteins involved in signaling through the two receptors are shown. Chemical structures of the synthetic adjuvants selected for this study are also presented.

Three cellular systems were selected to investigate the effects of single vs. double ligand activation: a D1 murine cell line system, which is a long-term immature DC cell line from cultured mouse spleen cells;[16] human monocyte-derived dendritic cells (moDCs); and two cloned human T cell lines specific for mycobacterial Heat shock protein 65.[17] Flow cytometry was employed to assess if double vs. single stimulation would result in increased expression of activation markers and T cell co-stimulatory molecules on APCs. Analysis of the level of pro- and anti-inflammatory cytokines released in the cell supernatants upon stimulation with nine different mixtures of UPam and TDS, was performed in order to identify potential synergistic combinations of the two ligands. Antigen-presentation studies using the two T cell clones were also performed to analyse the influence of selected single vs. double stimulations with UPam and/or TDS on T cell proliferation.

Results

In vitro results using murine D1 cells system

First, the expression of Mincle on the D1 cell line was verified using a cross species reactive anti-Mincle antibody (anti-CLEC4E Clone 16E3). As shown in supporting Figure S1, Mincle is expressed on the cell surface of immature D1 cells. Subsequently, D1 cells were assessed for their responsiveness to Mincle ligands, following stimulation with either synthetic TDS or commercial trehalose 6-6'-dibehenate (TDB). ODN1826, a TLR9 ligand was taken along as positive control. Upon treatment with these ligands, the cells shifted from an immature DC-like phenotype to mature DC-like phenotype which resulted in increased expression of CD40 and CD86 activation markers, as determined by flow cytometry (see supporting Figure S1). Stimulation of D1 cells using TDS and TDB also resulted in production of IL-12p40, as determined by ELISA (see supporting Figure S2).

In line with previous results,[13] UPam stimulation resulted in an increased number of $CD40^{+}CD86^{+}$ cells and production of IL-12p40 as compared to the unstimulated control (Figure 2A and 2B). Notably, TDS stimulation induced an even stronger cellular activation with significantly higher levels of IL-12p40 production as compared to UPam stimulation. Combinations of UPam/TDS were investigated using a 3 by 3 concentration matrix, with concentrations ranging from 50 - 10 - 2 μM for both ligands. As shown in Figure 2C, stimulation of the cells with 10 μM UPam in combination with TDS (50 - 10 - 2 μM) resulted in increased numbers of $CD40^{+}CD86^{+}$ cells as compared to stimulation with UPam or TDS alone. However, no increase in IL-12p40 production was observed (Figure 2D).

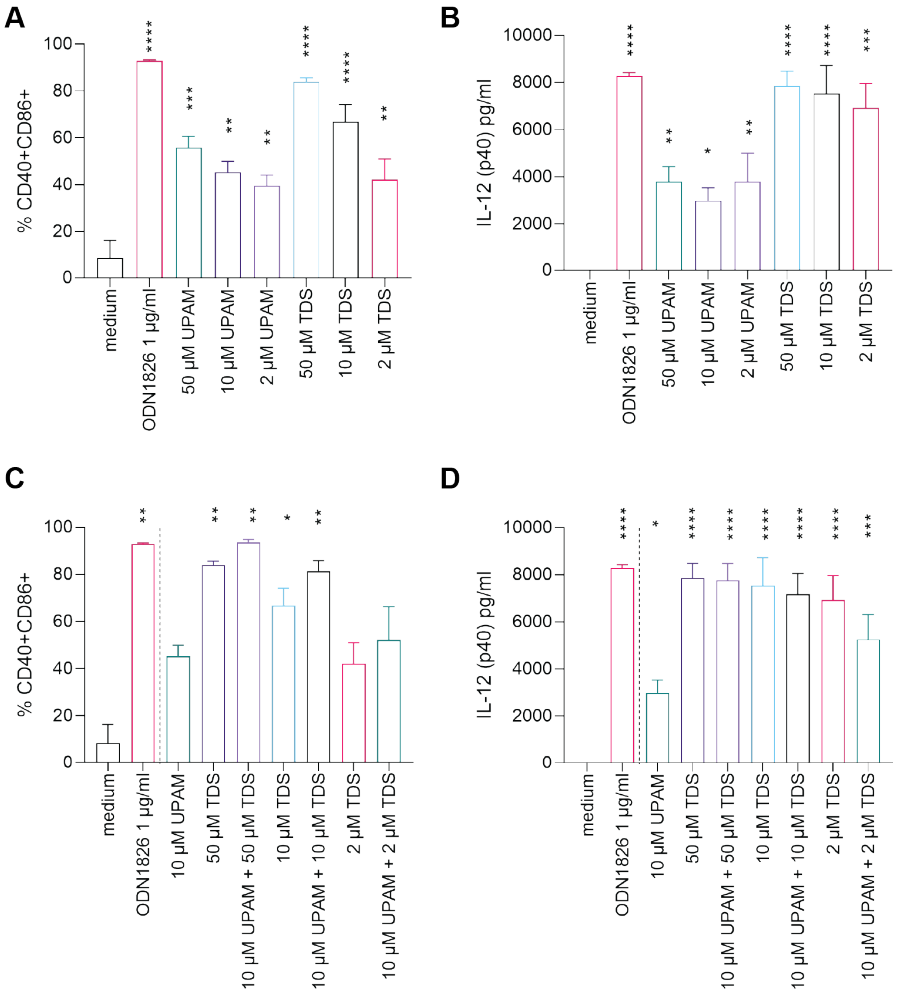

Figure 2 - Effects of UPam/TDS stimulation on D1 DC cells. Bar plots depicting: **(A)** percentage of CD40-CD86 double positive D1 cells as measured by flow cytometry; **(B)** amount of IL-12p40 cytokine detected in the supernatant as measured by ELISA after 20 hours stimulation with UPam or TDS; **(C)** percentage of CD40-CD86 double positive D1 cells as measured by flow cytometry and **(D)** amount of IL-12p40 cytokine detected in the supernatant as measured by ELISA after 20 hours stimulation with UPam and TDS or their combination. Error bars represent mean + SD of two independent experiments as calculated using GraphPad Prism. Statistical significance with reference to cells exposed to medium + DMSO was calculated through one-way ANOVA method (****p < 0.0001; ***p < 0.001; **p < 0.01; *p < 0.05). CpG ODN1826 (1 µg/ml) was used as positive control.

In vitro results using a human moDCs cell system

Immature monocyte-derived dendritic cells (DC) were differentiated as previously described and analysed for correct differentiation by expression of CD14, CD163, CD11b, CD1a.[18,19]

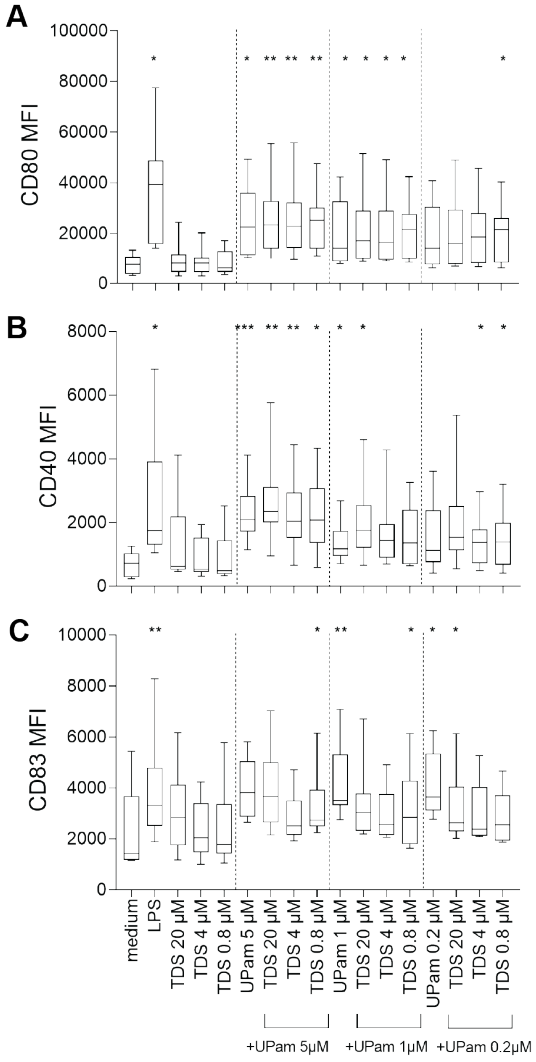

Figure 3 - Box and whiskers plots depicting the expression of selected surface markers from 9 different donors, as measured by flow cytometry. Box plots indicate the median value of the dataset (n = 9 donors) with error bars from min to max values as calculated using GraphPad Prism. Statistical significance with reference to cells exposed to medium + DMSO was calculated through one-way ANOVA method (***p < 0.001; **p < 0.01; *p < 0.05). LPS (100 ng/ml) was used as a positive control.

In order to verify that this human cell model could be used to investigate the response to the Mincle/TLR2 ligands, immature moDCs were further characterised for expression of human Mincle and TLR2. As shown in supporting Figure S3, both receptors were expressed in immature moDCs, and the expression of TLR2 but not Mincle further increased upon stimulation by UPam and LPS.

Studies conducted with immature moDCs showed that stimulation with a concentration range of UPam (5 - 1 - 0.2 μM) resulted in cell activation with an increased expression of CD40 and CD80 T cell co-stimulatory markers and CD83 activation marker. By contrast, stimulation with a concentration range of TDS (20 - 4 - 0.8 μM) resulted only in an increase in CD83 but not CD40 or CD80 expression.

To determine the immunogenic profile of simultaneous Mincle/TLR2 receptor stimulation, moDCs were stimulated using matrixed combinations of UPam (5 - 1 - 0.2 μM) and TDS (20 - 4 - 0.8 μM). When TDS was added to UPam, only minor changes were observed for CD83 and CD40 (Figure 3C, 3B). Interestingly, TDS did not promote CD40 expression, although co-stimulation using UPam and TDS, for the two lowest concentrations (1 and 0.2 μM) of UPam selected in this study, led to upregulation of this surface protein to somewhat higher levels than the corresponding UPam stimulus. In the case of CD80 (Figure 3A), upregulation of this marker could be observed when the cells were treated with UPam, in a dose dependent manner. In contrast TDS stimulation, by itself, did not lead to an increase in CD80 expression. The simultaneous stimulation using TDS and UPam resulted in increased expression of CD80 as compared to single UPam stimulation only for the suboptimal 0.2 and 0.8 μM concentrations of UPam and TDS, respectively.

Cell supernatants were analysed by ELISA for the quantification of IL-12p40, IL-10, IL-6 cytokines and by Luminex for TNF-α, IL-8, IL-1β and GM-CSF. Neither UPam nor TDS stimulation resulted in detectable IL-1β and GM-CSF production (data not shown). Interestingly, when moDCs were stimulated using UPam, medium to high levels of IL-12p40, IL-10, IL-8, IL-6 and TNF-α were released in the cell supernatant after 20 hours (see Figure 4). Neither of these cytokines could be detected in the supernatants of TDS-stimulated cells.

Stimulation of DCs using mixtures of TDS 0.8 μM with UPam (5 - 1 - 0.2 μM) resulted in increased production of IL-6 and TNF-α as compared to stimulation by single ligand, with statistically significant differences for one defined concentration of ligands. In the selected concentration window, the release of IL-6 in the cell supernatants tended to increase, with twice as much IL-6 produced when UPam 1 μM was combined with TDS 0.8 μM as compared to the amount of cytokine induced by UPam 1 μM alone (see Figure 4). For the same concentrations of ligands, also the amount of TNF-α increased significantly, doubling the amount released upon UPam stimulation of DCs. The amount of IL-12p40 and IL-10 increased slightly upon double ligand activation, although comparison to the single ligand activation did not result

in a statistically significant change (Figure 4C and 4D). However, the amount of IL-8 slightly decreases upon TLR2/Mincle stimulation as opposed to single TLR2 stimulation in the studied concentration range (see supporting Figure S4).

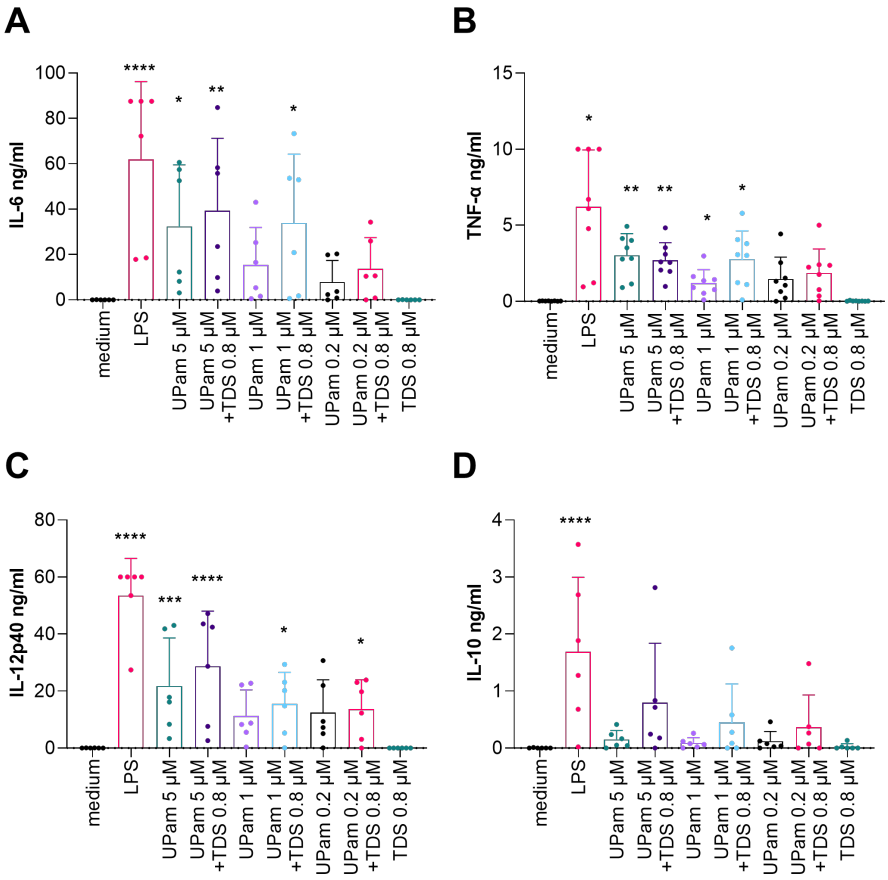

Figure 4 - Cytokine production profile of human moDCs stimulated for 20 hours using single adjuvants or mixtures thereof, as measured by ELISA or milliplex. (A, C, D) Dots shown in the scatter dot plots represent IL-6, IL-12p40 and IL-10 data from 6 different donors (each dot corresponds to the mean of duplicate measurements), as measured by ELISA; **(B)** Dots shown in the scatter dot plots represent TNF-α data from 8 different donors, as measured by milliplex. Bars indicate mean value + SD. Statistical significance with reference to cells exposed to medium + DMSO was calculated through one-way ANOVA method (****p < 0.0001; ***p < 0.001; **p < 0.01; *p < 0.05). LPS (100 ng/ml) is used as a positive control.

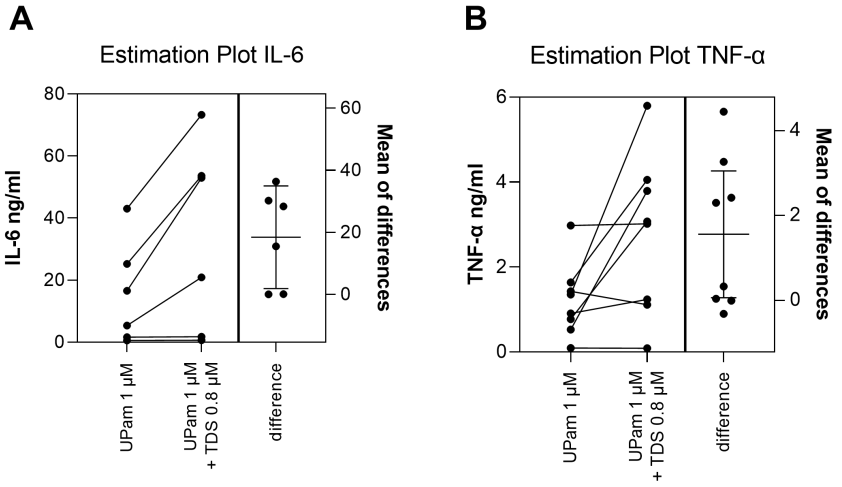

Figure 5 – Estimation plots for cytokines produced by human moDCs using UPam 1 µM or UPam 1 µM in combination with TDS 0.8 µM. Comparison of change in cytokine concentration for depicted cytokines is visually facilitated connecting with a line the cytokine concentration per each donor after stimulation with single or double adjuvants. The difference in cytokine concentration of the two selected conditions per each donor is visualized on the right side of each plot. **(A)** Dots shown in the scatter dot plots represent IL-6 data from 6 different donors (each dot corresponds to the mean of duplicate measurements), as measured by ELISA; **(B)** Dots shown in the scatter dot plots represent TNF-α data from 8 different donors, as measured by Luminex. Error bars indicate mean value of differences + 95% confidence interval, as calculated by GraphPad Prism.

5

For comparison purposes, paired t-test for each relevant pair of conditions was performed and the resulting estimation plots for the statistically significant difference are shown in Figure 5. These plots clearly show that dendritic cells from 4 out of 6 donors produced a higher amount of IL-6 when stimulated with the mixture of ligand as compared to UPam only. In contrast, UPam stimulation on cells from the remaining 2 donors resulted in very low amounts of this cytokine, and addition of TDS did not increase production. Additionally, TNF-α production increased for 4 out of 8 donors for double ligand stimulation as opposed to UPam stimulation (Figure 5B).

In vitro results using human T cell clones

To study the effect of TDS/UPam co-stimulation on antigen-presentation by monocyte-derived dendritic cells of peptide antigen to T cells, a T cell proliferation assay was performed. Here several combinations of TDS (0.8 and 4 μM) and UPam

(0.2, 1 and 5 μM) were selected in the presence of varying amounts of antigen. Two T cell clones were selected, namely R2F10, a DR2-restricted T cell clone generated against the peptide p418-427 from *Mycobacterium leprae* heat shock protein 65, and Rp15 1-1, a DR3-restricted T cell clone generated against the peptide p3-13 from *Mycobacterium leprae/Mycobacterium tuberculosis* heat shock protein 65 matching the HLA DR type of the moDC donor.

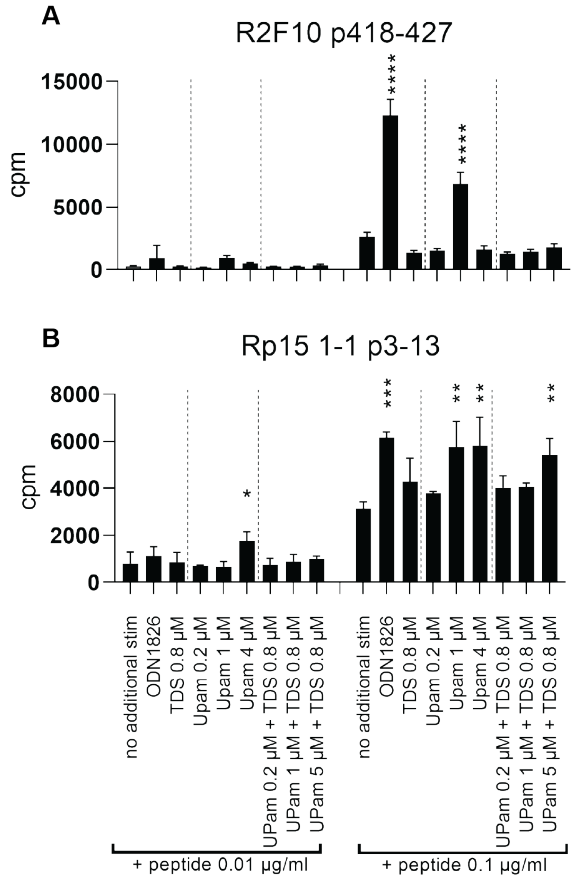

Figure 6 - Antigen presentation experiment using moDCs and T cell clones. T cell proliferation for the R2F10 p418-427 clone (subplot A) and for the Rp15 1-1 p3-13 clone (subplot B) was measured on a Microbetaplate counter after 18 hours pulsation with [^{3}H]thymidine and it is expressed as counts per minute (cpm). Values represent mean + SD of triplicate measurements from one experiment as calculated using GraphPad Prism. Statistical significance with reference to cells exposed to reference peptide was calculated through one-way ANOVA method (****$p < 0.0001$; ***$p < 0.001$; **$p < 0.01$; *$p < 0.05$). Peptide (at described concentration) is used as positive control.

Only UPam at a very narrow single concentration (1 μM) (seen for both T cell clones) and ODN1826, a TLR9 ligand used as positive control, induced an increase in proliferation of T cells from the R2F10 clone (see Figure 6). For clone Rp15 1-1 there was a slight to moderate increase in T cell proliferation by addition of all ligands, but no synergistic effect was observed, indicating the effect on the antigen presenting capacity of the treated moDC not to be interfering nor beneficial for T cell antigen presentation.

Discussion

There is increasing evidence that vaccine adjuvants containing PAMPs not only function to amplify an immune signal,[20] but can also influence and direct the type of immune response.[3,21] Single-molecule PRR ligands allow for the study of these immune pathways and represent valuable tools to deepen our understanding of how the immune system responds to single PAMP molecules. When a pathogen interacts with cells from the host, several immunostimulatory molecules are present simultaneously that activate different receptors expressed by antigen-presenting cells.[22] It has been shown that distinct combinations of pathogenic molecules lead to very specific responses.[5] PRRs can cooperate to produce amplified responses, a phenomenon known as synergistic activation. Many combinations of ligands acting synergistically have been identified within the TLR family.[4,23–30] Recently, combinations of nucleotide-binding oligomerization domain-like receptors, retinoic acid-inducible gene-I-like receptors, CLRs and TLRs have also been studied.[31–34] Not all combinations lead to synergy.[35,36] Here, the effect of simultaneous TLR2/Mincle stimulation on murine and human DCs as key players in innate and adaptive immune responses was studied, because the effect of co-stimulation by ligands for Mincle and TLR2 on this type of antigen-presenting cells had not been investigated previously. Synthetic small molecules, namely TDS, a synthetic analogue of mycobacterial cord factor and an established Mincle ligand, and UPam, a synthetic ligand very similar in structure to Pam_3CSK_4 which is able to activate the TLR1/TLR2 heterodimer[13,15] were selected for this study. One of the advantages of using small molecules is their synthetic and commercial potential, in addition to the ease of chemical modification, which allows for the generation of multiple epitope/adjuvant conjugates, the insertion of molecular scaffolds to optimise the immune response and/or their facile incorporation in nanoparticles. Two model cellular systems were used, the murine D1 DC cell line and human monocyte-derived DCs for the study of potential Mincle/TLR2 co-stimulation. It was first verified that both cell types expressed Mincle in their immature state. The D1 DC cells expressed Mincle and they responded to TDS stimulation by upregulating the expression of CD40 and CD86, and by producing the pro-inflammatory cytokine IL-12p40. As expected,[13] also UPam stimulation resulted in upregulation of selected activation markers and production

of IL-12p40, although to a lower extent than when stimulating these cells with TDS. No synergy, however, was detected when stimulating the D1 DC cells with the two ligands. Human DCs, generated by culturing monocytes in the presence of IL-4 and GM-CSF, were stimulated using a matrix of nine combinations of the two ligands and the effects of co-stimulation were assessed using flow-cytometry to study the expression of activation markers and T cell co-stimulatory molecules, and ELISA and Luminex to detect cytokine-production. Notably, TDS stimulation induced only CD83 upregulation in moDCs and no production of IL-10, IL-6, IL-8, IL-12 nor TNF-α. When Decout *et al.* treated human monocyte-derived DCs or peripheral blood monocytes with TDB, a synthetic compound structurally very similar to TDS, they also observed that no TNF-α nor IL-6 was detected in the cell supernatants.[37] A different study by Smith *et al.* reported on Brartemicin derivatives, which are synthetic aryl-6,6'-trehaloses, being able to induce the production of cytokines, including TNF-α and IL-6, by human peripheral blood monocytes.[38] It is possible that the physicochemical properties of the different trehalose derivatives influence the interaction with Mincle and the uptake by APCs. This has also been suggested by Kiyotake *et al.* for cholesterol in the soluble or crystalline form.[39] Additionally, Hunter *et al.* have described how different supra-molecular structures of trehalose dimycolate are responsible for very different activities on human or murine macrophages.[40] Further studies, including structure-activity relationship studies using human Mincle, are required to fully explain the absence of cytokine production by human moDCs stimulated with TDS, as observed in our experiments. It is possible that the interaction to Mincle of the solubilized/suspended ligand differs from the interaction of the same ligand in a plate-bound form. However, with the overarching goal of including TDS or analogues in a single molecule vaccine modality containing two adjuvants, the studies reported in this Chapter required evaluation of the immune-stimulatory properties of the solubilized/suspended form of this compound.

On the contrary, UPam stimulation, performed as described in the materials and methods section of this Chapter, induced upregulation of all selected markers and production of both pro-inflammatory and anti-inflammatory cytokines. These results are in agreement with published data, where it has been shown that stimulation of moDCs by UPam induced upregulation of CD83, CD86 and HLA-DR in addition to production of several chemokines and cytokines, including IL-12, IL-8 and IL-10.[14] Interestingly, mixtures of the two ligands, in the assessed concentration window, induced increased production of TNF-α and IL-6 (up to 2-fold), as compared to the corresponding amounts released by only UPam stimulation. High inter-donor variability in terms of extent of the cytokine response to stimuli, with some DCs producing high amounts of cytokines and others responding with low production, was observed and this may be related to TLR1 polymorphisms.[41–43] Future studies should include DNA analysis to detect TLR1 polymorphisms with the aim of selecting donors who may better respond to UPam treatment.

Finally, to study the effect of TDS/UPam co-stimulation on antigen-presentation by monocyte-derived dendritic cells in the presence of peptide antigen, and to exclude inhibitory effects on T cell activation, a T cell proliferation assay was performed. No decrease or increase in T cell proliferation was observed upon co-stimulation with the two PRR ligands, suggesting that the combination of UPam and TDS, in the selected concentration range, does not improve antigen presentation by dendritic cells. However, antigen presentation of peptide p418-427 to the R2F10 clone was strongly enhanced in the presence of single adjuvant UPam (1 μM) and CpG control as compared to stimulation with peptide alone, and this was the case to a lesser extent for the p3-13 specific T cell clone. TLR ligands, such as CpG oligonucleotides and Pam_3CSK_4, have been shown to enhance T cell activation and proliferation when combined with anti-CD3 stimulation but this work did not address physiological HLA class II dependent antigen-presentation.[44–46]

In summary, the present study describes the immune-stimulatory effect of TLR2/Mincle co-stimulation using synthetic PRR ligands on murine and human dendritic cells, key players in the induction of T cell immune responses. Experiments performed using the murine D1 DC cell line, indicated that admixture of TDS and UPam induced a minor further increase in cell activation as compared to single ligand stimulation. Detailed quantification of cytokine production by human moDCs, however, allowed for the identification of only one synergistic/additive combination of the two synthetic PRR ligands, although minimal or no upregulation was observed for CD80, CD83 or CD40. Functional ELISA and Luminex assays identified concentrations of TDS and UPam which induced increased production of TNF-α and IL-6, as compared to the corresponding amount released following UPam stimulation alone. Notably, TDS alone failed to induce detectable amounts of any of these cytokines. Further studies are required to discover which cellular mechanisms may be responsible for these observations. Taken together, these first results suggest the potential of co-stimulation of the human TLR2 and Mincle receptor for the enhancement of immune responses typically associated with TLR2 stimulation.

Materials and methods

Synthesis of ligands

The two synthetic ligands employed in this study were synthesized according to published procedures.[13,15] Synthetic compounds were tested using LAL assay to exclude the possibility of LPS contamination.

Culturing and stimulation of murine D1 cells

The D1 cell line[16] was obtained from the department of Immunohematology and Blood Transfusion of the Leiden University Medical Centre. The cells were cultured in IMDM medium (Lonza, Belgium) containing 10% heat inactivated FBS (Sigma, St.Louis, MO, USA), 2 mM GlutaMAX™ (Gibco, PAA, Linz, Austria), 50 μM β-mercaptoethanol (Sigma, St.Louis, MO, USA) and 30% supernatant from R1 cells (mouse fibroblast NIH/3T3 cells transfected with mouse GM-CSF gene), which was collected from confluent cultures and filtered. Cells were harvested using PBS containing 2 mM EDTA (Sigma, St.Louis, MO, USA), counted and transferred to 96 well-plates (round bottom, Corning Costar TC-Treated Microplates, Corning, NY) at approximately 50.000 cells/well. Immediately after plating, the cells were stimulated at described concentrations (see results section) of UPam, trehalose 6-6'-distearate and combination thereof. Synthetic compounds were dissolved in DMSO (Sigma, St.Louis, MO, USA) at a concentration of 5 nmol/μL, further diluted and premixed in culture medium. ODN1826 (1 μg/ml; 5'-TCCATGACGTTCCTGACGTT-3'; InvivoGen, San Diego, CA) and TDB (50 – 10 – 2 μM; Avanti Polar Lipids, Alabama) were used as positive control for cell stimulation. Supernatants were harvested 20 hours after the addition of stimuli and cells were stained as described below.

Generation and stimulation of immature human moDCs

Buffy coats of healthy human Blood Bank donors were purchased from Sanquin, Amsterdam, the Netherlands. $CD14^+$monocytes were isolated from whole blood using Ficoll-Paque density gradient followed by purification on autoMACS® Pro Separator instrument using CD14 MicroBeads (MACS, Miltenyi Biotec, Bergisch Gladsbach, Germany). The monocytes were differentiated to monocyte-derived dendritic cells (moDCs) at a concentration of 106 cells/mL in RPMI 1640 (Gibco, PAA, Linz, Austria) medium containing 10% FCS (HyClone, GE Healthcare Life Sciences, Eindhoven, the Netherlands), 2 mM GlutaMAX™ (Gibco, PAA, Linz, Austria), 100 U/ml penicillin, and 100 µg/ml streptomycin (Life Technologies-Invitrogen), 10 ng/mL GM-CSF (Life Technologies-Invitrogen, Bleiswijk, the Netherlands) and 10 ng/mL IL-4 (Peprotech, Rocky Hill, NJ). On day 3 of culturing, fresh medium (RPMI 1640 + 10% FCS, 2 mM GlutaMAX™ + 100 U/ml penicillin + 100 µg/ml streptomycin) supplemented with 30 ng/mL GM-CSF and 30 ng/mL IL-4 was added to the cell culture plates (0.5 mL fresh medium per 1 ml old medium). Cells were differentiated for a total of 5 days at 37°C and in a 5% CO_2 atmosphere. Differentiated $CD14^+$ monocytes were harvested, counted and transferred to 96 wells plates (round bottom, Corning Costar TC-Treated Microplates, Corning, NY) at approximately 50.000 cells/well. The next day, cells were stimulated with described concentrations (see results section) of UPam, trehalose 6-6'-distearate and combination thereof. Synthetic compounds were dissolved in DMSO (Sigma, St.Louis, MO, USA) at a concentration of 5 nmol/μL, further diluted and premixed in RPMI 1640 medium containing

10% FCS, 2 mM GlutaMAX™, 100 U/ml penicillin, and 100 µg/ml streptomycin. LPS (InvivoGen, San Diego, United States) (100 ng/ml) was used as positive control for stimulated cells. Supernatants were harvested 20 hours after the addition of stimuli and cells were stained as described below.

Cytokine detection

The concentration of cytokines in culture supernatants was measured by ELISA according to the manufacturer's instructions. Mouse IL-12/IL-23 (p40), human IL-12/IL-23 (p40) and human IL-10 ELISA kits were purchased from Biolegend (ELISA MAX™ Standard Set; London, UK). Human IL-6 ELISA kit was purchased from Invitrogen (Thermo Fisher scientific, Merelbeke, Belgium). Microlon high binding 96 well plates (Greiner Bio-One International, Alphen a/d Rijn, The Netherlands) were used for the assays. Sample absorbance was measured using a Spectramax i3x (Molecular Devices, CA, USA) spectrometer. All samples were tested in duplicate. The concentration of TNF-α was determined using a MILLIPLEX MAP Human TH17 Magnetic Bead Panel (Merck, Darmstadt, Germany) according to manufacturer's protocol and also contained reagents for the quantification of IL-6, IFN-γ and GM-CSF. Milliplex data were measured using a Bio-Plex 200 system and analysed using Bio-Plex Manager software v6.2 (Bio-rad, Belgium).

Flow cytometric analysis of D1 cells

After 20 h stimulation, murine D1 cells were incubated for 30 minutes at 4 °C with the following dye-labelled antibodies: PE anti-mouse CD40 clone 3/23 (Biolegend, London, UK) and FITC anti-mouse CD86 clone B7-2 (eBioscience, San Diego, CA). Alternatively, cells were stained with Alexa-Fluor 647 anti-CLEC4E (clone 16E3; Novus Biologicals, Littleton, CO). Samples containing the stained cells were characterized on a BD FACSLyric™ flow cytometer and analysed using FlowJo v10 software (Treestar Inc).

Flow cytometric analysis of human moDCs

For quality check of the cells prior to stimulation, immature moDCs were stained for 30 minutes at 4°C with the following dye-labelled antibodies: Alexa Fluor 647 anti-human CD1a clone HI149 (Biolegend, London, UK), BB515 Mouse Anti-Human CD11b clone ICRF44 (BD Biosciences, San Diego, CA), PE anti-human CD163 Antibody clone GHI/61 (Biolegend, London, UK), Brilliant Violet 510 anti-human CD14 Antibody clone 63D3 (Biolegend, London, UK). Human moDCs were incubated for 10 minutes at room temperature with 5% human serum (Sigma, St.Louis, MO, USA) in PBS to prevent nonspecific binding of dye-labelled antibodies. Subsequently, cells were stained for 30 minutes at 4°C with the following dye-labelled antibodies: CD40 - APC (clone 5C3), CD80 - APC-R700 (clone L307.4), CD83 - PE (clone HB15e); all antibodies were purchased from BD Biosciences (San Diego, CA). Alternatively, cells were stained with Alexa-Fluor 488 mouse anti-human CD282 (clone 11G7; BD Pharmingen, San Diego, CA) and Alexa-Fluor 647 anti-CLEC4E (clone 16E3; Novus Biologicals, Littleton, CO). All samples were characterized on a BD FACSLyric™ flow cytometer and analysed using FlowJo v10 software (Treestar Inc).

T cell proliferation

Thawed T cell clones, R2F10 (DR2 restricted, specific for p418-427 of hsp65 Mlep) and Rp15 1-1 (DR3 restricted, specific for p3-13 of hsp65 Mlep/Mtb), were cultured in triplicate in 96-

wells round-bottom plates (10.000 cells/well) together with HLA-DR-matched monocyte-derived dendritic cells (2500 cells/well) and cognate peptide (0.0001, 0.001, 0.01, 0.1, 1 and 10 μg/ml) in combination with TDS (0.8 and 4 μM) and/or UPam (0.2, 1, 5 μM) at 37◦C, 5% CO_2 in IMDM (Gibco, PAA, Linz, Austria) supplemented with GlutaMAX™ (Gibco, PAA, Linz, Austria) and 10% pooled human serum. After 72 hours, cells were pulsed for an additional 18 hours with [3H]thymidine (0.5 μCi/well; Thermo Fisher scientific, Merelbeke, Belgium), harvested with a TomTec cell harvester, and counted on a Microbetaplate counter (Wallac Turku).

Supporting figures:

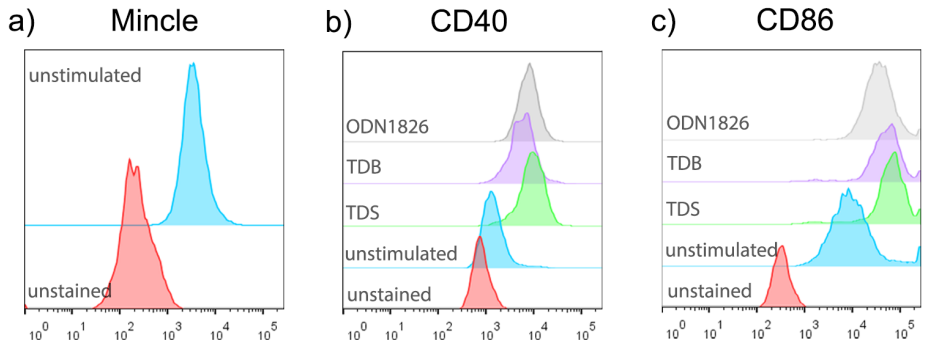

S1 Figure - Expression of surface proteins on D1 DC cells, as measured by flow cytometry. (A) Mincle expression. From front to back: in red unstained cells; in blue unstimulated stained cells. **(B)** CD40 expression and **(C)** CD86 expression. From front to back: in red unstained cells; in blue unstimulated stained cells; in green cells stimulated with TDS (50 μM); in purple cells stimulated with TDB (50 μM); in grey cells stimulated with CpG ODN1826 (1 μg/ml).

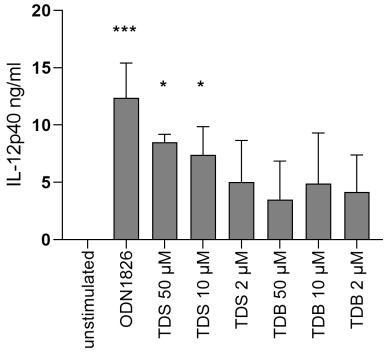

S2 Figure - Quantification of IL-12p40 produced by D1 DC cells, as measured by ELISA. Bar plot showing the amount of IL-12p40 cytokine detected in the supernatant of D1 DC cells as measured by ELISA after 20 hours stimulation with TDS and TDB. Error bars represent mean + SD of two independent experiments as calculated using GraphPad Prism. Statistical significance with reference to cells exposed to reference peptide was calculated through one-way ANOVA method (****p < 0.0001; ***p < 0.001; **p < 0.01; *p < 0.05). CpG ODN1826 (1 μg/ml) is used as positive control.

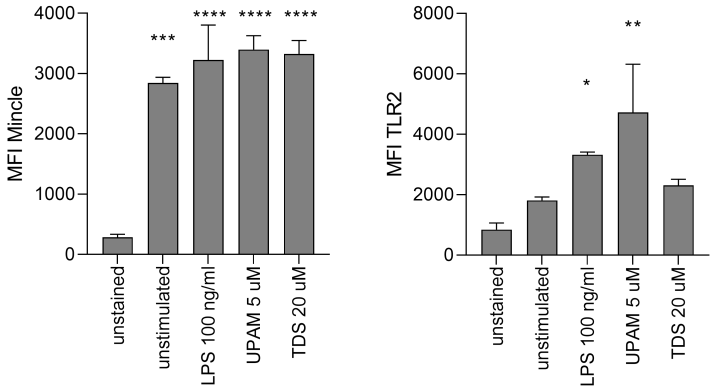

S3 Figure - Human moDC expression of pattern recognition receptors, as measured by flow cytometry. (A) Mincle expression; **(B)** TLR2 expression. Representative data from one human donor are shown. LPS is used as positive control. From front to back: in red unstained cells; in blue unstimulated stained cells; in orange cells stimulated with UPam (5 μM); in light green cells stimulated with TDS (20 μM); in dark green cells stimulated with LPS (100 ng/ml). **(A)** Median fluorescence intensity of Mincle receptor; **(B)** Median fluorescence intensity of TLR2 receptor. Bar plots represent mean value + SD (n = 2 donors) as calculated using GraphPad Prism. Statistical significance with reference to unstained cells exposed to medium + DMSO was calculated through one-way ANOVA method (***p < 0.001; **p < 0.01; *p < 0.05). LPS (100 ng/ml) was used as a positive control.

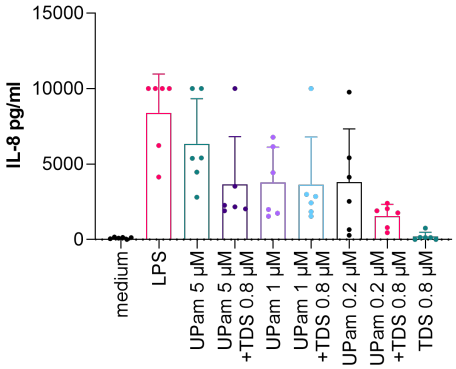

S4 Figure – IL-8 production profile of human moDCs stimulated for 20 hours using single adjuvants or mixtures thereof, as measured by milliplex. Dots shown in the scatter dot plots represent IL-8 data from 6 different donors, as measured by milliplex. Bars indicate mean value + SD.

References

1. Kawai T, Akira S. Toll-like receptors and their crosstalk with other innate receptors in infection and immunity. Immunity. 2011 May;34(5):637–50.

2. Tan RS, Ho B, Leung BP, Ding JL. TLR cross-talk confers specificity to innate immunity. Int Rev Immunol. 2014 Jun;33(6):443–53.

3. Duthie MS, Windish HP, Fox CB, Reed SG. Use of defined TLR ligands as adjuvants within human vaccines. Immunol Rev. 2011 Jan;239(1):178–96.

4. Napolitani G, Rinaldi A, Bertoni F, Sallusto F, Lanzavecchia A. Selected Toll-like receptor agonist combinations synergistically trigger a T helper type 1–polarizing program in dendritic cells. Nat Immunol. 2005 Jul;6(8):769–76.

5. Tom JK, Albin TJ, Manna S, Moser BA, Steinhardt RC, Esser-Kahn AP. Applications of immunomodulatory immune synergies to adjuvant discovery and vaccine development. Trends Biotechnol. 2019 Apr;37(4):373–88.

6. Thakur A, Andrea A, Mikkelsen H, Woodworth JS, Andersen P, Jungersen G, et al. Targeting the Mincle and TLR3 receptor using the dual agonist cationic adjuvant formulation 9 (CAF09) induces humoral and polyfunctional memory T cell responses in calves. PloS One. 2018 Jul;13(7).

7. Yamamoto M, Sato S, Hemmi H, Sanjo H, Uematsu S, Kaisho T, et al. Essential role for TIRAP in activation of the signalling cascade shared by TLR2 and TLR4. Nature. 2002 Nov;420(6913):324–9.

8. Schoenen H, Bodendorfer B, Hitchens K, Manzanero S, Werninghaus K, Nimmerjahn F, et al. Cutting edge: Mincle is essential for recognition and adjuvanticity of the mycobacterial cord factor and its synthetic analog trehalose-dibehenate. J Immunol. 2010 Mar;184(6):2756–60.

9. Ostrop J, Jozefowski K, Zimmermann S, Hofmann K, Strasser E, Lepenies B, et al. Contribution of MINCLE–SYK signaling to activation of primary human APCs by mycobacterial cord factor and the novel adjuvant TDB. J Immunol. 2015 Sep;195(5):2417–28.

10. Schick J, Etschel P, Bailo R, Ott L, Bhatt A, Lepenies B, et al. Toll-like receptor 2 and Mincle cooperatively sense corynebacterial cell wall glycolipids. Infect Immun. 2017 Jun;85(7):e00075-17.

11. Matsumura T, Ikebe T, Arikawa K, Hosokawa M, Aiko M, Iguchi A, et al. Sequential Sensing by TLR2 and Mincle Directs Immature Myeloid Cells to Protect against Invasive Group A Streptococcal Infection in Mice. Cell Rep. 2019 Apr;27(2):561–71.

12. Lee W-B, Kang J-S, Choi WY, Zhang Q, Kim CH, Choi UY, et al. Mincle-mediated translational regulation is required for strong nitric oxide production and inflammation resolution. Nat Commun. 2016 Apr;7(1):1–14.

13. Willems MM, Zom GG, Khan S, Meeuwenoord N, Melief CJ, van der Stelt M, et al. N-tetradecylcarbamyl lipopeptides as novel agonists for toll-like receptor 2. J Med Chem. 2014 Jul;57(15):6873–8.

14. Zom GG, Welters MJ, Loof NM, Goedemans R, Lougheed S, Valentijn RR, et al. TLR2 ligand-synthetic long peptide conjugates effectively stimulate tumor-draining lymph node T cells of cervical cancer patients. Oncotarget. 2016 Oct;7(41):67087.

15. Huber A, Kallerup RS, Korsholm KS, Franzyk H, Lepenies B, Christensen D, et al. Trehalose diester glycolipids are superior to the monoesters in binding to Mincle, activation of macrophages in vitro and adjuvant activity in vivo. Innate Immun. 2016 Aug;22(6):405–18.

16. Winzler C, Rovere P, Rescigno M, Granucci F, Penna G, Adorini L, et al. Maturation Stages of Mouse Dendritic Cells in Growth Factor–dependent Long-Term Cultures. J Exp Med. 1997 Jan;185(2):317–28.

17. Geluk A, van Meijgaarden KE, Janson A, Drijfhout J, Meloen R, de Vries R, et al. Functional analysis of DR17 (DR3)-restricted mycobacterial T cell epitopes reveals DR17-binding motif and enables the design of allele-specific competitor peptides. J Immunol. 1992 Nov;149(9):2864–71.

18. Verreck FA, de Boer T, Langenberg DM, Hoeve MA, Kramer M, Vaisberg E, et al. Human IL-23-producing type 1 macrophages promote but IL-10-producing type 2 macrophages subvert immunity to (myco) bacteria. Proc Natl Acad Sci. 2004 Mar;101(13):4560–5.

19. Verreck FA, de Boer T, Langenberg DM, van der Zanden L, Ottenhoff TH. Phenotypic and functional profiling of human proinflammatory type-1 and anti-inflammatory type-2 macrophages in response to microbial antigens and IFN-γ-and CD40L-mediated costimulation. J Leukoc Biol. 2006 Feb;79(2):285–93.

20. Shi S, Zhu H, Xia X, Liang Z, Ma X, Sun B. Vaccine adjuvants: Understanding the structure and mechanism of adjuvanticity. Vaccine. 2019 May;37(24):3167–78.

21. Bachmann MF, Jennings GT. Vaccine delivery: a matter of size, geometry, kinetics and molecular patterns. Nat Rev Immunol. 2010 Oct;10(11):787–96.

22. Mishra A, Akhtar S, Jagannath C, Khan A. Pattern recognition receptors and coordinated cellular pathways involved in tuberculosis immunopathogenesis: emerging concepts and perspectives. Mol Immunol. 2017 Jul;87:240–8.

23. Short KK, Miller SM, Walsh L, Cybulski V, Bazin H, Evans JT, et al. Co-encapsulation of synthetic lipidated TLR4 and TLR7/8 agonists in the liposomal bilayer results in a rapid, synergistic enhancement of vaccine-mediated humoral immunity. J Controlled Release. 2019 Dec;315:186–96.

24. Liu B, Liu Q, Yang L, Palaniappan SK, Bahar I, Thiagarajan P, et al. Innate immune memory and homeostasis may be conferred through crosstalk between the TLR3 and TLR7 pathways. Sci Signal. 2016 Jul;9(436):ra70–ra70.

25. Bayyurt B, Tincer G, Almacioglu K, Alpdundar E, Gursel M, Gursel I. Encapsulation of two different TLR ligands into liposomes confer protective immunity and prevent tumor development. J Controlled Release. 2017 Feb;247:134–44.

26. Surendran N, Simmons A, Pichichero ME. TLR agonist combinations that stimulate Th type I polarizing responses from human neonates. Innate Immun. 2018 Apr;24(4):240–51.

27. Blufstein A, Behm C, Gahn J, Uitz O, Naumovska I, Moritz A, et al. Synergistic effects triggered by simultaneous Toll-like receptor-2 and-3 activation in human periodontal ligament stem cells. J Periodontol. 2019 Oct;90(10):1190–201.

28. Hu Y, Cong X, Chen L, Qi J, Wu X, Zhou M, et al. Synergy of TLR3 and 7 ligands significantly enhances function of DCs to present inactivated PRRSV antigen through TRIF/MyD88-NF-κB signaling pathway. Sci Rep. 2016 Apr;6:23977.

29. Fischetti L, Zhong Z, Pinder CL, Tregoning JS, Shattock RJ. The synergistic effects of combining TLR ligand based adjuvants on the cytokine response are dependent upon p38/JNK signalling. Cytokine. 2017 Nov;99:287–96.

30. Nouri-Shirazi M, Tamjidi S, Nourishirazi E, Guinet E. TLR8 combined withTLR3 or TLR4 agonists enhances DC-NK driven effector Tc1 cells. Immunol Lett. 2018 Jan;193:58–66.

31. Pashenkov MV, Murugina NE, Budikhina AS, Pinegin BV. Synergistic interactions between NOD receptors and TLRs: Mechanisms and clinical implications. J Leukoc Biol. 2019 Apr;105(4):669–80.

32. Fritz JH, Girardin SE, Fitting C, Werts C, Mengin-Lecreulx D, Caroff M, et al. Synergistic stimulation of human monocytes and dendritic cells by Toll-like receptor 4 and NOD1- and NOD2-activating agonists. Eur J Immunol. 2005 Aug;35(8):2459–70.

33. Tukhvatulin AI, Dzharullaeva AS, Erokhova AS, Scheblyakov DV, Naroditsky BS, Gintsburg AL, et al. NOD1/2 and the C-Type Lectin Receptors Dectin-1 and Mincle Synergistically Enhance Proinflammatory Reactions Both In Vitro and In Vivo. J Inflamm Res. 2020 Jul;13:357.

34. Toy R, Keenum MC, Pradhan P, Phang K, Chen P, Chukwu C, et al. TLR7 and RIG-I dual-adjuvant loaded nanoparticles drive broadened and synergistic responses in dendritic cells in vitro and generate unique cellular immune responses in influenza vaccination. J Controlled Release. 2021 Feb;

35. Van Haren SD, Dowling DJ, Foppen W, Christensen D, Andersen P, Reed SG, et al. Age-specific adjuvant synergy: dual TLR7/8 and mincle activation of human newborn dendritic cells enables Th1 polarization. J Immunol. 2016 Dec;197(11):4413–24.

36. Tukhvatulin AI, Gitlin II, Shcheblyakov DV, Artemicheva NM, Burdelya LG, Shmarov MM, et al. Combined stimulation of Toll-like receptor 5 and NOD1 strongly potentiates activity of NF-κB, resulting in enhanced innate immune reactions and resistance to Salmonella enterica serovar Typhimurium infection. Infect Immun. 2013 Jul;81(10):3855–64.

37. Decout A, Silva-Gomes S, Drocourt D, Barbe S, André I, Cueto FJ, et al. Rational design of adjuvants targeting the C-type lectin Mincle. Proc Natl Acad Sci. 2017 Mar;114(10):2675–80.

38. Smith AJ, Miller SM, Buhl C, Child R, Whitacre M, Schoener R, et al. Species-specific structural requirements of alpha-branched trehalose diester Mincle agonists. Front Immunol. 2019 Feb;10:338.

39. Kiyotake R, Oh-Hora M, Ishikawa E, Miyamoto T, Ishibashi T, Yamasaki S. Human Mincle Binds to Cholesterol Crystals and Triggers Innate Immune Responses. J Biol Chem. 2015 Oct;290(42):25322–32.

40. Hunter RL, Olsen MR, Jagannath C, Actor JK. Multiple roles of cord factor in the pathogenesis of primary, secondary, and cavitary tuberculosis, including a revised description of the pathology of secondary disease. Ann Clin Lab Sci. 2006;36(4):371–86.

41. Hawn TR, Misch EA, Dunstan SJ, Thwaites GE, Lan NT, Quy HT, et al. A common human TLR1 polymorphism regulates the innate immune response to lipopeptides. Eur J Immunol. 2007 Aug;37(8):2280–9.

42. Mikacenic C, Reiner AP, Holden TD, Nickerson DA, Wurfel MM. Variation in the TLR10/TLR1/TLR6 locus is the major genetic determinant of interindividual difference in TLR1/2-mediated responses. Genes Immun. 2013 Jan;14(1):52–7.

43. Dittrich N, Berrocal-Almanza LC, Thada S, Goyal S, Slevogt H, Sumanlatha G, et al. Toll-like receptor 1 variations influence susceptibility and immune response to *Mycobacterium tuberculosis*. Tuberculosis. 2015 May;95(3):328–35.

44. Kranzer K, Bauer M, Lipford G, Heeg K, Wagner H, Lang R. CpG-oligodeoxynucleotides enhance T-cell receptor-triggered interferon-γ production and up-regulation of CD69 via induction of antigen-presenting cell-derived interferon type I and interleukin-12. Immunology. 2001 Dec;99(2):170–8.

45. Gelman AE, LaRosa DF, Zhang J, Walsh PT, Choi Y, Sunyer JO, et al. The adaptor molecule MyD88 activates PI-3 kinase signaling in CD4+ T cells and enables CpG oligodeoxynucleotide-mediated costimulation. Immunity. 2006 Nov;25(5):783–93.

46. Komai-Koma M, Jones L, Ogg GS, Xu D, Liew FY. TLR2 is expressed on activated T cells as a costimulatory receptor. Proc Natl Acad Sci. 2004 Mar;101(9):3029–34.

6

Summary and prospects

The research described in this Thesis was aimed at designing and synthesizing nature-inspired compounds as part of TB vaccine discovery. A variety of synthetic analogues of mycobacterial cell wall components, from peptide and glycolipid antigens to glycolipid pathogen-associated molecular patterns (PAMPs) has been accessed. Evaluation of the immune stimulatory activity of the novel compounds in combination with preliminary immunization studies *in vivo,* suggested the potential of selected synthetic conjugates as single molecule vaccines against TB. Further research is needed to verify the efficacy of these vaccine modalities.

Chapter 1 provides an overview of the interaction of *Mtb* with the human immune system, with emphasis on new TB vaccine strategies in preclinical and in clinical trials. The key players of the human immune system are introduced and a general overview of the tools available for the rational design of vaccines is provided to set the context for the research presented in this Thesis.

Chapter 2 focuses on the design and synthesis of *Mtb* glycolipid CD1c binding molecules. Three stabilized mannosyl phosphomycoketide (MPM) analogues, comprising a carba-mannose and two C-mannosides, were generated and evaluated for their ability to bind to CD1c molecules and elicit a T cell response. Antigens presented by the CD1c system are of great value for vaccine discovery, given the non-polymorphic nature of the different CD1 (a-e) proteins across humans.[1] This research aimed at generating MPM analogues with improved stability as compared to the natural mycobacterial glycolipid by creating hydrolysis-resistant bonds between the carbohydrate and phospholipid moiety. As it is not possible to determine *a priori* how these modifications impact the binding to the CD1c protein and presentation to T cells, three different stabilized analogues were generated. One of the three MPM analogues, the difluoro-C-mannoside, was shown to be resistant to degradation in APCs and to be cross-reactive with the natural MPM, while the other two were shown to be less effective mimics. Further studies are needed to explore the function and potential of the stabilized difluoro antigen including immunization studies in CD1c-expressing species, such as transgenic mice expressing the human CD1c protein or guinea pigs that naturally express several CD1c genes.[2] Depending on the outcome of these studies, immunization experiments followed by infection with *Mtb* are envisioned to assess the potential of this antigen in prophylactic vaccines.

Chapter 3 combines the design and synthesis of conjugation-ready *Mtb* glycolipid Mincle ligands with the synthesis and *in vitro/in vivo* immunological evaluation of a fully synthetic single molecule vaccine modality. Two trehalose dimycolate (TDM) and two glucose monomycolate (GMM) analogues are synthesized and their ability to interact with Mincle was assessed. A validated peptide antigen, derived from the Mtb Rv1733 latency protein-antigen, was chemically linked to the TDM analogues to generate two synthetic conjugates and the innate stimulatory activity of these compounds was assessed on human DCs, M1 and M2 cells. Finally, one conjugate was employed in a study to immunize HLA-DR3/Ab^0 mice, and the results of these studies indicated the potential of the conjugate to induce humoral and protective immunity against *Mtb*, interestingly and unexpectedly in the absence of detectable T cell responses. In a preliminary immunization study, it was shown that IgG1 and IgG2b antibody responses could be induced accompanied by a reduction of the bacterial load in the spleen of immunized mice. For the synthesis of the conjugates containing Mincle ligands, a maleimido-propionic acid was used to extend the oligopeptide at the N-terminus end and the generated peptide was conjugated to the

thiol-functionalized adjuvants in solution. This conjugation strategy required the design of conjugation-ready Mincle ligands which had not been described before. Two factors were considered in the design of the ligands: orthogonality of the ligation handle in anticipation of the extension of the single molecule strategy to include multiple PAMPs (in this case to include the TLR2 ligand described in Chapter 4); the position of the ligation handle and the definition of the length (and number) of lipid chains to prevent loss of binding to the receptor. The results from the HEK-murine Mincle revealed that functional binding to murine Mincle was retained for the two synthetic analogues generated. The length of the 6'-OH lipid chain influences the extent of the stimulatory activity of the two Mincle ligands on selected human antigen-presenting cells and further research is needed to determine the relationship between the lipid chain length and the biological activity. Although most studies have been focused on defining the biological function of trehalose glycolipids in relation to Mincle, there is recent evidence that the natural Mincle ligand, TDM, and its well-known analogue TDB are regulating macrophage response in a Mincle-dependent and Mincle-independent way.[3–5] Preliminary experiments performed using soluble human Mincle, DC-SIGN, Dectin-1 and Mannose receptor suggest that the trehalose derivatives used in this research can interact with human Mincle and other C-type lectin receptors (see Figure 1).

However, these results do not formally prove that the two Mincle ligands generated in this Chapter would interact with C-type lectin receptors in a cellular system nor that binding would be functional. To better understand the result of binding to these lectins, further studies could address the binding affinities of TDM analogues to a panel of relevant CLRs, and determine the influence of binding to these receptors on the immunological and functional effects of the different analogues on APCs.

A vaccine formulation containing the TDM analogue TDB has been previously studied and shown to polarize cellular immune responses towards a Th1/Th17 phenotype in a murine model.[6] In that study, TDB was used in combination with the surfactant dimethyldioctadecylammonium (DDA) forming the cationic liposomal CAF01 adjuvant system. However, there is no clear definition, nor consensus, how the formulation affects binding and activation of Mincle. No explanation can yet be provided to account for potential interspecies differences in Mincle. In the case of Mincle-cholesteryl stearate interaction, it has been hypothesized that multivalent presentation of the ligand may be necessary for binding to the human, but not murine receptor.[7]

To compare the immune-stimulatory effects of the synthetic conjugate in solution to that of the conjugate incorporated in a cationic liposomal formulation, containing 1,2-dioleoyl-*sn*-glycero-3-phosphocholine (DOPC) and N-1-(2,3-Dioleoyloxy)propyl-N,N,N-trimethylammonium methyl-sulfate (DOTAP) in a 4:1 ratio, the innate stimulatory activity was assessed on human DCs. The extent of cellular activation and expression of T cell co-stimulatory molecules on DCs was significantly increased

upon incorporation of the conjugate in the liposomal formulation (data not shown), and so was the amount of IL-12p40 and IL-10 released by the cells as shown in Figure 2. The evaluation of the vaccine potential of the cationic formulations containing the conjugate in a murine system is ongoing.

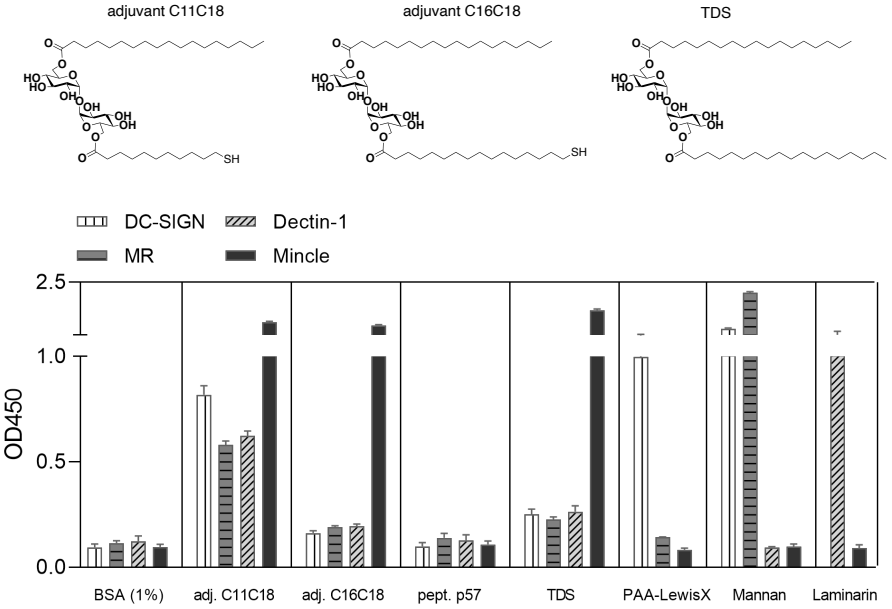

Figure 1 - Binding of compounds to soluble forms of DC-SIGN, Dectin-1, Mannose receptor (MR), Mincle. ELISA experiment was performed using plate-bound glycolipids (chemical structures shown above) and control compounds. TDS = Trehalose distearate (5 nmol/well), PAA-LewisX (10 μg/ml), Mannan (10 μg/ml) and Laminarin (3 μg/ml) and the reference peptide (5 nmol/well) were chosen as negative controls. The soluble human receptors carrying an Fc-portion were used for assaying binding interaction. Bars represent mean + SEM of duplicates from two independent experiments.

Chapter 4 describes the synthesis and immunological evaluation of conjugates containing UPam, a known TLR2 ligand, and three antigenic *Mtb*-derived peptides. The ability of the constructs to bind to human TLR2 was demonstrated. The innate immune system stimulatory activity of these conjugates was assessed on DCs, M1 and M2 cells. One conjugate was tested in an antigen-presentation assay with the available T cell clone to verify that the peptide antigen presentation to $CD4^+$ T cells was not affected by conjugation to the TLR2 ligand. Finally, the *in vivo* vaccine potential of one conjugate was suggested by the ability of the synthetic compound to induce, after subcutaneous immunization of HLA-DR3/Ab^0 mice, a Th17 cellular and a highly diversified humoral immune response, together with protective immunity against *Mtb*.

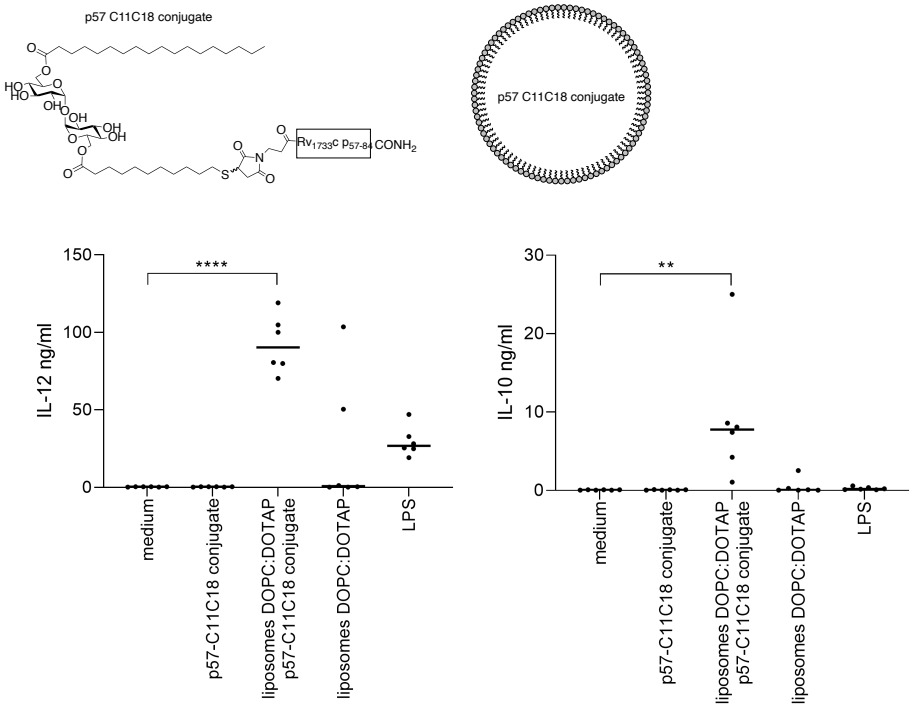

Figure 2 - Cytokine production profile of human monocyte-derived dendritic cells stimulated with the solubilized p57-C11C18 conjugate or the same conjugate incorporated in a liposomal formulation containing the lipids DOPC:DOTAP in a 4:1 molar ratio. IL-12p40 and IL-10 amounts present in supernatant were measured by ELISA for n = 6 donors. Each dot corresponds to mean of two replicates from one donor; horizontal line corresponds to the grand median for each treatment group, as calculated using GraphPad Prism. p values are indicated in the graph above the relative couple of conditions and they are calculated using one-way ANOVA by GraphPad Prism (****$p < 0.0001$, **$p < 0.01$). LPS (100 ng/ml) is used as a positive control.

A major asset of the use of peptide antigens is that they can be synthesized using automated solid phase synthesis without the need of intermediate purification steps. Final purification of the full-length peptide, usually carried out on an automated HPLC system, delivers a highly pure compound that is free of biological impurities. Chemical methods can be developed to extend the peptide with other molecular components in-line during the automated solid phase synthesis without removal of the peptide from the resin before conjugation. In view of the generation and immunological assessment of a single-molecule vaccine, UPam which is a synthetic lipopeptide analogue of Pam_3Cys, was selected for conjugation to the three *Mtb*-derived peptides. This TLR2/1 agonist was built via peptide couplings directly on the growing oligopeptide at the N-terminal end. Despite the differences in

physicochemical properties of the three peptides, all synthetic conjugates retained the ability to activate HEK-293 cells via the human TLR2, albeit to a different extent. Overall, the work presented provided evidence for the ability of *Mtb*-derived peptide conjugates containing a TLR2/1 ligand to induce strong *in vitro* activation of human DCs and macrophages, key players in bridging the innate and adaptive immune response. The results further suggested that antigen-presentation by DCs and monocytes to human cloned $CD4^+$ T cells is neither increased nor decreased by stimulation with the conjugate as compared to stimulation with the reference peptide. Whether the activation of human APCs results in the induction of a protective humoral or cellular adaptive immune response requires further investigation.

The vaccine potential of one of the UPam-peptide conjugates described in this Thesis was preliminarily assessed using a murine model system, suggesting that a cellular Th17 immune response is initiated and that antigen-specific IgG antibodies are present in the sera as a result of immunization. This response corresponded to the induction of protective immunity against a live *Mtb* challenge in the same transgenic murine model. While differences in the murine and human immune system limits the generalizability of the results, this approach provides new insight in the efficacy of a single molecule vaccination strategy. The versatility and modularity that is intrinsic to peptide-conjugate vaccines represents a powerful tool to screen for different adjuvant-antigen couples. To expand this strategy to known synthetic PAMPs recognized by either TLR9 or TLR4, the synthetic strategies shown in Figure 3 were devised and partly implemented for the generation of two other synthetic conjugates.

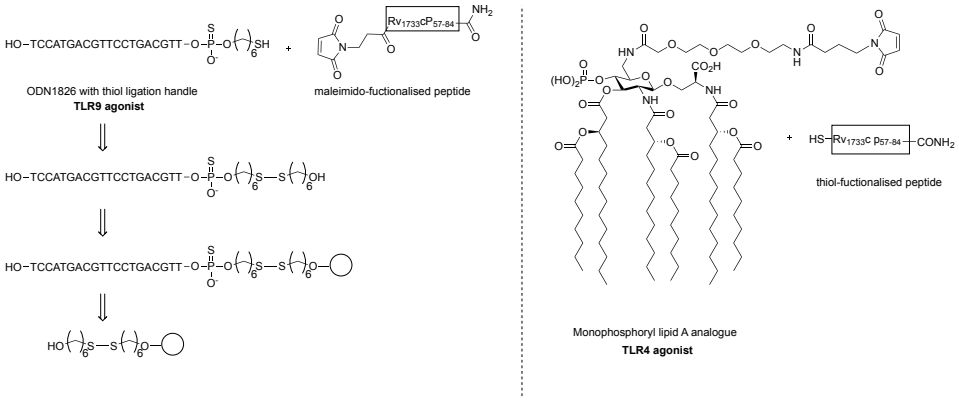

Figure 3 – Synthetic strategies devised for the generation of novel TLR9 ligand-peptide and TLR4 ligand-peptide conjugates.

In summary, the 3'-disulfide modified CpG oligonucleotide was synthesized using an automated solid phase synthesizer, then purified using ion-exchange chromatography and treated with dithiothreitol to reduce the disulfide. A conjugation to the maleimide-functionalized peptide would lead to the generation of desired target ODN1826-peptide conjugate. The CpG oligonucleotide ODN1826, whose sequence is shown in Figure 3, has previously been shown to function as molecular adjuvant in combination with SLPs and induce protective responses against *Mtb*.[8] To target TLR4, a conjugate containing a peptide linked to a monophosphoryl lipid A (MPL) analogue, CRX-527, can be readily generated via a maleimide-thiol conjugation, as previously demonstrated for a different peptide.[9] MPL has been shown to possess strong adjuvanticity and diminished toxicity as compared to the naturally occurring TLR4 agonist, lipid A.[10,11]

Chapter 5 provides insight in the effects of Mincle/TLR2 co-stimulation on murine and human dendritic cells. For this purpose, two synthetic adjuvants were generated, namely trehalose distearate, a Mincle agonist,[12] and Upam-SK_4, a TLR2 agonist.[13] To improve the composition of current or novel vaccines, it is of relevance to understand possible synergistic/antagonistic effects of different PAMPs. With the overarching goal of eventually generating single molecule conjugate vaccines containing a peptide and two or more different adjuvants, explorative studies were performed to identify the innate stimulatory/inhibitory activity of the combination of different synthetic PAMPs. Although studies using murine macrophages suggest potential synergistic activation by TLR2 and Mincle stimulation,[14] co-stimulation of murine or human dendritic cells using well-defined agonists for these two receptors has not yet been explored. In murine dendritic cells, signaling via both receptors increases the expression of activation markers with respect to single TLR2 or Mincle activation, although to a limited extent. The studies performed on human monocyte-derived dendritic cells showed that an increase in production of IL-6 and TNF-α could be detected, but only at a specific concentration range. However, the absence of cytokine production when only Mincle was activated, points to possible synergistic activity of TDS with UPam. To better define the role played by the two ligands in the activation of human DCs and understand the interaction between the two receptors, mechanistic studies are required. Experiments using blocking antibodies for TLR2 and Mincle would be a logical first step to obtain further molecular proof of ligand receptor interaction.

Overall, the research described in this Thesis encompasses design and synthesis of several synthetic vaccine components, antigens and adjuvants, of relevance in the context of mycobacterial infection. Organic synthesis is combined to immunological assays to identify relevant biologically active analogues of naturally occurring compounds to be used as ingredients in soluble or liposomal subunit vaccines. This research resulted in the identification of novel interesting CD1c ligands, which are stable to most common hydrolytic conditions, novel analogues of the Mincle-binding

trehalose dimycolate and a library of Mincle-ligand or TLR2-ligand peptide conjugates with *in vitro* and/or *in vivo* activity.

Materials and methods

ELISA using C-type lectin receptors

Recombinant Human DC-SIGN/CD209 Fc Chimera Protein and recombinant Human CLEC4E Fc Chimera Protein were purchased from RD systems and used at concentrations of 1.5 μg/ml and 0.83 μg/ml respectively. Fc-hDectin-1a was purchased from InvivoGen and used at a concentration of 3 μg/ml. Cys-MR-Fc fusion protein (hydrophobic signal sequence and the first 139 residues of human MR, a 2-residue linker, and the Fc region of human IgG1) was produced in 293T cells, according to published procedure[15] and supernatant was directly used in the ELISA experiments without further purification. Control compound PAA-Lewis X was purchased from Lectinity (MW approx. 20 KDa, Carbohydrate content around 20% mol). Laminarin (from Laminaria digitata) and Mannan (from Saccharomyces cerevisiae) were purchased from Sigma-Aldrich. All synthetic compounds were dissolved in iso-propanol and were transferred to 96 well plates (Nunc MaxiSorp, Biolegend) at three different concentrations (5 - 1 - 0.2 nmol/well) for a total volume of 50 μL/well. The solvent was evaporated at 50°C. Control compounds Laminarin (3 μg/ml), PAA-Lewis X (1 μg/ml) and Mannan (1 μg/ml) were diluted in PBS and used to coat remaining wells for a total volume of 50 μL/well. After coating for 2 hours at room temperature, all the wells were washed twice with TMS (20 mM tris(hydroxymethyl)aminomethane (Tris)-HCl, pH 8.0; 150 mM NaCl; 1 mM $CaCl_2$; 2 mM $MgCl_2$) (150μL) and blocked with 100 μL TMS with 1% of BSA (Fraction V, Merk Millipore) for 30 min at room temperature. The plates were then incubated for 1 hour at room temperature with 50 μL soluble receptor in TMS with 1% of BSA. The wells were washed two times with TMS (150μL) and incubated at room temperature with 50 μL of Goat-anti human HRP (0.8 μg/mL, JacksonImmuno) in TMS with 1% of BSA for 30 min. After two washes with TMS (150μL), 50 μL of substrate solution (3,3,5,5-Tetramethylbenzidine, TMB, in citric/acetate buffer, pH=4, and H_2O_2) were added and after 2 min at room temperature the reaction was stopped with 50 μL of H_2SO_4 (0.8M). Sample absorbance at 450 nm was measured using a Spectramax i3x (Molecular Devices, CA, USA) spectrometer. All samples were tested in duplicate.

ODN1826 and p57-ODN1826 synthesis

Thiol-functionalized ODN1826 was synthesized on an Expedite automated solid phase synthesizer (PerSeptive Biosystems), using 3' Thiol Modifier C6 SS Glyc CPG (Biosearch technologies) as solid support. Reaction scale 10 μmol based on solid support loading. Oligonucleotide elongation was performed using an established protocol.[16] In summary, elongation was performed using 5'-DMT-protected 3'-phosphoramidite derivatives in the presence of dicyanoimidazole as coupling agent. After each coupling, remaining free 5'-hydroxyls were capped using a solution of t-butylphenoxyacetic anhydride/1-methylimidazole in THF/pyridine, followed by sulfurization of the phosphite to phosphorothioate using the Beaucage reagent. The DMT protecting groups on the 5'-position were then removed using trichloroacetic acid, after which the elongation process was

continued. Cleavage from the resin was performed using a solution of 25% NH_4OH in water to give the desired 3'-disulfide modified ODN (ODN-SS-hexyl-OH). This compound was purified with ion exchange chromatography on an AKTA Explorer system using a Q-Sepharose column (source-Q 10 x 100 mm) and the following running buffer solutions: buffer A = 25 mM NaOAc with 25 mM $NaClO_4$; buffer B = 25mM NaOAc with 500 mM $NaClO_4$. Gradient used for purification: 25% to 75% B in A, over 50 minutes (flow 4 ml/min). Fractions containing the pure product were combined and lyophilized three times using new aliquots of Endotoxin-free water (Sigma) to yield disulfide ODN compound as a white solid (9.1 mg, 1.35µmol, 13.5%). Quantification was performed by UV absorbance at 260 nm. LC-MS analysis: (C18 column with 10 mM NH_4OAc, linear gradient 00→50% B, 11 min): Rt = 5.980 min. CpG-SS-hexyl-OH (3.4 mg, 0.5µmol, 1 eq) was deprotected overnight in 2 ml dithiothreitol (DTT) buffer (350 mg DTT, 260 mg of NaOAc 3 H_2O in 10ml endotoxin-free water). The resulting reduced CpG-SH was purified using a PD-10 column which was pre-equilibrated using a 50 mM phosphate solution (25 mM Na_2HPO_4, 25 mM NaH_2PO_4, 1 mM EDTA) which was already degassed and flushed with Argon. The filtrate (3.25 ml) was directly transferred to a tube containing the maleimide-functionalized peptide (10 mg, 3µmol, 6 eq). The resulting solution was degassed, sonicated and stirred under Argon for two days at RT. The CpG-peptide conjugate was isolated after gel-filtration on a superdex 75 column (16 x 60 mm) with isocratic gradient of 0.15 M NH_4OAc and further purified by RP-HPLC using a C18-column (10 x 250 mm) with 10 mM NH_4OAc and a gradient of 5 to 30% acetonitrile in water over 15 minutes. Fractions containing the pure product were combined and lyophilized three times using new aliquots of Endotoxin-free water to yield the synthetic conjugate as a white powder (2.6 mg, 272 nmol, 54%). Quantification was performed by UV absorbance at 260 nm. LC-MS analysis: (C18 column with 10 mM NH_4OAc, linear gradient 50→90% B, 15 min): Rt = 7.222 min, ESI-MS $[M+H]^{10+}$=972.5 found, 971.7 calculated, ESI-MS $[M+H]^{8+}$= 1215.7 found, 1214.4 calculated. MALDI-TOF $[M+NH_4]^+$: 9724.051 found, 9725.164 calculated.

Generation of DOPC:DOTAP liposomes

DOPC/DOTAP (4:1 molar ratio) liposomes were prepared using the thin-film hydration method. First, a thin lipid film was formed by adding stock solutions of DOTAP and DOPC in chloroform (25 mg/mL) to a round-bottomed flask, followed by evaporation of the organic solvent of the lipids using a rotary evaporator. Hereafter, p57-C11C18 conjugate in DMSO (nothing was added for the empty liposomes) was added to the round-bottomed flasks, and the formulation was homogenized by adding 5 glass beads and swirling them around to remove the lipid film from the glass wall. The formulations were transferred to 15 ml tubes, and the round-bottomed flask was rinsed 4 times, each time with 1 mL of Milli-Q water, which was added to the tubes to make sure that the main part of the formulation was transferred. The liposomes were snap-frozen in liquid nitrogen followed by lyophilization overnight. The resulting lipid cakes were rehydrated in 10 mM phosphate buffer (PB) (pH 7.4) to reach a total lipid concentration of 10 mg/mL and 77.2 nmol of p57-C11C18 conjugate (305 µg/mL). Rehydration was performed in three steps, where 25%, 25%, and 50% of the total volume (2 mL) were added with 30 min intervals at 60°C. After the last addition, the formulations equilibrated for 1 hour at 60°C, the obtained liposomes were extruded (Lipex 1.5 mL extruder, TransferraNanosciences, Burnaby, Canada) simultaneously through stacked polycarbonate filters with a pore size of 400 and 200 nm, six times at 60°C. Free molecules were removed by dialysis (24 hours, RT) using a Float-A-Lyzer G2 with a 100 kDa molecular weight cut-off

(MWCO) (Repligen, Waltham, MA, USA) and 10 mM PB in the dialysate. The obtained liposomal formulations were stored at 4°C until further use.

Particle size and zeta potential measurements

The formulations were diluted twenty-fold in 10 mM PB. The intensity-weighted average hydrodynamic diameter (Z-average) and polydispersity index (PDI) of the particles were determined by dynamic light scattering (DLS) and the zeta potential was determined by laser Doppler electrophoresis. Measurements were conducted in triplicates at 25°C using a nano ZS zetasizer coupled with a 633 nm laser and 173° optics (Malvern Instruments, Worcestershire, UK) and analyzed using Zetasizer Software v7.12 (Malvern Instruments).

Liposomes (DOPC:DOTAP 4:1)	***Size (nm)***	***PDI***	***ZP (mV)***
Empty	*121,2333*	*0,0959*	*33,69*
p57-C11C18 conjugate	*136,3667*	*0,1216*	*28,39*

Generation and stimulation of immature human moDCs using liposomes

Buffy coats of healthy human Blood Bank donors were purchased from Sanquin Amsterdam. $CD14^+$ monocytes were isolated from whole blood using Ficoll-Paque density gradient followed by purification on autoMACS® Pro Separator instrument using CD14 MicroBeads (MACS, Miltenyi Biotec, Bergisch Gladsbach, Germany). The monocytes were differentiated to monocyte-derived dendritic cells (moDCs) at a concentration of 10^6 cells/mL in RPMI 1640 (Gibco, PAA, Linz, Austria) medium containing 10% FCS (Hyclone, GE Healthcare Life Sciences, Eindhoven, the Netherlands), 2 mM GlutaMAX™ (Gibco, PAA, Linz, Austria), 100 U/ml penicillin, 100 μg/ml streptomycin and 10 ng/mL GM-CSF (Life Technologies-Invitrogen, Bleiswijk, the Netherlands) and 10 ng/mL IL-4 (Peprotech, Rocky Hill, NJ). On day 3, all cultures were replenished with fresh culture media with the appropriate concentrations of GM-CSF and IL-4. Cells were incubated for 5 days at 37°C and in a 5% CO_2 atmosphere incubator. Immature dendritic cells were then harvested, counted and transferred to 96 well plates (round bottom, Corning Costar TC-Treated Microplates, Corning, NY) at 50.000 cells/well. The next day cells were stimulated for three hours, before the supernatant was discarded and replaced by medium before overnight incubation, using synthetic compounds (20 μM concentration) or liposomes (100 μg/ml concentration of the lipids DOPC:DOTAP in a 4:1 molar ratio; 0.89 μg/ml = 0.22 nmol/ml synthetic conjugate concentration in the final formulation). The synthetic compounds were dissolved in DMSO at a concentration of 5 nmol/μL, further diluted and premixed in RPMI 1640 medium containing 10% FCS, 2 mM GlutaMAX™, 1% Pen-Strep; the liposomes were diluted in the same medium at described concentration. LPS (100 ng/ml) was used as positive control for stimulated cells. Supernatants were harvested 20 hours after the initial addition of stimuli for subsequent analysis of cytokines.

Human IL-12(p40) and IL-10 ELISA

Human IL-12/IL-23 (p40) and human IL-10 ELISA kits were purchased from Biolegend (ELISA MAX™ Standard Set; London, UK). All supernatants were tested in triplicates according to manufacturer's instructions. Sample absorbance was measured using a Spectramax i3x (Molecular Devices, CA, USA) spectrometer.

References

1. Moody DB, Zajonc DM, Wilson IA. Anatomy of CD1–lipid antigen complexes. Nat Rev Immunol. 2005 May;5(5):387–99.

2. van Rhijn I, Ly D, Moody DB. CD1a, CD1b, and CD1c in Immunity Against Mycobacteria. In: The New Paradigm of Immunity to Tuberculosis. New York, NY: Springer New York; 2013. p. 181–97. (Advances in Experimental Medicine and Biology; vol. 783).

3. Braganza CD, Teunissen T, Timmer MSM, Stocker BL. Identification and Biological Activity of Synthetic Macrophage Inducible C-Type Lectin Ligands. Front Immunol. 2018 Jan 17;8:1940.

4. Hansen M, Peltier J, Killy B, Amin B, Bodendorfer B, Härtlova A, et al. Macrophage Phosphoproteome Analysis Reveals MINCLE-dependent and -independent Mycobacterial Cord Factor Signaling. Mol Cell Proteomics. 2019 Apr;18(4):669–85.

5. Ostrop J, Jozefowski K, Zimmermann S, Hofmann K, Strasser E, Lepenies B, et al. Contribution of MINCLE–SYK signaling to activation of primary human APCs by mycobacterial cord factor and the novel adjuvant TDB. J Immunol. 2015 Sep;195(5):2417–28.

6. Lindenstrøm T, Woodworth J, Dietrich J, Aagaard C, Andersen P, Agger EM. Vaccine-Induced Th17 Cells Are Maintained Long-Term Postvaccination as a Distinct and Phenotypically Stable Memory Subset. Infect Immun. 2012 Oct;80(10):3533–44.

7. Kiyotake R, Oh-Hora M, Ishikawa E, Miyamoto T, Ishibashi T, Yamasaki S. Human Mincle Binds to Cholesterol Crystals and Triggers Innate Immune Responses. J Biol Chem. 2015 Oct;290(42):25322–32.

8. Coppola M, van den Eeden SJF, Wilson L, Franken KLMC, Ottenhoff THM, Geluk A. Synthetic Long Peptide Derived from *Mycobacterium tuberculosis* Latency Antigen Rv1733c Protects against Tuberculosis. Pascual DW, editor. Clin Vaccine Immunol. 2015 Sep;22(9):1060–9.

9. Reintjens NRM, Tondini E, de Jong AR, Meeuwenoord NJ, Chiodo F, Peterse E, et al. Self-Adjuvanting Cancer Vaccines from Conjugation-Ready Lipid A Analogues and Synthetic Long Peptides. J Med Chem. 2020 Oct 22;63(20):11691–706.

10. Qureshi N, Takayama K, Ribi E. Purification and structural determination of nontoxic lipid A obtained from the lipopolysaccharide of Salmonella typhimurium. J Biol Chem. 1982 Oct;257(19):11808–15.

11. Behzad H, Huckriede ALW, Haynes L, Gentleman B, Coyle K, Wilschut JC, et al. GLA-SE, a Synthetic Toll-like Receptor 4 Agonist, Enhances T-Cell Responses to Influenza Vaccine in Older Adults. J Infect Dis. 2012 Feb 1;205(3):466–73.

12. Williams SJ. Sensing Lipids with Mincle: Structure and Function. Front Immunol. 2017 Nov 27;8:1662.

13. Willems MM, Zom GG, Khan S, Meeuwenoord N, Melief CJ, van der Stelt M, et al. N-tetradecylcarbamyl lipopeptides as novel agonists for toll-like receptor 2. J Med Chem. 2014 Jul;57(15):6873–8.

14. Lee W-B, Kang J-S, Choi WY, Zhang Q, Kim CH, Choi UY, et al. Mincle-mediated translational regulation is required for strong nitric oxide production and inflammation resolution. Nat Commun. 2016 Apr;7(1):1–14.

15. Liu Y, Chirino AJ, Misulovin Z, Leteux C, Feizi T, Nussenzweig MC, et al. Crystal Structure of the Cysteine-Rich Domain of Mannose Receptor Complexed with a Sulfated Carbohydrate Ligand. J Exp Med. 2000 Apr 3;191(7):1105–16.

16. Khan S, Bijker MS, Weterings JJ, Tanke HJ, Adema GJ, van Hall T, et al. Distinct Uptake Mechanisms but Similar Intracellular Processing of Two Different Toll-like Receptor Ligand-Peptide Conjugates in Dendritic Cells. J Biol Chem. 2007 Jul;282(29):21145–59.

Nederlandse Samenvatting

Het onderzoek in dit proefschrift beschrijft het ontwerp en de synthese van natuurlijke verbindingen als onderdeel voor een toekomstig tuberculose (TB) vaccin. De natuurlijke verbindingen hierin beschreven bestaan uit peptides, glycolipide antigenen en glycolipidische pathogen associated molecular patterns (PAMPs). Evaluatie van de gesynthetiseerde verbindingen in combinatie met voorlopige *in vivo* immunisatiestudies, lieten de potentie zien van synthetische conjugaten als "single molecule" vaccins tegen TB. Verder onderzoek is nodig om de werkzaamheid van deze potentiele vaccins te verifiëren.

Hoofdstuk 1 bevat een overzicht van de interacties tussen *Mycobacterium tuberculosis* (Mtb) en het menselijk immunsysteem. Verder wordt hier dieper ingegaan op huidige vaccin strategieën en vaccins die op dit moment klinische proeven ondergaan. Tot slot wordt de gedachte achter het ontwerp van de verbindingen, die in dit proefschrift beschreven worden uitgelegd.

Hoofdstuk 2 beschrijft het ontwerp en de synthese van gestabiliseerd mannose fosfomycoketide (MPM), een stof die de menselijke T-cel reactie tegen de natuurlijke Mtb glycolipiden stimuleert. Drie gestabiliseerde MPM analogen zijn gesynthetiseerd en getest op hun antigeniciteit and kruisreactiviteit met natuurlijk MPM. Deze testen gaven belangrijke inzichten wat betreft MPM presentatie door het CD1c eiwit.

Het eerste biologisch actieve conjungaat vaccin dat bestaat uit een peptide covalent gebonden aan een synthetisch analoog van een Mtb glycolipide (trehalose dimycolate, TDM) staat beschreven in **Hoofdstuk 3**. De synthese van vier verschillende op TDM geinspireerde glycolipides wordt hier beschreven samen met de *in vitro* karakterisatie van de conjungaten hiervan. Data verkregen uit muisproeven wijst naar een sterkere humorale immuniteits reactie, als gevolg van deze conjungaten.

In **Hoofdstuk 4** wordt de activatie van TLR2 door verscheidene Upam peptide conjungaten verkend, voor de inductie van antimycobacteriële reacties. Drie conjungaten zijn gesynthetiseerd, waarvan biologische experimenten lieten zien dat ze activatie van menselijke dendritische cellen en macrofagen sterk opwekken *in vitro*. Verdere *in vitro* experimenten suggereerde dat antigeen presentatie aan T-cellen niet werd beïnvloed door de conjungatie aan een TLR ligand. Één van deze conjungaten is gebruikt bij een immunisatie studie in muizen, waarbij voorlopige data leek te wijzen op zowel een humorale als een cellulaire reactie.

In **Hoofdstuk 5** wordt de de synthese van twee liganden beschreven, die in staat zijn te binden met Mincle en TLR2. Deze liganden zijn vervolgens *in vitro* onderzocht op functionele synergieën. Hieruit kwam naar voren dat bij bepaalde concentraties inderdaad een synergetisch effect kon worden bereikt. Dit effect leidde tot een toename van cytokine productie in menselijke dendritische cellen, die zijn afgeleid van monocyten. T-cel antigen presentatie experimenten zijn uitgevoerd, die er op wezen dat co-stimulatie de presentatie niet verder zou verhogen.

Hoofdstuk 6 bevat een samenvatting van de behaalde resultaten, die in dit proefschrift beschreven staan, samen met een uiteenzetting van de volgende stappen die nodig zijn voor de toemkomstige ontwikkeling, verfijning en implementatie voor synthetische Mtb vaccins.

About the Author

Laura Marino was born on the 9th of October 1990 in Villaricca, Italy. After completing her secondary education at the Istituto Pluricomprensivo Renato Cartesio in 2008, she commenced her studies in Chemistry at the Università degli Studi di Milano, Italy. She received her bachelor's degree in 2012 after completing her research internship in the group of dr. Giorgio Molteni. After one sabbatical year spent in the United Kingdom, she started her Master's degree in Chemical Sciences at the Università degli studi di Milano, Italy. To sponsor her studies, she undertook a paid 10-months internship at the European Patent Office in Rijswijk, the Netherlands. After being awarded two scholarships, she conducted a joint research internship in Biochemistry under the supervision of Tim P. Hogervorst in the groups of prof. dr. Gijs A. van der Marel, Universiteit Leiden, and prof. dr. Luigi Lay, Università degli studi di Milano, focusing on the synthesis of carbohydrates to investigate their immunomodulatory properties. After obtaining her master degree in Chemical Sciences in 2016, she started her doctoral studies at the Universiteit Leiden with the guidance of prof. dr. Jeroen D.C. Codée and prof. dr. Tom H.M. Ottenhoff, combining chemistry and immunology. At the time of submission of her dissertation, Laura is working as a Scientist at Sanquin Reagent B.V. in Amsterdam.

Acknowledgments

First of all, I would like to thank Prof. dr. Jeroen Codée and Prof. dr. Gijs van der Marel for giving me the opportunity to pursue my PhD in their group, for their guidance and for granting me with the freedom to explore and create my own path. I would like to thank Prof. dr. Tom Ottenhoff for welcoming me at the INZI group, providing mentorship and making me feel part of a team. I thank Dr. Ildiko van Rhijn and Prof. dr. Adriaan Minnaard for our productive collaboration on the phosphomycoketide project, and Prof. dr. Annemieke Geluk, Prof. dr. Ferry Ossendorp and Dr. Dimitri Filippov for their valuable contribution to the research on self-adjuvanting peptides. I also want to thank our scientific director Prof.dr. H.S. Overkleeft, our secretaries Mionne and Jessica, and our technicians Fons, Karthick and Hans for their help from behind the scenes.

A special thank you goes to Susan: without your teachings, support, positivity, hard work and the happy ELISA songs, my PhD would have not been the same. Krista and Nico: thank you for sharing your knowledge with me, for contributing greatly to the work contained in this thesis and for always being open to a nice conversation. I thank Malene and Mikolaj for their collaboration, reliability and friendliness. I also want to thank Robert and Simone for their kindness and readiness to help with sample measurements, even on a short notice.

Thank you to the whole Biosyn and INZI groups for contributing to the creation of many nice memories of my time in Leiden. Elko, Tim, Jacopo, Francesca, Daniel and Anouk: in one way or another you have inspired me and you have been good friends throughout the years. I would also like to thank Marta, Jeanine, Sara, Anne Geert, Casper, Niels, Tony, Thijs and Jim for creating a stimulating work atmosphere and for making my coffee breaks more enjoyable. A big thank you to Fabrizio, for providing new insights and for his motivating energy. I would also like to thank my students

Mirjam, Jelle and Dennis for their contribution, and for their friendly and positive attitude.

A special thank you to my paranymphs, Mickey and Deniz: since the beginning of my PhD you have been there for me, bringing a smile and a distraction when things were more difficult. You have helped me in so many ways that a whole page would be too short to properly describe my gratitude. To my family and friends, in the Netherlands and abroad, thank you for your love and support during the past 5 years. Thank you, Roberta for designing the cover of my thesis and much more.

Finally, my deepest gratitude goes to Ruben, my husband and my best friend: you have lived the ups and downs of my PhD path, possibly as vividly as I did, and you have decided to stand by my side unconditionally; you have shown so much compassion and love that I was inspired to overcome the challenges encountered and celebrate every success with a renewed joy.